

©2016

Annie D'Souza Palaparthi

ALL RIGHTS RESERVED

**POTENTIAL APPLICATIONS OF LIPID NANOPARTICLES IN
EDIBLE PACKAGING AND NUTRACEUTICAL DELIVERY**

By

ANNIE D'SOUZA PALAPARTHI

A dissertation submitted to the

Graduate School-New Brunswick

Rutgers, The State University of New Jersey

In partial fulfillment of the requirements

For the degree of

Doctor of Philosophy

Graduate Program in Food Science

Written under the direction of

Dr. Qingrong Huang

And approved by

New Brunswick, New Jersey

OCTOBER 2016

ABSTRACT OF THE DISSERTATION

**POTENTIAL APPLICATIONS OF LIPID NANOPARTICLES
IN EDIBLE PACKAGING AND NUTRACEUTICAL
DELIVERY**

By ANNIE D'SOUZA PALAPARTHI

Dissertation Director

DR. QINGRONG HUANG

Lipid nanoparticles are emulsion-type nanoscale aqueous dispersions that have been extensively used as delivery systems for drugs and active ingredients of lipophilic nature in pharmaceutical and cosmetic industry through different administration routes. These nanoparticles are made from food-grade ingredients which make them desirable approach to create new fortified and functional foods.

In my work, lipid nanoparticles were investigated for the very first time as a potential nanofiller in biopolymer films in improving moisture barrier properties and further extended their role in creating multifunctional edible films. Further, a new lipid nanoparticle/nanocarrier from cocoa butter was developed and evaluated as an effective delivery system of non-polar bioactives for functional beverage applications. Finally, this nanocarriers were tested as nanofillers in biopolymer films that improve its moisture

interactions as an edible film and examine whether these films can serve an ‘encapsulating matrices’ to delivery systems.

Candelilla wax, a highly hydrophobic plant wax was utilized to create a nano dispersion using microemulsion technique. Selection of emulsifiers and proportions of the emulsions were carried out by using effective HLB concept for emulsifiers and ternary phase diagrams respectively. Particle size analysis using dynamic light scattering and imaging of Candelilla wax nanoparticles using atomic force microscopy were examined to understand their storage stability and morphology. Chitosan, an antimicrobial natural polymer was used as a model nanocomposite film to analyze its physical properties and antibacterial nature with wax nanoparticles. The film was preparing film solution by blending polyvinyl alcohol, glycerol and wax nanoparticles to create a thin film which can be used for practical purposes. After conditioning at ambient conditions (relative humidity of 53% and room temperature 25°C, moisture barrier properties (surface hydrophilicity, % water uptake, moisture isotherms and water vapor permeability) of the films were studied. Mechanical strength and elasticity of the films were calculated and microstructure of the surface and cross-sections of the film were examined to understand their physical state. Inclusion of fillers might affect the anti-bacterial nature of chitosan and to understand the effect of wax nanoparticles, growth and interaction of gram-negative and gram-positive bacteria on these films were measured to establish the nanocomposite films’ anti-microbial activity. Optimization of preparation of hot emulsions of Candelilla wax with Tween 80 (polysorbate 80) gave nanoparticles of smallest average hydrodynamic diameter of ~ 212 nm with good storage stability. On visualizing the nanoparticle with AFM and cross-sectional analysis, it was found that they have a platelet structure with dimensions ~145nm

as the horizontal size and ~15nm as its vertical height. Films were prepared with different percentages of nanoparticles keeping chitosan and glycerol ratio constant. From surface hydrophilicity studies using water droplet method with contact angle analysis, it was noted that hydrophobicity of the film with wax nanoparticles was slightly increased and at a higher concentrations of nanoparticles (> 3% w/w), contact angle with water did not change. From moisture isotherms of films with different concentrations of nanoparticles, adsorption of water was significantly decreased as the movement of water molecules were restricted in nanocomposites. Water uptake capacity of the nanocomposites were drastically lowered as percentage of nanoparticles in the film increased. On increasing nanoparticle content from 1% to 10% w/w, water vapor permeability values decreased by 19% to 55%. Tensile strength and elongation % values of nanocomposites were compared with the control film without nanoparticles, showing that nanoparticles have no plasticizing effect. Effects of wax nanoparticles in the films were further supported by its homogenous structure and chemical interaction analysis by FTIR. Antibacterial nature of chitosan was not affected at low content (< 5% w/w) of nanoparticles. From these observations, it can be concluded that Candelilla wax nanoparticles can serve as potential nanofiller in chitosan films and these nanocomposites can effectively be used as primary packaging material as stable over a wide range of relative humidity and increase shelf-life with its controlled water transfer and anti-microbial nature.

Health-promoting bioactives due to their chemical nature are not effective due to their instability, poor bioaccessibility and bioavailability on digestion. In pharmaceutical industry, lipids based delivery systems have shown to overcome this problem. Lipid based nanoparticles, also called as nanocarriers were developed to deliver beneficial non-polar

molecules that promote wellness and alleviate diseases conditions. In my study, emulsion based nanoparticles are prepared from cocoa butter with Coenzyme Q10 (CoQ10) as a test bioactive which has poor bioavailability due to its hydrophobic nature. Selection of lipid for suitable for nanoparticle preparation is dependent on the chemical properties of the bioactive. Solubility of the bioactive is the key factor that governs the encapsulation and stability of a delivery system. Cocoa butter (CB) was chosen due to high solubility of CoQ10 ($110 \pm 4.7\%$ w/w) among the soft fats considered for the study and its polymorphic crystal states that enables better loading capacity and stability of nanocarriers. Cocoa butter emulsions were prepared with polysorbate and fatty acid esters based non-ionic emulsifiers using HLB systematic approach and further, ternary phase diagrams were created to narrow down compositions of stable oil-in-water (O/W) emulsions. According to the solubility studies with CoQ10, these stable O/W emulsions were loaded with CoQ10 and particle size analysis was conducted to obtain the most stable formulation with highest loading capacity (2% w/w). These hot emulsions were subjected to homogenization above melting temperatures to create nanoscale emulsion droplets with CoQ10 and quickly cooled to 4°C. The process conditions of high pressure homogenization (1000 bar and 20 cycles) were optimized to obtain nanoemulsions of smallest diameter required for maximum saturation solubility and better dissolution velocity of encapsulated CoQ10. To understand the effect of CoQ10 concentration on cocoa butter nanocarriers, three different formulations were prepared 0.5% (low-level), 1.0% (mid-level) and 2.0% (high-level) CoQ10 with 2% w/w emulsifier (1.74% Span60 and 0.36% Tween60), 10% cocoa butter and remaining DI water. Storage stabilities of three formulations show that they are stable with no significant difference in particle size over 7 weeks. Due to high solubility of CoQ10 in CB, 85-90%

entrapment efficiency was achieved in nanocarriers. Formulations did not destabilize after sterilization which is a crucial HACCP step for beverage applications. Crystallization state of components and structural information of these nanocarriers can throw light on its stability and behavior on consumption. Most of cocoa butter exists a metastable α polymorph form in an empty nanocarriers form and in presence of CoQ10, different polymorphs existed. CoQ10 remains as a super-cool melt during recrystallization process as there were no phase transition peak from liquid to solid crystal state. Structural data about nanoparticles can be elucidated from scattering intensity profiles generated by synchrotron small-angle X-ray scattering (SAXS) method. Using Porod's law, structural information extracted from scattering intensity profile shows that the interface thickness is affected by loading % of CoQ10 at intermediate q range. Empty and low load nanocarriers have interface thickness of 4.5 nm and in high load nanocarriers, interface thickness increases by only 9%. This shows that interfaces of nanocarriers is not affected by encapsulate.

Performance of this novel CoQ10-CB nanocarriers by evaluating the bioaccessibility (a measure for amount of *solubilized* CoQ10 that is available for absorption) and relative bioavailability (a measure for amount of CoQ10 that reaches systemic circulation over time of observation) with *in vitro* and *in vivo* models. *In vitro* lipolysis with pancreatic lipase in fed and fast state buffers were conducted and compared on 0.5%, 1.0% and 2.0% CoQ10 in both mixture and nanoparticle form without changing material composition. Extent of lipolysis is a parameter studied to understand lipase activity on different types of formulations and measure amount of fatty acids released during lipolysis. Upon 2-way ANOVA analysis, there was no significant difference in

extent of lipolysis on comparing fed and fast state between mixture and nanoparticle form. CB lipolysis in nanoparticle form was significantly greater than that of mixture due to greater surface area and better exposure to enzyme in nanodispersions. However, it was interesting to find that addition of CoQ10 in CB mixtures and nanocarriers have significantly lowered the lipolysis of CB by 32-42%. Bioaccessibility of CoQ10 significantly improved when incorporated in cocoa butter nanoparticles. Among different formulations with different levels of CoQ10, formulations with lowest amount of CoQ10 (0.5% CoQ10-CBLN) had highest bioaccessibility suggesting that there is a limiting concentration of CoQ10 in mixed micelles of hydrolysis products of nanocarriers and is controlled by lipase activity on the delivery system. Since bioaccessibility is accounted by CoQ10 that is able to solubilize in gastric environment after lipolysis, it only reflects a portion of CoQ10 that can be absorbed. Bioaccessibility tests doesn't consider other transport mechanisms involved. Pharmacokinetic studies were performed on pure CoQ10 and 2% CoQ10-CBLN in rats and pigs to evaluate relative bioavailability and absorption kinetics into systemic circulation. The results were inconclusive due to inconsistencies with the results and previous studies with solubilized CoQ10 formulations and time window of observation for the experiments were too short to get comparable results. Tissue uptake kinetics of Coenzyme Q10 from nanocarriers was very similar to studies on CoQ10 dissolved in oils and fats. Three hours after single dose administration of 2% CoQ10-CBLN, concentrations of the bioactive was highest in small intestine which confirms the interaction of CoQ10 with enterocytes in small intestinal epithelium. Overtime, CoQ10 was absorbed into liver with its concentration highest in 24 h. On comparing with control, it can be concluded that CoQ10 in CB nanocarriers is absorbed into circulation and reaches

liver. Long chain fatty acids and glycerides trigger absorption through lymphatic route and is favored by hydrophobic compounds to reach blood circulation. It is suggested that further lymphatic transport studies on *in vivo* lymph duct cannulated animal models which have similar lipid absorption capacity (apobec-1 knockout mice) would give better understanding of pharmacokinetics of bioactives in CB nanocarriers.

To extend functionality of lipid nanoparticles in edible packaging film matrix, novel starch nanocomposite edible films using lipid nanoparticles as fillers with enhanced moisture barrier properties and its ability to stabilize and controlled release bioactive loaded in nanoparticles, were developed. A potent antioxidant from rosemary with anti-inflammatory and anti-carcinogenic properties, Carnosic acid (CA) was loaded in cocoa butter (CB) nanocarriers in a similar approach to that CoQ10 delivery system. CA has very poor solubility in water (135 ppm) and CB nanocarriers can be potential delivery system to enhance its bioaccessibility and bioavailability to exhibit its health benefits. Solubility of CA in CB (555 ± 7.05 ppm/ $^{\circ}\text{C}$) increased with temperature and process temperature (60°C and 80°C) was chosen. Hot-melt homogenization method for preparation of CA-CB nanoparticles was optimized for process pressure and cycles (1500 bar and 20 cycles) to obtain smallest and most stable nanoparticles. Encapsulation efficiency was dependent on CA loading % in CB nanoparticle formulations. Formulation with highest loading, 5.3% (w/w) CA had encapsulation efficiency ($87.81 \pm 0.2\%$ EE) and stability over a month and at higher temperatures. In-vitro lipolysis of these CA-CB nanoparticles in fed and fast state buffers have no significant difference in extent of lipolysis but bioaccessibility % in fed state buffer ($31.52 \pm 0.71\%$) was improved and was significantly higher than that in fast state buffer by 36%.

CA-CB nanoparticles (CA-NP) were incorporated in hydroxypropylated starch (HPS) films with film forming capabilities but have high moisture affinity. Films solutions with different concentrations of CA-CB nanoparticles (HGNC-0.5, 1 and 2% w/w) were used to prepare different films. On analyzing microstructure of different films using SEM, significant microphase separation of lipid in matrix were observed in HGNC-2 films which effects its transparency and other physical properties. DSC observations of films suggest that nanoparticles in starch films have plasticizing effect due to loss of crystallinity and thermograms of CA-NP show polymorphism in CB which is important for stability and integrity of nanoparticles. Loss of crystallinity could be a reason for lower tensile strength of films. Elastic modulus of all films are around 2.65 MPa with their elongation around at 214%. Surface hydrophilicity of nanocomposite films didn't change with increase in CA-NP. Moisture isotherms indicate that nanocomposite edible films are stable over a range of humidity as they show poor solubility of water vapor in their matrix. All nanocomposites have similar swelling behavior with water uptake around 155% and was 40% lower than the control film (HGNC-0). HGNC-0.5 films had lowest water vapor permeability which can be attributed to homogenous matrix and smoothness of the surface. Uniform embedment of CA-CB nanoparticles in starch matrix and hydrophobic nature of CB would obstruct diffusion of the water vapor. From these findings, we can conclude that moisture barrier properties effectively improved in nanocomposite films and can be used in multicomponent food systems. Release of CA from HGNC films was assessed by measuring antioxidant capacity of aqueous phase of digested films with pure HPS film as control using DPPH assay. Comparing with pure CA, only 40% of antioxidant capacity was retrieved from digested films after 2 hours of *in vitro* digestion. From these results, we

can conclude that edible films with lipid NP possess good moisture barrier properties and can slowly release non-polar bioactives in limited, controlled way.

ACKNOWLEDGEMENT

I am deeply grateful to Dr. Qingrong Huang for giving me an opportunity to work in his group and his encouragement during my graduate studies which gave a thorough grounding in food chemistry and nanotechnology. I am immensely thankful for providing me recommendations for teaching assistantship and other competitions. Overall, I am very thankful for having Qingrong Huang for being kind hearted and a very considerate advisor.

I would like to thank Dr. Kit L. Yam, Dr. Chi-Tang Ho, Dr. Alan King and Shiming Li for their willingness to be my committee members, and for their valuable suggestions and help with my research. I am very grateful for Dr. Yam for their time and effort on writing a recommendation letter for me for a scholarship and provide me motivation and suggestions during his term as a graduate director.

I would also like to thank a number of visiting scholars whom I closely worked with. Their valuable suggestions and encouragement has helped immensely in shaping my thesis and gave me insights about different areas of research in food science. I would also like to thank Dr. Schaich, Dr. Karwe and Dr. Cordana who allowed me to use their laboratory facilities. I am grateful for all my previous and current lab mates for their help and support to my work. I am thankful to all my friends and colleagues in Food Science Department who made my time at Rutgers a memorable experience.

I also want to express my gratitude to Dr. Gregg Transue, my teaching advisor for his support with my teaching and career development. I am also grateful for the teaching assistantship from Office of Undergraduate Instruction, Division of Life Sciences and part-time lectureship in Instruction Support and Development from Department of Physics and Astronomy.

DEDICATION

To my father and my inspiration, Daniel D'Souza Palaparthi who instigated my love for sciences by introducing me to theory of relativity at the age of seven.

To my mother and my best friend, Pramila Rajeswari Victor who believed in my ambitions and supported me in every step of my life.

To my fiancé and love of my life, Vinodh Kotipalli who was helped me realize my dream of earning a PhD.

TABLE OF CONTENTS

ABSTRACT OF THE DISSERTATION	ii
ACKNOWLEDGEMENT	xi
DEDICATION	xii
TABLE OF CONTENTS.....	xiii
LIST OF TABLES	xx
LIST OF ILLUSTRATIONS.....	xxii
RATIONALE AND HYPOTHESIS.....	xxvii
CHAPTER 1. INTRODUCTION.....	1
1.1 Lipid based delivery systems: Background and definitions	1
1.2 Factors affecting structure and integrity of Lipid Nanoparticles.....	7
1.3 Mechanism of Lipid Nanoparticles in Oral Delivery of Nutraceuticals.....	7
1.4 Materials for lipid nanocarriers	10
1.4.1 Candelilla wax	10
1.4.3 Cocoa butter.....	13
1.5 Bioactives encapsulated in lipid nanocarriers	14
1.5.1 Coenzyme Q10	14
1.5.2 Carnosic acid	18
1.6 Biopolymer based packaging.....	24
1.6.1 Chitosan films.....	27
1.6.2 Starch films.....	33

1.6.3	Hydroxypropyl starch	47
1.7	Biopolymer nanocomposites	52
CHAPTER 2. CANDELILLA WAX NANOPARTICLES: DESIGN AND CHARACTERIZATION		53
2.1	Abstract.....	53
2.2	Materials and Methods	53
2.2.1	Materials	53
2.2.2	Selection of emulsifiers	54
2.2.3	Preparation of Candelilla wax nanoparticles	56
2.2.4	Particle Size Analysis by Dynamic Light Scattering (DLS)	56
2.2.5	Atomic Force Microscopy (AFM) Imaging	57
2.3	Results and Discussion	58
2.3.1	Tween 80 was the choice of surfactant.....	58
2.3.2	Particle Size Analysis of CW formulations with Tween 80-Oleic Acid surfactant mixture.....	60
2.3.3	Optimization of Candelilla wax nanoparticles preparation	62
2.4	Conclusion	73
CHAPTER 3. CHITOSAN-PVA NANOCOMPOSITES WITH CANDELILLA WAX NANOPARTICLES: PHYSICAL AND ANTIBACTERIAL PROPERTIES		74
3.1	Abstract.....	74
3.2	Materials and Methods	75
3.2.1	Materials	75
3.2.2	Preparation of CS-PVA nanocomposite films with CW nanoparticles	75

3.2.3	SEM Imaging of CPGW films.....	78
3.2.4	Contact Angle Measurements on CPGW films.....	78
3.2.5	Moisture Sorption Isotherms of CPGW films	78
3.2.6	Water absorption Studies on CPGW films.....	79
3.2.7	Water Vapor Transmission Rate and Water Vapor Permeability of CPGW films:	80
3.2.8	Mechanical properties of CPGW films	80
3.2.9	Molecular Interactions Analysis: Fourier Transform Infra-Red Spectroscopy 81	
3.2.10	Antibacterial Properties of CPGW films	81
3.3	Results and Discussion	82
3.3.1	Visual Appearance of Chitosan-PVA nanocomposite films with Candelilla wax nanoparticles.....	82
3.3.2	Microstructure of CPGW films	84
3.3.3	Surface hydrophobicity of CPGW films	86
3.3.4	Moisture Sorption Isotherms	89
3.3.5	Water Absorption studies of CPGW films	92
3.3.6	Film permeability	94
3.3.7	Mechanical Strength and Elasticity of CPGW films	96
3.3.8	Molecular Interactions Analysis: Fourier Transform Infra-Red Spectroscopy 99	
3.3.9	Antibacterial Activity of films.....	102
3.4	Conclusion.....	105

CHAPTER 4.	COENZYME Q10 LOADED COCOA BUTTER NANOPARTICLES: PRODUCTION AND CHARACTERIZATION.....	106
4.1	Abstract.....	106
4.2	Materials and Methods	107
4.2.1	Materials	107
4.2.2	Solubility Studies.....	107
4.2.3	Preparation of Coenzyme Q10 loaded cocoa-butter nanoparticles	107
4.2.4	Particle Size analysis – Dynamic Light Scattering.....	108
4.2.5	Stability studies after sterilization	109
4.2.6	Encapsulation efficiency measurements.....	109
4.2.7	Crystallization behavior studies.....	110
4.2.8	Synchrotron Small-angle X-ray scattering (SAXS) studies	110
4.3	Results and Discussion	111
4.3.1	Maximum solubility of Coenzyme Q10 in different fats and oils.....	111
4.3.2	Optimization of Process Conditions	113
4.3.3	Storage stability of the formulations	116
4.3.4	Stability after sterilization	119
4.3.5	Encapsulation Efficiency of Coenzyme Q10 in Cocoa butter nanocarriers .	121
4.3.6	Crystallization behavior of Cocoa butter and Coenzyme Q10 in formulations	123
4.3.7	Small Angle X-Ray Studies.....	127
4.4	Conclusions	129

CHAPTER 5.	COENZYME Q10 LOADED COCOA BUTTER NANOPARTICLES: BIOACCESSIBILITY AND BIOAVAILABILITY	130
5.1	Abstract.....	130
5.2	Materials and Methods	130
5.2.1	Materials	130
5.2.2	In-vitro lipolysis of CoenzymeQ10 in Cocoa butter formulations	131
5.2.3	Calculations for the percent bioaccessibility	133
5.2.4	Calculations for extent of lipolysis.....	133
5.2.5	Quantitative assay of coenzyme Q10	134
5.2.6	Animals.....	134
5.2.7	Pharmacokinetics studies and Body distribution of Coenzyme Q10 in Rats and Pigs	134
5.2.8	Data analysis.....	136
5.2.9	Statistical Analysis	136
5.3	Results and Discussion	137
5.3.1	Effect of Coenzyme Q10 loading on extent of lipolysis in lipid mixtures and in CB nanocarriers.....	137
5.3.2	Improved bioaccessibility of Coenzyme Q10 in CBSLNs.....	141
5.3.3	Pharmacokinetics studies in Rats	145
5.3.4	Body distribution of Coenzyme Q10 on single dose administration.....	150
5.3.5	Pharmacokinetics studies in Pigs.....	153
5.4	Conclusion	156

CHAPTER 6. CARNOSIC ACID LOADED COCOA BUTTER

NANOPARTICLES: PRODUCTION AND CHARACTERIZATION..... 157

6.1 Abstract..... 157

6.2 Materials and Methods 157

6.2.1 Materials 157

6.2.2 Solubility studies of CA in water, gastric buffers and lipids..... 158

6.2.3 Preparation of CA loaded CB Nanoparticles..... 158

6.2.4 Stability studies of CA-CB nanoparticles..... 159

6.2.5 Encapsulation Efficiency 160

6.2.6 Bioaccessibility Studies 160

6.3 Results and Discussion 162

6.3.1 Solubility of CA in water, gastric buffer and lipids 162

6.3.2 Preparation of Carnosic acid loaded cocoa butter nanoparticles 165

6.3.3 Storage stability of Carnosic acid loaded cocoa butter nanoparticles 169

6.3.4 Encapsulation Efficiency of CA loaded CB Nanoparticles..... 172

6.3.5 In-vitro lipolysis studies on CA-CB Nanoparticles 174

6.4 Conclusion 183

CHAPTER 7. HYDROXYPROPYL STARCH NANOCOMPOSITES WITH

CARNOSIC ACID LOADED COCOA BUTTER NANOPARTICLES: PHYSICAL

AND ANTIOXIDANT PROPERTIES..... 184

7.1 Abstract..... 184

7.2 Materials and Methods 185

7.2.1 Materials 185

7.2.2	Preparation of nanocomposite films	185
7.2.3	SEM Imaging.....	186
7.2.4	Differential Scanning Calorimetry	186
7.2.5	Mechanical properties.....	186
7.2.6	Moisture barrier properties	187
7.2.7	Antioxidant activity measurements	189
7.3	Results and Discussion	191
7.3.1	Preparation of nanocomposite films	191
7.3.2	Microstructure of HGCN films.....	193
7.3.3	Differential Scanning Calorimetric studies	197
7.3.4	Mechanical Properties of HGCN films	201
7.3.5	Moisture Barrier Properties of HGCN films	204
7.3.6	Antioxidant Activity in HGCN films	214
7.4	Conclusion	219
CHAPTER 8. SUMMARY AND FUTURE WORK		220
8.1	Summary.....	220
8.2	Future Work.....	221
8.2.1	Comparative study with other alternative nanocomposite films in real food systems	221
8.2.2	Response surface methodology for optimization of film composition.....	221
8.2.3	Lymphatic transport studies for bioactive loaded lipid nanoparticles	222
BIBLIOGRAPHY		224

LIST OF TABLES

Table 1 Chemical Composition and Melting point of selected lipids.....	12
Table 2 Common components of biopolymer based films	26
Table 3 List of natural starches and their crystallinity percentages.....	35
Table 4 Mechanical Properties of Amylose and Amylopectin Films.....	43
Table 5 Water vapor transmission of starch films at initial time and stored for 90 days at 64% relative humidity and 20°C.....	46
Table 6 Effective HLB Values of Surfactant Mixtures of Tween 80 and Oleic acid	55
Table 7 Visual Appearance of formulations with 10% w/w CW and 1.5% w/w surfactant/blends	59
Table 8 Hydrodynamic Diameter and Polydispersity of formulations with 10% Candelilla Wax and different surfactants	61
Table 9 Composition of CPGW films.....	77
Table 10 PCS diameter and polydispersity index in 0.01M NaCl of 10% Cocoa butter and 2% emulsifiers (87% w/w Span60 and 13% w/w Tween60).....	115
Table 11 Encapsulation Efficiency (EE%) of Coenzyme Q10 in SLN formulations with different loading % before and after sterilization	122
Table 12 Chemical composition of Fasted and fed state buffer for in-vitro lipolysis	132
Table 13 Extent of Lipolysis of different Cocoa butter based mixtures and SLN formulation of CoenzymeQ10	139
Table 14 Pharmacokinetic Parameters of CoQ10 Nanoparticles in rats.....	149
Table 15 Pharmacokinetic Parameters of CoQ10 Nanoparticles in pigs.....	155
Table 16 Composition and Stability of CA loaded in CB nanodispersions.....	166

Table 17 Encapsulation Efficiency of stable CA-NP formulations	173
Table 18 In-vitro Lipolysis of CA & CB Mixture (CA+CB) and CB Nanoparticle with 5.3% CA (CA-NP-6).....	182
Table 19 Composition of the HGCN film solutions	192
Table 20 Endothermic peaks of HGCN-0 (control), CA loaded nanoparticles and nanocomposites.....	200
Table 21 Mechanical Properties of HGCN films.....	203
Table 22 Contact measurements and surface absorption kinetics of HGCN films.....	205
Table 23 Antioxidant Capacity (%) of CA+CB mixture, nanoparticles and HS nanocomposite film.....	218

LIST OF ILLUSTRATIONS

Figure 1 Illustration summarizing characteristics of oil-in-water emulsion based nanoscale delivery systems of nutraceuticals	2
Figure 2 Schematic diagram of solid lipid nanoparticle (SLN) and nanostructured lipid carrier (NLC). Adapted from (12)Lipid based delivery systems in functional foods.....	4
Figure 3 Mechanisms of absorption promoting effect of lipids in lipid nanoparticle formulations. Adapted from (28)	9
Figure 4 Different oxidation states of Coenzyme Q10	16
Figure 5 In-vitro antioxidant mechanisms of Coenzyme Q10 (40)	17
Figure 6 Major antioxidant components in Rosemary extract.....	20
Figure 7 Oxidation Products of Carnosic Acid.....	21
Figure 8 Proposed antioxidant mechanism of carnosic acid, LOOH, LOO* and OH denote hydroperoxide, peroxy radical and hydroxide, respectively. Adapted from (51)	22
Figure 9 Proposed antioxidant mechanism from carnosic acid quinone where carnosic acid, CAR and rosmanol have antioxidant ability. Adapted from (51)	23
Figure 10. Preparation of Chitosan from Chitin. Adapted from (131)	29
Figure 11. Structure of Cellulose, Chitin and Chitosan. Adapted from (131).....	30
Figure 12 Retrogradation mechanism involving intermolecular hydrogen bonding between amylose and amylopectin in Potato Starch. Adapted from (144).....	37
Figure 13 Intermolecular hydrogen bonding among short chains of amylopectin between amylose- amylopectin and amylopectin-amylopectin molecules in starches. Adapted from (144).....	38
Figure 14. Preparation of hydroxypropyl starch by etherification reaction of corn starch	49

Figure 15 Ternary Phase diagram of Candelilla Wax-Tween 80-Water	63
Figure 16 Effect of Tween80 Concentration on 10% (w/w) Candelilla wax nanoparticle size	65
Figure 17 Storage studies on Candelilla wax nanoparticles stabilized by 2% (w/w) Tween80.....	68
Figure 18 Tapping mode -Atomic Force Microscopy Height image (A) and Phase image (B)	71
Figure 19 Sectional Analysis of Candelilla Wax SLN	72
Figure 20 Appearance of freshly prepared films with 0% (A) and 2% (B), films stored for a month 2%(C), 4%(D), 5% (E) and 10% (F).....	83
Figure 21 FESEM Images of the surface (A-E) and cross-sectional (F-J) areas of CPGW films with no SLN (A, F), 1% SLN (B, G), 2% SLN (C, H), 4% SLN (D, I) and 10% SLN (E, J) using in lens detector	85
Figure 22 Effect of SLN% on water contact angles in CPGW films conditioned at 53% RH and 25°C.....	88
Figure 23 Moisture sorption isotherms of CPGW films.....	91
Figure 24 Photographs of 0% (A) and 2% (B) SLN containing CPGW and their corresponding swollen gels, (C) and (D). Effect of %SLN in CPGW films on water absorption capacity %	93
Figure 25 Water Vapor Permeance Values for CPGW films	95
Figure 26 Effect of % SLN (w/w) and relative humidity on tensile strength of CPGW films	97

Figure 27 Effect of % SLN (w/w) and relative humidity on elongation % of CPGW films	98
Figure 28 FTIR generated absorbance spectrum of Candelilla Wax and CPGW films	100
Figure 29 FTIR offset absorbance spectrum of Candelilla wax and CPGW films.....	101
Figure 30 Antibacterial activity against <i>E. Coli</i> K12 of CS-PVA films with wax NP...	103
Figure 31 Antibacterial activity against <i>S. aureus</i> of CS-VA films with wax SLN.....	104
Figure 32 Solubility of CoQ ₁₀ in fats. Data shown as mean (n=3), p <0.05.....	112
Figure 33 Effective diameter of the cocoa butter nanoparticles with loading 0.5% (A) and 2% (B) at different pressures and number of cycles.....	114
Figure 34 Effective diameter of CoQ ₁₀ CB SLN formulation over 7 weeks of storage at 25°	117
Figure 35 Optical Images of the CoQ ₁₀ CBSLN formulations after 7 weeks of storage	118
Figure 36 Effect of Sterilization on the particle size of CoQ ₁₀ CBSLN formulations ..	120
Figure 37 DSC thermograms of the components, Coenzyme Q10 (I) and Cocoa butter (II) and control CBSLN (III) during melting (A) and recrystallization (B).....	125
Figure 38 DSC thermograms of the formulations, 0.5% (IV), 1% (V) and 2% (VI) CoQ ₁₀ -CBSLN during melting (A) and recrystallization (B).....	126
Figure 39 SAXS intensity profile of CBSLN loading CoQ ₁₀	128
Figure 40 Consumption of NaOH during the lipolysis for different SLN formulations in fed state condition	140
Figure 41 HPLC spectrogram of aqueous phases of 0.5%CoQCBSLN and mixture after in-vitro lipolysis in fed state buffer.....	143

Figure 42 % Bioaccessibility of CoQ10 CBSLN formulations and equivalent lipid mixtures in fed and fast state for in-vitro lipolysis	144
Figure 43 Concentration-Time profiles of 2% CoQ10 CB nanoparticles vs. pure CoQ10 in rats.....	148
Figure 44 Distribution of Coenzyme Q10 amounts in organs: a) Heart, b) Kidney, c) Liver and d) Small intestine at different time points after a single dose oral administration	152
Figure 45 Concentration-Time profiles of 2% CoQ10 CB nanoparticles vs. pure CoQ10 in pigs.....	154
Figure 46 Solubility of carnosic acid (CA) in medium chain triglycerides, Neobee® (NM5, NM20, N895, N1053), cocoa butter (CB) and cocoa butter substitutes, Wecobee® (WM, WFS) at different temperatures (60°C and 80°C). Data shown as n=4, p<0.05 ..	164
Figure 47 Effect of HPH Cycles on Particle analysis on Stable Formulations (1500 Bar)	167
Figure 48 Effect of HPH pressure on Particle analysis on Stable Formulations (20 cycles)	168
Figure 49 Effective diameter of CA-NP formulation over 4 weeks of storage at 25°C .	170
Figure 50 Optical Images of CA-NP formulations after 4 weeks of storage where A = control, B-D = 0.8%, 1.6%, 2.4%, 3.2%, 4%, 5.3% (w/w) of loaded CA in NP and H = 7.7% of loaded CA in NP (400X magnification).....	171
Figure 51 In-vitro Lipolysis of CA+CB mixture (Mixture) and CA-NP -6(Nanoparticle) in fed state and fast state buffers.....	179

Figure 52 HPLC Spectrogram of aqueous phase of CA & CB Mixture (CA+CB) and CB Nanoparticle with 5.3% CA (CA-NP-6) after in-vitro lipolysis in fed state buffer.....	180
Figure 53 HPLC Spectrogram of aqueous phase of CA & CB Mixture (CA+CB) and CB Nanoparticle with 5.3% CA (CA-NP-6) after in-vitro lipolysis in fast state buffer	181
Figure 54 Surface morphology of HP starch (A), nanocomposites HGCN-0.5 (B), HGCN-1 (C) and HGCN-2 (D).....	195
Figure 55 Morphology of the cross-section of films: HP starch (A), HGCN-0.5 (B), HGCN-1 (C) and HGCN-2 (D).....	196
Figure 56 DSC thermograms of HP starch (1), CA-NP (2), nanocomposites HGCN-0.5 (3), HGCN-1 (4) and HGCN-2 (5)	199
Figure 57 Tensile-strain curves of the films cast at 25 °C and 50% of relative humidity. Water content (17.3% ± 0.3).....	202
Figure 58 Water sorption isotherm of HP starch and nanocomposite films at different relative humidity at 25°C.....	207
Figure 59 Moisture Isotherms of HP starch (HGCN-0) and nanocomposites (HGCN-0.5, HGCN-1 and HGCN-2) at 25°C.....	208
Figure 60 Water uptake % by swelling in HP starch and nanocomposite films (Mean comparison by Tukey test, p < 0.05)	210
Figure 61 Water vapor permeance of HP starch and nanocomposite films (Mean comparison by Tukey test, p < 0.05)	213
Figure 62 HPLC spectrogram of aqueous phase of digested HGCN-6 nanocomposite film	217

RATIONALE AND HYPOTHESIS

Nanotechnology approaches have been used effectively in different areas in food industry especially in packaging with improved properties, functional food by nanoencapsulation and nanosensors to estimate various quality attributes. Many recent research endeavors in this area, is to create safer and high quality food products by utilizing nanoscale forms of ingredients and additives.

Motivation behind this research thesis is to generate safe and novel approaches using nanotechnology to solve challenges in food science. Also, in this pursuit, I want to develop a systematic approach that can identify and verify a nanoscale system as an effective solution. More specifically, I am studying lipid nanoparticles as a solution to specific research gaps in packaging material, functional foods and functional edible films.

Currently, naturally occurring biopolymers are favored over the synthetic petro-based plastics in food packaging due to their abundance and eco-friendly attributes. The biggest challenge facing biopolymers in packaging is their relatively poor mechanical and moisture barrier properties. Nanocomposite films where nanoscale fillers like clays and metals to improve their physical properties are extensively used in material science, electronics, and biomedical sciences. Unfortunately, these fillers have regulatory limitations and cannot be used in applications that have direct interactions with food. For this reason, safer alternatives to nanoscale fillers are desired in primary packaging materials. Different nanostructured systems can be created from basic building blocks of life, simple macromolecules like carbohydrates, proteins, lipids and nucleic acids which are safe on consumption. Among them, lipid based nanostructures like solid lipid nanoparticles, nano-structured lipid carriers and nanoemulsions are extensively used in

pharmaceutical industry as non-toxic and effective drug delivery systems. It is hypothesized that lipid nanoparticles can be a safe and effective nano-filler in improving moisture barrier properties of biopolymer films due to the lipid's hydrophobicity and high aspect ratio of lipid nanoparticles.

Functional beverages are the fastest growing sector of functional food industry mainly for the health benefits and convenience they offer. These health benefits are attributed by nutraceuticals present in functional foods. Chemical characteristics of nutraceuticals, like molecular weight, conformations, polarities etc. and further, their physiochemical properties like solubility, physical state, chemical stability etc. interfere the effectiveness of functional beverages. Different delivery systems are developed to overcome these challenges associated with functional beverages. Lipid nanoparticles can be a carrier vehicle for nutraceutical delivery. It is hypothesized that lipid with polymorphism could be a suitable candidate for delivering non-polar molecule with health-promoting benefits on oral consumption.

Edible functional films can function as carriers for water soluble antibacterial, antifungal, colors and antioxidant agents. It is difficult to incorporate non-polar bioactives due to their hydrophilic nature, one way this could be done is by incorporating them in lipid nanoparticles. These films can serve dual functions: (1) lower the moisture transfer of the films and (2) stabilize and release non-polar bioactives on consumption. This could extend our knowledge of behavior of lipid nanoparticles in a solid state system, for example a food matrix. It is a lipid nanoparticle can serve as potential nano-filler and also an effective delivery system of a bioactive in polysaccharide based films by improving its

water barrier properties and thus creating a functional edible films to preserve fresh and processed food.

This work is aimed to explore applications of lipid nanoparticles in different food systems which possibly lead to new paths in food product development which combines nanotechnology, material science and pharmaceutical sciences

CHAPTER 1. INTRODUCTION

1.1 Lipid based delivery systems: Background and definitions

Oral delivery of lipophilic bioactive/drug molecules has been a constant challenge in both pharmaceutical and food industry. Lipophilic molecules can be orally administered in two broad categories of formulations: (i) lipid-based(1, 2) and (ii) polymer-based(3, 4) formulations. From functional food industry perspective, lipids have advantages over polymers: (i) Lipids are non-toxic whereas the polymers have a narrow range of cytotoxicity (ii) Lipid based formulations can be produced on large-scale using cost-effective methods and (iii) Lipids can readily dissolve the lipophilic molecules whereas, polymer based delivery systems may require an organic solvent for dissolution of active ingredient which may not be permissible by food regulatory laws.(5)

Different lipid based and nano-sized emulsion systems are explored and utilized in different areas of applications for example, pharmaceuticals, and cosmetic and food industry. These systems are derived from the conventional oil-in-water (lipid: dispersed phase and water: continuous phase) emulsion system which has 100-1000 nm sized droplets of oil stabilized by emulsifiers in water. Conventional oil-in-water emulsions are kinetically unstable because the free energy of oil and water separately is lower than that of the emulsion.(6) There are three most common nano-systems resulting from conventional emulsions have greater stability and multiple functionalities as shown in Figure 1. In this section, the definitions and terminology of these systems are discussed in detail to understand and differentiate them.

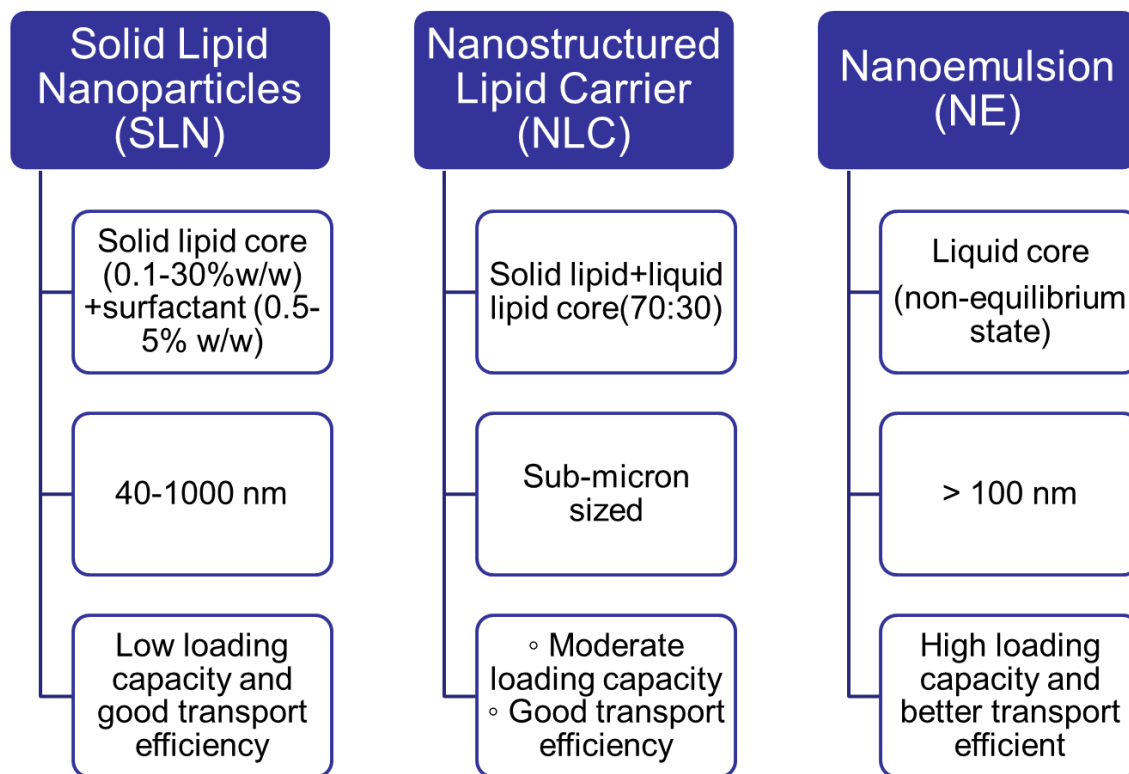


Figure 1 Illustration summarizing characteristics of oil-in-water emulsion based nanoscale delivery systems of nutraceuticals

Nanoemulsions are similar to the conventional emulsions but with a very small particle size (< 100 nm). Oil droplet size of a nanoemulsion is smaller than wavelength of the visible light ranging 400-700nm (λ) due to which they are optically transparent or translucent and possess better stability to gravitational separation and aggregation over conventional emulsions.

Lipid nanoparticles (LN) are colloidal drug carrying particles with submicron size ranging from 50 to 1000 nm. They are composed of lipids and stabilized by surfactants.(7) They are used as an alternative delivery systems to nanoemulsions, liposomes, and polymeric nanoparticles. Solid lipid nanoparticles (SLN) were first designed by research groups lead by Prof. M.R. Gaso and Prof. R.H. Müller in 1990.(8) The lipid matrix of the first published carriers is composed of solid fat. Later in late 1990s, newer forms of lipid nanoparticles were developed and are called nano-structured lipid carriers (NLC) as shown in Figure 2. NLCs' lipid core are composed of blend of solid and liquid lipid (oil) which remained in solid state at ambient temperatures.(9) A major advantage of NLC applications is that NLC possess better drug loading capacity over SLN. Lipid nanoparticles are suited for incorporation of lipophilic bioactives and low amounts of hydrophilic drugs (lysozyme, β -interferon etc.).(10) To overcome the problem of poor loading of hydrophilic molecules, lipid-drug conjugates (LDC) were introduced in 2001 in which lipid core had fatty acid salts of the hydrophilic drugs were used or has a lipophilic complex in which the drug molecule was covalently attached to a lipid structure.(11)

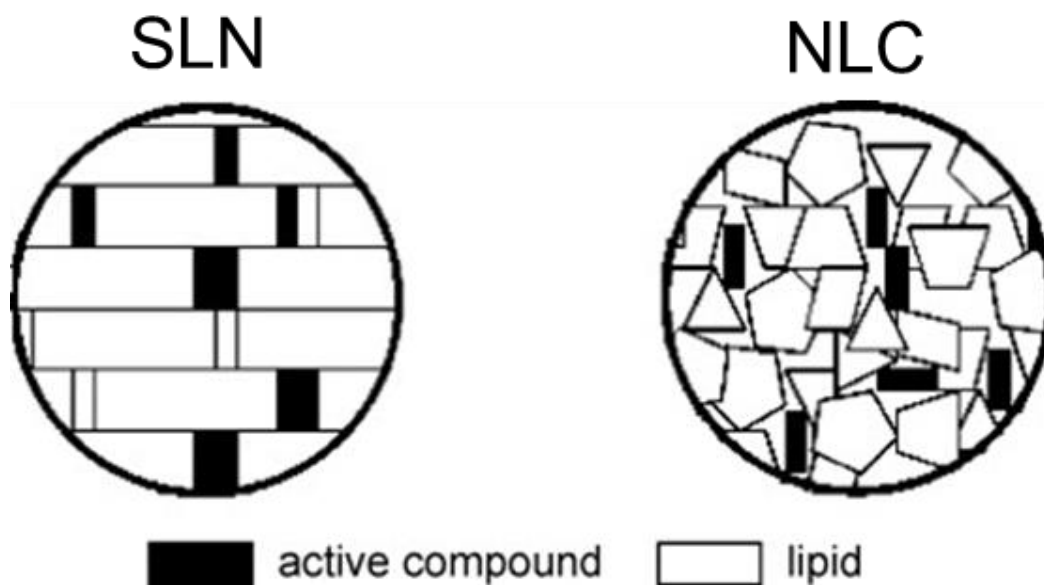


Figure 2 Schematic diagram of solid lipid nanoparticle (SLN) and nanostructured lipid carrier (NLC). Adapted from (12) *Lipid based delivery systems in functional foods*

Functional foods are described as the food products fortified with special components that have beneficial physiological effects (13-15). Functional food can improve general health of the body and alleviate the disease causing conditions on their consumption. For a long time, research in nutritional sciences pioneered in identification of nutritional and health benefits of different compounds found in various plant and animal sources which lead to quantification of these compounds in various processed food products. This growing knowledge about lack of effective concentration of these active compounds or nutraceuticals in most of the processed food revolutionized the idea of food and paved way to product development of functional foods. Functional food is described as the food products fortified with special components that have beneficial physiological effects (13-15). Functional food can improve general health of the body and alleviate the disease causing conditions on their consumption. There is no single definition to describe functional food and it is assumed that food is considered as a functional if it leads to betterment of general health or specifically lowers the risk of chronic disease apart from supplying nutritional benefits. The trends of functional food has been evolving with time starting with vitamins and mineral – fortified foods, omega-3 fatty acids, phytosterol and soluble fiber – micronutrients and more recently sport drinks, probiotics and weight management diet foods.(16-18).

The key step in product development of a functional food is to identify an effective delivery system for a particular bioactive making it highly accessible and absorptive in desirable amounts at sites of absorption like small intestine in oral delivery route. A delivery system for several drug compounds (active synthetic or chemical molecules, proteins, genes etc.) are coined by researchers in pharmaceutical to overcome problems of

poor solubility and rapid metabolism of drugs, prevent tissue damage due to extravasation, achieve desired pharmacokinetics and biodistribution, and most importantly, ensure selectivity to specific tissues with different types of drug administrations (parental, nasal, oral routes etc.).(19) Similarly, a delivery system in food products have several functions:

- (i) They serve as a protective barrier that can preserve the activity of the bioactive by not affecting or improving their chemical stability during processing, storage and consumption.
- (ii) Controlled release of a bioactive at the site of absorption for target delivery can be manipulated by the choice of a delivery system.
- (iii) Incorporating a bioactive in different delivery systems allow fortification of a wide range of food products from beverages to processed food.

For active compounds of lipophilic nature, lipid based nutraceutical delivery systems are commonly used that are very simple in nature where the bioactive is dissolved in oil to more complex systems that utilize various lipids, surfactants and co-surfactants.

One such strategy in field of food nanotechnology is development of nano-sized delivery systems that increase their efficacy in humans by improving physiochemical properties of bioactives. Nano-sized delivery systems proved to be effective due to chemical and thermal stability, dissolution and enhanced solubility of encapsulated bioactives. Most common technique that involve nanoencapsulation with lipid as carrier of bioactives is emulsification process to create nano-sized particles like nanocapsules, nanospheres, nanostructured lipid carriers and solid lipid nanoparticles and transparent to translucent solutions of nanoemulsions.(20)

1.2 Factors affecting structure and integrity of Lipid Nanoparticles

Lipid nanoparticles are prepared from oil-in-water nanoemulsions where liquid lipid is replaced by solid lipid. Due to the state of lipid core, this system enables controlled release of the encapsulated drug molecules. Solid lipids used in SLN can form highly crystalline form (i.e. tristearin) which expulses the drug making the system ineffective. 'Nanostructuring' with liquid oil in a solid lipid core increases the drug loading capacity in NLCs. For example, loading of retinol is increased from 1% to 5% by addition of oil to solid lipid.(21) Imperfections in the crystal structure of the lipid core can also be introduced by using natural lipids (e.g. cocoa butter) or blends that have different crystal forms.(22) Other factors that affect the localization of the drug are hydrophobicity index of the lipid and the crystal structure of the drug. Also pure lipids can undergo polymorphic changes because on cooling, the lipid in SLN stays in less stable and low melting point crystal forms and over time, change into a stable modification.

1.3 Mechanism of Lipid Nanoparticles in Oral Delivery of Nutraceuticals

The primary goal of an effective delivery system of a bioactive is to improve solubility of the bioactive in the intestinal lumen so that it can effectively be absorbed by enterocytes lined in the small intestine. Physiochemical properties of the delivery system are determinants of the bioavailability of the bioactive.

Three mechanisms are involved in absorption enhancement and increased bioaccessibility and bioavailability of nutraceuticals in lipid nanoparticles and shown in Figure 3. They are as follows:

(1) *Adhesiveness of nanoparticles*: Due to high aspect ratio or high surface area of the nanoparticles, the interactions forces between the surface of the nanoparticles and the gut walls are high which enables absorption. Once the particle is absorbed, the encapsulated bioactive is released locally leading controlled delivery.(23, 24)

(2) *Less variation in Bioavailability*: A lot of studies have shown that there is low variation in bioavailability of drug via lipid nanoparticles, irrespective of fed and fast state in a rat model and suspension vs microemulsion systems.(25)

(3) *Lipid absorption enhancing effect*: The lipids are hydrolyzed by enzymes in the gut and mono- and di- glycerides released from the surface of the lipid droplets or solid lipid particles and they are surface-active which form micelles. Bioactive entrapped in the lipid is also simultaneously released which is solubilized into the micelles. The formed micelles interact with surface-active bile salts (e.g., sodium cholate) leading to the formation of so-called “mixed micelles.” In the subsequent absorption process of the lipid degradation product, the bioactive is simultaneously absorbed. This process is described in Figure 3. The length of the fatty acid chains affects the primary place of absorption. Fatty acids with C-14 chains to C-18 chains promote lymphatic absorption.(26, 27)

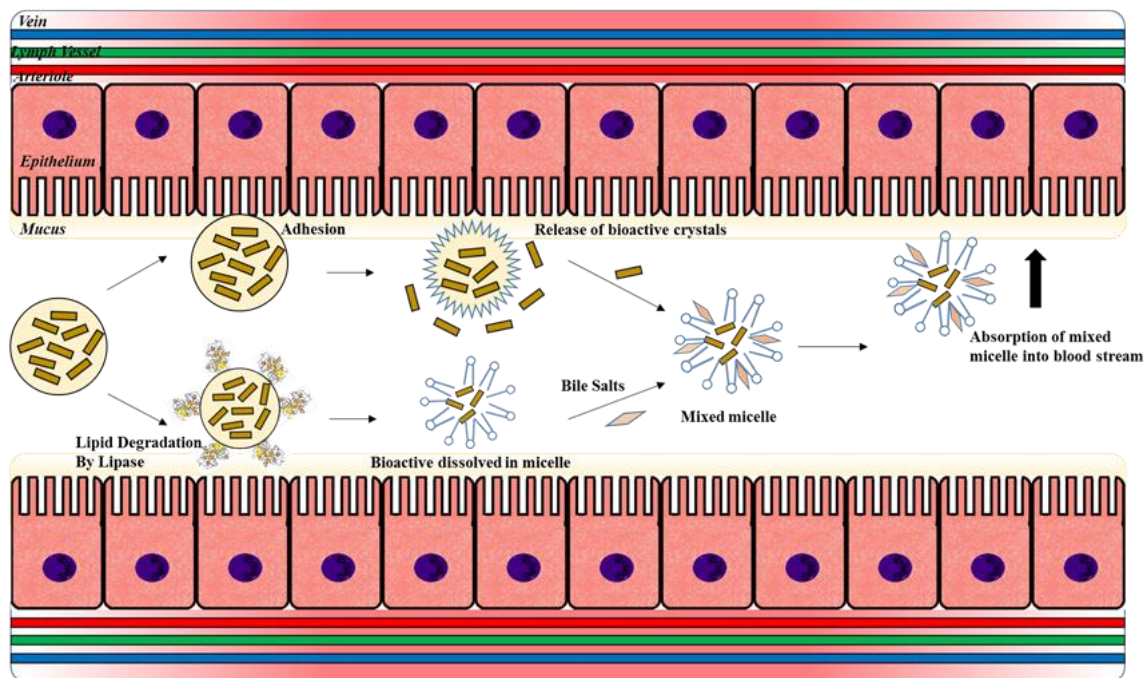


Figure 3 Mechanisms of absorption promoting effect of lipids in lipid nanoparticle formulations. Adapted from (28)

1.4 Materials for lipid nanocarriers

In our study, candelilla wax was used to prepare solid lipid nanoparticles and cocoa-butter to prepare lipid nanocarriers.

1.4.1 Candelilla wax

Candelilla wax is extracted from desert plant *Euphorbia antisiphilitica*, which grows in the southwestern United States and northern Mexico. It has chemical composition of hydrocarbons of carbon chain length C₂₉-C₃₃(50%), wax acid esters (28.5%), free alcohols (13%), wax acids (8%) and moisture (0.5%) with melting point around 66-71°C and very different from rest of the waxes as shown in Table 1.(29, 30) Candelilla wax (CW) is a worldwide recognized food additive approved by the FDA (under regulations 21CFR, 175.105, 175.320, 176.180) and, in accordance with regulation 184.1976, might be used in food with no limitation other than current good manufacturing practice(30). CW is used mainly as a glazing agent and binder for chewing gums. It also finds use in the cosmetic industry as a component of lip balms and lotion bars, and in the paint industry to make varnishes. Additionally, CW can be used as a substitute for carnauba wax and beeswax in different food systems. It is mainly used in coatings of citrus fruits and bananas that have high permeance to oxygen and carbon dioxide.(31) Citrus fruits with candelilla wax based coatings have low weight loss and good gloss.(32, 33). On comparing water vapor (WVP) and oxygen (P_[O₂]) permeabilities of free standing films with beeswax (BSW), candelilla wax (CNW), carnauba wax (CRW) and microcrystalline wax (MCW), both CNW and CRW showed low P_[O₂] values which is approximately half of P_[O₂] value for high-density polyethylene but P_[O₂] of beeswax and MCW were 6-9times than that of CNW and CRW.(34) In similar study, it was found that WVP of CNW was comparatively

lower than that of polypropylene yet greater than that of high-density polyethylene. Crystal forms of wax determined by X-ray diffraction and chemical composition of CNW and other waxes are the primary factors that could explain its effect on WVP and $P_{[O_2]}$.(34)

Table 1 Chemical Composition and Melting point of selected lipids

Components (% w/w)	Candelilla wax	Carnauba Wax	Beeswax	Milkfat fraction
Hydrocarbons	50	2	12	0
Wax acid esters	28.5	84.5	71	0
Fatty alcohols	13	2.5	1	0
Free wax acids	8	3	14	0
Moisture	0.5	0.5	1	0
Lactides	0	2.5	0	0
Fatty acid esters	0	0	1	0
Resins	0	5	0	0
Triacylglycerides	0	0	0	98
Mono- and diglycerides	0	0	0	2
Avg. melting points (°C)	70	84	63	45

1.4.3 Cocoa butter

Cocoa butter (CB) is the lipid component of chocolate which is processed from cocoa beans of cocoa tree (*Theobroma cacao*). Among all the natural animal and plant based fats, CB has a simpler composition. CB is a mixture of triglycerides (TG) mostly composed of monosaturated TG (~80%) with palmitic-oleic-stearic or POS (~42%), stearic-oleic-stearic or SOS (~26.4%), palmitic-oleic-palmitic or POP (~18.3%) and other triglycerides.(35) Polyunsaturated and trisaturated TG correspond to about 13 and 3%, respectively, of the total TG content. CB has melting point around 35-37°C that gives chocolate desirable organoleptic properties on consumption. CB also exhibits polymorphism due to its TG composition. Polymorphism of TG is defined by the possible arrangements of molecules within a crystal lattice due to different ways of lateral packing of the fatty acid chains and of longitudinal stacking of molecules in lamellar structures. Six different polymorph forms of CB are identified (36, 37)- (i) γ polymorph (orthorhombic subcell), (ii) α polymorph (hexagonal subcell), (iii) β'_1 and β'_2 polymorphs (orthorhombic subcell), (iv) β_1 and β_2 polymorphs (triclinic). Due to polymorphism in CB, the lipid molecules can effectively reorient themselves in presence of bioactive to form a disordered packing compared to other solid fats (i.e. stearin) that have tight packing due to homogenous chemical composition of these fats. Also, crystallization of fats like CB can be manipulated by addition of additives (i.e. emulsifiers) and processing conditions to obtain and stabilize the less stable α modification which in turn, possibly improve loading capacity of their nanocarriers. Crystallization of lipid droplets in emulsions is very complex to study and yet, is an important factor for stability, protection and controlled

release of bioactive. Based on its physical properties, it is hypothesized that CB makes it a good candidate for lipid core in design of a lipid nanocarrier.

1.5 Bioactives encapsulated in lipid nanocarriers

In our study, coenzyme Q10 and carnosic acid are used as they are strong antioxidants that have multiple benefits but have poor bioavailability.

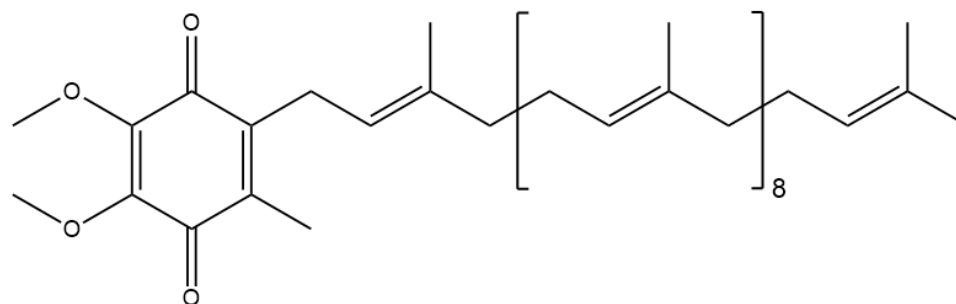
1.5.1 Coenzyme Q10

Coenzyme Q are group of homologous quinones (Figure 4), found in inner membrane of mitochondria and functions as an electron carrier between enzyme complexes from NADH to reduce O₂ into H₂O in electron-transfer-chain (ETC) of cellular respiration.

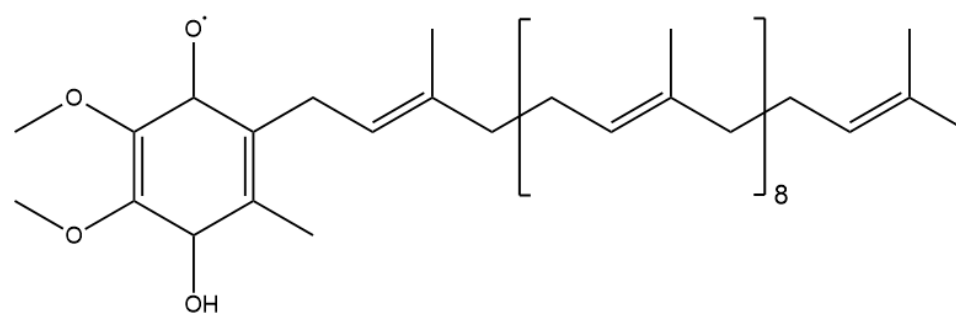
IUPAC name for Coenzyme Q is 2,3-dimethoxy,5-methyl, 6-polyisoprene parabenzoquinone. The polyisoprene chain present in Coenzyme Q10 (CoQ10) has 10 isoprene units (5 carbons each) or a total of 50 carbons, giving it a high molecular weight around 862g/mol. CoQ10 remains in the interior of cell membranes due to the affinity of *trans* polyisoprene to the inner membrane in mitochondria. The enzyme specificity is contributed by the methoxy groups present on quinone ring. Further addition reactions with other reactive groups (eg. Thiol groups in glutathione, thioredoxin or thioctic acid) cannot take place on the ring due to presence of 2 methoxy groups and polyisoprene tail.(38)

The quantity of CoQ10 can affect efficiency of electron transport rate and ability of the ATP production. The biosynthesis of CoQ10 occurs in most tissues with 110, 60, and 70 µg/g tissue in heart, liver and kidney respectively, where major portion is present in reduced form.(39) The functional group is the quinone ring. By reduction of the quinone

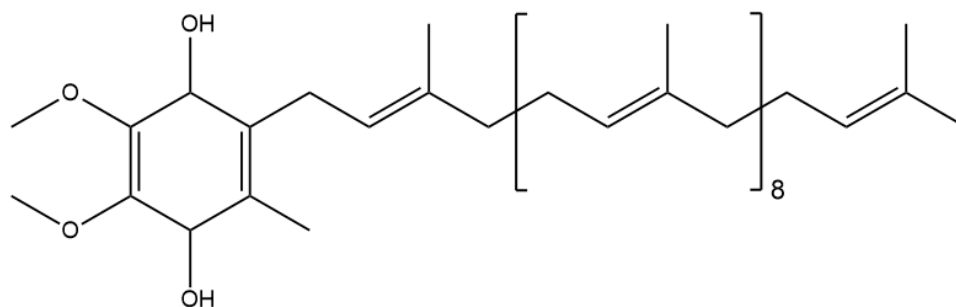
to quinol a carrier of protons and electrons is produced. It acts as biological antioxidant by quenching free radicals and protects cell membranes and plasma lipoproteins. It is considered safe and well tolerated at dosages of up to 1200 mg/d. Physiological amounts of CoQ10(reduced form) or ubiquinol-10 scavenges peroxy and superoxide radicals which are generated within the liposomal membranes as shown in Figure 5 and has no prooxidant activity.(40) Administration of CoQ10 reduces LDL oxidation by making LDL resistance to lipid peroxidation and therefore, prevents cardiovascular disease.(41) Tissue content and blood levels of CoQ10 is lowered in patients of heart failure and dilated cardiomyopathy.(42) CoQ10 had positive effects on subjects performing fatigue-inducing workloads and possibly prevent effects of physical fatigue.(43-45) Supplementation of CoQ10 has a preventive role against cancer(46) and tolerance towards cancer treatment.(47) The progressive decline in abilities due to Parkinson disease can be managed and lowered by high dosage of CoQ10. (48, 49) Other studies provided conflicting evidences about health benefits of CoQ10 which necessitates to create effective formulations that can deliver significant dosages and alleviate disease conditions. In this study, cocoa butter based lipid nanoparticles was chosen to orally administer coenzyme Q₁₀ (CoQ10), which has poor oral bioavailability due to its high molecular weight and poor water solubility.



a) Oxidized form of Coenzyme Q₁₀ - Ubiquinone (CoQ)



b) Intermediate form of Coenzyme Q₁₀ - Semiquinone (CoQH)



c) Reduced form of Coenzyme Q₁₀ - Ubiquinol (CoQH₂)

Figure 4 Different oxidation states of Coenzyme Q10

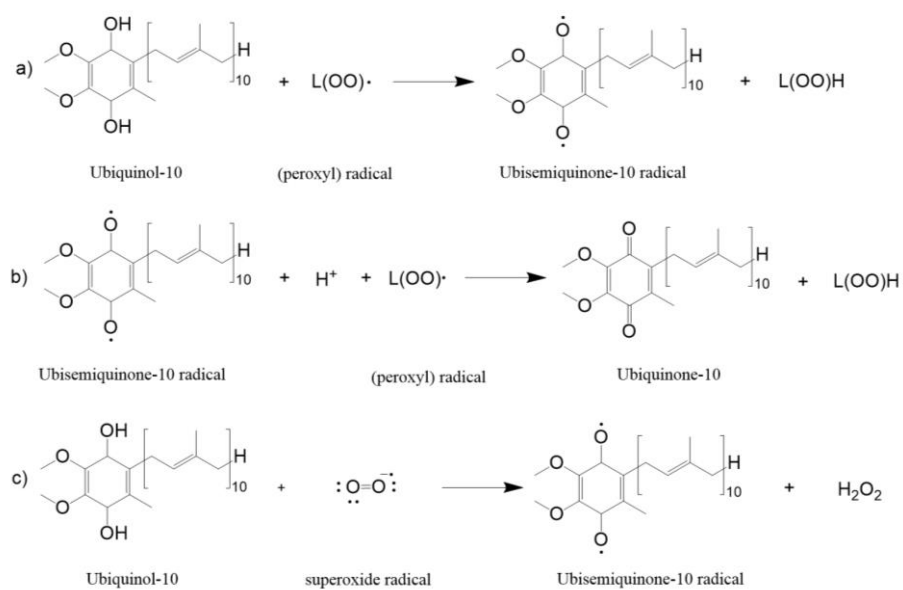


Figure 5 In-vitro antioxidant mechanisms of Coenzyme Q10 (40)

1.5.2 Carnosic acid

Carnosic acid (CA) is one of active components of Rosemary (*Rosmarinus officinalis* L) extracts. Carnosol (CAR) and CA (Figure 6) are phenolic compounds known to have antioxidant properties. CA protects chloroplasts from oxidative stress in plants in vivo by following a highly regulated compartmentation of oxidation products.(50)

CA is a phenolic diterpene and its phenolic hydroxyl group is easily oxidized and degraded under alkaline conditions. CA is unstable in form of solution as it can be converted into CAR by air oxidation. (Figure 6)

Phenolic compounds in foods have garnered a lot of attention as effective antioxidants that would prevent oxidative deterioration of food components. A primary mechanism involves the trapping and stabilizing of species generated from the radical chain oxidation of food components. The chain-breaking antioxidation process is thought to be divided into 2 stages as follows:

(i) Radical trapping stage



(ii) Radical termination stage

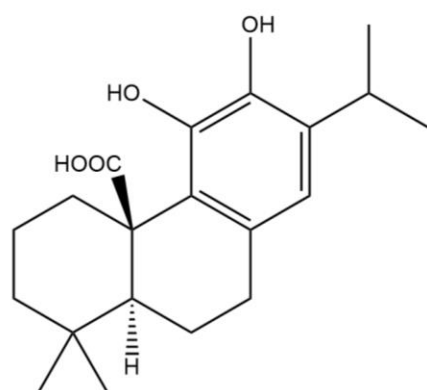


The mechanism was investigated in presence of ethyl linoleate and radical oxidation initiator 2,2'-azobis-(2,4-dimethylvaleronitrile).(51) As shown in Figure 7 and Figure 8, compound 1 and 2 are produced independently and are not time-dependent. The phenolic group at 11 position undergoes hydrogen donation to a radical species such a lipid peroxy radical, to produce the carnosate radical. Radical coupling reaction proceeds by radical termination of 3 with a second lipid peroxy radical. When coupling proceeds at the

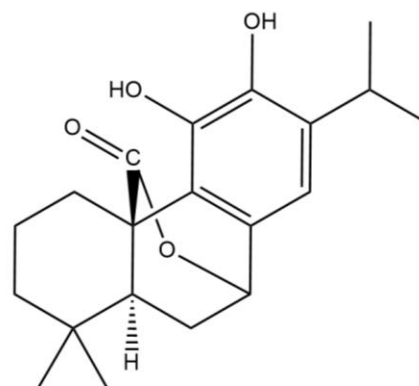
14-position (para-position), a peroxide 5 is formed. Since 5 is unstable, an intermediate epoxide 6 and peroxide cleavage. Isomerization of 6 leads to formation of 2. The last step of this pathway is very similar to antioxidation products of Vitamin E.

Compound 2, carnosic acid quinone which is a radical chain-termination product and with no antioxidant activity, can recover its activity upon standing in solution. The mechanism is shown in Figure 9.(52) The proposed mechanisms reveals that CA has high antioxidant potency due to the ability of its termination product to convert back to active forms.

Compared to synthetic antioxidants, BHA and BHT, the antioxidant activity of the flavones and flavanones from sage and rosemary are relatively weak. Absence and poor antioxidant potency is due to the fact that there is no hydroxyl group on the C3 position of the molecule.



(i) Carnosic Acid



(ii) Carnosol

Figure 6 Major antioxidant components in Rosemary extract

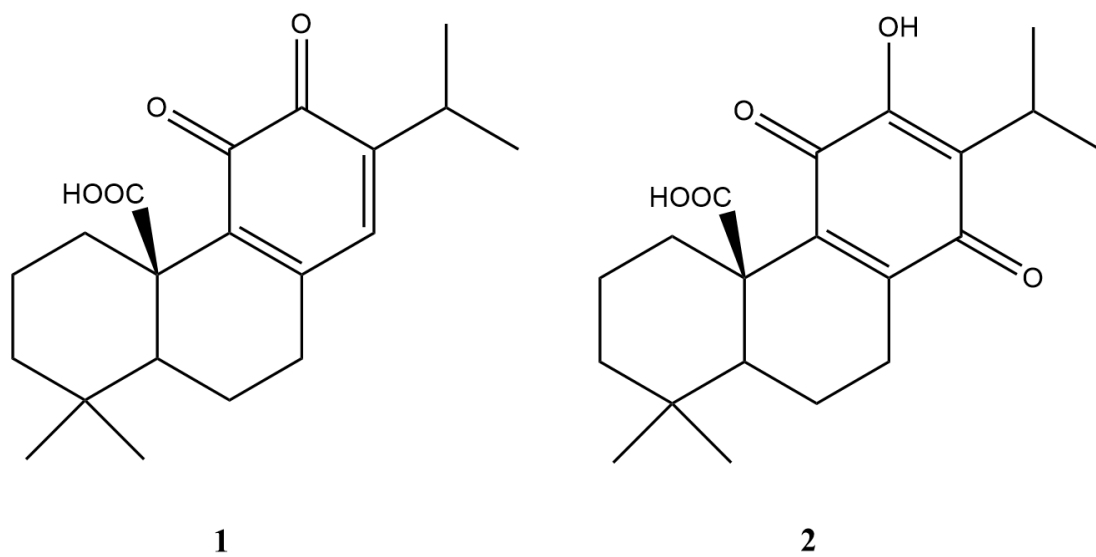


Figure 7 Oxidation Products of Carnosic Acid

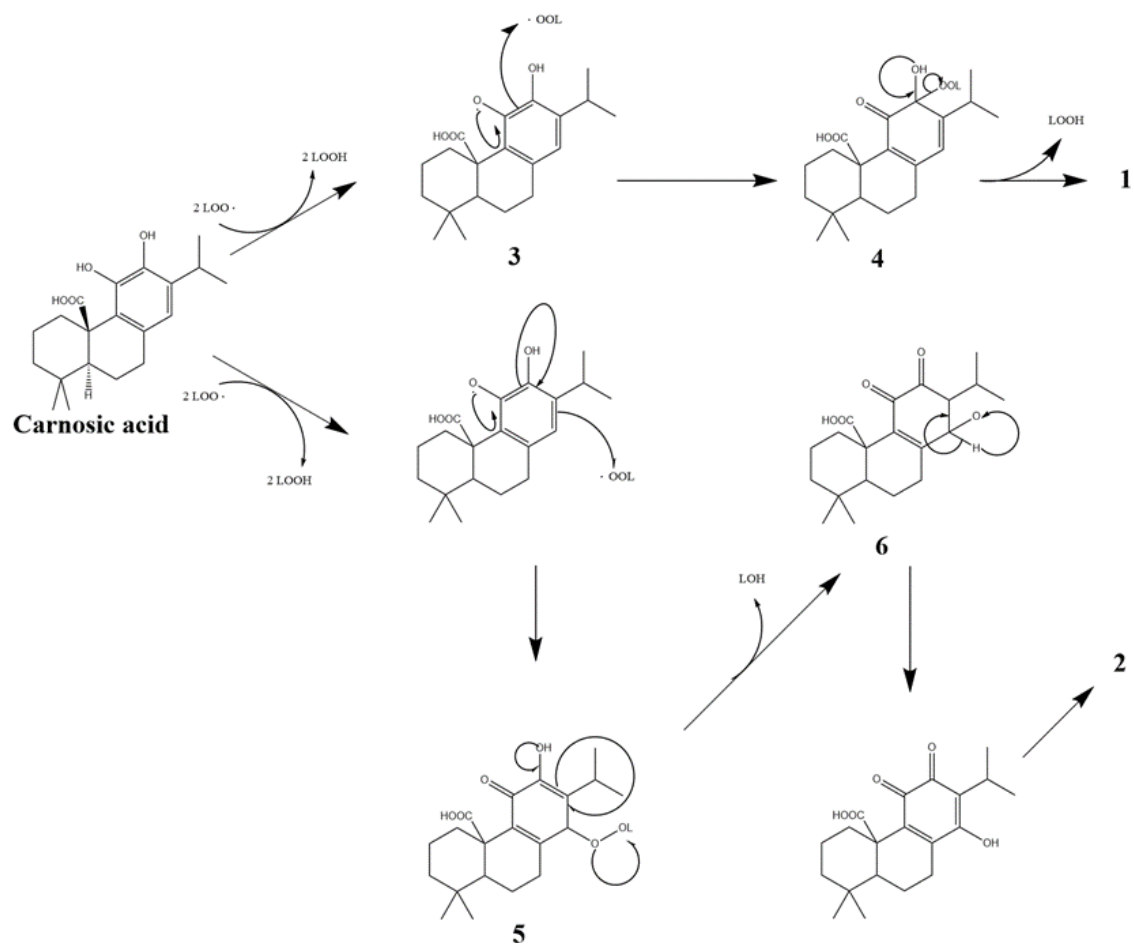


Figure 8 Proposed antioxidant mechanism of carnosic acid, LOOH, LOO* and OH denote hydroperoxide, peroxy radical and hydroxide, respectively. Adapted from (51)

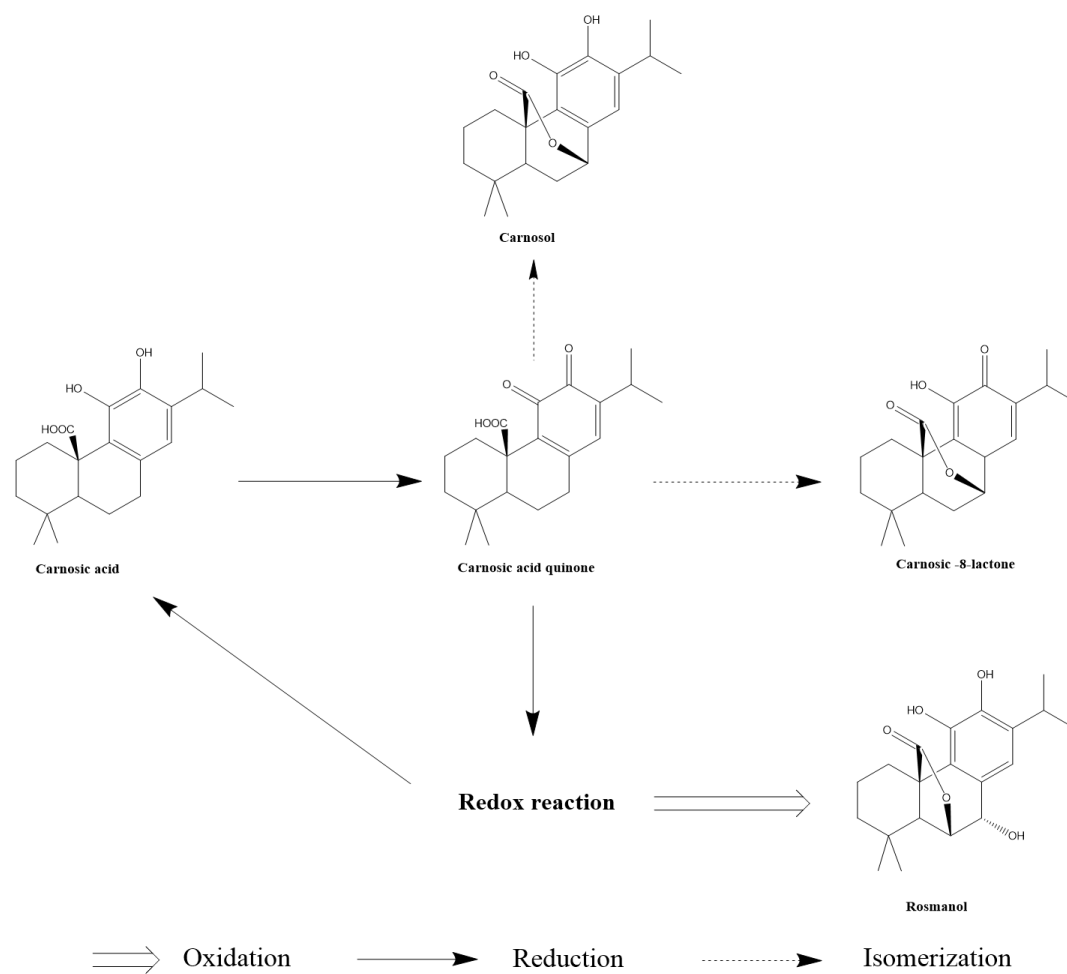


Figure 9 Proposed antioxidant mechanism from carnosic acid quinone where carnosic acid, CAR and rosmanol have antioxidant ability. Adapted from (51)

1.6 Biopolymer based packaging

Packaging based on different natural biopolymers are gaining more and more interest due to social consciousness in clean and sustainable technologies. Conventional packaging that are based on petrochemicals has been subjected to criticism from both scientific and consumer communities due to its negative effects to the environments and ecology by accumulation and toxicity. Three different techniques using agricultural raw materials (fully renewable raw materials) to make bio-packaging are proposed: synthetic polymer/biopolymer mixtures (first and second generations), agricultural materials used as fermentation substrates to produce microbial polymers and finally agricultural/aquacultural polymers used directly as basic packaging material. Polysaccharides are the most abundant and cost effective biodegradable material that are used in packaging recently as shown in Table 2.

Novel strategies and technology in material science and engineering are adopted to achieve economic and environmental sustainability by replacing petro-chemical based plastics in food packaging applications to meet increasing demand of high-quality foods. Biopolymers like polysaccharides and proteins with lipids from renewable resources are low cost, safe and biodegradable making them as 'greener' alternative to existing packaging materials. Films made from polysaccharides (starch and starch derivatives(53-55), cellulose derivatives(56-60), alginate(61-64), pectin(65-67), carrageenan(68-70), chitosan(71-73), and various gums(74, 75)), plant proteins (soy protein(76-78), wheat gluten(79-81), cottonseed protein(82, 83) and protein extracted from sorghum kafirin(84-86), rice bran(87-89), peanuts(90-92), corn zein(93-95) and pea(96-98), and animal

proteins (collagen(99-101), gelatin(102-104), fish myofibrillar protein(105-107), keratin(108-110), egg white(111-113), casein(114-116), and whey protein(117-119)) were investigated in several studies. These biopolymers have film-forming capacity and good gas barrier properties, the major limitations of most of the natural polymer based films is their low mechanical and poor barrier properties. The performance efficiency of films and other products made from polysaccharides and proteins can be manipulated by various approaches like blending with other polymers and addition of additives (plasticizers, antimicrobials, crosslinkers, fillers, bioactives etc).

Table 2 Common components of biopolymer based films

Macromolecule	Polymer	Additive	Compounds	
Polysaccharides	• Starch	Plasticizers	• Glycerol	
	• Cellulose derivatives		• Propylene glycol	
	• Pectin		• Polyethylene glycol	
	• Alginate		• Sorbitol	
	• Carrageenan		• Water	
	• Chitosan		• Antimicrobials	
	• Pullulan		• Antioxidants	
	• Natural gums		Functional ingredients	• Flavor
	• Milk proteins			• Colorants
	• Collagen			• Vitamins
• Gelatin	• Other nutraceuticals			
Proteins	• Keratin			
	• Fish myofibrillar protein			
	• Soy protein			
	• Wheat gluten			
Lipids	• Corn zein			
	• Neutral lipids			
	• Fatty acids			
	• Wax			

1.6.1 Chitosan films

1.6.1.1 Chitosan: chemical properties

Chitosan, a linear polysaccharide consisting of (1,4)-linked 2-amino-deoxy-b-D-glucan, is a deacetylated derivative of chitin produced from shellfish waste or from mycelia of fungi which is the second most abundant polysaccharide found in nature after cellulose (Figure 11). Chitosan has been found to be nontoxic, (120) biodegradable, bio-functional, biocompatible with antimicrobial characteristics. It is essentially a natural, water-soluble derivative of cellulose with unique properties (Figure 11).

Chitosan has multiple uses as a (i) anti-cancer agent, (ii) antimicrobial agent (iii) clarifier, (iv) fiber, (v) film, (vi) flocculent, (vii) gas-selective membrane, (viii) affinity chromatography column matrix, (ix) plant disease resistance promoter, (x) thickener, and (xi) wound healing promoting agent. It can be used in pet food and has GRAS (generally regarded as safe) status. It is used as a processing aid and is used for applications in fruit preservation, wound dressings, cosmetics, artificial organs and pharmaceuticals. Chitosan is usually prepared from chitin and chitin has been found in a wide range of natural sources (crustaceans, fungi, insects, annelids, molluscs, coelenterata etc.). However chitosan is only manufactured from crustaceans (crab, krill and crayfish) primarily because a large amount of the crustacean exoskeleton is available as a byproduct of food processing. (121)

Chitosan is a weak base and is insoluble in water and organic solvent. However, it is soluble in dilute aqueous acidic solution (pH 6.5), which can convert glucosamine units into soluble form $R-NH_3^+$. It gets precipitated in alkaline solution or with poly-anions and forms gel at lower pH. (122)

Chitosan oligomers, which can be achieved by degradation of chitosan polymer chain, are water-soluble. In addition, water-soluble chitosan can be obtained through a chemical modification in which the degree of substitution is controlled. For instance, it is known that water-soluble chitosan with about 50% DD can be obtained from chitin by hydrolysis with alkali(123) or from chitosan by N-acetylation with acetic anhydride.(124)

In the solid state, chitosan is a semi-crystalline polymer. The electron diffraction diagram can be indexed in an orthorhombic unit cell ($P2_12_12_1$) with $a= 0.807$ nm, $b=0.844$ nm, $c=1.034$ nm; the unit cell contains two antiparallel chitosan chains, but no water molecules. Low molecular chitosan predominantly exhibit high crystallinity in their amorphous form.(125) The solution properties of a chitosan depend not only on its average degree of acetylation but also on the distribution of the acetyl groups along the main chain in addition of the molecular weight.(126-128) The deacetylation, usually done in the solid state, gives an irregular structure due the semi-crystalline character of the initial polymer. The degree of ionization of the chitosan is dependent on the pH and pKa of the acid (acetic acid(129) and hydrochloric acid(130)) used which causes protonation on the chain and influences its solubility. Chitosan with varying degrees of deacetylation can be solubilized at pH 6 or lower.(129) The solubility is dependent on various factors: (i) DA, (ii) the ionic concentration, (iii) the pH, (iv) the nature of the acid used for protonation, and (v) the distribution of acetyl groups along the chain, as well as (iv) the conditions of isolation and drying of the polysaccharide.

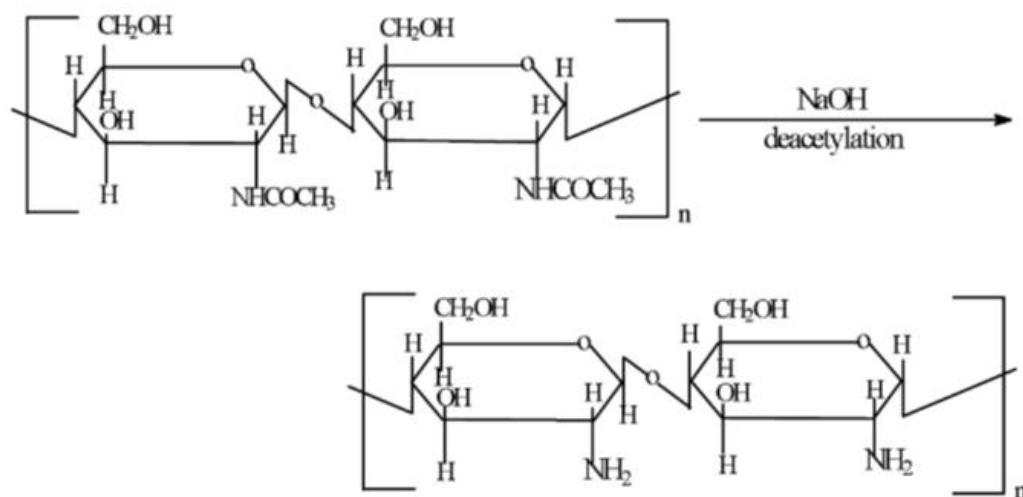
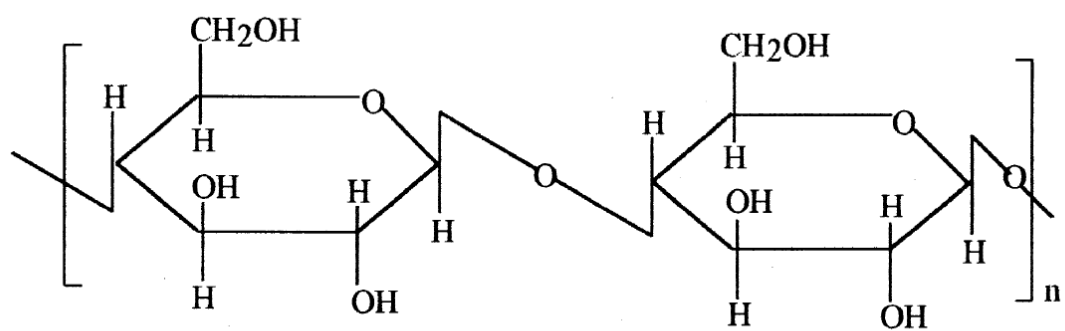
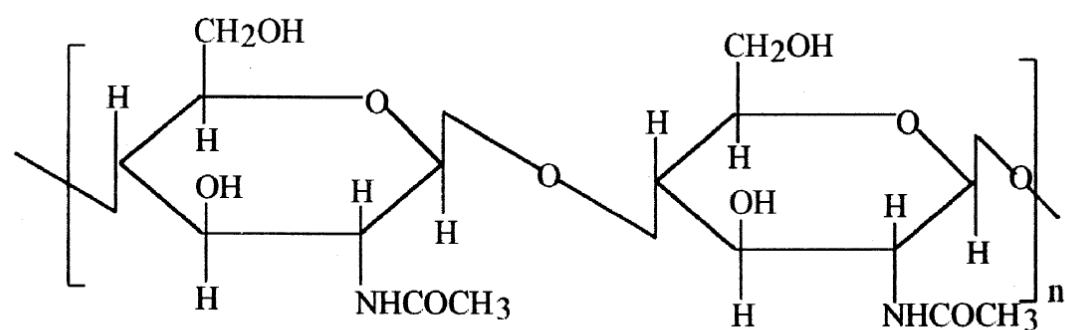


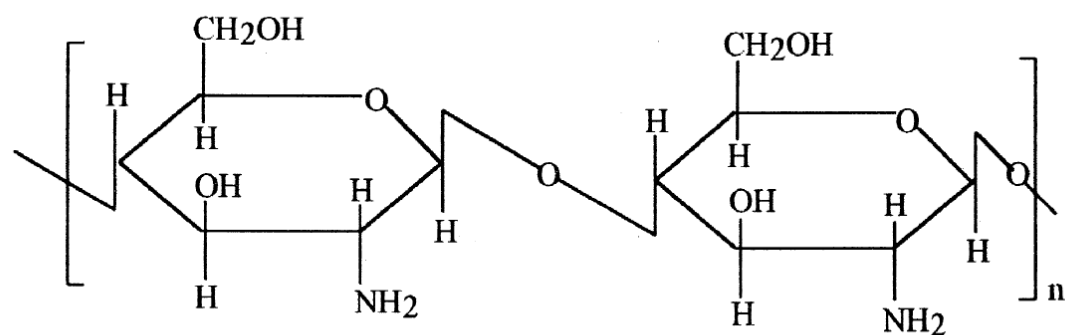
Figure 10. Preparation of Chitosan from Chitin. Adapted from (131)



Cellulose



Chitin



Chitosan

Figure 11. Structure of Cellulose, Chitin and Chitosan. Adapted from (131)

1.6.1.2 Optical Properties

Film color can be a factor in terms of consumer acceptance. Effect of drying of chitosan films on its optical properties were studied.(132) Oven dried films were more colored than infra-red dried and air dried films. L value indicates lightness and as the L value increases films are less colored. Air-dried films were more transparent than heat-dried films. The *a* value (red+/green-) did not vary significantly, indicating that the films became brown due to heating and hence variation in *b* value (yellow+/blue-) (indicating yellowness) was significant between the three methods of drying. Brownness was observed in oven-dried films, due to the preferential drying of surface layers, and also it could be attributed to Maillard reaction products due to amide groups, whereas in infra-red drying, electromagnetic waves penetrate deep inside the solution and remove the moisture mass from inside out, and films were of less yellowness. Also the infrared rays provide some bleaching action as well. Addition of a transparent polymer to the chitosan polymer will produce light and more transparent films with slight yellowish tinge. It was also noted that the yellowness of chitosan is also dependent on the source and the purification technique employed to obtain the polymer.(133)

1.6.1.3 Mechanical properties

Chitosan in its purest form is a very brittle polymer. Often chitosan films are made using plasticizers to provide mechanical strength. The tensile strength (TS), % elongation (%e) and modulus of elasticity (ME) could be used to describe how the mechanical properties are related to their chemical structure. TS indicates the maximum tensile stress that the film can sustain, %e is the maximum change in length of a test specimen before breaking, and ME is a measure of the stiffness of the film. The type and concentration of

the plasticizers and storage time effect the tensile strength and % elongation. A low molecular weight chitosan with 25% (v/w) glycerol had a tensile strength comparable to that of commercial HDPE and LDPE films.(134) Increase in glycerol content can reduce the tensile strength of the films. The TS and %e are inversely correlated. The glycerol and sorbitol blend films showed a drastic decrease in ME with small addition. This may partly be due to the introduction of glycerol or sorbitol moieties resulting in drastic chain flexibility, thereby the rigidity of native chitosan disappears. Also the smaller size of glycerol influences the mechanical property of the film, giving more elongation to the film compared to other plasticizers.(135)

1.6.1.4 Barrier properties

Chitosan is of interest as a potential edible film component because of its excellent oxygen barrier properties.(136) Chitosan can form a semipermeable coating which can modify the internal atmosphere, thereby decreasing transpiration rates in food products.(137)

For a relative humidity lower than 0.6, chitosan films keep low permeability coefficients (0.06 barrer), but at higher water partial pressures, the gas permeability greatly increases. This phenomenon is more pronounced for CO₂ than for O₂ and leads to an increase in the CO₂/O₂ selectivity (17 at a relative water pressure equal to 1), which can be an important parameter, especially for the packaging of breathable food products.(138)

As for water sorption, two domains are distinguished for water permeation. At relative pressures lower than 0.4, the permeability and diffusion coefficients are low and easy to determine. For a higher relative humidity, the plasticization effect leads to variation of the permeability coefficient as a function of the pressure gradient applied to the

membrane, but average permeability coefficients can be determined. They increase with the partial pressure, especially at high relative pressures (P/P_0 ; 0.9 –1). This plasticization effect also has an influence on the gas permeation because a loss of the gas barrier properties is observed for relative humidities greater than 0.8. The behavior of both the gas uptake and sorption rate with the hydration state of the membrane can explain this behavior.(138)

1.6.2 Starch films

Starch is the most commonly used agricultural raw material, since it is inexpensive, widely available and relatively easy to handle. Most of the food application use starch due to its versatility in function and biodegradability making it sustainable in the environment.

1.6.2.1 Chemistry

Commercially available starch is extracted from carbohydrate rich food plants like corn, potato, rice, tapioca, peas etc. Starch is formed by light assisted biological reaction called photosynthesis in plant cell structures called starch granules. Starch is composed of two polysaccharide structures called amylose and amylopectin. Mostly linear in structure, amylose is α -D-(1→4) glucan, whereas amylopectin is a highly branched α -D-(1→4) glucan with α -D-(1→6) linkages and higher molar mass than amylose. Molecular weight, % branching and crystallinity are few intrinsic properties of the starch that determines their behavior in various applications. From XRD results of different natural starches, it has been shown that higher amylose content results in higher crystallinity. There is a range of crystallinity observed in starch granules which is not the only mode of organization of the

polymers. (139) Botanical origins influence crystallinity and some of the natural starches and their % crystallinity are shown in Table 3.(140)

Table 3 List of natural starches and their crystallinity percentages

Natural starches	%Crystallinity
Maize	43-48
Wheat	36-39
Potato	23-53
Pea	17-20
Barley	2-24
Rice	38

Starch is hydrophilic and biodegradable polymer due to which they have multiple advantages as edible films. Native starch granules are partially crystalline particles. Starch films are produced often by heating starch in water which leads gelatinization after losing its semi-crystalline structure. Due to high moisture and temperature, the starch granules are irreversibly swollen and solubilizing the amylose and amylopectin.(141) It was found that the amylopectin is swollen into granules but the amylose is completely solubilized forming the continuous phase around these swollen granules of amylopectin.(142) But when the starches are heated beyond their glass transition temperatures (T_g), they achieve a rubbery state with high molecular mobility. Due to this state and presence of high moisture content at high RH and plasticizers (143), recrystallization occurs which is also called retrogradation. Retrogradation explains the phenomenon of cooling and storage of the gelatinized starches. Starch retrogradation occurs as a result of intermolecular hydrogen bonding between O-6 of D-glucosyl residues of amylose molecules and OH-2 of D-glucosyl residues of short side-chains of amylopectin molecules as shown in Figure 12 and intramolecular hydrogen bonding between O-3 and OH-3 of D-glucosyl residues on different amylopectin molecules shown in Figure 13.(144) Existence of intramolecular hydrogen bonding is not observed in case of amylopectin but it took place in case of amylose between OH-6 and OH-6 and its adjacent hemi-acetal oxygen atoms of the D-glucosyl residues.(144) Initial crystallization in the starch gels is due to the gelation and crystallization of the amylose alone.(145) Long-term changes during storage of starch films are contributed due to amylopectin fraction. (146) Lipids have shown to inhibit retrogradation in starches.(147, 148)

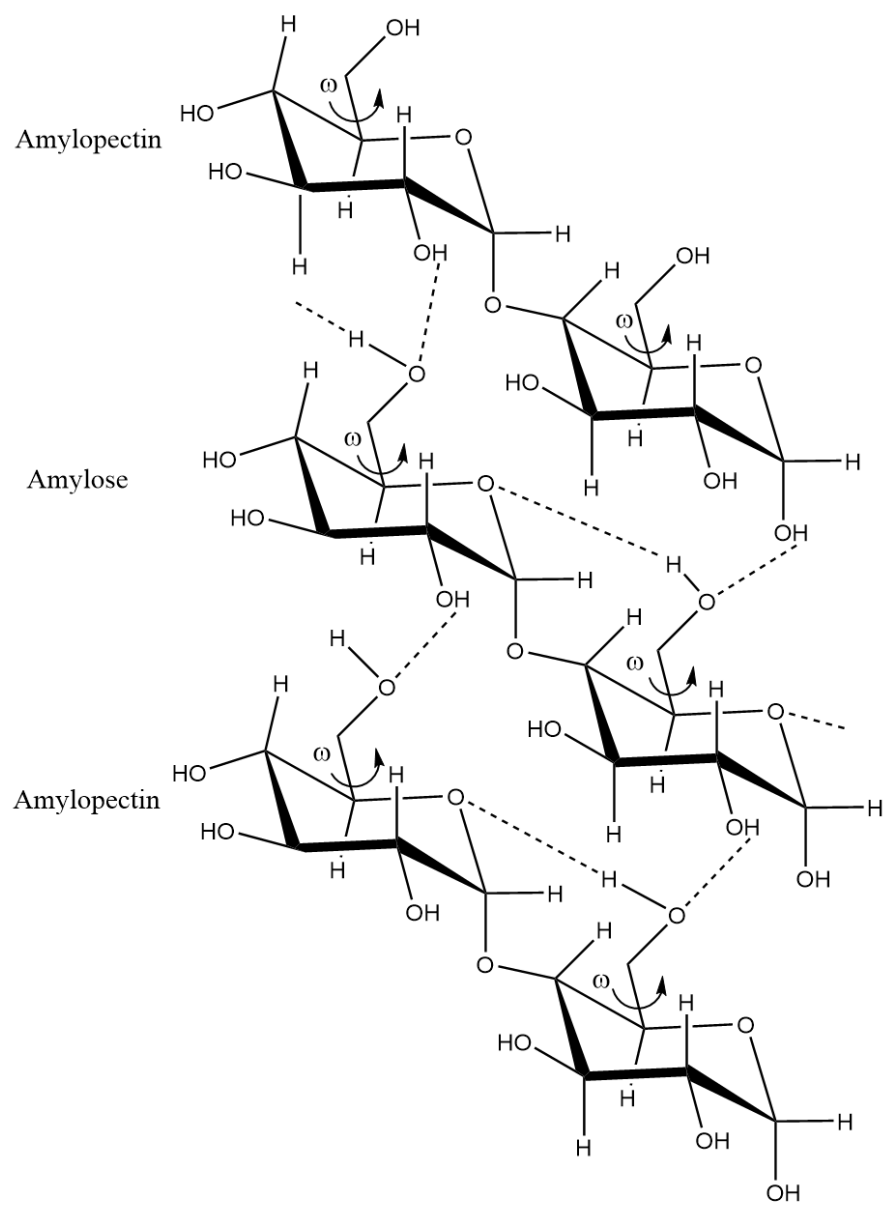


Figure 12 Retrogradation mechanism involving intermolecular hydrogen bonding between amylose and amylopectin in Potato Starch. Adapted from (144)

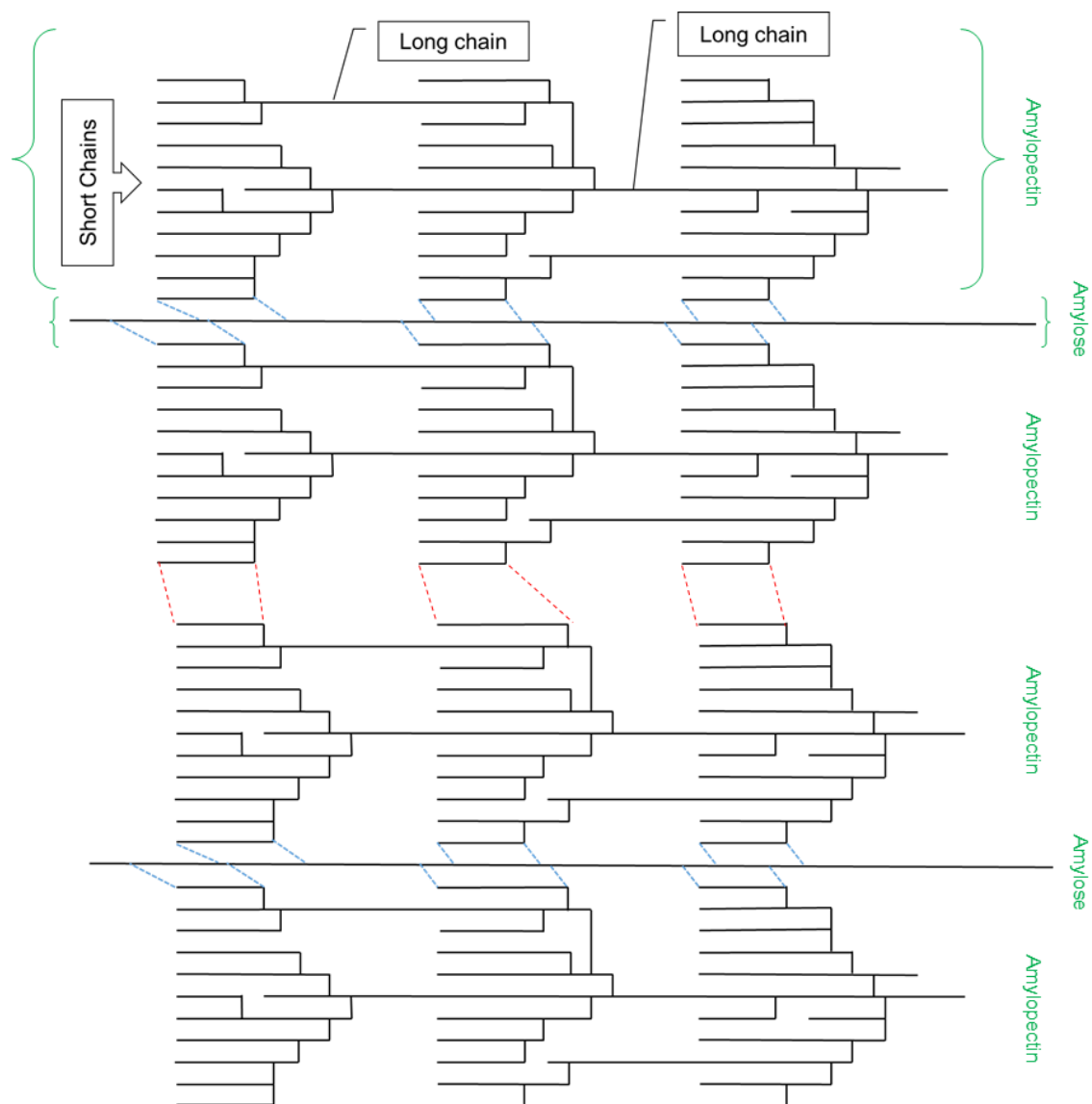


Figure 13 Intermolecular hydrogen bonding among short chains of amylopectin between amylose- amylopectin and amylopectin-amylopectin molecules in starches. Adapted from (144)

Mechanism of starch retrogradation originates from formation of crystalline lamellae of packed double helices of amylopectin short chains which leads to further packing into crystalline clusters.(143) Crystallization in starch can be affected by water and plasticizer content. Higher the water content, the degree of crystallinity and kinetics of crystallization was increased, whereas in case of increase in glycerol content, the kinetics slowed down in rubbery state of amorphous starch.(143) Other factors that influence crystallization of starch films are processing conditions such % dissolution of amylose in water, drying conditions, source of the starch and storage conditions. Due to presence of two different polymers (amylose and amylopectin) in starch, there is a possibility of phase separation.(149) Crystallization in starch determines the mechanical properties of starch films. There are two types of crystals due to their helical arrangement forms – A mainly found in cereal starches(150), B found in tuber and high amylose starches(151) and C is newly discovered formed by coexistence of A and B crystal types, found mostly in seed starches.(152)

To understand the gelatinization and retrogradation of starches which are crucial processing stages of starch film preparations, thermal properties are studied using differential scanning calorimetry (DSC). The gelatinization enthalpy (ΔH_{gel}) measures the crystallinity of the amylopectin which is a factor influencing the quality and quantity of starch crystals and ranges between 15.6 and 23.9 Jg⁻¹.(153) Potato starches show higher crystallinity than that of pea with cereals having the lowest values.(154) Also exothermic complex formation with amylose with lipid can lower this value of ΔH_{gel} . The gelatinization always takes place over a temperature interval ΔT_{gel} , which in excess water may be 1-2°C for a single granule, and for the whole population of granules the interval

may be $> 10^{\circ}\text{C}$. (147) At intermediate or high water content, the onset (T_o) and peak minimum temperatures (T_m) are independent of the water content, whereas the offset temperature (T_f) is much influenced by the water available during gelatinization. (155) Starch from potato Desiree also showed a relatively high $T_{o,gel}$ value around 65°C . Starches from potato Prevalent, normal-amylose barley and high-amylose barley exhibited an intermediate $T_{o,gel}$ between $60\text{-}65^{\circ}\text{C}$ while the lowest $T_{o,gel}$ was recorded for the pea, rye, and wheat starches. $T_{o,gel}$ for maize and barley are 67 and 58°C , respectively. Gelatinization temperatures are directly related to the degree of crystallinity along with other factors like amount of damaged starch, isolation techniques and variation in climatic conditions during growth.(154)

Retrogradation endotherms are not influenced by the periods of storage times. Starches from rye, wheat, normal-amylose barley and high-amylose barley have bell-shaped endotherm curves during retrogradation with exception for waxy barley starch which is bimodal.(154) This characteristic behavior of the retrogradation of starches can be attributed to differences in the quality of the recrystallized amylopectin which is dependent on the botanical origin. The melting enthalpy (ΔH_2 and ΔH_4) related to recrystallized amylopectin was calculated from the area of retrogradation endotherms. Retrograded amylopectin from different sources evidently shows the same B-polymorphic crystal pattern, other factors, such as structural differences in the amylopectin molecule, could cause the variations found in the rate and extent of amylopectin recrystallization. Also, high amylose starch has a higher melting enthalpies than those of normal amylose content starches because of co-crystallization of the two polymers in starch. The crystallinity of amylose and amylopectin films was studied to understand the mechanical,

thermal and barrier properties. The microstructure of any polymer based film can significantly influence its behavior.

To make edible films from starch, starch powder and water are heated to high temperatures beyond its gelatinization (T_{gel}) temperature to completely dissolve its polysaccharide components and prepare low viscous starch film solutions. These processing temperatures are high which are undesirable to high-temperature sensitive encapsulates or fillers.

1.6.2.2 Optical Properties

Native starch films and starch films blended with plasticizers are transparent and colorless. Addition of monomers like glucose etc. give yellowish color to the starch film. CMC can produce clearer films than starch, therefore, addition of CMC to starch films, can improve their optical properties and reduce their yellowness.

1.6.2.3 Mechanical Properties

Past several years, starch is extensively used to develop biodegradable films due to its ability to form a continuous matrix. But one of the major disadvantage of pure starch films that limits its usage in various food applications are its hydrophilic nature and poor mechanical properties. The two major components of starch are amylose and amylopectin and their films were strong and had a Young's modulus (E) and the stress at break (σ_b) which are comparable to low density polyethylene (LDPE) as shown in Table 4.

Studies conducted by A. Rindlav-Westling *et al* showed that all the films exhibited low strain around 2.5% and hence, it can be said that these film are brittle in nature. They showed that amylose films are stiffer and stronger than amylopectin films. Different studies

have shown significant differences in their mechanical properties due to different sources and preparation of the films. Different approaches to improve starch mechanical properties are blending (156), chemical modifications (modified starch) and using additives like plasticizers(157-160), clay(161-164) and other nano-fillers (165-167). In starches from different sources, tensile stress and Young's Modulus decreased and strain increased with increase of glycerol.(157) The plasticizer in the starch network reduces the direct interactions and the proximity between starch chains and when force is applied then starch chains were enabled which leads to a decrease in the glass transition temperature of the starch and improvement in their flexibility. Addition of 30% and more clay was added to the starch film to achieve reinforcing effect where the Young modulus increased by 50% on comparing with unplasticized starch films.(163) Another strategy to improvise mechanical properties of starch based films are incorporation of natural cellulose fibers as a reinforcing phase in thermoplastic matrices. Cellulose fibers are constituted of long threadlike bundles, called microfibrils, of cellulose molecules stabilized laterally by hydrogen bonds between hydroxyl groups of adjacent molecules.(165)

Table 4 Mechanical Properties of Amylose and Amylopectin Films

Polymer	Stress at Break, σ_b (MPa)	Strain at Break, E_b (%)	Conditions and References
Amylose	20	31	$\frac{\text{Glycerol}}{\text{Amylose}} = 0.4$, films formed and measured at 50%RH(168)
Amylose	20	46	$\frac{\text{Glycerol}}{\text{Amylose}} = 0.3$, films formed and measured at 65%RH (169)
Amylose	11	17	$\frac{\text{Glycerol}}{\text{Amylose}} = 0.29$, films formed and measured at 50%RH and 20°C(170)
Amylose	32	3	$\frac{\text{Glycerol}}{\text{Amylose}} = 0.19$, films formed and measured at 50%RH and 20°C(170)
Amylose	48	5	$\frac{\text{Glycerol}}{\text{Amylose}} = 0$, films formed and measured at 50%RH and 20°C(170)
Amylopectin	6	29	$\frac{\text{Glycerol}}{\text{Amylopectin}} = 0.4$, films formed and measured at 50%RH(168)
Amylopectin	2	5	$\frac{\text{Glycerol}}{\text{Amylopectin}} = 0.28$, films formed and measured at 50%RH and 20°C

1.6.2.4 Barrier Properties

Primary function of a packaging or an edible film is providing a barrier between the food surface and its surrounding environment. Barrier properties are divided into two categories: water vapor transmission rate and gas transmission rate which is very essential if the coatings are applied on fresh fruit and vegetables.

In a study conducted by S. Mali et. al(157), water vapor permeability rates of the starches from different sources conditioned at RH 64% and 20°C were studied and are given in Table 5.

Plasticizers like glycerol at moderate amounts (20% (w/w)) has lower values of water vapor permeability. This result can be supported by the possible structural modifications of starch network that occurs when glycerol is added. The unplasticized starches form brittle films facilitating water vapor transfer due to presence of pore or cracks.(171) By addition of glycerol, the pore formation is avoided by creating a compact structure. At low concentrations, plasticizers tend to bind to the starch molecules leading to an anti-plasticization effect. (172) By increasing the content of glycerol, the density of the starch is lowered and acquires the hydrophilic character of glycerol making it vulnerable for adsorption and desorption of water molecules. On long term storage of starch films, the water vapor permeability doesn't depend on glycerol content but on the ratio of crystallinity and amorphous phases of the starch where water vapor permeability decreases with an increase in crystallinity because permeation occur through the amorphous zones of the film.(34)

Oxygen permeability (OP) is one of the most commonly studied transport properties of edible films. The increasing content of the starch increases the OP of film,

because of hydrophilic nature as well as higher amylopectin content of starch.(173) Plasticizers such as glycerol generally increase gas and water vapor permeabilities of hydrophilic films. Glycerol is a relative small hydrophilic molecule and has a similar chemical structure to glucose, thus glycerol can easily interact with starch chains reducing packing between chains. Thus, the polymer chain movements could be facilitated, resulting in an increase of water vapor and gas permeation through the film matrix.(174) Also, use of sorbitol (plasticizer) and Tween 80 (surfactant) can reduce the water vapor and oxygen permeability of the corn maize starch films due to decrease in molecular mobility of polymer molecules in the matrix.(173) In case of tapioca starch based edible films, glycerol has increased the water vapor permeability and oxygen permeability significantly due to its hydrophilic nature and plasticizing nature.(175) Similar trend was observed for yam starch films.(176)

Table 5 Water vapor transmission of starch films at initial time and stored for 90 days at 64% relative humidity and 20°C

Starch Base	Glycerol (g/100g starch)	Water Vapor Permeability ($\times 10^{-10} gm^{-1} s^{-1} Pa^{-1}$)	
		Initial Time	Storage Samples
Corn	0	8.33 ± 0.21	5.13 ± 0.51
	20	5.37 ± 0.21	5.00 ± 0.75
	40	6.70 ± 0.21	5.95 ± 0.75
Cassava	0	7.59 ± 1.26	5.59 ± 0.89
	20	4.02 ± 1.26	4.02 ± 1.01
	40	6.25 ± 1.26	5.65 ± 0.99
Yam	0	6.75 ± 1.05	5.25 ± 0.58
	20	4.46 ± 1.05	4.00 ± 0.55
	40	7.59 ± 1.05	6.66 ± 0.99

1.6.3 Hydroxypropyl starch

Hydroxypropyl starch (HPS) is modified starch which is substituted by hydroxypropyl groups that are hydrophilic in nature and influence the interaction of starch polysaccharides in granular form and affect its physical properties in solution.

1.6.3.1 Preparation

Hydroxypropyl starch (HPS) is prepared by reacting starch with propylene oxide to low levels of etherification with most common molar substitution (MS) of 0.1. HP starch with MS between 0.9 and 2.7 can be dissolved in DMSO.

Starch dispersed in ethanol solution and NaOH is added to make the solution alkaline. Use of ethanol in the reaction mixture maintains the integrity of the granules and facilitates in removal of undesired products during reaction by simple step of density separation. Swelling of granules can be inhibited by addition of swelling -inhibiting salts before adding propylene oxide. Alkalinity of starch slurry acts as a catalyst that speeds up the reactivity between starch nucleophile and unstable 3-membered epoxide ring. Propylene oxide is added and flushed with nitrogen gas in a closed container. This solution is heated at 60-70°C for a day. High temperatures facilitate diffusion of the alkaline catalyst and promotes permeation of the etherifying agent to the polymer in the starch granule. Finally, the pH is adjusted to 5-6.⁽¹⁷⁷⁾ The precipitated starch is hydroxypropylated at -OH groups on starch polymers. The parameters in a reaction like epoxide concentration, starch/water ratio, reaction time and amount of catalyst to control the MS of HPS as shown in Figure 14. ⁽¹⁷⁸⁾

Amylose and amylopectin fraction of HPS can be isolated using size exclusion chromatography. It is observed that greater extent of modification occurs in amorphous

regions comprising the amylose and branching sites of amylopectin due to accessibility of the reagent. The substitution of hydroxypropyl group occurs in the order of C-2 > C-6 > C-3 on α -D-glucose unit of the starch. (179)

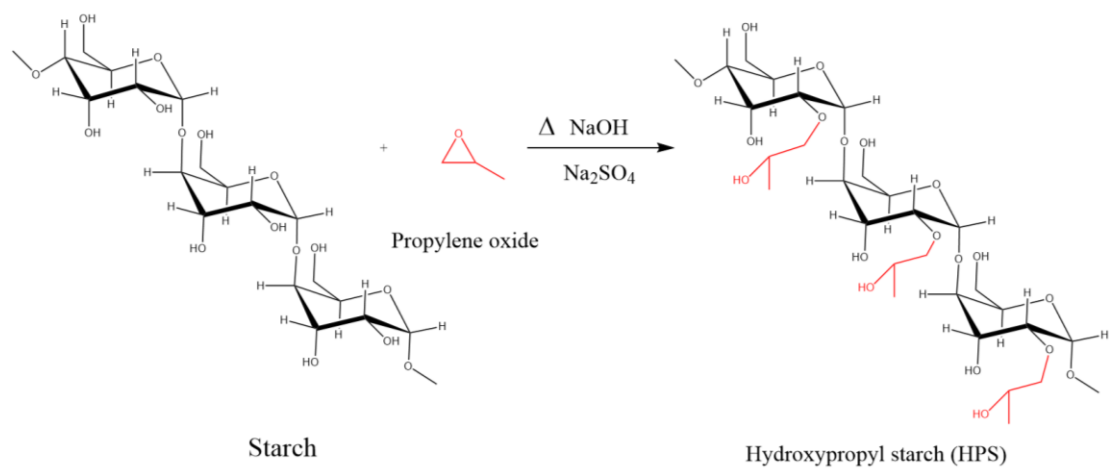


Figure 14. Preparation of hydroxypropyl starch by etherification reaction of corn starch

1.6.3.2 Chemical properties

Introduction of hydroxypropyl (HP) group on the starch chains weakens the interactions of amylose and amylopectin and increases its water binding capacity.(180) Improved dispersibility in cold water is observed when the molar substitution of HP increases from 0.4 to 1.0 . This modification also improves its freeze thawing stability by retaining water and preventing syneresis. By decreasing intermolecular interactions between polysaccharides in the starch by chemical substitution, the crystallinity of the starch is significantly reduced and inhibits the process of retrogradation. This further enables the viscosity stability of its solution with high temperature resistance, low pHs and mechanical shear and therefore making them as stabilized starches. Absorption of water is greater in amorphous regions of the HP starch granules compared to native starch which increases its rate of gelatinization.

Hydroxypropyl groups are hydrophilic in nature and their substitution on starch reduces the strength of the bonds that hold the granule structure. With increase in degree of substitution, the pasting temperature gradually decrease until the starch becomes cold water swelling. Retrogradation that involves close alignment of the chains in starch is interrupted by the HP groups and creates a fluid-like paste with better clarity.

1.6.3.3 Film properties

HPS films are highly transparent which are desirable for edible films. The tensile strength of pure HPS films are higher than those of plasticized with polyols. On storage at ambient temperature over 12 months, the HPS films have increased tensile strength and lower elongation modulus which makes them extremely brittle. (178) Processing temperatures during preparation of casting HPS-gelatin solutions are crucial in determining

physical properties of the film. The low temperature method resulted in films with more densely packed polymer chains, increased molecular ordering, higher percentage crystallinity and higher tensile strength and limited gas and water transmission rates. The presence of a plasticizer in the HPS-gelatin blends led to greater mobility of the polymer matrix and tensile strength but higher elongation and gas/water permeation values.(159)

D. Lourdin and group studied physical properties of acid-hydrolyzed starch films.(181) The crystal structure of the starch films is a B-type crystalline structure. Films with high molecular weight showed no crystallinity compared to low molecular weight. Drying temperatures also influenced crystallinity which an increase in temperature created films with no crystallinity. Crystallinity in films prepared with different molecular weight of HPS showed no effect on mechanical properties.

1.6.3.4 Applications of Hydroxypropyl starch

Hydroxypropyl starch is used in various applications in food industry. Hydroxypropyl substitution, cross-linking and inherent properties of starch improves the shelf-life, free/thaw stability, cold storage stability, cold water swelling and reconstituting products in formulated products.(182) This enable HPS use in a wide range of food applications such as gravies, dips, sauces, fruit pie fillings and puddings.(179) It is used as a thickener in food products. They are used as binders for building materials or gelling aids for perfumes or organic liquids due to their adhesive properties and solvent solubility of these starches. During drying of concentrated aqueous starch solutions, film-forming properties were observed.

1.7 Biopolymer nanocomposites

Nanocomposites are extensively used in different applications due to their superior functionality and performance. By definition, nanocomposites are typically composed of polymer based matrix with organic or inorganic nano-sized fillers. Though the matrix and filler material do not interact effectively in macroscopic scale, it is found that on reducing the dimensions of the fillers to a nanometric scale can increase interactions with the matrix and thus, improving thermal, mechanical and barrier properties of the nanocomposites. Mineral nanoscale fillers like silica, clay and talc are extensively used to create bionanocomposites.(183)

Nanocomposites films prepared using different nanoscale forms of nanocellulose like microfibril, microfibrillated cellulose, cellulose whiskers and microcrystalline cellulose have improved mechanical properties, low oxygen permeability and high transparency.(184)

Nanocomposites are being developed to ensure food safety to different high water activity foods by protecting contact surfaces. Silver nanoparticles are used in creating antibacterial nanocomposite films for biopolymer packaging.(185) These Ag nanoparticles have dose-dependent cytotoxicity as shown in zebrafish model which limits its usages directly in food safety.(186)

There is a need to investigate more nanostructures that can address the research gap in nanocomposite edible packaging and extend its functionality more than that of its traditional usage to improve qualitative properties and shelf-life of foods that are encased in them.

CHAPTER 2. CANDELILLA WAX NANOPARTICLES: DESIGN AND CHARACTERIZATION

2.1 Abstract

Candelilla wax, a highly hydrophobic plant based wax is used to prepare lipid nanoparticles that can be used filler in biopolymer based nanocomposites. Hot microemulsions of this wax were prepared by using HLB concept for selection of emulsions and ternary phase diagrams for optimum concentration of emulsifiers. Wax nanoparticles (NP) were formed on cooling at a controlled environment. Polysorbate 80 (Tween80), a non-ionic surfactant at concentration of 2% (w/w) produced nanoparticles with smallest hydrodynamic radius (~212 nm) with high storage stability over 2 months. On imaging with atomic force microscopy (AFM), wax NP were observed to have a round spherical structure with diameter of 140nm.

2.2 Materials and Methods

2.2.1 Materials

Candelilla wax (CW), Tween 80 (Polyethylene glycol sorbitan monooleate), and oleic acid were purchased from Sigma-Aldrich (St. Louis, MO). Other chemicals used for analytical purposes are acquired from VWR International (Radnor, PA) and Fischer Chemicals (Hampton, NH).

2.2.2 Selection of emulsifiers

The selection of emulsifiers was based on their HLB (hydrophobic-lipophilic balance) values derived from the structure of the molecule. A widely used semi-empirical method of calculating the HLB number for a surfactant is given by (187):

$$HLB = 7 + \sum(\text{hydrophilic group numbers}) - \sum(\text{lipophilic group numbers})$$

'Effective' HLB number can be achieved by a weighted mixture of two or more surfactants of the same class with different HLB numbers.(188, 189).

$$\begin{aligned} & \text{Effective HLB number of binary emulsifier mixture} \\ & = (\%[A] \times HLB_A) \times (\%[B] \times HLB_B) \end{aligned}$$

Where, %[A] = % of A in the mixture, HLB_A = HLB number of A), %[B] = % of B in the mixture, HLB_B = HLB number of B. Calculation for Tween 80 and Oleic acid was shown in Table 6.

In this study, emulsifiers used are class 300 (Tween and Spans) defined by the producer ICI Americas Inc. surfactants which represent hydrophilic non-ionic surfactants that are ideal to create oil-in-water (O/W) emulsions.(190)

Different mixtures of non-ionic surfactants Tween and Span surfactants and anionic surfactant oleic acid whose effective HLB above 10 were used. Wax (10% w/w) was heated above its melting point (68-72 °C) at 85°C and stirred continuously with a magnetic bar. The surfactants (1.5% w/w) were added into hot water around 85°C and mixed vigorously.

Table 6 Effective HLB Values of Surfactant Mixtures of Tween 80 and Oleic acid

Weight % of Tween 80 (HLB 15)	Weight % of Oleic acid (HLB 1)	Effective HLB Value
25	75	4.5
50	50	8
75	25	11.5
100	0	15

2.2.3 Preparation of Candelilla wax nanoparticles

Based on the knowledge of O/W emulsion preparation and ternary phase diagram results, most stable composition of mixture was found. Several compositions of candelilla wax (2-20% w/w) and surfactant mixture (0.3-3% (w/w)) and water were prepared.

CW nanoparticles were prepared by hot homogenization method. 10% (w/w) candelilla wax was melted at 90°C using temperature controlled oil bath. Solution of 2% (w/w) Tween 80 was prepared at 85°C. This solution was added to the melted wax and was mixed using magnetic stirrer. Hot nanodispersions were obtained using high-speed homogenization equipment, Ultra-Turrax stirrer T25 with S 25 N - 18 G dispersing element (IKA® Works, Inc., Wilmington, NC). These liquid wax droplets were solidified by cooling the dispersions to room temperature and formed solid lipid nanoparticles. The size and morphological measurements of nanoparticles were determined by DLS method and AFM imaging.

2.2.4 Particle Size Analysis by Dynamic Light Scattering (DLS)

DLS-based BIC 90plus particle size analyzer equipped with a Brookhaven BI-9000AT digital correlator (Brookhaven Instrument, New York, NY) at a fixed scattering angle of 90° at 25°C was used to determine mean hydrodynamic diameters (D_h) and the corresponding polydispersity index (PDI) of the nanoparticles. The light source of the particle size analyzer is a solid state laser operating at 658 nm with 30 mW power, and the signals were detected by a high sensitivity avalanche photodiode detector. The normalized field-field autocorrelation function $g(q,t)$ is obtained from the intensity-intensity autocorrelation function, $G(q,t)$ via the Sigert relation: $\alpha \cdot g(q, t) = \left[\frac{G(q,t)}{A} - 1 \right]^{0.5}$ where, A is the experimentally determined baseline, α is the contrast factor which is less than 1,

due to the fact that only a fraction of dynamic scattering intensity falls within the correlator window and due to a pinhole of certain size is used in the experiment. For all particle size measurements, the measured baseline A is in agreement with the theoretically calculated baseline to 0.01%. The diffusion coefficient D was calculated according to $D = \tau^{-1}q^2$, where q is the amplitude of scattering vector defined as $q = \left(\frac{4\pi n}{\lambda}\right) \times \sin\left(\frac{\theta}{2}\right)$, n is the solution refractive index, λ is the laser wavelength and θ is the scattering angle. The diffusion coefficient D can be converted into mean emulsion droplet diameter d using the Stokes-Einstein equation: $d = \frac{\kappa T}{3\pi\eta D}$, where κ is the Boltzmann constant, T is the absolute temperature, and η is the solvent viscosity. Cumulant analysis method was used in our size measurements, where $g(q,t)$ was decomposed into a distribution of decay rate Γ ($= 1/\tau$), given by $g(q, t) = \int G(\Gamma)e^{-\Gamma t}. d\Gamma$. The first two moments of the distribution $G(\Gamma)$ are as follows: (1) $\Gamma = Dq^2$, (2) $\mu^2 = (D^2 - D^{*2})q^4$, where, D^* is the average diffusion coefficient. The polydispersity term defined in the Cumulant analysis is: $polydispersity = \mu_2/\Gamma^2$ (no units). It is close to zero for monodisperse or nearly monodisperse samples, and larger for broader distribution.

2.2.5 Atomic Force Microscopy (AFM) Imaging

Images of wax nanoparticles were collected by a commercial Nanoscope IIIa Multi-Mode AFM (Veeco Instruments, CA) equipped with a J scanner, which was operated in tapping mode using silicon cantilever. The scanned images were obtained at the scan size of $3.0 \mu\text{m} \times 3.0 \mu\text{m}$ and the scan frequency of 0.75 Hz. A diluted solution with Candelilla wax nanoparticles was dropped and allowed to spread on silicon wafers, later washed by MilliQ water and dried by nitrogen gas prior to morphological measurements.

2.3 Results and Discussion

2.3.1 Tween 80 was the choice of surfactant

To identify the most stable formulations of Candelilla wax emulsions, visual appearance of the formulations was observed. For 10% (w/w) wax in the emulsions, Tween 80 (1.5%) was able to form most stable emulsion as shown in Table 7.

Important control variables that influence emulsification of a system are (1) Process temperature, (2) HLB value of the system and (3) chemical class of surfactants used. In our study, the process temperature was 90°C which was kept constant. Required HLB value of candelilla wax to create a O/W emulsion was unknown. Therefore, different types of surfactants were investigated to create stable emulsions

From empirical observations, it is suggested that maximum emulsion stability for O/W emulsions is obtained using surfactants with a HLB 10-12. (191). Emulsifiers with a low HLB number (below 9.0) is lipophilic in nature and those with a high HLB number (above 11.0) are hydrophilic. Other with HLB values between 9 and 11 are intermediate in nature. Different effective HLB values were achieved by using mixture of Tween and Span surfactants which have different chemical structures as suggested.(192) It was found that required HLB of Candelilla wax for O/W emulsions is 15 which is similar to another plant wax Carnauba wax and its mixtures as shown in previous studies.(193) Studies have shown that Tween 80 is a common and effective hydrophilic emulsifier (HLB = 15) with C_{18:1} oleic carbon chain that occupy the lipid and water interface and reduces high energy interface barrier in Self-Emulsifying Drug Delivery Systems (SEDDS).(194)

Table 7 Visual Appearance of formulations with 10% w/w CW and 1.5% w/w surfactant/blends

Surfactant/Blend (1.5% w/w)	Ratio	Effective HLB (± 1)	Visual Appearance (after a week)
Span 20/Tween 20	3:1	10.6	phase separation
	1:1	12.6	phase separation
	1:3	14.7	phase separation
Tween 20		16.7	phase separation
Span 40/Tween 40	3:2	10.2	phase separation
	1:1	11.1	phase separation
	1:3	13.3	phase separation
Tween 40		15.6	phase separation
Span 60/Tween 60	1:1	9.8	phase separation
	2:3	10.8	phase separation
	1:3	12.4	phase separation
Tween 60		14.9	phase separation
Span 80/Tween 80	1:1	9.6	emulsion with creaming
	2:3	10.7	emulsion with creaming
	1:3	12.3	emulsion with slight creaming
Oleic acid/Tween 80	1:1	8	emulsion with slight creaming
	1:3	11.5	emulsion with slight creaming
Tween 80		15	Stable Emulsion

2.3.2 Particle Size Analysis of CW formulations with Tween 80-Oleic Acid surfactant mixture

After visual observations of the stable formulations of Candelilla wax SLN, particle size analysis using Dynamic Light Scattering approach to further understand its stability as shown in Table 8. In this case, Tween 80 effectively reduces the surface tension and facilitates the particles during homogenization than oleic acid. Also oleic acid is more lipophilic than Tween 80 and can possibly solubilized into the hydrophobic matrix of Candelilla wax nanoparticle than its interface. The nature and concentration of suitable surfactant are important factors that contributes to the stability for nanoparticles. (195-197)

Table 8 Hydrodynamic Diameter and Polydispersity of formulations with 10% Candelilla Wax and different surfactants

Weight % of Tween 80 (HLB 15)	Weight % of Oleic acid (HLB 1)	Effective HLB Value	Effective diameter (nm)	Polydispersity
25	75	4.5	-	-
50	50	8	517.5±0.5	0.005
75	25	11.5	421±0.9	0.005
100	0	15	267.7±1.3	0.005

2.3.3 Optimization of Candelilla wax nanoparticles preparation

2.3.3.1 Analysis of Ternary Phase Diagram

Phase behavior of a tertiary system is determined by its composition at room temperature. Different compositions of CW formulations were calculated based on surfactant-to-lipid ratio (S/W) and their visual appearance is shown in the ternary phase diagram – Figure 15.

For formulations with higher concentration of lipid phase (>15%), the emulsions were creamy and viscous. For high melting point lipids like waxes, stability of O/W emulsions is influenced by a destabilization mechanism called partial coalescence. Partial coalescence occurs due to penetration of lipid crystals from one droplet into another droplet and these crystals bring the droplets together by overcoming Laplace pressure.⁽¹⁹⁸⁾ This can be explained by increased particle size due to aggregation at higher lipid concentrations and broader particle size distributions.⁽¹⁹⁷⁾ At lower concentrations of lipid phase (<5%), phase separation was observed. Destabilization of nanoparticles occurs due to aggregation of lipid crystals in absence of sufficient surfactant concentrations.⁽¹⁹⁹⁾

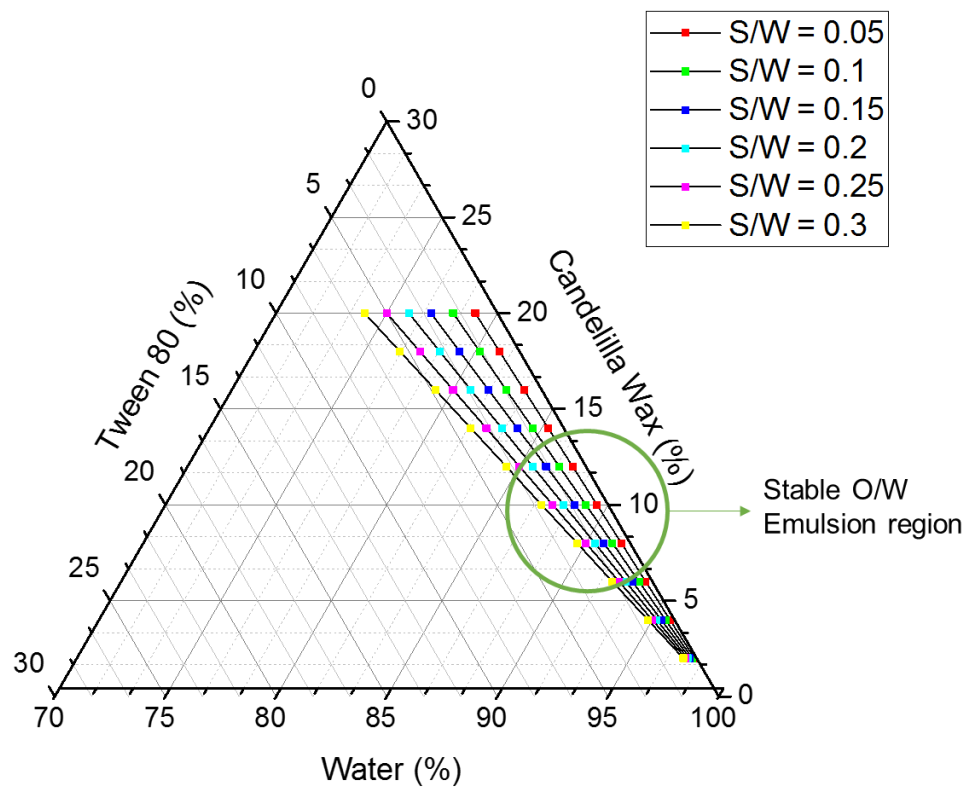


Figure 15 Ternary Phase diagram of Candelilla Wax-Tween 80-Water

2.3.3.2 Particle size Analysis of stable CW O/W emulsions

The particle size of emulsified CW formed from 10% (w/w) CW and different concentrations of Tween 80 were measured. Figure 16 shows that 2% (w/w) Tween 80 formed candelilla wax particles of smallest size (~ 212 nm).

The factors that influence the particle size of SLN are (i) the nature of lipid matrix, (ii) type of surfactant and its concentrations, and (iii) process parameters (temperature, homogenization parameters). With increase in Tween80 concentration, the particle size has effectively reduced. Decrease in particle size can be achieved by introducing sufficient surfactant molecules at the lipid-water interface and reduce high energy barrier between binary system. Since Tween80 is a non-ionic surfactant, stability of nanoparticle dispersions is attributed to steric hindrance of the groups that occupy at the interface in the aqueous phase. At higher concentrations (>3%) of Tween80 (not shown) the CW formulations were creamy and highly viscous, probably due to increase in rate of recrystallization of lipid in the droplets that leads aggregation.

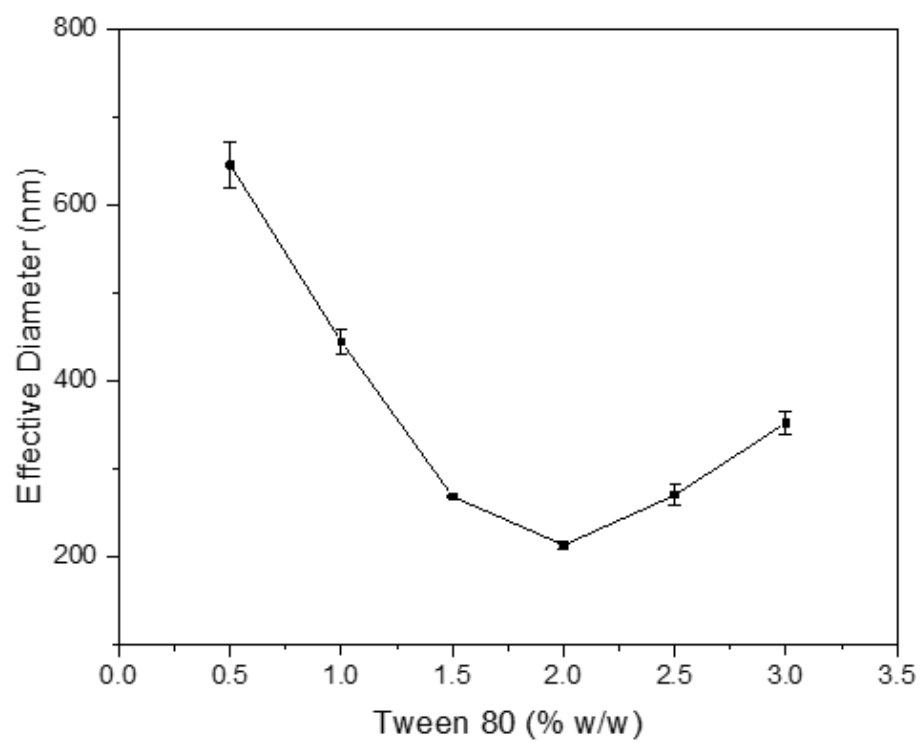


Figure 16 Effect of Tween80 Concentration on 10% (w/w) Candelilla wax nanoparticle size

2.3.3.3 Storage Stability of CW nanoparticles

To further confirm the most stable formulation of CW nanoparticles, storage studies were conducted on CW formulation with 10% CW and 2% Tween80. Lipid dispersions are considered as kinetically stable in nature, when their particle size doesn't significantly change over time. The kinetic aspect of the surface coverage process by the emulsifiers influence the particle size and its stability. Rate of the process of primary coverage of the surfactant on wax droplets competes with the rate of cooling and the agglomeration of liquid droplets. Since nanoparticles have solid lipid matrix instead of liquid core, destabilizing features like coalescence and Ostwald ripening. One major destabilizing process associated with SLN is creaming due to flocculation and gravitational separation. Flocculation occurs due to collision frequency and electrostatic interactions. Collision frequency doesn't play a role in SLN due to their solid lipid core and use of a non-ionic surfactant like Tween 80 lowers the interactions through steric repulsions. Sterically stabilized emulsions are usually less susceptible to pH and ionic strength than electrostatically stabilized emulsions.(200) Reduction in particle size of the system prevents gravitational separation which is physically governed by Stokes' law that predicts the creaming rate of an emulsion. Smaller the creaming rate, more stable the formulation will remain.

The equation for creaming rate (v_{stokes}) of an isolated spherical particle in a liquid:

$$v_{stokes} = -\frac{2gr^2(\rho_2 - \rho_1)}{9\eta}$$

$$v_{stokes} \propto r^2$$

Where, g is acceleration due to gravity, r is the radius of the particle, ρ_2 is density of the dispersed phase and ρ_1 is the density of the continuous phase and η is the shear viscosity.

Formulations that are based on emulsion preparations are not thermodynamically stable and their properties change with time. In our application, this is undesired and can cause changes in the behavior of the products over storage time. The kinetic stability of the non-creaming formulation with 10% Candelilla wax and 2% Tween 80 was observed over a few months and is shown in Figure 17. The particle size increases slightly from ~ 271 nm to ~ 287 nm over 2 months. There is no drastic change in particle size during storage which indicates that the formulation is kinetically stable.

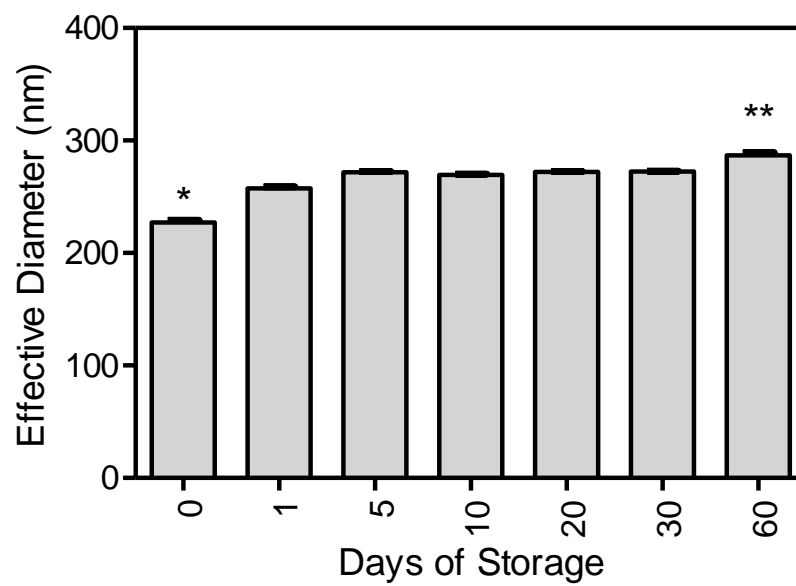


Figure 17 Storage studies on Candelilla wax nanoparticles stabilized by 2% (w/w)

Tween80

2.3.3.4 Morphology of Candelilla Wax SLN using Atomic Force Microscopy

To understand the shape and size of the SLN formed, AFM imaging with section analysis was performed using tapping mode of atomic force microscopy.(201) Figure 18 displays the tapping mode AFM height and phase image of Candelilla wax SLN in dry state on the silicon wafer, which indicates their pseudo-spherical morphology. Some particles were significantly smaller than others but they were in smaller amounts. They could possibly be remaining surfactants. Section analysis embedded in the software Nanoscope5.30 was applied to calculate the particle size on the wafer surface as shown in Figure 19. The vertical distance from the upper edge of the particle to the bottom of the silicon wafer was taken as particle size, which was previously utilized to calculate size of CS-TPP nanoparticles in dry state.(202) The individual particle sizes of the nanoparticles (prepared at initial wax concentration of 10g/g emulsion) from section analysis are approximately 140-150 nm as its diameter. Smaller artifacts were observed on AFM images which were measured to have a diameter of 28 to 40 nm. The minimum particle size calculated from curve fitting through Stocks-Einstein's equation from DLS studies turns out to be 271 nm. The difference between the particle sizes from AFM and DLS studies arises from the sample's state, in case of AFM, dry samples are analyzed while particles were in a solution during DLS tests. In the dry state, the particles are stripped out of the water layers that held by the hydrophilic part of the surfactants when dispersed in aqueous phase and causing increase in the effective diameter of the particles. Other studies have also shown that particle sizes from AFM are smaller than those from DLS measurements.(202, 203) Morphology of Candelilla wax SLN can be explained by the composition and polymorphic form of the lipid core. Nanoparticles with lipid in less stable

α polymorph tend to form more spherically shaped structures. Shape of SLN is also determined by the structure of the surfactant used. When present in stable β -modification polymorph, the lipid nanoparticles assume platelet like morphology.(204-214). Candelilla wax exists in β polymorph form in SLN which has a melting point at 64°C and it only forms unstable α polymorph during rapid cooling (10°C/min).(215)

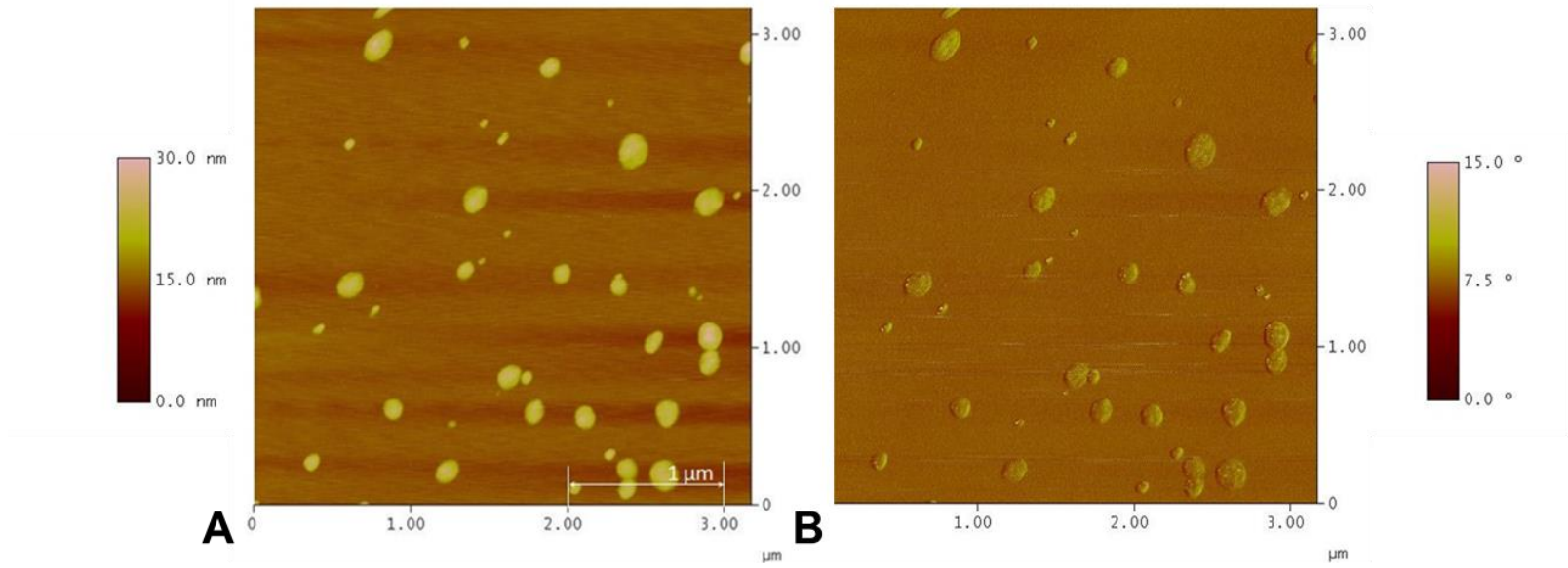


Figure 18 Tapping mode -Atomic Force Microscopy Height image (A) and Phase image (B)

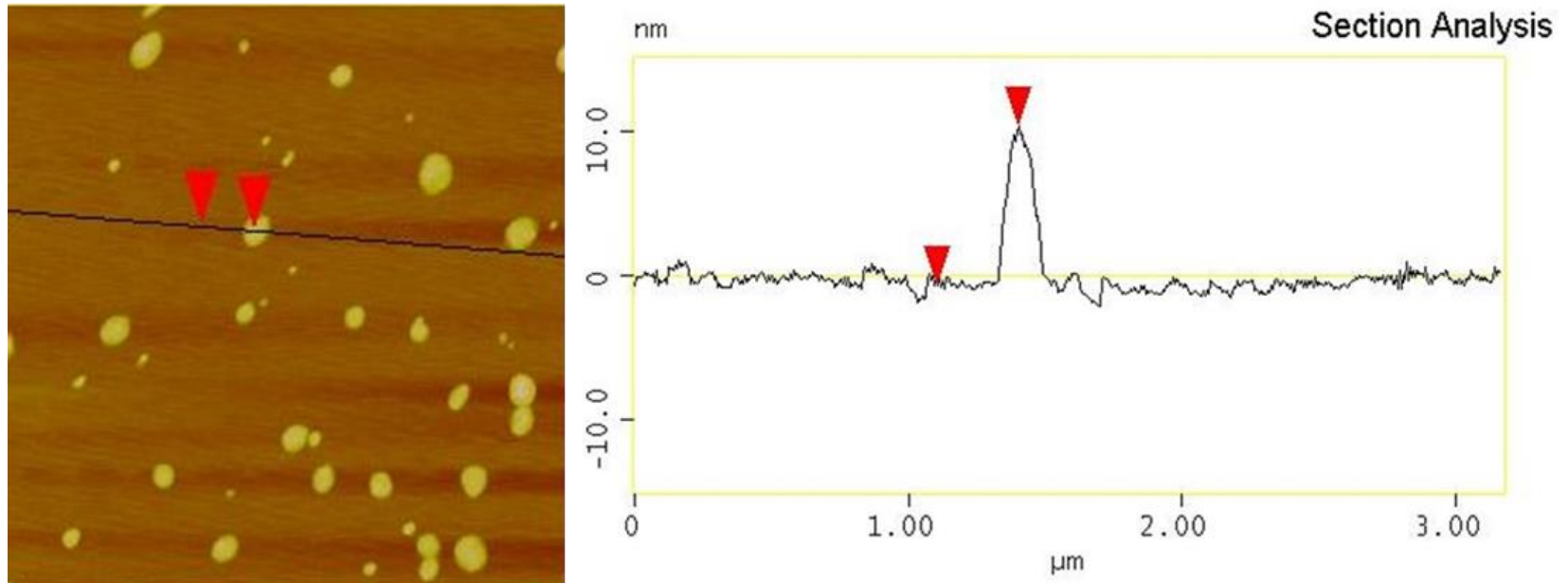


Figure 19 Sectional Analysis of Candelilla Wax SLN

2.4 Conclusion

In this study, wax nanoparticles were prepared in a systematic approach. Firstly, selection of surfactants for creating an emulsion system by using low molecular surfactants (Tween/Span) based on hydrophilic-lipophilic barrier concept. HLB value of this surfactant can be useful while using other surfactants with known HLB values to create emulsion systems of Candelilla wax. The composition of stable pre-emulsions was calculated using ternary phase diagram. To obtain nanoparticles, the pre-emulsions were subjected to high speed homogenization at optimal process temperature to create hot microemulsions and later, cooled down rapidly by storing them at cold temperatures. Characterization of wax nanoparticles were performed to ensure its size and stability by using dynamic light scattering methods and atomic force microscopy. This systematic approach can be employed to create nanoparticles with different types of lipids.

CHAPTER 3. CHITOSAN-PVA NANOCOMPOSITES WITH CANDELILLA WAX NANOPARTICLES: PHYSICAL AND ANTIBACTERIAL PROPERTIES

3.1 Abstract

Chitosan (CS), acetylated form of naturally occurring polymer from crustaceans has limited application in packaging due to presence of hydrophilic groups. To address this challenge, films from chitosan-poly(vinyl)alcohol (PVA) based nanocomposites with different amounts (% w/w) of wax nanoparticles and glycerol as plasticizer were prepared by pour casting. These nanocomposites (CPGW) were characterized for its moisture barrier properties, mechanical and antibacterial properties. Films with concentration of wax SLN greater than 3% (w/w) had significant increase in surface hydrophobicity. Moisture isotherm curves of nanocomposite films followed very similar absorption behavior to that of control film and their water vapor absorption rate linearly decreased with increase in SLN. Water uptake % was lowered by 19% to 55% when SLN content increased upto 3% (w/w), no significant difference was observed beyond 3% (w/w) SLN. Tensile strength and elongation E% of nanocomposites were affected by relative humidity they are stored and it is suggested that polymer-SLN interactions are complex. Microstructure of films up to 5% (w/w) SLN concentrations have homogenous matrix and no phase separation was observed. FTIR analysis of nanocomposites were performed to understand chemical interactions of different components of the film. It is observed that CS and PVA completely blended in the films and disappearance of CH stretching band characteristic to saturated carbon in wax confirms that wax exists in the nanoparticle form. Incorporation of wax NP

in chitosan/PVA film did not affect the inherent antibacterial properties of chitosan. The current work suggests that wax SLN can be used as a nanofiller to overcome the moisture sensitivity of certain biopolymer based films.

3.2 Materials and Methods

3.2.1 Materials

Chitosan (CS) with deacetylation degree (DD) of 98.0% and molecular weight (Mw) of 330 kDa was purchased from Kunpoong Bio. Co., Ltd. (Seoul, South Korea). Mowiol® 56-98 or poly (vinyl alcohol) (PVA) of Mw ~ 195,000 with DP ~ 4300 and degree of hydrolysis 98.0 – 98.8 % (molar fractions) was obtained from Sigma-Aldrich (St. Louis, MO). Other chemicals used for analytical purposes are acquired from VWR International (Radnor, PA) and Fischer Chemicals (Hampton, NH).

3.2.2 Preparation of CS-PVA nanocomposite films with CW nanoparticles

Chitosan-polyvinyl alcohol nanocomposite films with CW nanoparticles are prepared by casting/solvent evaporation method. Chitosan (CS) was dissolved in acetic acid (0.5 M) to yield a 4% (w/v) chitosan solution. Polyvinyl alcohol (PVA) was separately dissolved in deionized water at 80°C to make 4% (w/v) solution. The two solutions were mixed and an appropriate amount of 15% w/w glycerol (G) was added. The mixture was stirred thoroughly for 30 min at ambient temperature. Candelilla wax solid lipid nanoparticles (SLN) dispersion (10 % w/w) was added drop-wise according to wax weight percentage. The composition of the nanocomposite films (CPGW) are listed in the Table 9. The 25ml of film solution is poured into petri-dishes and dried under a hot air oven at

35°C. The films are peeled out and are conditioned at 52% relative humidity at ambient room temperature.

Table 9 Composition of CPGW films

Sample ID	CS (%w/w)	PVA (% w/w)	SLN (% w/w)	G (%w/w)
CPGW0	42.5	42.5	0	15
CPGW1	42	42	1	15
CPGW2	41.5	41.5	2	15
CPGW3	41	41	3	15
CPGW4	40.5	40.5	4	15
CPGW5	40	40	5	15
CPGW10	37.5	37.5	10	15
CPGW20	32.5	32.5	20	15
CPFW40	22.5	22.5	40	15
CPGW60	12.5	12.5	60	15
CPGW80	2.5	2.5	80	15

3.2.3 SEM Imaging of CPGW films

The CPGW films were mounted on a flat SEM pin (Tedpella Inc, Redding, CA) for surface images and with aid of 12mm carbon discs (SPI Supplies, West Chester, PA) on to which the sample is adhered. The vacuum dried samples are coated with a 10 nm with gold using in a Polaron (Hatfield, PA) SEM coating system. The specimens were scanned using Field Emission SEM (Zeiss Sigma, Jena, Germany) with Oxford INCA PentaFETx3 EDS system (Model 8100) at an accelerating voltage at 5kV. The images with digitally processed by Smart SEM software (Zeiss Sigma).

3.2.4 Contact Angle Measurements on CPGW films

The static water contact angle measurements were carried out using a VCA Optima XE Dynamic Contact Angle Analyzer (AST Products Inc., Billerica, MA) at ambient condition. The image was recorded by a CCD camera immediately after the water drop was deposited onto the CPGW film surface. At least six measurements were averaged for each sample.

3.2.5 Moisture Sorption Isotherms of CPGW films

Saturated salt solutions of lithium chloride, magnesium chloride, sodium bromide, sodium chloride, and potassium nitrate were used to obtain different RH combinations having a_w values of 0.11, 0.33, 0.58, 0.75 and 0.94 respectively. These saturated solutions were taken in different desiccators. Prior to keeping the film, specimens were conditioned to 53% RH (desiccator with saturated solution of magnesium nitrate) at 24°C. The initial moisture content of the blend films was measured in duplicate on dry basis (db in %) by drying in hot air oven at 100 ± 2 °C to constant weight. The sorption experiments were

carried out by keeping approximately 1 g of blend films (2 cm x2 cm) in desiccators, removing at frequent intervals and weighing until they reach constant weight (within $\pm 5\%$). All chemicals were of analytical grade from Sigma-Aldrich (St. Louis, MO). The equilibrium moisture content (% db) of the films when the weight of the film reaches a constant value.

$$\text{Equilibrium moisture content (\% db)} = \left(\frac{m_{eq} - m_{dry}}{m_{dry}} \right) \times 100\%$$

Where,

m_{eq} = Weight of the film in equilibrium at a certain relative humidity and temperature 25°C

m_{dry} = Dry weight of a certain relative humidity and temperature 25°C

3.2.6 Water absorption Studies on CPGW films

Small pieces of membranes were weighed and immersed in deionized water (30 mL), until equilibrium was reached. The swollen membranes were taken out and extra water was removed by carefully transferring swollen film into a dry dish. The water absorption capacity (WAC) was calculated using the equation:

$$WAC (\%) = \left[\frac{W_s - W_d}{W_d} \right] \times 100$$

Where “ W_d ” is the weight of the dry membrane and “ W_s ” is the weight of swollen membrane at equilibrium.(216) The results were reported as the average of three readings. The swelling response of films was also measured at different pH.

3.2.7 Water Vapor Transmission Rate and Water Vapor Permeability of CPGW

films:

The water vapor transmission rate (WVTR) and water vapor permeability (WVP) of the membranes were analyzed according to the ASTM Method E96/E96 M. Circular test cups were filled with calcium chloride (10.0 ± 0.5 g) as desiccant at 0% relative humidity (RH), and sealed with the test membranes. The membranes were tightly attached and the initial weights of the cups were recorded. The cups were placed in an environmental desiccator set at 25°C and 53% RH. After reaching equilibrium state in the desiccators, cups were weighed daily for 14 days. The WVTR was calculated as the slope of the regression line drawn between elapsed time and the weight change of the test cups. The actual WVTR and WVP of the membranes were calculated using the following equations.

$$WVTR = \frac{G}{tA}$$

$$WVP = \frac{WVTR}{\Delta P} \times S = \frac{WVTR}{S(R_1 - R_2)}$$

Where, G is weight change (g), t is the time (h), A is the test area (m²), and ΔP is vapor pressure difference (Pa) and S is saturation vapor pressure at test temperature (1.333×10^2 Pa), R_1 = relative humidity at the source expressed as a fraction and R_2 = relative humidity at the vapor sink expressed as a fraction.

3.2.8 Mechanical properties of CPGW films

The tensile strength (TS) and elongation at break (EB) of the films were measured on a TA.XT2 Texture Analyzer (Texture Technologies, New York, USA) at a speed of 0.1 mm/s. The appropriate sized films (1.0 × 10.0 cm) were cut using a razor blade and the

gauge length was set at 10.0 mm. For each sample, the measurements were replicated four times. TS was calculated by dividing the maximum load for breaking the film by cross-sectional area, and %E by dividing film elongation at rupture to initial gauge length, and the values were measured both in longitudinal and transverse directions to observe whether any difference in the orientation of polymer chain occurs. Percent elongation is the ratio of extension to the length of the sample. All means were compared with each other, the results of ANOVA indicated significance ($p < 0.05$).

3.2.9 Molecular Interactions Analysis: Fourier Transform Infra-Red Spectroscopy

The IR spectra of samples were determined in the range of 4000 to 400 cm^{-1} using a Fourier transform infrared (FTIR) spectrophotometer (Thermo Electron Corp., Nicolet 6700, Waltham Massachusetts, USA) at room temperature. Spectra were recorded with 200 scans at 6.0 cm^{-1} resolution using an attenuated total reflectance (ATR) technique with a diamond crystal tip.

3.2.10 Antibacterial Properties of CPGW films

Antibacterial activity of the films was assessed against the Gram's negative bacterium *E. coli* (CGSC4401) and the Gram's positive bacterium *Staphylococcus aureus* DB (ATCC 55585) using a modified agar well diffusion method. CPGW films of 100±2 mg were placed on BHI (Brain Heart Infusion) agar plates seeded with 20 μl of bacterial culture containing 10^5 - 10^6 CFU/ml and hydrated with inoculated nutrient broth. The plates were then incubated at 37°C overnight and were bacterial growth was observed. The antibacterial activity of CPGW films was quantitatively measured according to the method described by Zhai *et al.* with slight modifications.(217) CPGW films were initially washed in sterile distilled water, weighed and placed in test tubes containing BHI broth with

bacterial culture (0.5%) containing approximately 10^5 – 10^6 CFU/ml. The culture tubes were incubated overnight at 37°C with shaking (150 rpm). During incubation, the optical density of the medium was measured at 600 nm at regular time intervals until a constant reading was obtained. To estimate amount of viable bacteria after incubation, serial dilutions of the incubated cultures with CPGW films was performed and plated on BHI agar plates for overnight growth. Final CFU/ml was estimated from the bacterial colonies grown on the plates. All experiments were conducted in triplicate under aseptic conditions.

3.3 Results and Discussion

3.3.1 Visual Appearance of Chitosan-PVA nanocomposite films with Candelilla wax nanoparticles

Freshly prepared CPGW films are transparent and have a slight yellow color due to chitosan as shown in Figure 20. The moisture content of the dry films was $6.4 \pm 2.1\%$ (w/w). The yellowness of chitosan is dependent on its treatment process and extent of Maillard reaction. Air-dried films were more transparent than heat-dried films. More yellowness was observed in films formed by convective drying, due to the preferential drying of surface layers, and also it could be attributed to Maillard reaction products.⁽¹³²⁾ During storage, yellowness increases significantly. In CPGW films with more than 10% SLN, the films are not homogenous and SLN aggregates in the film.

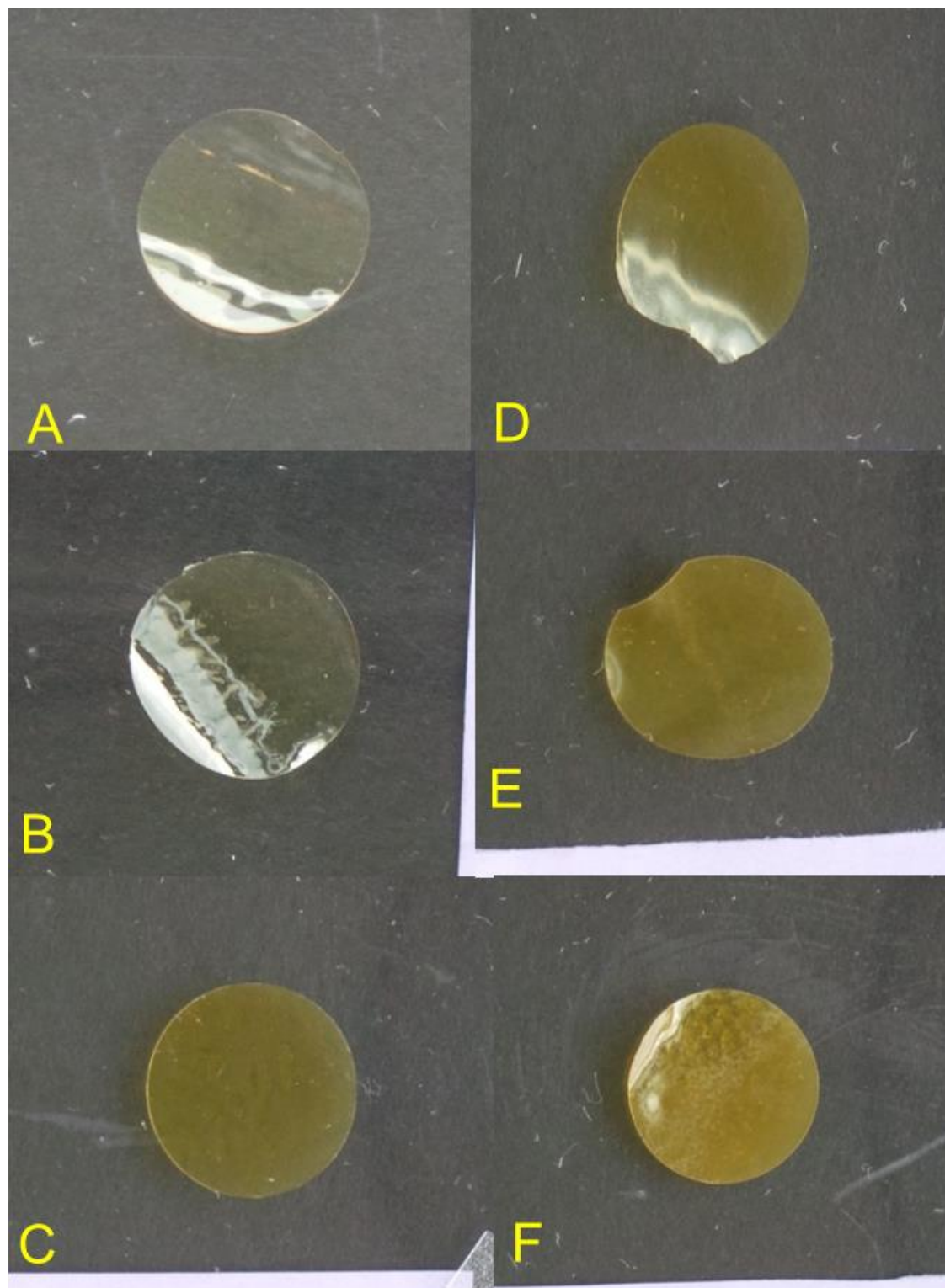


Figure 20 Appearance of freshly prepared films with 0% (A) and 2% (B), films stored for a month 2%(C), 4%(D), 5% (E) and 10% (F)

3.3.2 Microstructure of CPGW films

To understand the microstructure of the CPGW films, in-lens detector was used to study morphology and surface topography and additionally, work function (electronic variation) of the material which is characteristic property to the material. The difference in the work function is expressed by variations in image contrast.(218) From Figure 21 (A-E), surface of the films has no or very deposition of SLN and are embedded inside the matrix only at higher concentration (>10%), SLN plaques appear on the surface. The cross-sectional images using the conventional secondary electron detector (not shown) are compact and the film surface is smooth and without cracks or pores. **In Error! Reference source not found.**-F which shows the control, CPG film matrix and it is observed that CS and PVA in the dry state produced a fine mesh network of CS-PVA polymers with high porosity. In Figure 21 (F-J), the chitosan and PVA polymers are completely miscible to form the matrix in control CPGW film and at low SLN% in the film, the nanoparticles are homogenously mixed into the matrix. There is phase separation of SLN and the polymer matrix in the films with 10% SLN (w/w).

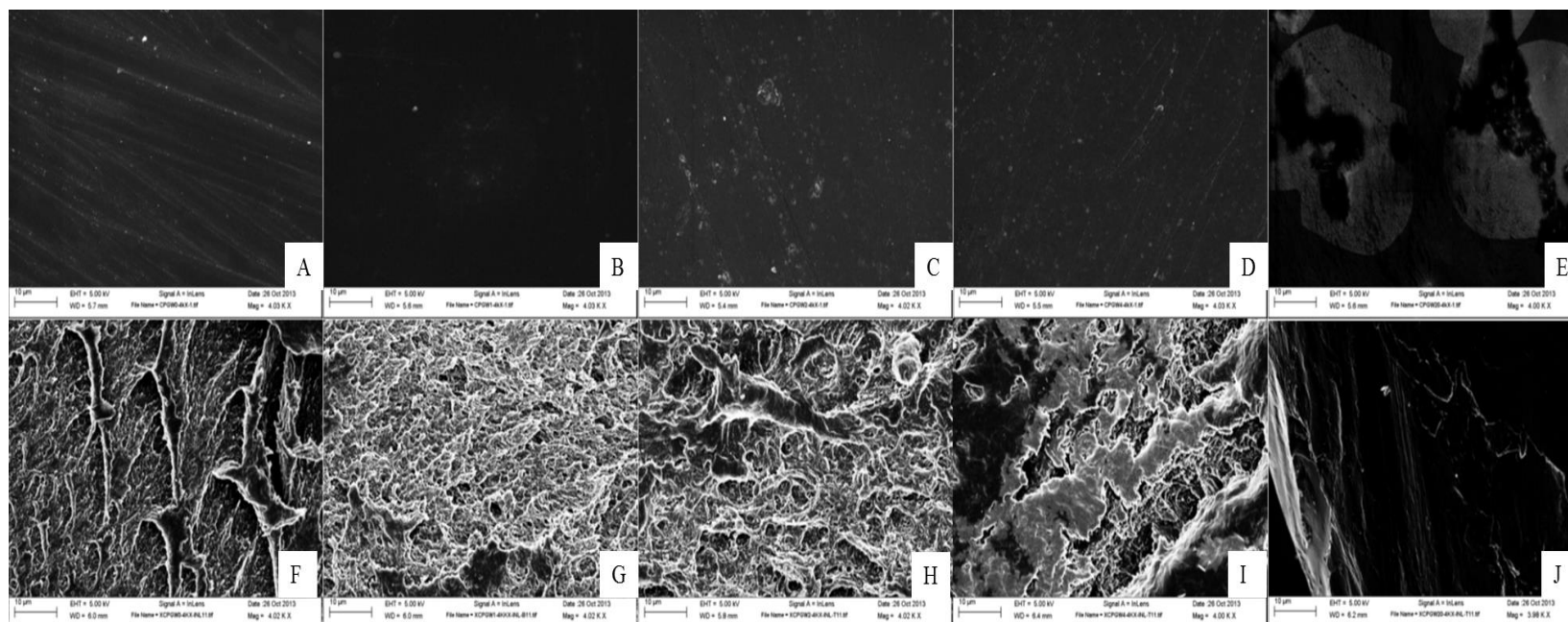


Figure 21 FESEM Images of the surface (A-E) and cross-sectional (F-J) areas of CPGW films with no SLN (A, F), 1% SLN (B, G), 2% SLN (C, H), 4% SLN (D, I) and 10% SLN (E, J) using in lens detector

3.3.3 Surface hydrophobicity of CPGW films

Hydrophobic nature of the surface of materials are measured quantitatively from water contact angle and surface tension. Intermolecular forces at any surface is estimated by surface tension (γ). Contact angle measurement is an indirect and semi-empirical method for determining surface energy and tension. The contact angle measurements have been used extensively to study surface homogeneity, changes in surface composition, hydrophilicity and hydrophobicity, migration of functional groups and low-energy component to the surface.(219) Contact angle measurements of different liquids/solvents on material surfaces are used to characterize surface properties of plasticized films. The contact angle is defined as the angle between the substrate surface and the tangent line at the point of contact of the liquid droplet with the substrate.(220) The interaction between the substrate and the liquid is governed by adsorption. Hydrophilicity on the surface of CPGW films is contributed by the hydrophilic groups (-OH and -NH₂ on chitosan and -OH on PVA) on their polymeric backbone. The strength of hydrophilicity is net effect of number of free hydrophilic groups of polymers to interact with water on the surface and hydrophobic wax from SLN. Another important factor that determines surface properties is the roughness of the surface where roughness increases surface area for water/solvent to interact. From Figure 22, significant decrease in water contact angles in the film with increasing SLN% (w/w) suggests that the surface became slightly hydrophobic. But there was no significant change in water contact angle for CPGW films with SLN% (w/w) higher than 3% which can possibly be the maximum amount of SLN occupying the water and air interface during drying. Small sized SLN have higher mobility to move in the polymer solution and occupy the interface due to the difference in the density of SLN and the

polymers after drying. At high concentrations of SLN, layer of SLN could possibly form over the film surface due to microphase separation.

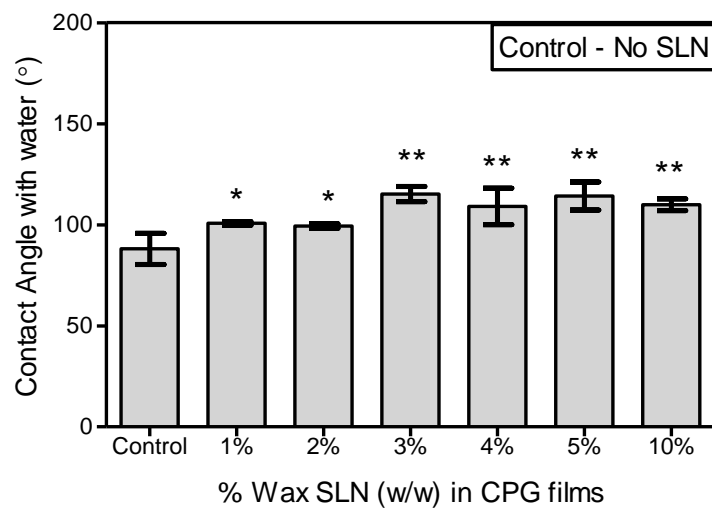


Figure 22 Effect of SLN% on water contact angles in CPGW films conditioned at 53% RH and 25°C

3.3.4 Moisture Sorption Isotherms

Moisture isotherms is determined by the sorption of water by the films stored at different relative humidity values at a constant temperature. Sorption considers both adsorption and absorption as a single mechanism. Adsorption is defined as the adhesion of molecules (adsorbate) which can possibly exist in different physical states (as a gas, a liquid, or a dissolved solid state) onto the surface of the adsorbent. In this study, the adsorbate is water vapor and the adsorbent is CPGW films. Absorption is defined as the mechanism in which a substance in one state is incorporated in another substance of a different state. Sorption of a liquid or gas by the film is dependent on the chemical nature of different components that the film is made from. The sorption isotherm curves for equilibrium moisture content (db) obtained from different CPGW films with varying SLN weight% is shown in Figure 23. The isotherm for moisture adsorption in CPGW films can be described by a sigmoidal curve and it is categorized by BET classification as a type II isotherm where equilibrium moisture content increases with increase in water activity, a_w but at high a_w , the increase is relatively high.(221) The sorption mechanism for chitosan-PVA based films is dependent on water activity (a_w) of the substance it is stored or the relative humidity of the environment. Previous studies on chitosan-PVA films show that there are 3 phases of water adsorptions: (I) Monomolecular phase relates to sorption of monolayer of water when $a_w < 0.2$ (II) Multimolecular phase relates to sorption of multiple layers of water when $0.2 < a_w < 0.7$ (III) Capillary condensation phase relates to condensation of water inside the matrix of the film and later, results dissolution of soluble components in the matrix for $a_w > 0.7$. (222) Adsorption of water is dependent on the surface properties of the film whereas absorption of water is dependent on the bulk of the film

matrix. The composition and quality of the material are determinants of sorption processes which are complex. Sorption in CPGW films is lowered due to decrease in polymer matrix and increase in SLN. Due to hydrophilic nature of PVA and chitosan, moisture is adsorbed into the matrix through the polymer network but by introducing wax nanoparticles into the matrix, the movement of water molecules can be restricted and possibly lower absorption. Crystallinity also determines the sorption in the films where water is only able to interact with monomers of chitosan in amorphous phase and crystalline regions are considered inaccessible to water molecules. (138)

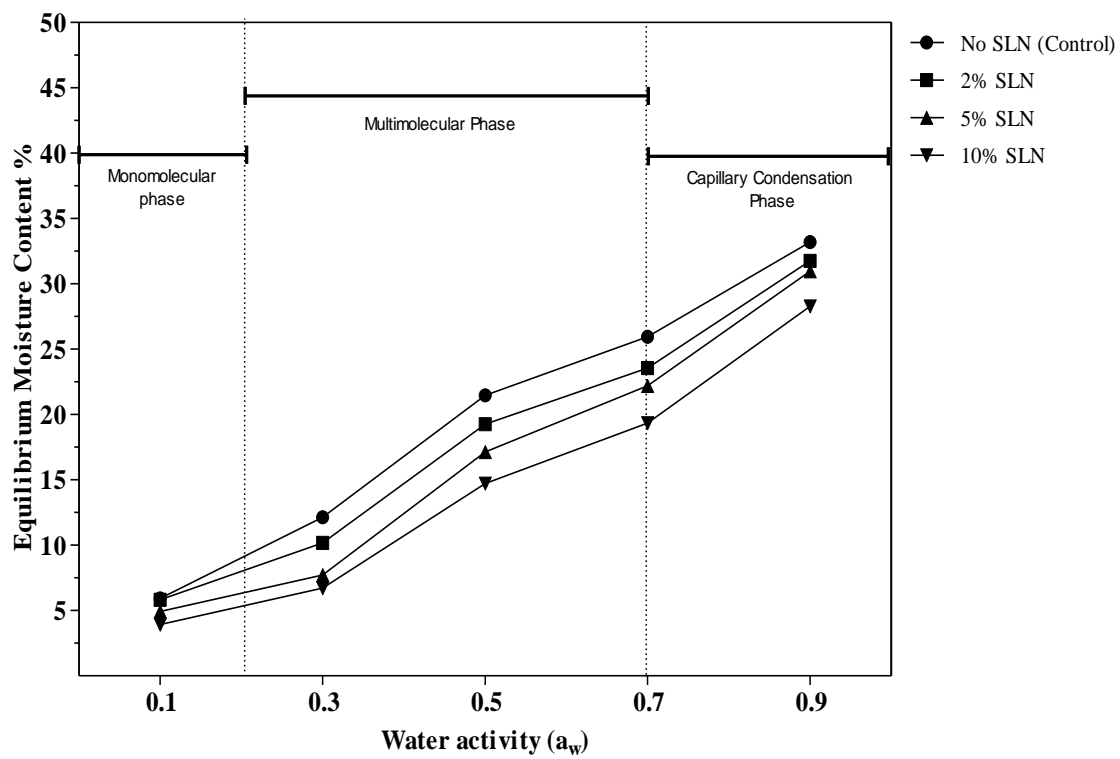


Figure 23 Moisture sorption isotherms of CPGW films

3.3.5 Water Absorption studies of CPGW films

With addition of Candelilla wax SLN, the water absorption capacity of the chitosan-PVA films was significantly lowered as given in Figure 24 E. From Figure 24 A-D, the control CPGW film is swollen larger than film with 2% (w/w) film. This observation clearly indicates that SLN effectively reduces its water absorption capacity.

Water absorption of film material is related to its chemical and structural properties of the film. It is known that chitosan and PVA solutions blend together due their good miscibility and form microporous structures by forming a network of chitosan-PVA through hydrogen-bonding between -OH and -NH₂ and -OH of PVA polymers.(223) The porosity of the films play an important role in water absorption as it allows bulk movement of the water to access different regions of the matrix. SEM images of the control CPG films show high porosity in the matrix which enable the water to move within and hydrate the polymers.

Inaccessibility of water to the polymer matrix by capillary action can be one reason to explain this phenomenon. From SEM images of the nanocomposites, the porosity is reduced due to presence of wax nanoparticles. Interaction of both SLN and polymers with water forms a gel like network which is more rigid and dense than that of the control film.

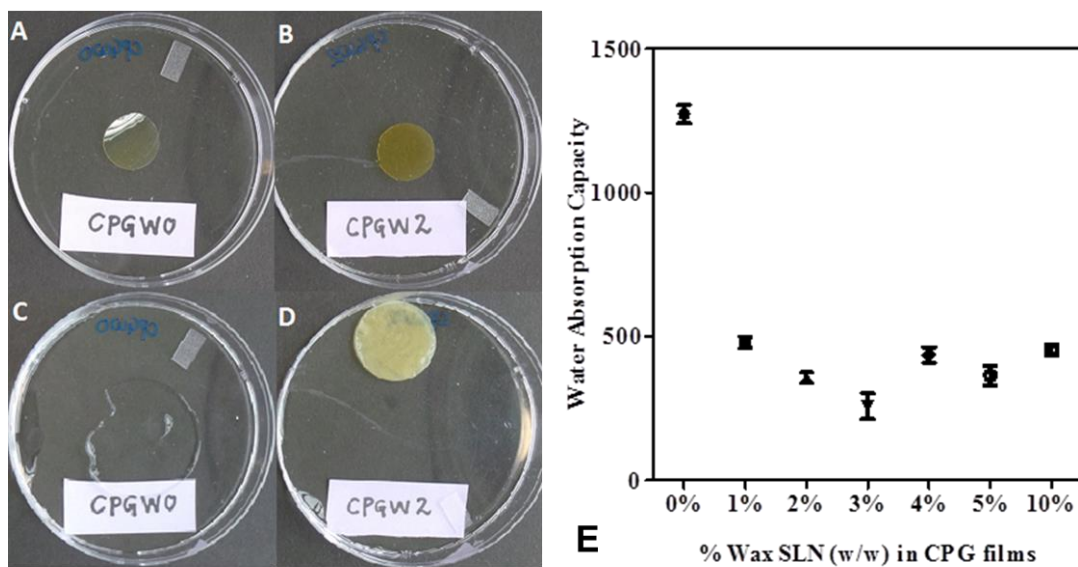


Figure 24 Photographs of 0% (A) and 2% (B) SLN containing CPGW and their corresponding swollen gels, (C) and (D). Effect of %SLN in CPGW films on water absorption capacity %

3.3.6 Film permeability

The WVTR and WVP values of any packaging films are important factors to understand their behavior in food applications of edible films and coating. The moisture barrier characteristics of these films are determined to estimate the shelf life of food products. Chitosan is used as biodegradable biopolymer with film forming capabilities with good gas barrier properties and antibacterial nature. These inherent properties of chitosan make it a suitable packaging material for improving the shelf-life of fruits and other processed food by retarding microbial growth and lowering lipid oxidation. The values for WVTR and WVP for the control CPGW film without no SLN were $390.45 \times \frac{10^{-3}g}{h.m^2}$ and $261.7 \times \frac{10^{-3}g}{Pa.h.m^2}$. This decrease in WVTR and WVP of CPGW films in Figure 25 indicates that a hydrophobic type physical obstacles can improve water barrier properties effectively. Reduction of WVP is around 19%-55% due to addition of SLN and lowest WVP was observed in films with 4-5% SLN (w/w). As observed before, reduced in porosity of the film with nanofiller and its hydrophobic nature can hinder the moisture transfer. Also SLN can aggregate and form localized micro regions in the film matrix that can prevent water vapor transmission. This property has been found extremely effective in preventing food contamination and spoilage. For 10% SLN formulations, the water vapor transfer has significantly increased due to non-uniformity of lipid distribution in polymer network. At higher concentration of SLN in the films, the surface becomes uneven and this increases the surface area and introduces gaps and cracks allowing movement of water vapor molecules.

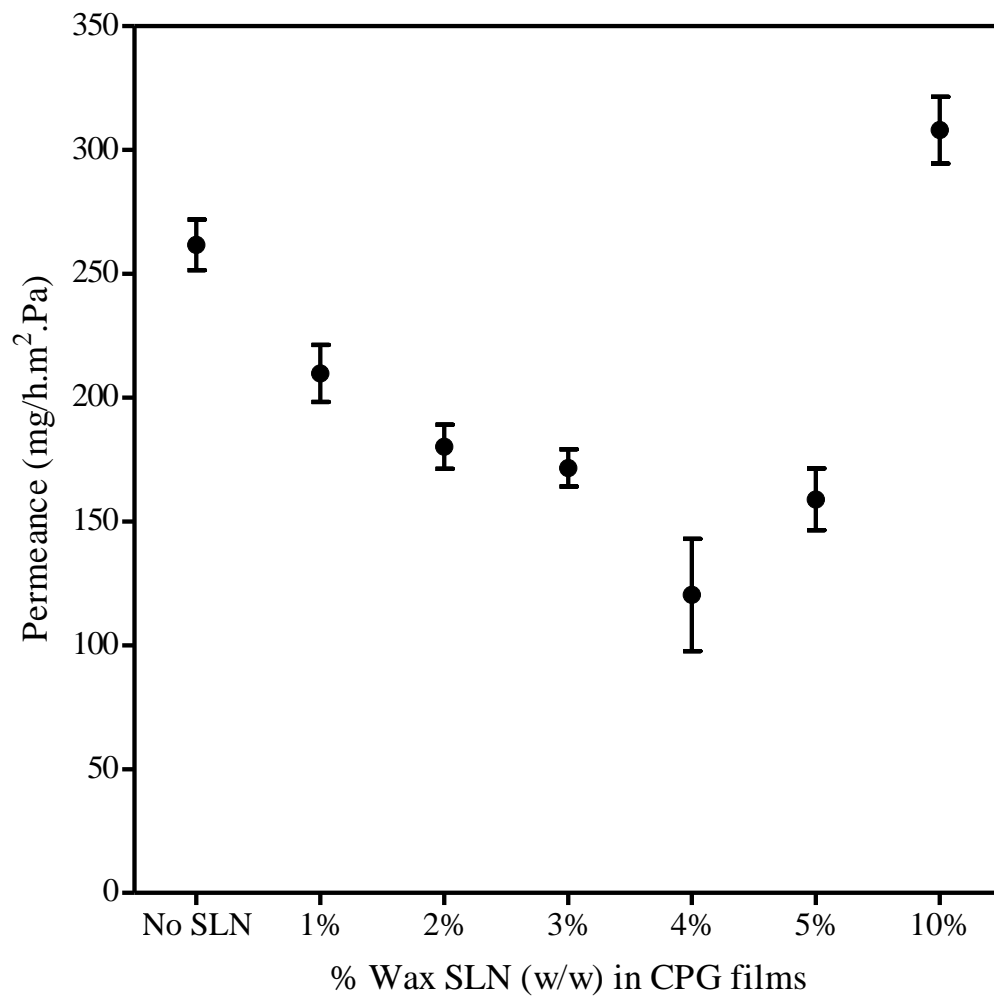


Figure 25 Water Vapor Permeance Values for CPGW films

3.3.7 Mechanical Strength and Elasticity of CPGW films

The tensile strength (TS) and elongation (%E) could be used to describe how the mechanical properties are related to their chemical structure. High TS and %E values are observed in materials with greater toughness whereas high %E with relatively low TS represents mechanical properties of a rigid substance. TS indicates the maximum tensile stress that the film can sustain and %E is the maximum change in length of a test specimen before breaking.

From statistical analysis of the results from Figure 26 and Figure 27, both relative humidity and % SLN (w/w) influence tensile strength and % elongation of the films ($p < 0.001$). % crystallinity in the film and amounts of plasticizers have different effects on chitosan films. High crystallinity in the films give high tensile strength and lower elongation, making the film strong and brittle. The degree of deacetylation of chitosan molecules effects the mechanical strength of films which allows denser packing of the polymer chains substituted with small amino groups, that causes a higher attraction within polymer chains and resulting higher mechanical strength for high degree of acetylation. (224) Plasticizers are often added to the material to increase the ductility which is an important for any packaging materials.

On comparing effect of SLN at RH 57% on tensile strength and elongation is non-linear which could be possibly explained by the complexity of the interactions between the polymers and SLN. On comparing effect of RH in films with different SLN% in them, there was only significant difference in both tensile strength and elongation was observed at RH greater than 53%.

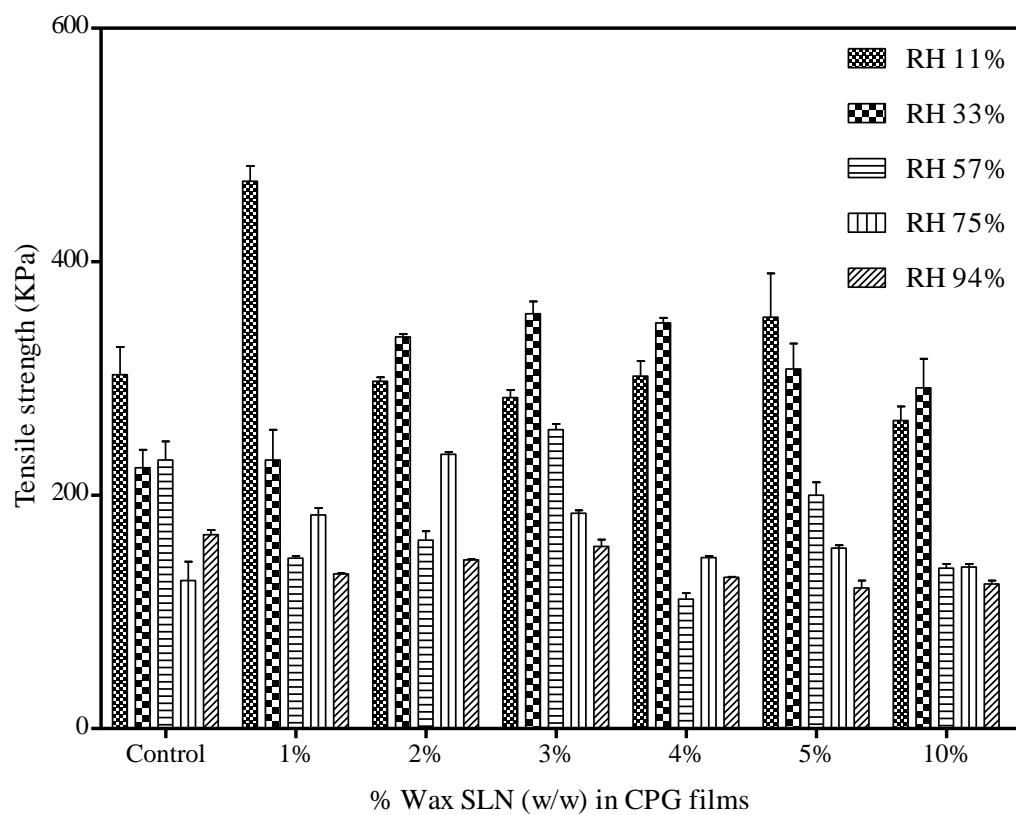


Figure 26 Effect of % SLN (w/w) and relative humidity on tensile strength of CPGW films

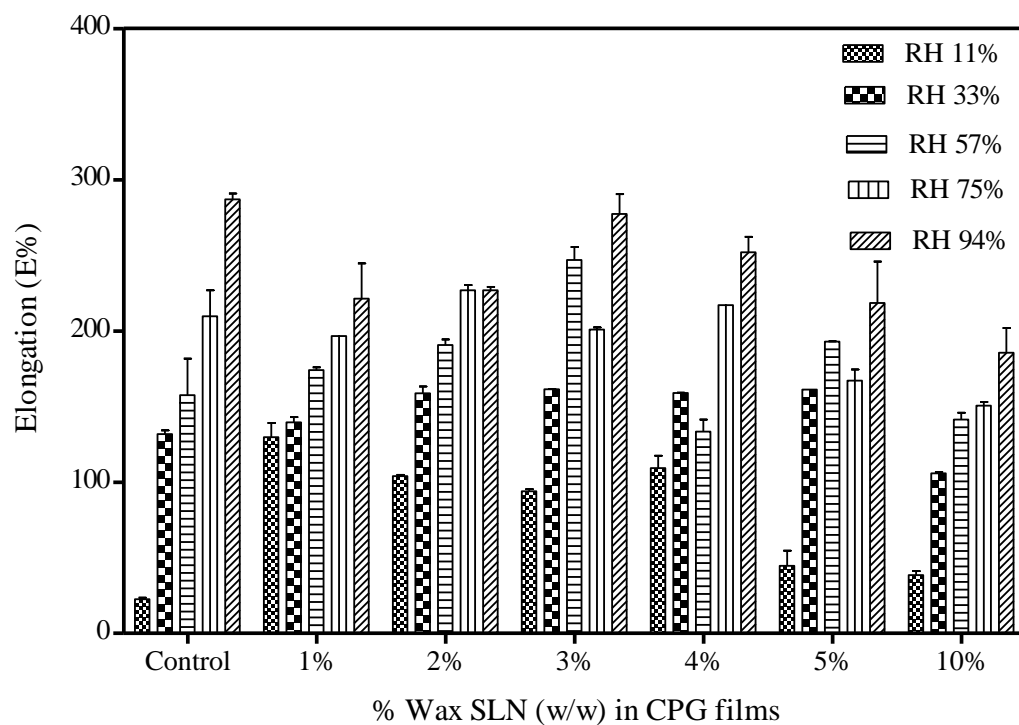


Figure 27 Effect of % SLN (w/w) and relative humidity on elongation % of CPGW films

3.3.8 Molecular Interactions Analysis: Fourier Transform Infra-Red Spectroscopy

Figure 28 and Figure 29 show the FTIR spectra of Candelilla wax and CPGW films with no SLN (Control), 1%, 3%, 5% and 10% SLN (w/w). To understand molecular interactions in the nanocomposite films, their absorbance spectra was generated by FTIR. The frequencies and their assignments of chitosan are indicated as followed: 655 and 1076 cm^{-1} for the characteristic peaks of crystallization of chitosan, (225, 226) 1642 cm^{-1} for the bending vibration of $-\text{NH}_2$ group, 1560 cm^{-1} for the bending vibration of amide group, and 3367 cm^{-1} for the combination of $-\text{OH}$ and $-\text{NH}$ functional groups.

In addition, the band appeared at 870 cm^{-1} , which represents the pyranose ring, confirms the presence of the chitosan moiety. (227) Presence of PVA in the blended films caused the band arising from the NH bending (amide II) at 1561 cm^{-1} of chitosan. Also, an increase in the intensity of CH group at around 2928 cm^{-1} was observed as the PVA content increases. (228) In the area of 1737 cm^{-1} is a band corresponding to stretching $\text{C}=\text{O}$, indicating the presence of carbonyl functions present in the wax, followed by the presence of the bands at 1462 cm^{-1} and 1377 cm^{-1} , corresponding to interactions O-C-H, which presents a characteristic band of Candelilla wax for the presence of these functional groups. (229) The presence of C-H stretching bands in Candelilla, characteristic of saturated carbon, appeared in a range from 2953-2849 cm^{-1} but was completely disappeared due to its form as a nanoparticle. (229)

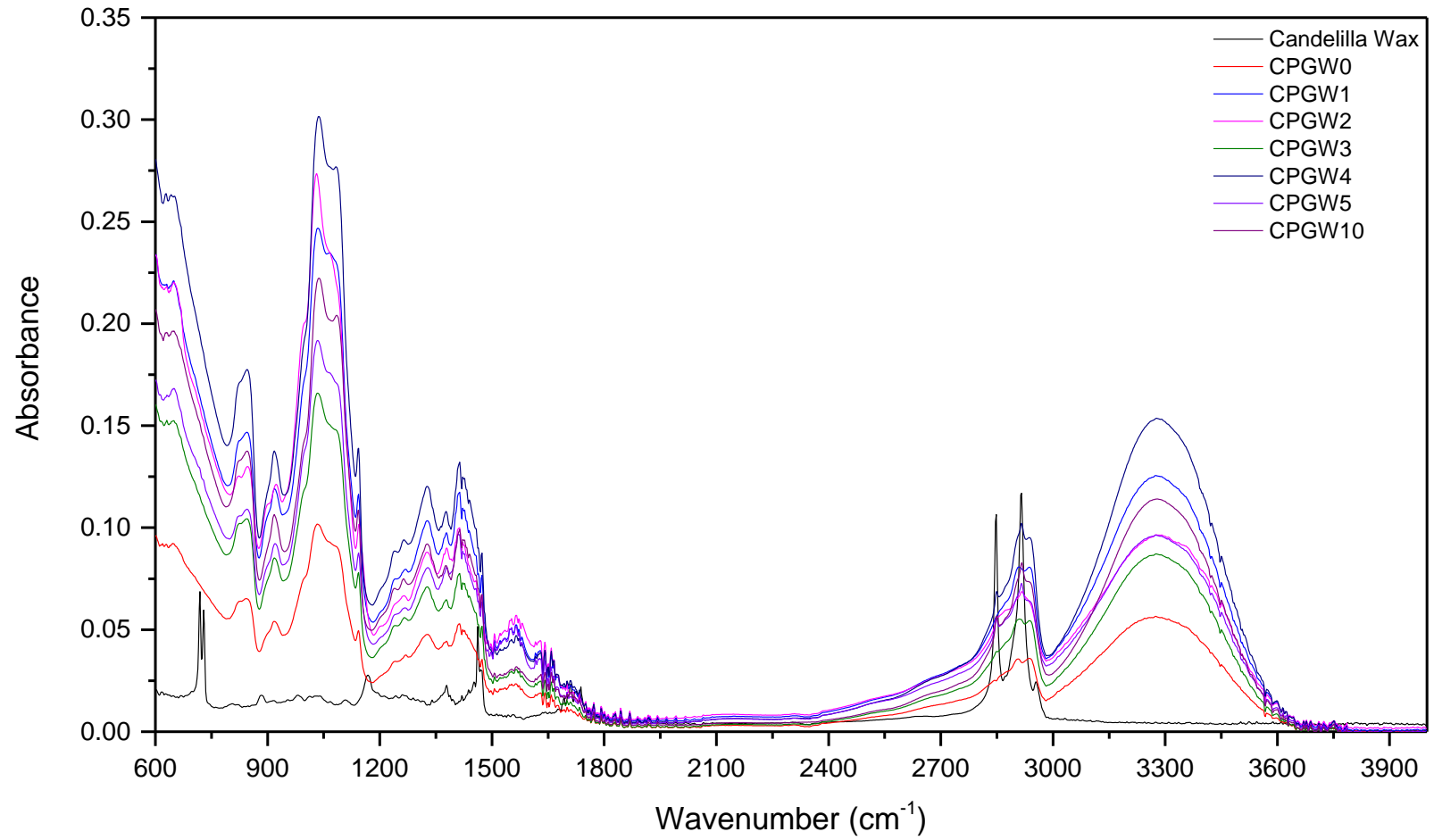


Figure 28 FTIR generated absorbance spectrum of Candelilla Wax and CPGW films

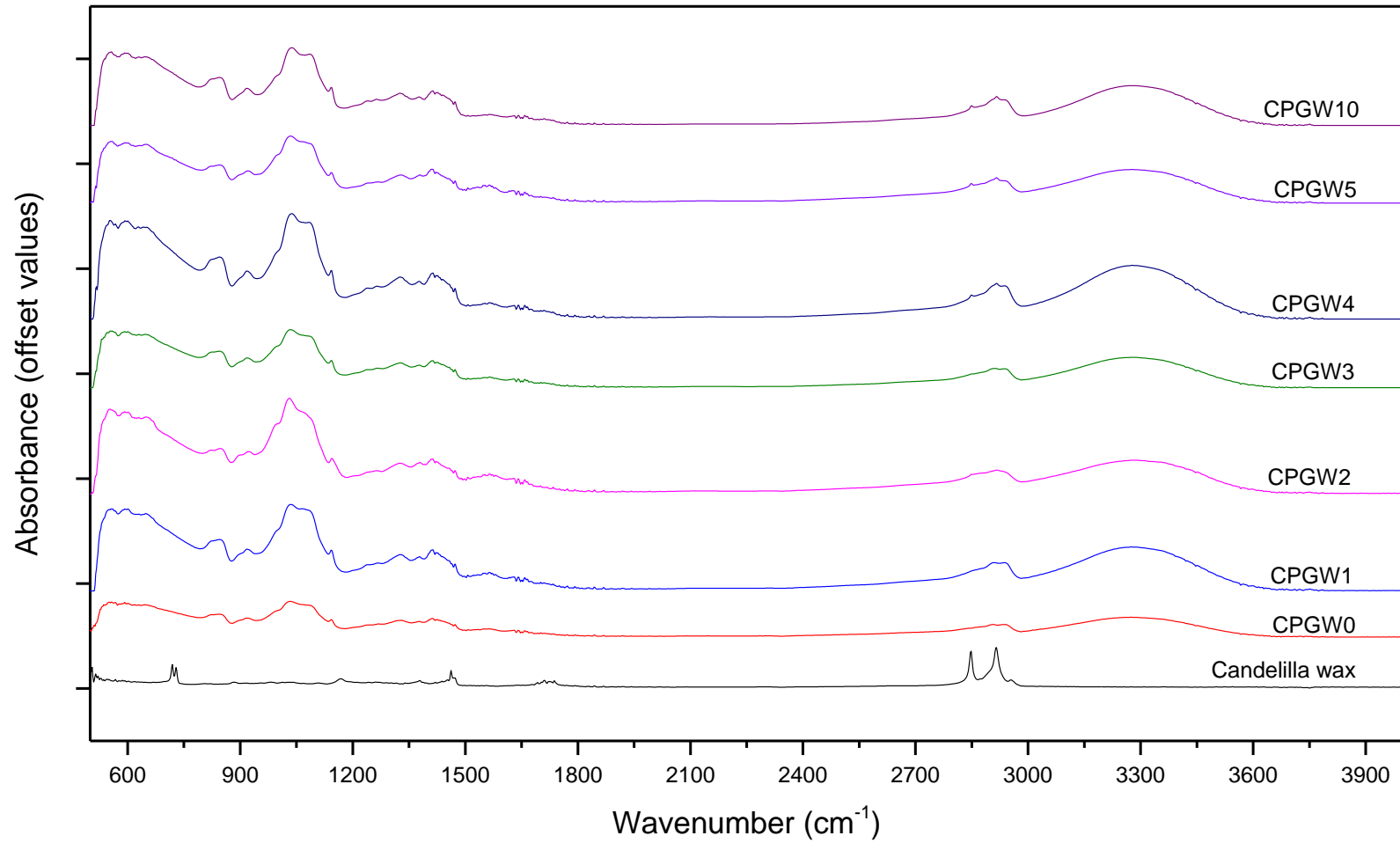


Figure 29 FTIR offset absorbance spectrum of Candelilla wax and CPGW films

3.3.9 Antibacterial Activity of films

No bacterial growth was observed on the films incubated in solid inoculated agar media. (Images not shown). However, there was some growth on higher SLN% based films. This could be on the regions of dispersed SLN phases in inhomogeneous matrix.

In Figure 30 and Figure 31, CPGW films effectively inhibited growth of Gram positive and Gram negative microorganisms in the liquid media. The polycationic structure of chitosan is a prerequisite for antibacterial activity. As environmental pH is below the pKa of chitosan and its derivatives, electrostatic interaction between the polycationic structure and the predominantly anionic components of the microorganisms' surface (such as Gram-negative lipopolysaccharide and cell surface proteins) plays a primary role in antibacterial activity. Besides protonation, the number of amino groups linking to C-2 on chitosan backbones is important in electrostatic interaction. Large amount of amino groups are able to enhance the antibacterial activity. Accordingly, native chitosan with higher DD shows a stronger inhibitory effect than that a molecule with a lower DD. Since chitosan with 98% DD was used in the films, it has high antibacterial effect on microorganisms due to strong electrostatic interactions. Inhibitory effect of the films on *E. coli* is higher than *S. aureus* due to the nature of the microorganism. MIC value for CS on *E. coli* is 0.025 (%) and on *S. aureus* is 0.05 (%).(230)

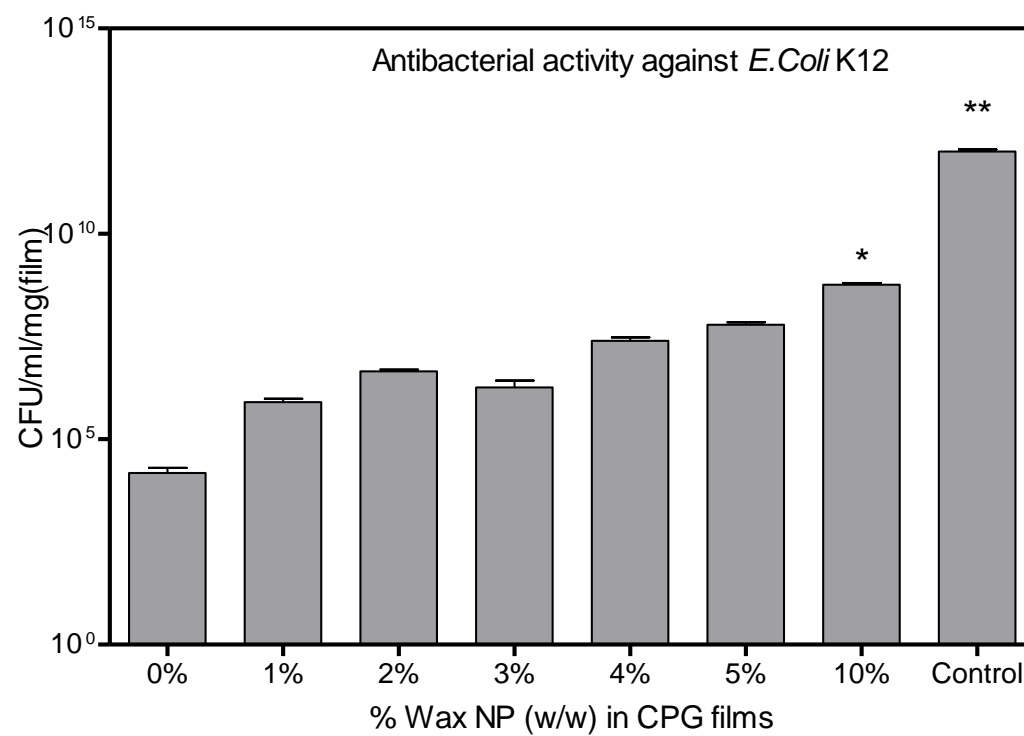


Figure 30 Antibacterial activity against *E. Coli* K12 of CS-PVA films with wax NP

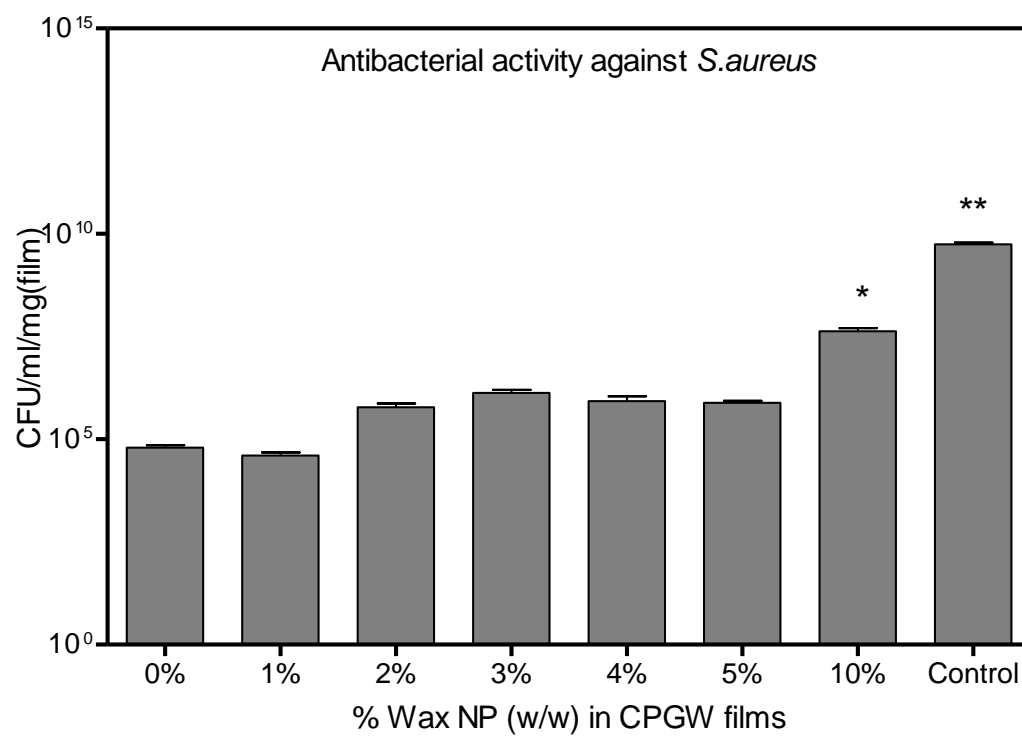


Figure 31 Antibacterial activity against *S. aureus* of CS-VA films with wax SLN

3.4 Conclusion

Addition of lipid nanoparticles in chitosan-PVA film have improved moisture barrier properties significantly. Embedment of nanoscale and hydrophobic materials in these films reduce porosity of the films and making pathway for water molecules tortuous to pass through the film. Introduction of low content of lipid nanoparticles in biopolymer film solution allows to create a homogenous lipid-polymer film with no aggregation or phase separation with good mechanical properties which can be used in food applications. These films can be applied on food with moderate water activity and prevent contamination on the food surfaces as they possess good anti-bacterial properties. The casings and films of these nanocomposite would improve the shelf life and protect the contact surfaces of the fresh and processed foods.

CHAPTER 4. COENZYME Q10 LOADED COCOA BUTTER NANOPARTICLES: PRODUCTION AND CHARACTERIZATION

4.1 Abstract

Studies on Coenzyme Q10 (CoQ10) have shown its potency against heart related diseases in humans but due to high molecular weight and hydrophobicity, it has low bioavailability. To improve its efficacy, CoQ10 loaded cocoa butter solid lipid nanoparticles (CBSLN) with loading range from 0.5% to 2% (w/w) were developed using high-speed and pressure homogenization of pure cocoa butter (CB) with Tween60 and Span60 as emulsifiers at 50°C and stored at 4°C. Particle size analysis, zeta potential and stability studies were performed by dynamic light scattering method. The novel CoQ10-CBSLN dispersions had non-ionic nanoparticles with average size 200 nm with 0.3 polydispersity index and possessed good stability at low and room temperatures. Due to high solubility of CoQ10 (110±4.7% w/w) in CB, 85-90% entrapment efficiency was achieved in their SLN form. DSC analysis of lyophilized CoQ10-CBSLN and their components showed that CB in SLN form exhibited polymorphism enabling co-crystallization with CoQ10. Sterilization process had major effects on the size and entrapment efficiency, confirming that CB recrystallization is influenced by cooling rates. On analyzing the SAXS intensity profiles of CBSLN and CoQ10-CBSLN, it was concluded that there is a slight decrease in thickness of the interface due to increase in loading.

4.2 Materials and Methods

4.2.1 Materials

Cocoa butter (manufacturer: Spectrum Chemical Mfg. Corp.) is purchased from vendor, VWR International. Coenzyme Q10, reduced form (95%, UV) was purchased from Hangzhou Joymore Technology Co., Ltd. China. Surfactants were acquired from Sigma-Aldrich (St. Louis, MO). Other chemicals used for analytical purposes are acquired from Sigma-Aldrich (St. Louis, MO), VWR International (Radnor, PA) and Fischer Chemicals (Hampton, NH).

4.2.2 Solubility Studies

The fats (1 ml) were pipetted into a shading tube at 45°C. CoQ10 was added to the tubes up to saturated concentration with stirring at 200 rpm at 45°C. The mixtures were then equilibrated for 24 h and centrifuged at ~2000g for 1 min to separate the insoluble part. Aliquots of the supernatant (0.5 ml) were diluted with hexane, and the total volume of the solutions was adjusted to 25 ml. In order to determine the CoQ10 concentration of the solutions, optical density at 270 nm was determined at 37°C using UV-spectroscopy (CARY Eclipse UV spectrometer). The fat-hexane solutions without CoQ10 were also investigated as blanks. The molar absorptivity was determined, on a preliminary basis, to be 13.368 mol/l/cm. The tests were done in triplicates. Statistical significance was expressed at the $P < 0.05$ level.

4.2.3 Preparation of Coenzyme Q10 loaded cocoa-butter nanoparticles

0.5%, 1% and 2% (w/w) of Coenzyme Q10 was melted into 10g cocoa butter heated at 50°C based on our results from solubility tests. Using HLB system, Tween 60 and Span

60 (Sigma-Aldrich, St. Louis, MO) was selected after different non-ionic polysorbates (Tweens) and ethoxylated polysorbates were tested at 1% (w/w) and 2% (w/w). The emulsifiers are added into the lipid phase and constantly at 50°C with magnetic bar to get a clear mixture. DI water at 50°C was added at the lipid phase to form a pre-emulsion. The pre-emulsion was subjected to high speed homogenizer (High-speed homogenizer, ULTRA-TURRAX T-25 basic, IKA Works Inc., Wilmington, USA) for 5 minutes at 24,000 rpm and was transferred into high pressure homogenization using High pressure homogenizer, EmulsiFlex-C3, AVESTIN Inc., Ottawa, Canada. Different pressures (500 (HP500), 1000 (HP1000), and 1500 (HP1500) bars) and number of cycles (5, 10, 15, 20, 25) were optimized to obtain a stable nanoparticle dispersion. (231) The sizes of emulsion droplets can be varied by the speed and the pressure in the homogenization processes. The morphology and droplet size of emulsions were measured using an inverted optical microscopy (Nikon TE 2000, Nikon Corporation, Japan) and photon correlation spectroscopy (PCS) – based BIC 90 plus particle size analyzer equipped with a Brookhaven BI-9000AT digital correlator (Brookhaven Instrument Corporation, New York, NY, USA), respectively.

4.2.4 Particle Size analysis – Dynamic Light Scattering

The morphology and droplet size of emulsions were measured over a period of time by dynamic light scattering technique. The samples were diluted with DI water (pH 6.8 and 25°C) at 200 dilutions. Hydrodynamic diameter of the particle and their size distribution were observed and calculated using an inverted optical microscopy (Nikon TE 2000, Nikon Corporation, Japan) and photon correlation spectroscopy (PCS) – based BIC

90 plus particle size analyzer equipped with a Brookhaven BI-9000AT digital correlator (Brookhaven Instrument Corporation, New York, NY, USA), respectively.

4.2.5 Stability studies after sterilization

All cocoa butter formulations with different Coenzyme Q10 loading % were diluted 0.5 times with distilled water and are autoclaved for 15 minutes at 121°C. The samples were cooled down by storing it in refrigerating temperature. The stability of the formulations is studied by observing the particle size based DLS techniques.

4.2.6 Encapsulation efficiency measurements

The encapsulation efficiency (E.E.) of CoQ10 in cocoa butter SLN before and after sterilization was determined indirectly by ultrafiltration method using centrifugal filter tubes (Nanosep®, Pall life Sciences) with a 30 kDa molecular weight cut-off. The amount of encapsulated active was calculated by the difference between the total amount used to prepare the systems and the amount of Q10 that remained in the aqueous phase after isolation of the systems:

$$E. E. = \left[\frac{\text{Total amount of CoQ10} - \text{Amount of Free CoQ10}}{\text{Total amount of CoQ10}} \right] \times 100\%$$

The amount of free CoQ10 in the solution is determined by HPLC analysis. An UltiMate 3000 HPLC system with 25D UV-VIS absorption detector (Dionex) was used with a C₁₈ reversed-phase column (Phenomenex™ Luna™ 5 μm C18 (2); 150x4.6 mm). An isocratic mobile phase was composed of ethanol/methanol in 6:4 ratios with a flow rate 1.0 ml min⁻¹ and 50 μl as injection value. UV detection wavelength for CoQ10 is maximum at 275 nm. Standard curve was calculated by using low concentration of CoQ10 (10, 25, 50, 75 and 100 μg/ml).

4.2.7 Crystallization behavior studies

A differential scanning calorimeter (TA instruments, USA; DSC Q2000 V24.10 Build 122 with DSC Standard Cell RC) was used to examine the thermal properties of the nanoparticles and CoQ10 loaded nanoparticles. The test was performed under nitrogen purge. The sample was two-step with single heating and cooling cycle. All the samples were equilibrated at 20°C (room temperature). Firstly, the sample was heated from 20°C to 90°C with a heating rate of 2°C/min to generate the heating curve and cooling curve was recorded by cooling the heating sample to 4°C at a controlled cooling rate of 2°C/min. The results were later analyzed for crystallization peaks and their corresponding melting points.

4.2.8 Synchrotron Small-angle X-ray scattering (SAXS) studies

SAXS datasets were collected from two sets (undiluted and 200X dilution) of 3 formulations – (i) Control (10 % w/w CB LN), (ii) 0.5% CoQ10 loaded in 10% w/w CB LN and (iii) 2% CoQ10 loaded in 10% w/w CB LN at the BIOCAT undulator beamline 18-ID of APS, Argonne National Laboratory. To minimize damage due to radiation during the run, samples were continuously pumped through a 1.5 mm-wide quartz capillary at 12.5 $\mu\text{L/s}$ for an average exposure time of 0.6 s. The scattering intensity profiles were obtained by negating the average of 15 water-only profiles from the average of 15 CB LN–water or CoQ10–CB LN–water profiles, which were performed with the program IGOR Pro (WaveMetrics), and macros written by the BIOCAT staff.

4.3 Results and Discussion

4.3.1 Maximum solubility of Coenzyme Q10 in different fats and oils

Coenzyme Q10 has highest solubility in MCT oils (Neobee M-5, 895, 1053) among the oils as shown in Figure 32. Among soft fats, cocoa butter has shown highest solubility. The difference in solubility for CoQ10 in different oils is dependent on temperature and viscosity.(232) Also solubility of CoQ10 also depends on fatty acid composition of the triglycerides in oils. Fats having medium-chain-length fatty acids provided higher solubility than those consisting of long-chain fatty acids. Neobee oils are composed of caprylic and capric acids in triglycerides. Cocoa butter is composed of oleic acid (34g/100g), palmitic acid (25g/100g), linoleic acid (3g/100g), and stearic acid (35g/100g). Wecobees are tailored made cocoa butter substitutes from palm kernel fats.(233)

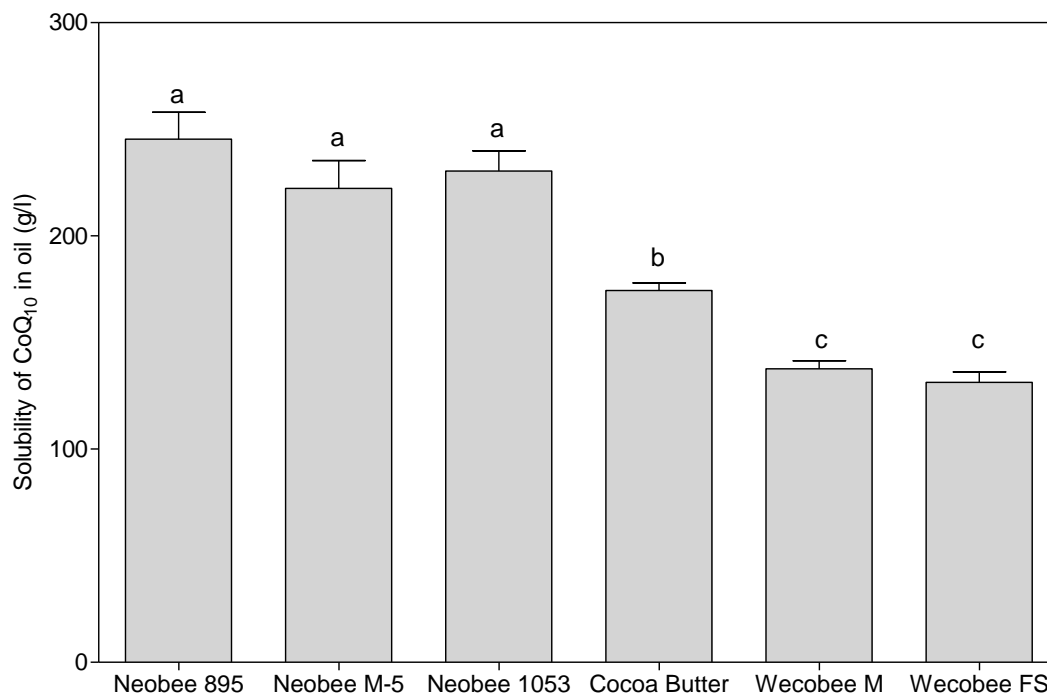


Figure 32 Solubility of CoQ₁₀ in fats. Data shown as mean (n=3), p <0.05

4.3.2 Optimization of Process Conditions

The colloidal carriers have shown to improve the bioavailability of orally administered poorly soluble drugs since the reduction of drug particles to the nanoscale increases dissolution velocity and saturation solubility, leading to improve in vivo drug performance. (234-236) High pressure homogenization has proved to be the most effective method to minimize the large particles in the dispersion.(195) Among different pressure and number of cycles conditions for high pressure homogenization, processing at 1000 bar and 20 cycles gave the smallest and stable nanoparticles, as shown as Figure 33. Initial decrease of particle size with increasing number of cycles occurs due to further dispersion of lipid phase. After 20 cycles, there is a slight increase in the emulsion droplet size due to coalescence. The droplets coalesce due to high kinetic energy gained from homogenization step. The kinetic energy beyond the barrier of electrostatic/steric repulsion can destabilize the system and promote coalescence that would increase the particle size. When subjected to higher pressures (not shown), the emulsions had a gel-like consistency.

Particle size of the SLN was slightly increased with increase in loading of CoQ10 as shown in Table 10. Mixed system of lipids do not have organized crystal form and the packing of fat triglycerides is effected by formation of a mixed crystal.(237)

CoQ10 can also be emulsified with Span60/Tween60 mixture of surfactants. The particle size is also significantly higher than lipid mixture of Coenzyme Q10 and cocoa butter. In contrast of micro particles, recrystallization and formation of nanocrystals can be delayed by hours, days or months with decreasing particle size, decreasing lipid and increasing surfactant content.(196)

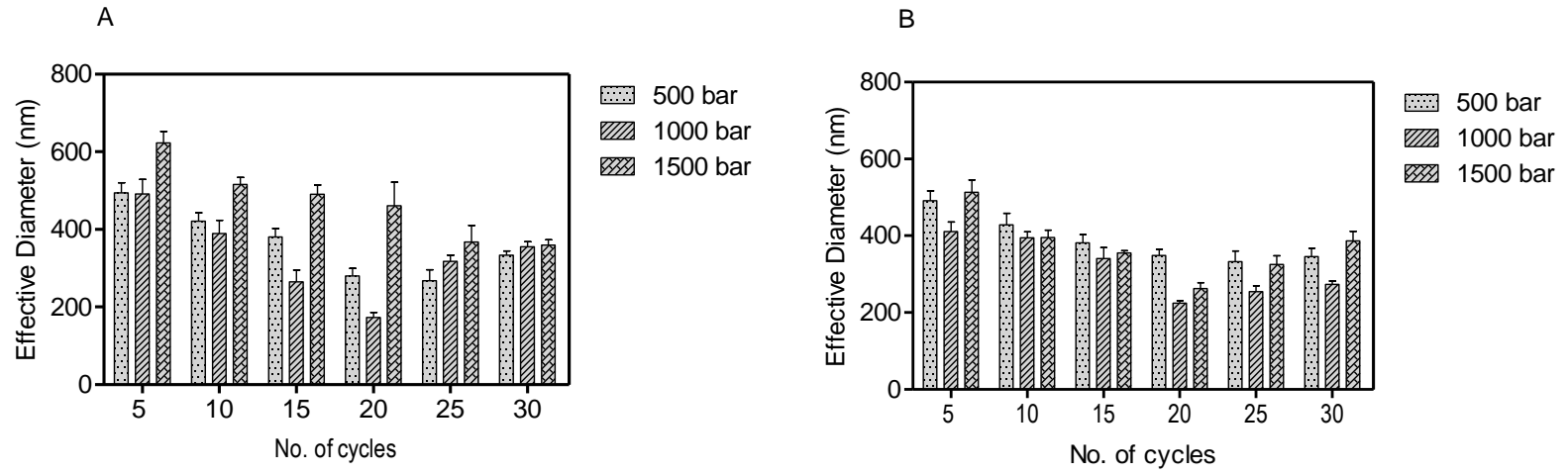


Figure 33 Effective diameter of the cocoa butter nanoparticles with loading 0.5% (A) and 2% (B) at different pressures and number of cycles

Table 10 PCS diameter and polydispersity index in 0.01M NaCl of 10% Cocoa butter and 2% emulsifiers (87% w/w Span60 and 13% w/w Tween60)

CoQ10 (w/w)	0% (w/w)		0.5% (w/w)		1.0 % (w/w)		2.0 % (w/w)		10.0% (w/w)		
	Pressure (bar)	D _{eff}	PI	D _{eff}	PI	D _{eff}	PI	D _{eff}	PI	D _{eff}	PI
500		321.8±	0.324±0.	342.6±	0.321±0.	376.5±	0.421±0.	316.5±	0.421±0.	-	-
		1.5	002	4.2	021	3.5	011	2.8	011		
1000		163.9±	0.304±0.	224.9 ±	0.289±0.	239.8±	0.284	254.4±	0.281±0.	305.7±	0.288±0.
		10.46	003	14.5	014	23.4	±0.01	5.2	007	4.1	005
1500		365.4 ±	0.423±0.	274.3 ±	0.269±0.	293.8±	0.214	331.7±	0.241±0.	364.4±	0.327±0.
		5.7	005	2.9	034	3.0	±0.015	3.7	017	5.2	005

4.3.3 Storage stability of the formulations

The particle size of nanocarriers was not altered during the storage period for 7 weeks. The factors that cause instability of emulsions like coalescence or flocculation would have formed larger particles with progress of time. Figure 34 depicts the effective diameter of the cocoa butter nanoparticles with different loading of CoenzymeQ10 over 7 weeks and there is no significant change over time. The nanoparticles can be considered as kinetically stable over time without aggregation which would lead to creaming and phase separation. It also suggests that CoQ10 molecules are effectively entrapped in lipid matrix during the storage. Also optical images of each formulation (Figure 35) confirmed the absence of crystals or other forms suggesting stability of the system.

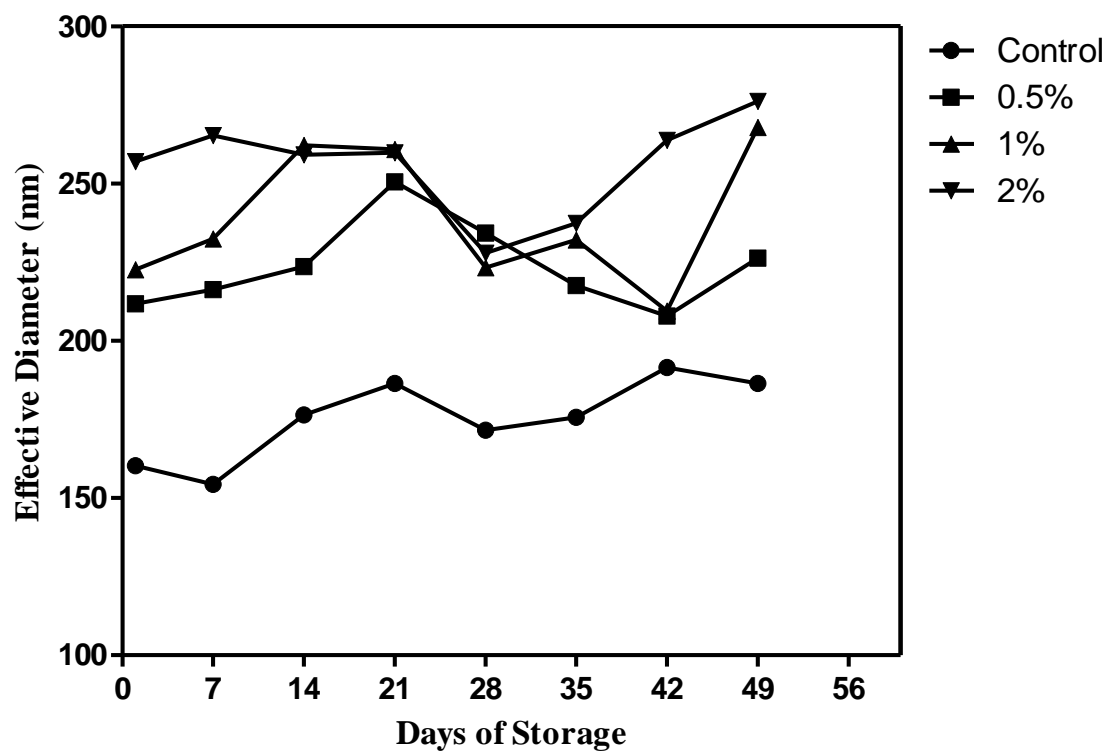


Figure 34 Effective diameter of CoQ10 CB SLN formulation over 7 weeks of storage at 25°

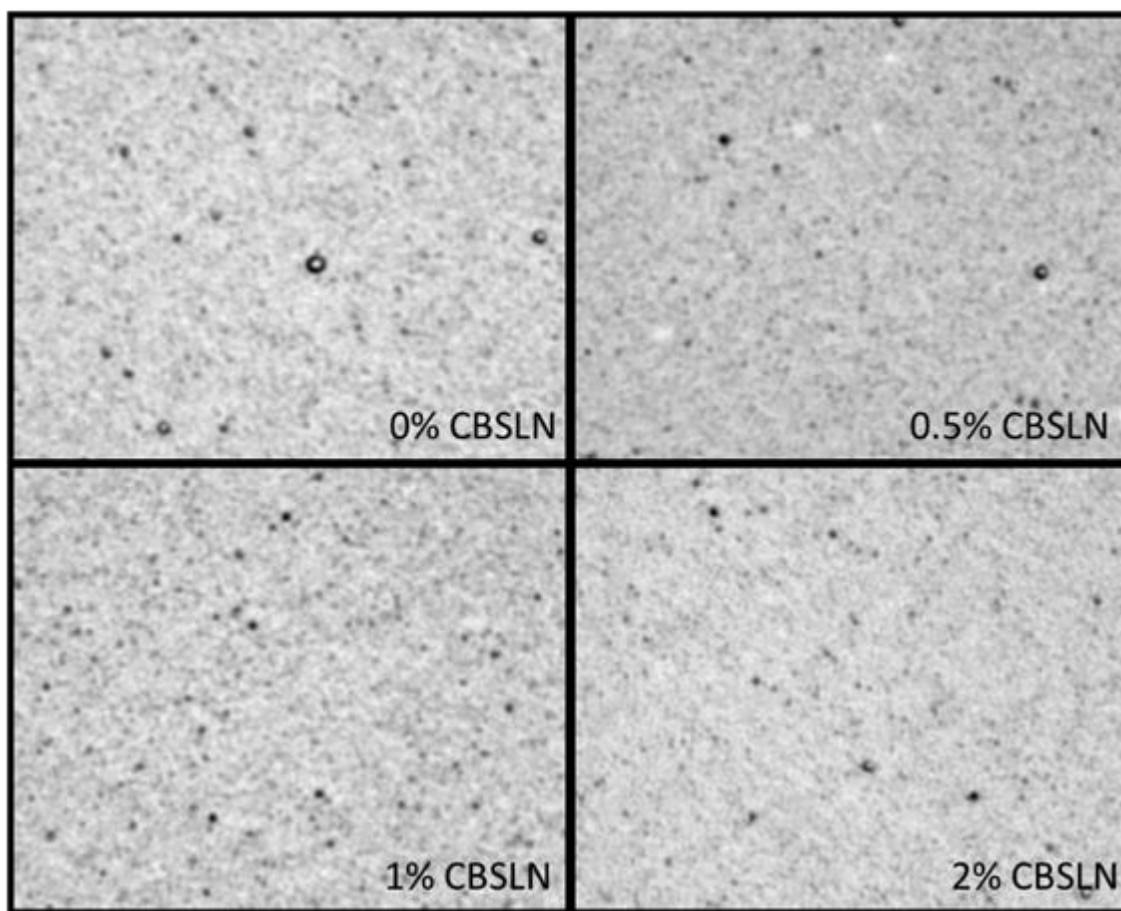


Figure 35 Optical Images of the CoQ10 CBSLN formulations after 7 weeks of storage

4.3.4 Stability after sterilization

To understand the stability of the SLN after sterilization, the formulations were autoclaved and the size of the particle was measured before and after sterilization. The hydrodynamic diameter of CoQ10-CBSLN increases due to sterilization by 9% but relatively insignificant change in CBSLN as shown in Figure 36. This could influence the stability and entrapment efficiency. The polydispersity index hasn't changes before and after sterilization. (0.21 ± 0.004) this confirms that SLN's stability towards sterilization treatments which is HACCP based processing step in beverages and pharmaceutical applications.(195, 238)

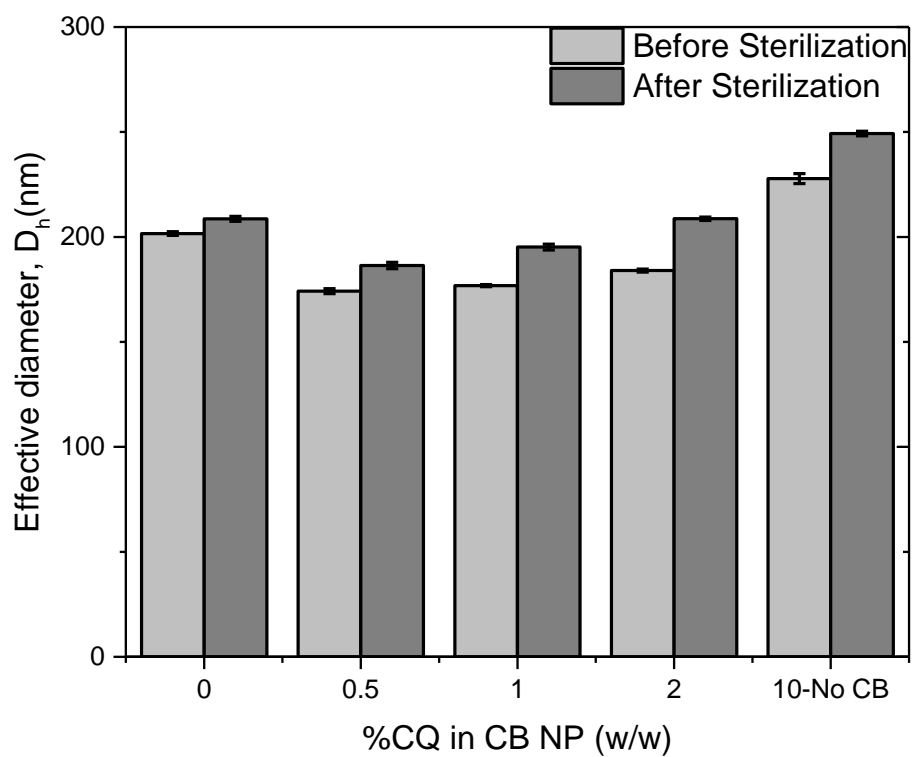


Figure 36 Effect of Sterilization on the particle size of CoQ10 CBSLN formulations

4.3.5 Encapsulation Efficiency of Coenzyme Q10 in Cocoa butter nanocarriers

Cocoa butter SLN show a very effective encapsulation for Coenzyme Q10 to almost 100% efficiency as shown in Table 11.

One of the contributing factor to increase encapsulation efficiency is due to polymorphic state of cocoa butter.(239) Since cocoa butter has multiple crystal forms than other hard fats which form ordered crystal structure, (β form)(240). Imperfection in crystals provide space in the lipid matrix for drug molecules to accommodate. This would increase the efficiency of encapsulation. To assess the encapsulation parameters in colloidal carriers such as lipid nanoparticles, previous separation of the systems from the aqueous external phase is required. This can be performed by ultracentrifugation and/or ultrafiltration techniques. Ultracentrifugation methods require application of centrifugal force for the separation of the nanoparticles from the aqueous medium, which might possibly destroy the carriers. Another factor that influences encapsulation of CoQ10 is due to its high hydrophobicity and also its high solubility in cocoa butter. Also, from optical images of the formulations have shown no CoQ10 crystals or other forms as shown in Figure 35. Other studies have also shown that SLN and other nano-sized lipid formulations have successfully entrapped drug and vitamins.

In a study conducted by Veerawat Teeranachaideekul et.al (241), similar results are were shown. This result is due to the high lipophilicity of CoQ10, the high solubility of the active both in the oil (Miglyol®812) and in the wax (cetyl palmitate), in addition to its low solubility in water (solubility of Q10 in water = 4 ng/ml)(242). However, Q10-loaded nanoparticles produced via microemulsions technique showed an E.E. of about 74%, most likely due to the type and the amount of surfactant used to stabilize the systems.(243)

Table 11 Encapsulation Efficiency (EE%) of Coenzyme Q10 in SLN formulations with different loading % before and after sterilization

SLN Formulations (loading % w/w)	Encapsulation Efficiency (%) Before Sterilization	Encapsulation Efficiency (%) After Sterilization
0.5%	98.4± 2.2	93.6±4.7
1%	96.4± 1.1	89.5±3.8
2%	95.2± 2.1	85.7±3.1

4.3.6 Crystallization behavior of Cocoa butter and Coenzyme Q10 in formulations

Different properties of cocoa butter are dependent on its fat crystal forms which have different types of crystal lattices and thermodynamic stabilities. CB can exist in 6 polymorphs termed Type I – Type VI which represent fat crystals of increasing thermodynamic stability. The crystal forms arise due to presence of triglycerides (TAG) that have C:16, C:18 and C18:1 fatty acid chains and their composition that varies among different sources. Tri-saturated TAGs form fractions with highest melting points above 50°C which are the most stable and highly organized crystal than polyunsaturated TAGs with melting points around 4°C. Saturated fatty acid chains of CB are packed closer and phase separate from unsaturated fatty acid chains due to their low solubility in mono-saturated fatty acids which makes ~80% of CB.(244) Polymorphism in CB makes it an ideal candidate for lipid based delivery system for non-polar bioactives as its fat crystals can reorganize itself after loading and remain stable.

From heating curve of CB (Figure 37- IIA), it was observed that most of CB exists in stable polymorphs (Type III-VI or α , β'' , β' and β forms) with high melting point around and above 25°C. Cocoa butter exhibits polymorphism in its natural state and mostly present as high melting point fractions. High melting fractions in pure CB indicates relatively high % of saturated fatty acid in TAGs. On cooling CB from 90°C at a steady rate of 2°C/min, two-thirds of CB was present in unstable form I / γ -form and rest was present in relatively stable form II-III. Cooling rates can manipulate the generation of different polymorphs and therefore, it becomes a crucial process parameter in preparation of lipid nanoparticles. Cocoa butter in nanoparticles transform into a metastable α polymorph and a small peak due to emulsifier around 50 °C (Figure 37– IIIA). Coenzyme Q10 has a melting point at

50°C and exists as super-cool melt during recrystallization (Figure 37 – IA and IB). This could one reason to explain the high loading and stability of formulations due to lack of phase transitions of CoQ10. With CoQ10 in the lipid core, different polymorphs of CB are formed. At low loading, CB has mostly metastable α form (Figure 38– IA and IB). Polymorphism is displayed in CB nanoparticles with higher amounts of CoQ10 (Figure 38 – IIA and IIIA). Recrystallization confirmed that cooling rates can influence the lattice stacking of acyl chains of CB triglycerides. (Figure 38 - IB, IIB and IIIB)

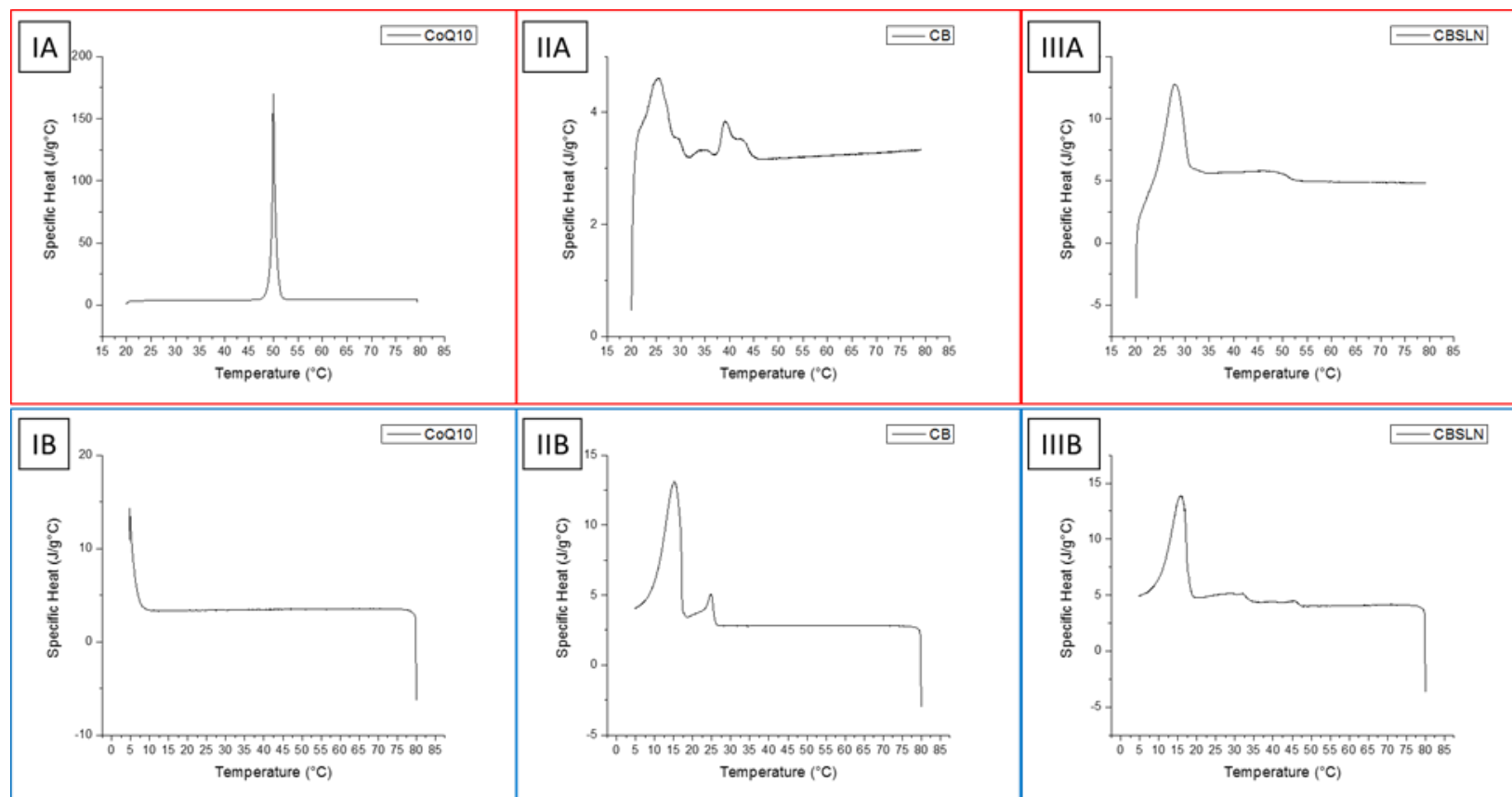


Figure 37 DSC thermograms of the components, Coenzyme Q10 (I) and Cocoa butter (II) and control CBSLN (III) during melting (A) and recrystallization (B)

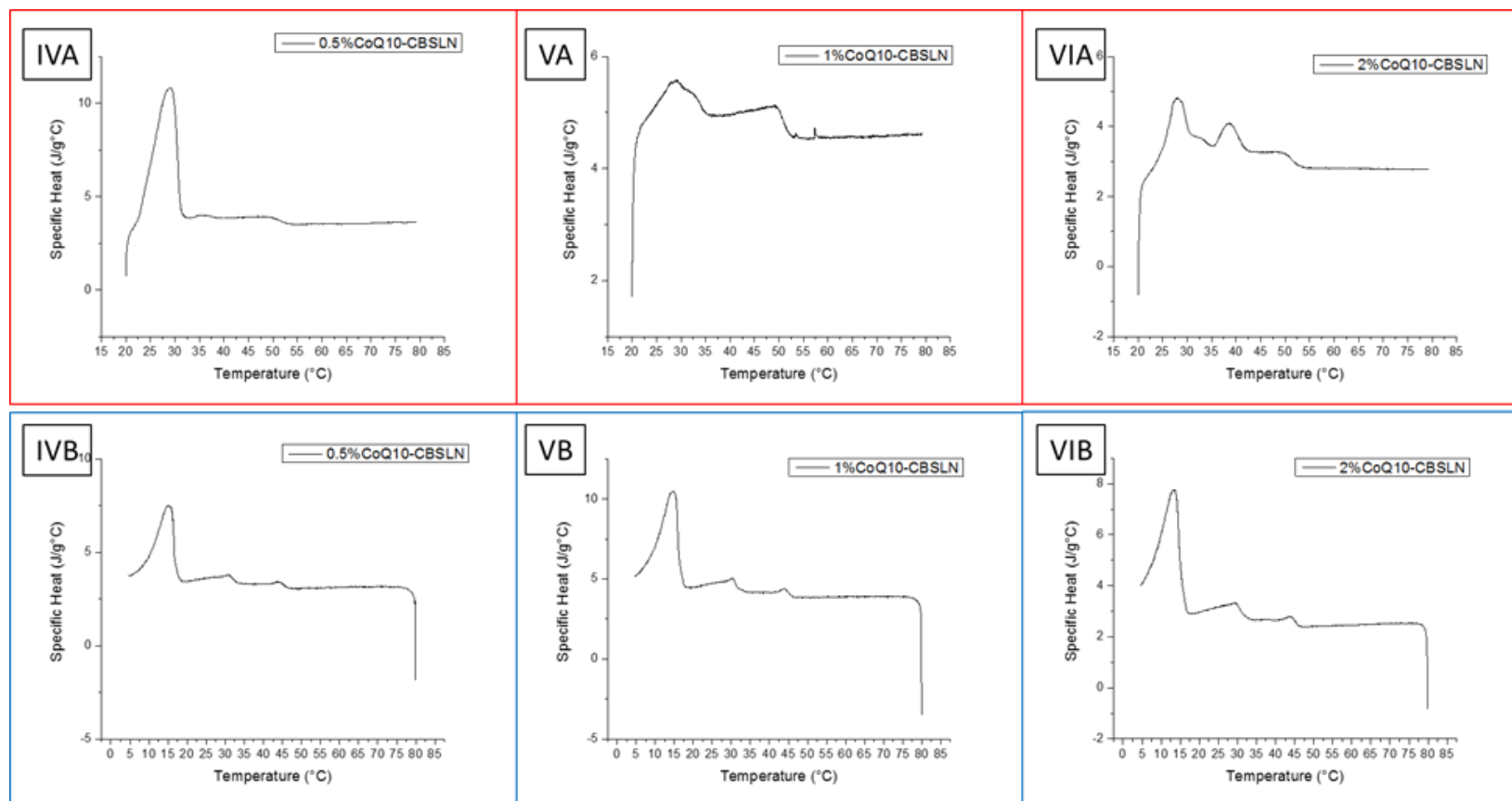


Figure 38 DSC thermograms of the formulations, 0.5% (IV), 1% (V) and 2% (VI) CoQ10-CBSLN during melting (A) and recrystallization (B)

4.3.7 Small Angle X-Ray Studies

SAXS intensity profile is recorded to understand the aggregation and nature of the interface in Figure 39. At small q range, aggregation of lipophilic droplets in the water-based emulsion can be viewed comparing the one with 200-fold dilution. This aggregation in the spatial scale larger than 65nm, which may suggest the scattering intensity majorly contributed from interfacial scattering since the hydrodynamic radius of the particles is around ~250 nm. Beyond the Porod region in intermediate q -range, the interfacial scattering show typical peaks at around 3.2nm and 5.0nm. Loading of CoQ10 has negligible impact on the peak in dilute CBSLN dispersion, but shift the thickness of one kind of interface from 4.9 to 4.5 nm upon 2% of CoQ10 loaded. The other peak keeps unchanged, which may not interact with the cargo. The peaks and the whole scattering profile in consideration of interfacial scattering is quite uniform. Additionally, the electron density contrast between surfactant and the continuous phase is the largest.

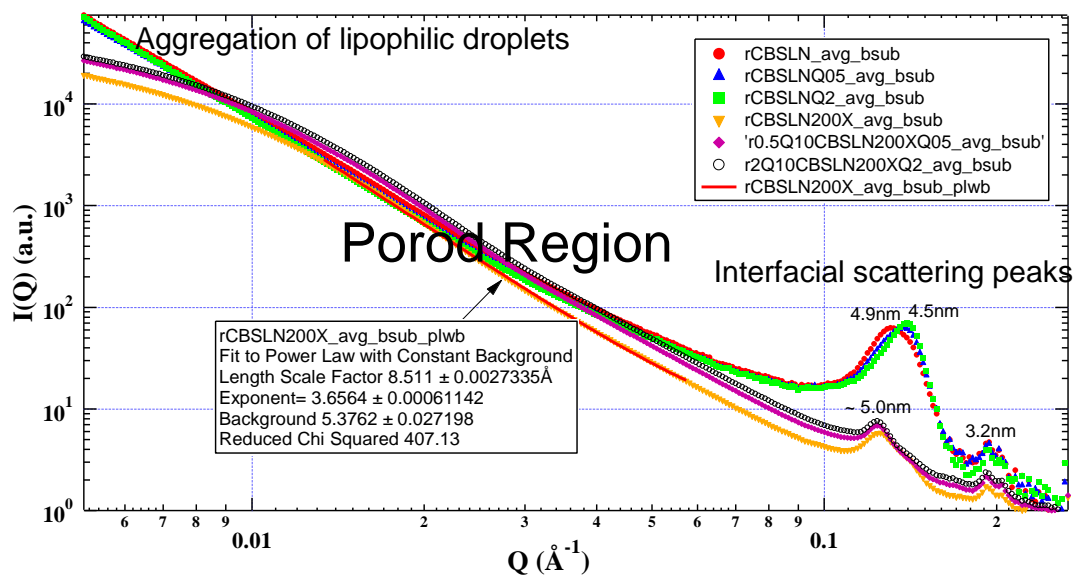


Figure 39 SAXS intensity profile of CBSLN loading CoQ10

4.4 Conclusions

Cocoa butter forms stable lipid nanoparticles which can carry lipophilic bioactive in their lipid core. Solubility of bioactive in the carrier lipid is a critical parameter for production and storage stability of these formulations. Stability of nanoparticle in different process conditions and treatment (eg. Sterilization for beverage application) is essential to test a formulation potentiality in upscaling its production for different applications. Cocoa butter nanoparticles could achieve high encapsulation efficiency for coenzyme Q10 which could be explained from crystallization studies and SAXS intensity profiles. Polymorphism of CB, super-cooled melt state of CoQ10 and interface properties contribute to the stability of CoQ10 loaded CB nanoparticles.

CHAPTER 5. COENZYME Q10 LOADED COCOA BUTTER NANOPARTICLES: BIOACCESSIBILITY AND BIOAVAILABILITY

5.1 Abstract

Studies on Coenzyme Q10 (CoQ10) have shown its potency against heart related diseases in humans but due to high molecular weight and hydrophobicity, it has low bioavailability. Bioaccessibility of CoQ10 in mixture of CoQ10 and CB, emulsified CoQ10 (with same surfactants used in SLN) and CoQ10-CBSLN were assessed and compared using in-vitro lipolysis and HPLC analysis of the aqueous and insoluble phases. Bioaccessibility due CoQ10-CBSLN of different loading was eight times greater than that of emulsified CoQ10. These results suggest that micelles formed from fatty acids released by increased lipolysis rate of CBSLN can act as vehicles to carry CoQ10 to make it more accessible for gastro-intestinal absorption. This nano delivery system can be extended to encapsulate other hydrophobic bioactives.

5.2 Materials and Methods

5.2.1 Materials

Cocoa butter (manufacturer: Spectrum Chemical Mfg. Corp.) is purchased from vendor, VWR International. Coenzyme Q10, reduced form (95%, UV) was purchased from Hangzhou Joymore Technology Co., Ltd. China. Surfactants were acquired from Sigma-Aldrich (St. Louis, MO). HPLC-grade water (0.22 μ m filtered), ethanol 200 proof (HPLC and spectrophotometric grade) and methanol (general use, HPLC-grade) were purchased

from Pharmaco-AAPER (Brookfield, CT). Lecithin (Phospholipon 85G) was a gift provided by American Lecithin Company (Oxford, CT). Pancreatin with 8X USP specification, Sodium taurodeoxycholate (Na TDC) and Tris maleate were obtained from Sigma Aldrich (St. Louis, MO).

5.2.2 In-vitro lipolysis of CoenzymeQ10 in Cocoa butter formulations

Food intake can influence the concentrations of bile salts and endogenous phospholipids in the small intestine lumen are higher in the fed state than in the fasted state. To replicate the same luminal environment, two lipolysis buffers were prepared corresponding to the fasted and fed states as shown in Table 12. The procedure of *in vitro* lipolysis experiments was described in the published literature (245) and was previously performed in lab. (246, 247) Briefly, pancreatin preparation was made by mixing 1 g pancreatin with 5 ml fasted/fed-state buffer, centrifuged and kept on ice. In 9 ml fasted/fed-state buffer, 0.25 g lipid phase and 1 ml pancreatin preparation were added to start the lipolysis. During the 2 hr lipolysis, the pH was maintained at 7.50 ± 0.02 by adding 0.25 N NaOH and temperature was kept at 37 ± 1 °C. The volume of consumed NaOH over time was recorded throughout the lipolysis experiments.

The final lipolysis solution after digestion were ultra-centrifuged at 50,000 rpm (Type 60 Ti rotor, about 180,000g, Beckman Coulter) for 60 min. The aqueous phase was filtered through 0.22 μm filters. The filtrate was directly used to measure the particle size of the mixed micelles. The filtrate is acidified to pH 7 using HCl and was mixed with one volumes of ethanol for HPLC analysis.

Table 12 Chemical composition of Fasted and fed state buffer for in-vitro lipolysis

Chemicals	Fasted state	Fed state
Tris maleate (mM)	50	50
NaCl (mM)	150	150
CaCl ₂ .2H ₂ O (mM)	5	5
Sodium taurodeoxycholate, NaTDC (mM)	5	20
Phosphatidylcholine (mM)	1.25	5

5.2.3 Calculations for the percent bioaccessibility

The percent bioaccessibility was calculated as:

$$\% \text{ Bioaccessibility} = \frac{\text{mass of solubilized Coenzyme Q10}}{\text{mass of Coenzyme Q10 in lipid}} \times 100$$

The mass of solubilized CoQ10 was the product of the concentration of solubilized CoQ10 in the aqueous phase after lipolysis and the volume of the aqueous phase. The mass of CoQ10 in lipid was calculated from the concentration of the CoQ10 in oil, mass of the oil (0.25 g) based on the entrapment efficiency and the density of the cocoa butter which is 0.876 g/ml.

5.2.4 Calculations for extent of lipolysis

The percentage amount of digested triglycerides is accounted by the extent of lipolysis. It was assumed that there were exclusively triglycerides in the basic oils, and that digestion of one molecule of triglycerides released exactly two molecules of fatty acids and consumed two molecules of NaOH. Consequently,

$$\text{Extent}_{\text{lipolysis}} = \frac{\text{Vol}_{\text{NaOH}} \times [\text{NaOH}]}{2 \cdot \text{Mole}_{\text{triglyceride}}} \times 100\%$$

Where Vol_{NaOH} is the volume of NaOH consumed in the lipolysis for digestion. $\text{Conc}_{\text{NaOH}}$ is the concentration of NaOH (i.e., 0.25 M). $\text{Mole}_{\text{triglyceride}}$ of 250 mg lipid was calculated from the average molecular weight of the triglycerides, which was estimated using the saponification value of the oil:

$$Mw_{\text{triglyceride}} = \frac{3 \times 1000 \times Mw_{\text{KOH}}}{SV}$$

Where Mw_{KOH} is the molecular weight of KOH, the mass of which is used to express the saponification value (SV). SVs used for cocoa butter is 193.

5.2.5 Quantitative assay of coenzyme Q10

An UltiMate 3000 HPLC system with 25D UV-VIS absorption detector (Dionex) and was used with a C₁₈ reversed-phase column (Phenomenex™ Luna™ 5 µm C18 (2); 150x4.6 mm); a 6/4 mixture of ethanol/methanol as an isocratic mobile phase; 1.0 ml min⁻¹ as a flow rate and 50 µl as injection value; UV detection at 275 nm. Standard curve was calculated by using low concentration of CoQ10 (10, 25, 50, 75 and 100 µg/ml).

5.2.6 Animals

Wistar WU rats aged seven weeks were purchased from Charles River Laboratories (NY, USA). Animals were randomly divided into control and experimental groups after 1 week of acclimation. All mice were maintained in a controlled atmosphere (25 ± 1 °C at 10% relative humidity) with 12 h light/12 h dark cycle. All animals were fed with Purina Laboratory Chow 5001 and ad libitum water (Ralston-Purina, Co., St. Louis, MO). The experimental protocol was approved by Rutgers University (no. 99-015).

Three castrated male pigs (PIC) weighing 32.1±3.45 kg, were used in this study. They were reared indoors and fed daily with drug-free commercial pellet diet. Pigs were allowed to free access to drinking water. The animals were humanely handled according to the approved IACUC protocols in China.

5.2.7 Pharmacokinetics studies and Body distribution of Coenzyme Q10 in Rats and Pigs

40 Wister mice used in the pharmacokinetics study were fasted overnight before administrating 100 mg/kg of CoQ10 and 2%CoQ10 CBLN formulation through oral gavage. At selected time intervals (3,6, 12 and 24h), blood samples were taken after the

animals were sacrificed by CO₂ asphyxiation and whole blood samples were acquired through cardiac puncture. Collected whole blood samples were immediately centrifuged at 5000g at 4 °C for 15 min. Plasma was collected and stored at –80 °C until later HPLC analysis.

For HPLC analysis, a final concentration of 10 µg/mL of CoQ-8 in hexane was added to 500 µl of thawed plasma sample as an internal standard. The inoculated plasma was then extracted by combining with 1 ml of ethanol and centrifuged at 16000g for 20 min at ambient temperature. The extract was further purified by mixing thoroughly 3 ml n-hexane, and centrifuged again at conditions above. After centrifuging, the supernatant was collected in a separate container and then dried under nitrogen. The dried samples were dissolved again in 100 µl of ethanol and were used for HPLC analysis. Peak concentration (C_{\max}) and time to peak concentration (T_{\max}) were recorded from the analysis of plasma concentration–time curves. The total areas-under-curve (AUC) of the time–concentration plot were calculated using the linear trapezoidal rule. The apparent elimination rate constant (K_{el}) was obtained from the terminal linear regression slope of logarithmic-transformed plasma concentration–time curves.

Concentration-time profiles of CoQ10 in blood plasma after oral administration in pigs were calculated using Latin Square design, which eliminates the effect of the body weight on the pharmacokinetic parameters. Three pigs were given a single dosage of pure CoQ10 and 2% CoQ10-CBLN formulations (100 mg/kg). Blood samples were collected from the superior vena cava by venipuncture into tubes containing CoQ-8 as internal standard before dosage and at 1, 2, 3, 4, 8 and 12 h after oral administration. All blood

samples were centrifuged at 1000g for 10 min at room temperature (25 °C). The separated plasma samples were kept at -20 °C until HPLC analysis.

To measure CoQ10 levels in different organs (heart, kidney, liver, small intestine), every organ was measured carefully, homogenized and acidified to pH 3 to break down the tissue. Methanol was used to precipitate the macromolecular components of the tissue suspensions. Extraction of CoQ10 was performed by using ethanol and hexane solvents before HPLC analysis.

5.2.8 Data analysis

Pharmacokinetic parameters of CoQ10 were calculated using non-compartmental methods. Concentration-time profile curves were constructed and parameters, maximum concentration peak (C_{max}) and t_{max} , (time when C_{max} appears) were noted.

The area under the plasma drug concentration-time curve (AUC) reflects the actual body exposure to drug after administration of a dose of the drug and is expressed in $\mu\text{g/ml}\cdot\text{h}$. The area under the curve, $AUC_{0-\infty}$ was calculated using trapezoidal rule in MS Excel® software.

5.2.9 Statistical Analysis

All experiments were performed in triplicates. Statistical analysis of the data from all the experiments was conducted using Origin 9.0 software. One-way analysis of variance (ANOVA) procedure followed by Tukey's mean comparison test was used for establishing the significance of differences among mean values at $p < 0.05$. The results were reported as the mean standard \pm deviation (SD).

5.3 Results and Discussion

5.3.1 Effect of Coenzyme Q10 loading on extent of lipolysis in lipid mixtures and in CB nanocarriers

The extent of lipolysis is crucial in determination of the solubility and structural stability in the gastrointestinal environment. In-vitro studies of lipolysis analyze the enzymatic reaction of pancreatic lipase on orally administered formulation. Mathematically, extent of lipolysis accounts for release of free fatty acids from triglycerides and other products of digestion. The release of fatty acids lowers the pH which reduces the activity of lipase by moving away from optimum pH. To counter this, sodium hydroxide (NaOH) is added which mimics the alkaline secretions from pancreas to maintain pH around 7.5.

Different factors can influence the reaction parameters of enzymatic action of pancreatic lipase. Temperature, pH, concentrations of bile salts and emulsifiers are maintained to represent two different conditions in small intestine— fed and fasted states. In post-meal conditions, increased amount of pancreatic secretions and micellar phase improves solubilization and composition of GI fluids and longer residence times increase absorption.

Structure and fatty acid composition of triglycerides that makes up the nano-delivery systems greatly influences the digestion and absorption process. Pancreatic lipase has greater activity on medium chain triglycerides (MCT) than long chain triglycerides (LCT) in duodenum.(248) Droplet sizes and their TAG composition can significantly affect enzymatic action of lipases. Enzymatic hydrolysis of smaller droplet diameter and higher

percentage of MCT in the core material of emulsions is higher than that of bulk material.(249)

Cocoa butter is primarily composed of long chain triglycerides with palmitic acid, oleic acid and stearic acid. By using CB in form of nanoparticles, they convert into nano dispersions on consumption at body temperature 37°C. Smaller size of droplets facilitates lipolysis by increasing the reactive interface area but has no effect of assimilation of the digestion products. (250) Pancreatic lipase acts on esters bonds between fatty acids and glycerol at positions *sn1* and *sn3* in a triglyceride which produces two free fatty acids (FFA) and one 2-monoacylglyceride.

In the *in vitro* lipolysis experiments, the extent of lipolysis of the cocoa butter mixtures and their SLN formulations was also estimated in Table 13. From two-way ANOVA analysis, there was no significant difference. In addition, the extent of lipolysis was higher in the fed state than in the fasted state, which was consistent with previous results. (245, 251) From Figure 40, it is observed that fatty acid release from CoenzymeQ10 loaded formulations was lower compared to control CB nanoparticles by 32-42%. There is no linear relationship of total % of CB and % of fatty acid release. A possible explanation could be interactions of lipase with the products of digestion and free CoQ10 that might inhibit the enzymatic activity. Also, the amount of fatty acids released from lipolysis also influence bioaccessibility of CoenzymeQ10.

Table 13 Extent of Lipolysis of different Cocoa butter based mixtures and SLN formulation of CoenzymeQ10

		Extent of Lipolysis	
		Fed State	Fast State
Cocoa Butter	Bulk	43.2±3.2	38.5±5.3
	SLN	55.4±4.3	51.8±3.9
0.5% CoQ10	Mixture	20.5±3.4	17.4±5.4
	SLN	27.6±4.1	24.6±3.7
1.0% CoQ10	Mixture	16.5±6.2	19.4±2.8
	SLN	25.6±3.7	21.5±2.7
2.0% CoQ10	Mixture	22.5±3.6	23.4±3.2
	SLN	28.5±4.3	26.8±5.7
10.0% CoQ10	Powder	2.4±1.2	3.2±0.9
	SLN (no CB)	3.2±2.1	4.3±1.2

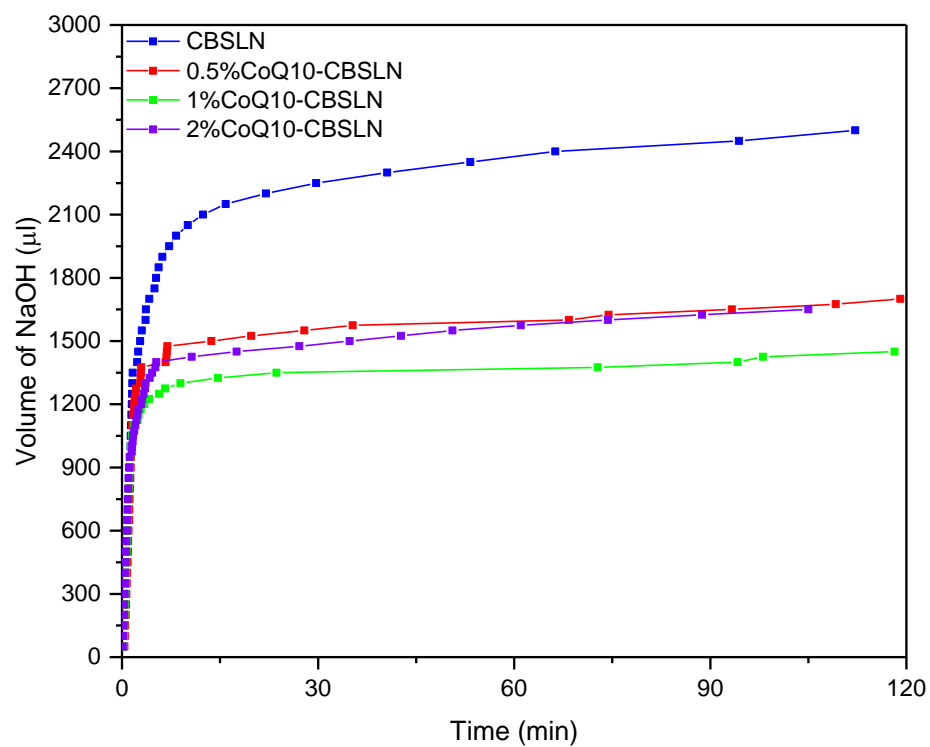


Figure 40 Consumption of NaOH during the lipolysis for different SLN formulations in fed state condition

5.3.2 Improved bioaccessibility of Coenzyme Q10 in CBSLNs

Different amounts of CoenzymeQ10 was encapsulated in cocoa butter in form of lipid nanoparticles and in similar way, same amounts of CoenzymeQ10 are mixed with cocoa butter to form lipid mixtures. The percent bioaccessibility of CoenzymeQ10 was determined after *in vitro* lipolysis in both fasted and fed states as shown in Figure 42.

Among all SLN formulations 0.5% CoQ10 CBSLNs had highest % bioaccessibility in fed state on analyzing dissolved CoQ10 in aqueous phase of formulation after in-vitro lipolysis (Figure 41). Results from Figure 42 also revealed that no significant difference was detected in the percent bioaccessibility between the fasted state and fed state (Two-Way ANOVA).

From the above results, release of free fatty acids after hydrolysis of TAG is crucial in creating the micellar phase that can solubilize the Coenzyme Q10. The ratio of lipid to loaded bioactive is positively correlated to % bioaccessibility of Coenzyme Q10. In-vitro lipolysis of CB in form of nanoparticles has shown generation of higher amount of free fatty acid release than compared to mixture form, creating higher concentration of micelles with CoQ10. CoQ10 loaded in CB NP has improved bioaccessibility around 70-80% compared to mixture form of same composition.

Results from Figure 40 were corrected by eliminating the solubility of free CoQ10 at 37°C in fed and fast state buffers. This eliminates the portion of solubility contributed by the mixed micelles from bile salts and lecithin alone. Digested reaction mixture after inhibiting enzymatic action by bringing its low temperature at 4°C is subjected to ultracentrifugation to separate the aqueous micellar phase. Since the hydrolysis of TAGs in CB is not complete, the reaction mixture is a multiphase system. Based on lipophilicity

of CoQ10, the partition coefficient between aqueous micellar phase and undigested lipid phase is an important factor that influences its bioaccessibility. Chemical nature of the payload strongly influences partition coefficient in multiphase system.

Another possible reason behind lower bioaccessibility in higher payload in CB nanoparticles is due to limiting concentration of CoQ10 that is entrapped in the lipid core. In our study, it was observed that CoQ10 has tendency to form aqueous nanodispersions with the surfactants that are used to create CB nanoparticles. CoQ10 can be emulsified to form a nanodispersions but has very poor bioaccessibility after in-vitro lipolysis. This could explain why CoQ10 was less bioaccessible in formulations with higher loading %.

Nanodispersions of CoQ10 can be absorbed into the blood stream in a different mechanism compared to CB based nanoparticles. The rate of dissolution of the drug in the stomach and residence time are important parameters that govern the absorption efficiency unlike the absorption of mixed micelles. There are 2 mechanisms for uptake of nutraceuticals: active and passive transport. Passive transport occurs by process of diffusion through epithelial cells which works well for hydrophobic substances. In case of active transport, the water soluble compounds can be transported through the transport channels in the enterocytes of the epithelial lining.

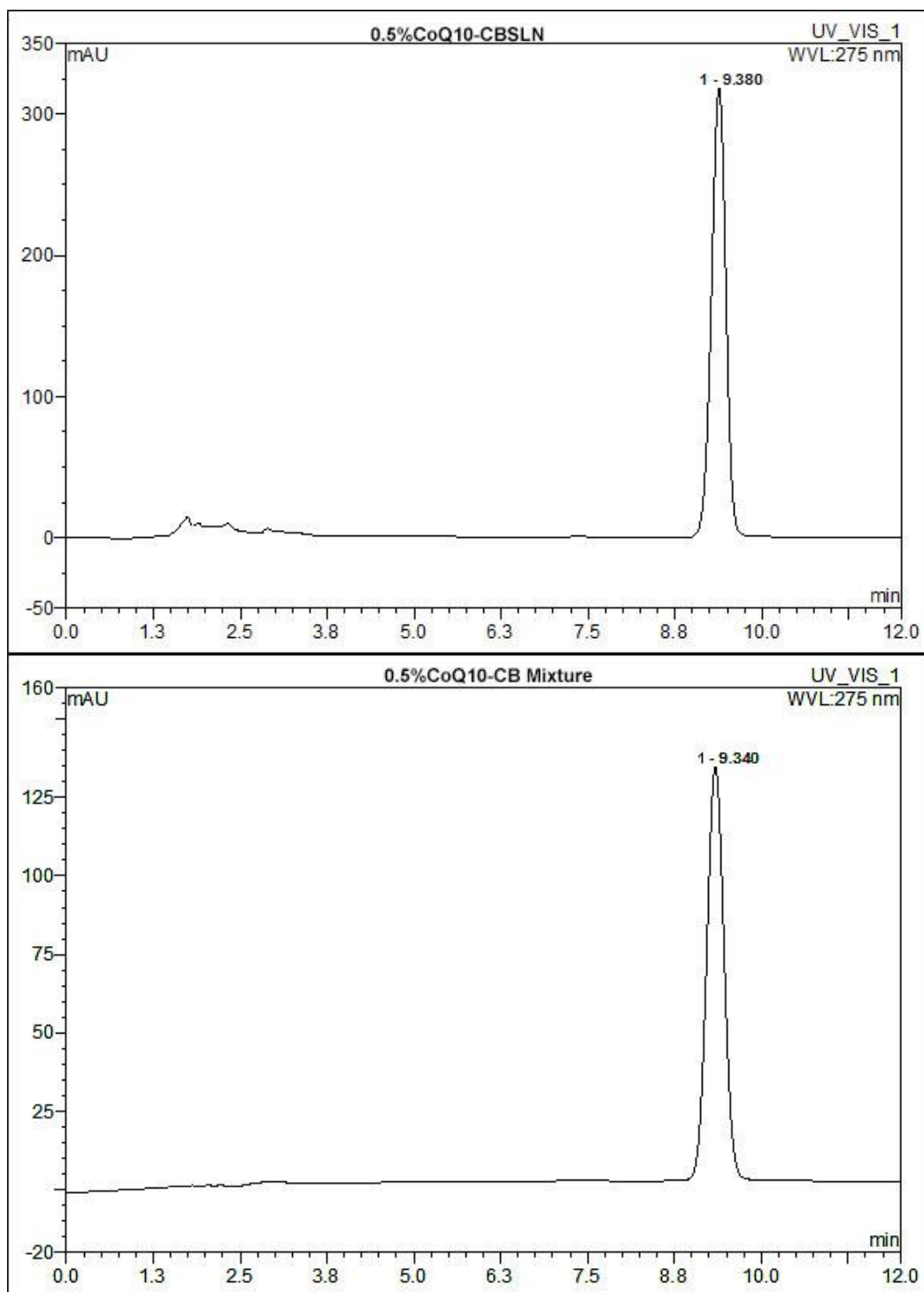


Figure 41 HPLC spectrogram of aqueous phases of 0.5%CoQCBSLN and mixture after in-vitro lipolysis in fed state buffer.

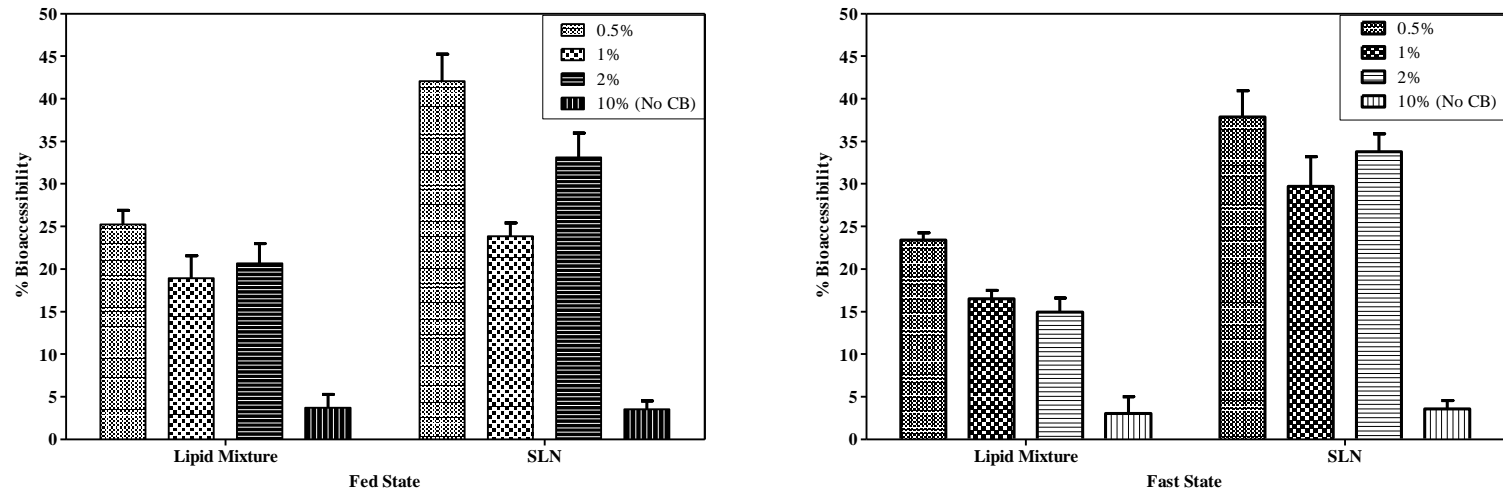


Figure 42 % Bioaccessibility of CoQ10 CBSLN formulations and equivalent lipid mixtures in fed and fast state for in-vitro lipolysis

5.3.3 Pharmacokinetics studies in Rats

To directly investigate the oral bioavailability of CoQ10 in the CB nanoparticles, pharmacokinetics analysis was performed on rats after oral administration with CoQ10 water suspension or in CB nanoparticles. Pharmacokinetic studies reveal the quantities of bioactives that are made bioavailable in different delivery systems which are dependent on physiological factors which include absorption, membrane permeation and metabolism.

As shown in Figure 43, the plasma concentrations of CoQ10 were slightly higher in 2%CoQ10 CBLN than those of unformulated CoQ10. The pharmacokinetics parameters are listed in Table 14. Notably, the C_{max} increased by 1.35 folds at $T_{max} = 3$ hr, and the $AUC_{0-\infty}$ remained the same for both, demonstrating that the nanoparticle formulation was able to improve the oral bioavailability (BA) very marginally. From pharmacokinetic profiles of pure CoQ10, C_{max} for CoQ10 appears only 12 hours. Comparing with other pharmacokinetic studies of powdered and solubilized forms of CoQ10, it can be concluded that this study needs to redone due to inconsistency of plasma profiles of the control, pure CoQ10. In humans, t_{max} for CoQ10 is 6 h and elimination half-life of CoQ10 is around 33.2h. (252) In a similar study, pure and solubilized CoQ10 powder have similar absorption rates (similar t_{max} values).(253) Absorption of pure CoQ10 is very similar to highly lipophilic molecules like Vitamin E. Before and during absorption, ubiquinone-10 is converted in a reduced state, ubiquinol-10. Around 95% of blood CoQ10 is in the reduced form.(254) Similar to fat soluble vitamins, which are absorbed from intestine primarily through lymphatic route. CoQ10 in CB nanoparticle allows rapid release and absorption of CoQ10 within few hours with C_{max} reaching around 1 $\mu\text{g/ml}$ but has poor retention time. This phenomenon could be explained by possible absorption of CoQ10 due to interaction

of nanoparticle and gut wall. On digestion of CB, C16 and C18 long chain fatty acids and their mono- and diglycerides are released which form mixed micelles with CoQ10 and might take lymphatic route during the absorption. Traditional plasma bioavailability studies have limitations in accessing total absorption due to transport of bioactives through lymph.(255) Lymphatic drug transport increases with increase in lymphatic lipid transport as shown in previous studies.(256) Highly hydrophobic molecules like CoQ10 can preferentially cleared from blood into the adipose tissue and effect the overall mass balance of drug absorption. It is suggested that lipophilicity of a drug (high solubility in carrier lipid, and high partition coefficient in 1-octanol/water mixture) has greater tendency to be absorbed in chylomicrons which are major lipoproteins composed of triglyceride core stabilized in aqueous environment of lymph by surface coating of proteins and phospholipids. (257) Molecules with log P values in excess of 5 and lipid solubility (expressed as solubility in triglyceride oil) in excess of 50 mg/ml have found to be lymphatically transported over portal vein route. From lipid absorption studies previously it is suggested that cocoa butter which is mostly composed of long chain fatty acids (C18, C18:1, C16) would preferentially restructure itself in the enterocytes of the small intestine epithelia, enter the core of a chylomicron on exiting the enterocyte and finally secreted into mesenteric lymph. Only medium and short chain fatty acids are quickly absorbed and directly enter the portal vein to reach liver and later into systematic circulation. Both CoQ10 and CB can influence the transport into blood and further their plasma concentrations that are being studied. Surface-active agents (emulsifiers) have shown to effect the lymphatic transport. (258) Since our studies can only quantify relative bioavailability of CoQ10, not the absolute bioavailability.

When working with new lipid based delivery systems, lymphatic transport and related bioavailability cannot be ignored. In addition to estimated systemic bioavailability in non-cannulated animals, lymphatic transport and simultaneous blood absorption should be studied in cannulated animal models. This approach gives a more accurate representation of overall mass balance of the drug before and after administration and subsequently, determines its fate in metabolic and elimination processes in model animals.(255, 259)

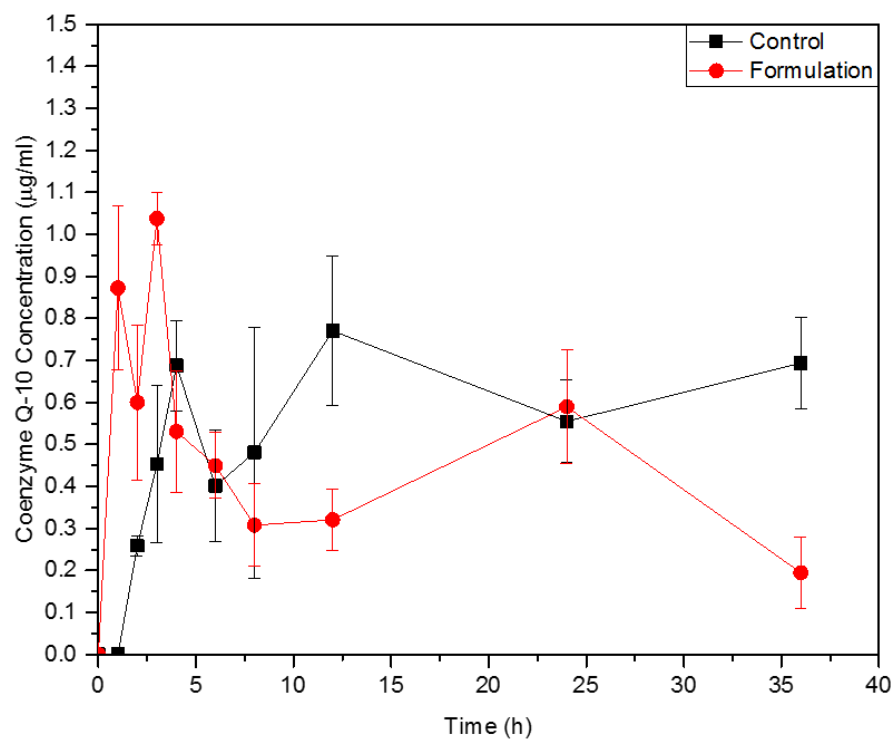


Figure 43 Concentration-Time profiles of 2% CoQ10 CB nanoparticles vs. pure CoQ10 in rats

Table 14 Pharmacokinetic Parameters of CoQ10 Nanoparticles in rats

Sample	CoQ10 Dose (mg/kg)	T_{max} (h)	C_{max} (µg/ml)	AUC 0-24 (µg/ml*h)	K_{el} (h⁻¹)	Relative Bioavailability
Control	100.0	12.0	0.8 ± 0.2	21.0	ND	-
Nanoparticle	100.0	3.0	1.0 ± 0.1	15.9	0.1	0.8

5.3.4 Body distribution of Coenzyme Q10 on single dose administration

Body distribution of a bioactive gives information about the tissue uptake capacity from blood during systemic circulation. From Figure 44, liver had the highest amount of CoQ10 ($33.87 \pm 5.70 \mu\text{g/g}$) on oral administration of 2%CoQ10-CBLN at 24 hours after single dosage (100mg/kg) which is 291% greater than pure CoQ10. Highest amount of CoQ10 was initially observed at 3hour after dosage of 2%CoQ10 in small intestine (210% greater than pure CoQ10) suggesting the entry of mixed micelles with CoQ10 into enterocytes after lipolysis. Other organs (heart and kidney) showed no signs of increase in CoQ10 concentrations even after 24 hours of oral administration. Initial concentrations of CoQ10 (at $t = 0$ hr) were not studied to measure overall uptake % in each tissue. These findings agree with previous studies on rats which have shown that liver and spleen were organs with highest amount of CoQ10 in rats after its dietary supplementation with lipids.(260, 261)

Ubiquinone is biosynthesized in animals which is a protective molecule in oxidative stress and with aging, endogenous synthesis is significantly decreased. Supplementation of CoQ from our diet is beneficial in promoting health and alleviate age-related diseases. Most common species of ubiquinone is CoQ9 in rats, but as much as 10–30% of the total is CoQ10. In humans, CoQ10 is the dominant species over CoQ9 which is just 2-7%.(254) High CoQ10 content are present in the heart, liver , kidney and muscle due to its involvement in electron transport chain in mitochondria and its requirement in metabolic activities with high energy input.(262)

Studies conducted by Zhang Y. *et. al.* have shown content of CoQ10 found in body is dose-dependent and beyond $12\mu\text{mol}/100\text{g}$ body weight dosage, the uptake reaches a

limit.(260) Absorption of Coenzyme Q10 after oral administration is very similar to Vitamin D and its analogs, and cholesterol and α -tocopherol. In a short window of observation (24 hours), CoQ10 is quickly absorbed by liver from blood as indicated in many studies.(263, 264) It can enter the liver in 2 ways: enterohepatic route and lymphatic route depending on type of lipid carrier.

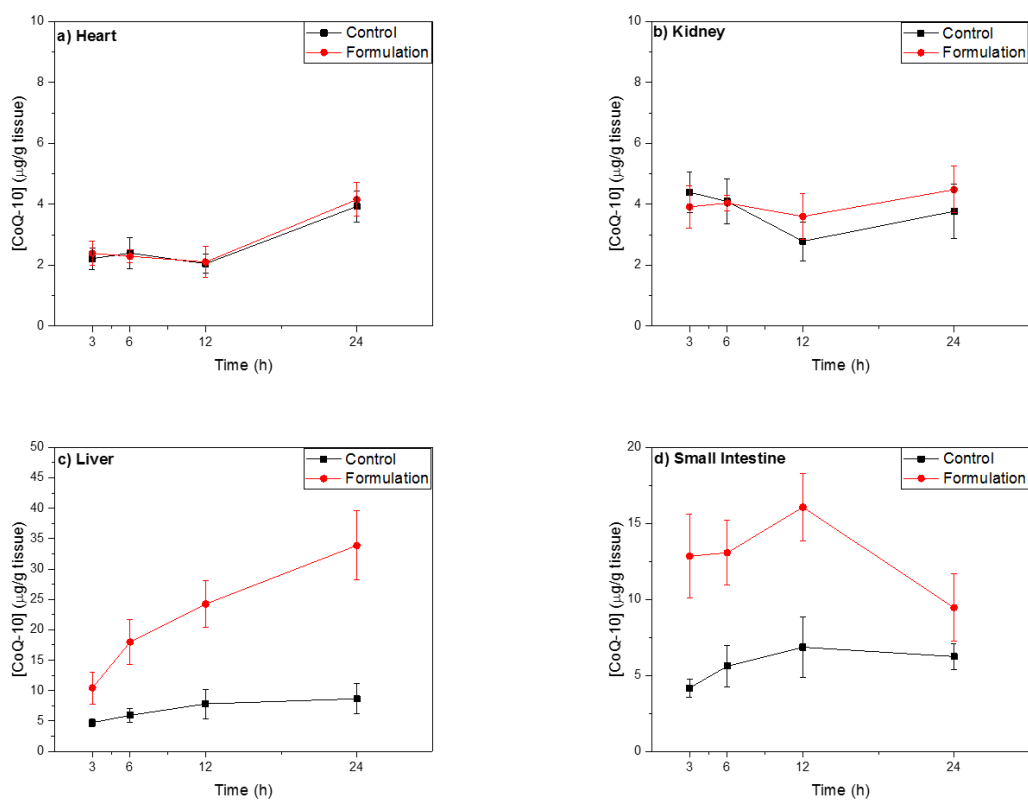


Figure 44 Distribution of Coenzyme Q10 amounts in organs: a) Heart, b) Kidney, c) Liver and d) Small intestine at different time points after a single dose oral administration

5.3.5 Pharmacokinetics studies in Pigs

The pharmacokinetic parameters of pure CoQ10 and 2% CoQ10-CBLN were not significantly different. This is inconsistent with other studies that absorption of CoQ10 improved in presence of lipid. This study needs to be repeated to get more meaningful results. The 2 peaks in the concentration-time profiles is the only consistent trend that was also observed in humans after oral administration.

In humans, CoQ10 peak concentration (C_{max}) reached around 6.5 h after dosage and terminal half-life was 33.2 ± 5 h.(252) In humans, pharmacokinetic profile of CoQ10 fits 3-compartment model which suggests that CoQ10 is absorbed in chylomicrons in enterocytes of small intestines, and then are taken up by liver cells. This phase occurs in first 6 h after dosage and is considered as the absorption phase. At the end of absorption phase, C_{max} is achieved and the following period between 6 and 12 h is called distribution phase. During the distribution phase, CoQ10 is stored in lipoproteins in liver and redistributed during enterohepatic recirculation which leads to appearance of 2nd peak in CoQ10 concentration at 24 h.(265)

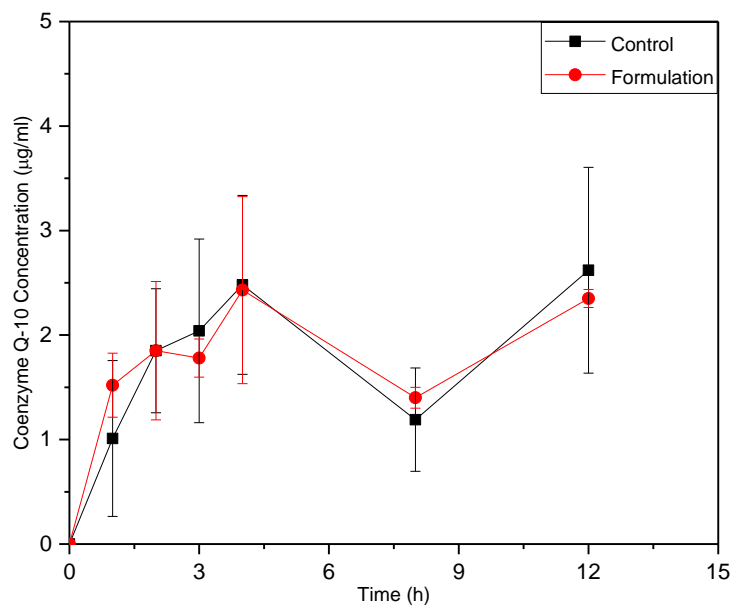


Figure 45 Concentration-Time profiles of 2% CoQ10 CB nanoparticles vs. pure CoQ10 in pigs

Table 15 Pharmacokinetic Parameters of CoQ10 Nanoparticles in pigs

Sample	CoQ10	T _{max} (h)	C _{max} (µg/ml)	AUC 0-24 (µg/ml*h)	K _{el} (h ⁻¹)	Relative Bioavailability
	Dose (mg/kg)					
Control	100.0	12.0	2.6 ± 1.0	21.1	ND	-
		4.0	2.4 ± 0.9	21.5	ND	1.0
Nanoparticle	100.0					

5.4 Conclusion

Bioaccessibility and bioavailability of a bioactive are two important parameters to assess its biological efficacy and these parameters are dependent on the type of delivery system. Bioaccessibility of a bioactive which represents its amount available for absorption across intestinal epithelium is increased significantly for CoQ10 with CB nanoparticles. After subjecting the formulation to lipolysis, the triglycerides of CB are hydrolyzed to fatty acids and glycerides in micellar structures and solubilize CoQ10 in aqueous phase. Later pharmacokinetic studies in rats and pigs are conducted to evaluate systemic exposure of CoQ10 in CB nanoparticles. The plasma concentration kinetics and relative bioavailability couldn't account for CoQ10 fate and mass balance suggesting that CB nanoparticle could possibly take lymphatic route to reach system circulation. Tissue uptake studies for CoQ10-CB SLN follow typical trend seen in other lipid based formulation with small intestine as organ with highest CoQ10 content immediately after dosage and liver having highest CoQ10 concentration at a later period. These studies suggest that lymph-cannulated animal models and related pharmacokinetic studies would give a better understanding of the fate of the bioactive in CB nanoparticles.

CHAPTER 6. CARNOSIC ACID LOADED COCOA BUTTER NANOPARTICLES: PRODUCTION AND CHARACTERIZATION

6.1 Abstract

Lipid based nanosystems are extensively used in pharmaceutical industry for drug delivery strategies and their potentiality in food applications is the central idea of the current research. Cocoa butter (CB) is lipid base of nanocarriers due to its polymorphic nature and carnosic acid (CA), a strong antioxidant and a bioactive from Rosemary was loaded in the carrier using hot-melt homogenization technique to create nanoparticles (NP). The maximum loading capacity of stable CA loaded CB NP was 5.3% dry weight basis with high encapsulation efficiency and improved the bioaccessibility of CA for absorption in in-vitro lipolysis studies.

6.2 Materials and Methods

6.2.1 Materials

Cocoa butter (manufacturer: Spectrum Chemical Mfg. Corp.) is purchased from vendor, VWR International. Carnosic acid (95%, purity) was purchased Wuling Yangguang Biotechnology Co., Ltd., Hunan province, China. Glycerol and surfactants were acquired from Sigma-Aldrich (St. Louis, MO). Medium chain triglycerides (Neobee®) and cocoa butter substitutes (Wecobee®) are obtained as free samples from Stepan Company (Northfield, Illinois). Other chemicals used for analytical purposes are

acquired from Sigma-Aldrich (St. Louis, MO), VWR International (Radnor, PA) and Fischer Chemicals (Hampton, NH).

6.2.2 Solubility studies of CA in water, gastric buffers and lipids

Solubility of CA in various solutions and different lipid was studied. 1g of solvent was taken in a shaded vial and 0.2 g of carnosic was added to it. This mixture was stirred at body temperatures (37°C) for aqueous solutions and in case of lipids, it was stirred at different temperatures (60°C and 80°C). The mixtures were then equilibrated for 24 hours. CA was extracted by adding 1 ml of acetonitrile to 1 ml of supernatants of the mixtures and centrifuged at ~2000g for 1 min to separate the insoluble components. The solvent extraction was repeated thrice and samples were diluted 200 times before HPLC analysis. The samples were evaluated in quadrates and Newman-Keuls Multiple Comparison Test was used for statistical significance of the solubility values ($p < 0.05$).

HPLC Analysis of Carnosic acid An UltiMate 3000 HPLC system with 25D UV-VIS absorption detector (Dionex) was used with a C₁₈ reversed-phase column (TOSOH Biosciences LLC, TSK gel ODS-100Z, 5 µm; 150x4.6 mm). A 6/4 mixture of acetonitrile/0.1% phosphoric acid is an isocratic mobile phase with 0.6 ml min⁻¹ as a flow rate and 50µl as injection value. Absorption peaks were observed as UV detection at 210 nm. Standard curve was calculated by using low concentration of CA (10, 20, 40, 60, 80 and 100 µg/ml).

6.2.3 Preparation of CA loaded CB Nanoparticles

Different amounts of Carnosic acid was melted into 10g cocoa butter heated at 60°C based on our results from solubility tests. Using HLB system, Tween 60 and Span 60 (Sigma-Aldrich, St. Louis, MO) was selected after different non-ionic polysorbates

(Tweens) and ethoxylated polysorbates were tested at 1% (w/w) and 2% (w/w). The emulsifiers are added into the lipid phase and constantly at 60°C with magnetic bar to get a clear mixture. DI water at 60°C was added at the lipid phase to form a pre-emulsion. The pre-emulsion was subjected to high speed homogenizer (High-speed homogenizer, ULTRA-TURRAX T-25 basic, IKA Works Inc., Wilmington, USA) for 5 minutes at 24,000 rpm and was transferred into high pressure homogenization using High pressure homogenizer, EmulsiFlex-C3, AVESTIN Inc., Ottawa, Canada. Different pressures (500 (HP500), 1000 (HP1000), and 1500 (HP1500) bars) and number of cycles (5, 10, 15, 20, 25) were optimized to obtain a stable nanoparticle dispersion.⁽²³¹⁾ The sizes of emulsion droplets can be varied by the speed and the pressure in the homogenization processes. The morphology and droplet size of emulsions were measured using an inverted optical microscopy (Nikon TE 2000, Nikon Corporation, Japan) and photon correlation spectroscopy (PCS) – based BIC 90 plus particle size analyzer equipped with a Brookhaven BI-9000AT digital correlator (Brookhaven Instrument Corporation, New York, NY, USA), respectively.

6.2.4 Stability studies of CA-CB nanoparticles

To understand the kinetic stability of the formulations prepared, the particle size and optical images are calculated and observed over a period of storage time. The morphology and droplet size of nanoparticles were measured over a period of time by using an inverted optical microscopy (Nikon TE 2000, Nikon Corporation, Japan) and photon correlation spectroscopy (PCS) – based BIC 90 plus particle size analyzer equipped with a Brookhaven BI-9000AT digital correlator (Brookhaven Instrument Corporation, New York, NY, USA), respectively.

6.2.5 Encapsulation Efficiency

The encapsulation efficiency (E.E.) of CA in cocoa butter SLN before and after sterilization was determined indirectly by ultrafiltration method using centrifugal filter tubes (Nanosep®, Pall life Sciences) with a 30 kDa molecular weight cut-off. The amount of encapsulated active was calculated by the difference between the total amount used to prepare the systems and the amount of CA that remained in the aqueous phase after isolation of the systems:

$$E.E. = \left[\frac{\text{Total amount of CA} - \text{Amount of Free CA}}{\text{Total amount of CoQ10}} \right] \times 100\%$$

The amount of free CoQ10 in the solution is determined by HPLC analysis.

6.2.6 Bioaccessibility Studies

In-vitro lipolysis: Food intake can influence the concentrations of bile salts and endogenous phospholipids in the small intestine lumen are higher in the fed state than in the fasted state. To replicate the same luminal environment, two lipolysis buffers were prepared corresponding to the fasted and fed states as shown in the Table. The procedure of *in vitro* lipolysis experiments was described in the published literature (245) and was previously performed in lab. (246, 247) Briefly, pancreatin preparation was made by mixing 1 g pancreatin with 5 ml fasted/fed-state buffer, centrifuged and kept on ice. In 9 ml fasted/fed-state buffer, 0.25 g lipid phase and 1 ml pancreatin preparation were added to start the lipolysis. During the 2 hr lipolysis, the pH was maintained at 7.50 ± 0.02 by adding 0.25 N NaOH and temperature was kept at 37 ± 1 °C. The volume of consumed NaOH over time was recorded throughout the lipolysis experiments. To simulate digestion of nanocomposite films, 370 µg of amylase was added to fed state buffer (83 µg for fast state

buffer) was added to 2g of HP nanocomposite films and stirred for 15 mins before addition of pancreatin preparation.

Chemicals	Fasted state	Fed state
Tris maleate (mM)	50	50
NaCl (mM)	150	150
CaCl ₂ .2H ₂ O (mM)	5	5
NaTDC (mM)	5	20
Phosphatidylcholine (mM)	1.25	5

The final lipolysis solution after digestion were ultra-centrifuged at 50,000 rpm (Type 60 Ti rotor, about 180,000g, Beckman Coulter) for 60 min. The aqueous phase was filtered through 0.22 µm filters. The filtrate was directly used to measure the particle size of the mixed micelles. The filtrate is acidified to pH 7 using HCL and was mixed with one volumes of ethanol for HPLC analysis.

Calculations for the percent bioaccessibility: The percent bioaccessibility was calculated as:

$$\% \text{ Bioaccessibility} = \frac{\text{mass of solubilized CA}}{\text{mass of CA in lipid}} \times 100$$

The mass of solubilized CA was the product of the concentration of solubilized CA in the aqueous phase after lipolysis and the volume of the aqueous phase. The mass of CA in lipid was calculated from the concentration of the CA in oil, mass of the oil (0.25 g) based on the entrapment efficiency and the density of the cocoa butter which is 0.876 g/ml.

Calculations for extent of lipolysis: The percentage amount of digested triglycerides is accounted by the extent of lipolysis. It was assumed that there were exclusively triglycerides in the basic oils, and that digestion of one molecule of triglycerides released exactly two molecules of fatty acids and consumed two molecules of NaOH. Consequently,

$$Extent_{lipolysis} = \frac{Vol_{NaOH} \times [NaOH]}{2 \cdot Mole_{triglyceride}} \times 100\%$$

Where Vol_{NaOH} is the volume of NaOH consumed in the lipolysis for digestion. $Conc_{NaOH}$ is the concentration of NaOH (i.e., 0.25 M). $Mole_{triglyceride}$ of 250 mg lipid was calculated from the average molecular weight of the triglycerides, which was estimated using the saponification value of the oil:

$$Mw_{triglyceride} = \frac{3 \times 1000 \times Mw_{KOH}}{SV}$$

Where Mw_{KOH} is the molecular weight of KOH, the mass of which is used to express the saponification value (SV). SVs used for cocoa butter is 193.

6.3 Results and Discussion

6.3.1 Solubility of CA in water, gastric buffer and lipids

Understanding and quantifying solubility of carnosic acid in different media is crucial in determining process parameters in preparation of nanoparticles and evaluate its biological efficiency in different studies.

Carnosic acid has very poor solubility (135 ppm) in distilled water (pH 6.83, 37°C). CA has higher solubility (1.1×10^4 ppm) in gastric buffer in fed-state (pH 4.6, 37°C). A phenolic diterpene by structure and owing to poor solubility in water, carnosic acid is

identified in insoluble extracts of rosemary and sage after alcohol extraction using Soxhlet apparatus.(266) Bile salts and lecithin in gastric buffer emulsify into micelles in which CA is solubilized.(267)

CA solubility in cocoa butter and its substitutes, Wecobee® is lower compared to medium chain triglycerides, Neobee® (Figure 46). Neobee® oils are composed of caprylic (C8) and capric(C10) acids in triglycerides. Cocoa butter is composed of oleic acid (34g/100g), palmitic acid (25g/100g), linoleic acid (3g/100g), and stearic acid (35g/100g). Wecobees® are tailored made cocoa butter substitutes from palm kernel fats.(233) Medium triglycerides have greater solubility due to low viscosity compared to structured fats like CB and Wecobees. Temperature increases solubility in all other lipids except cocoa butter. Solubility of CA in CB at 60°C is $(6.70 \pm 0.97) \times 10^4$ ppm and at 80°C is $(7.81 \pm 0.44) \times 10^4$ ppm. There is no significant difference in solubility in cocoa butter due to change in temperature. At these temperatures (60°C and 80°C), the crystal forms of CB are completely melted to liquid phase which behaves like a Newtonian fluid. (268)

60°C was chosen to be emulsifying temperature in preparation of CA-CB nanoparticles.

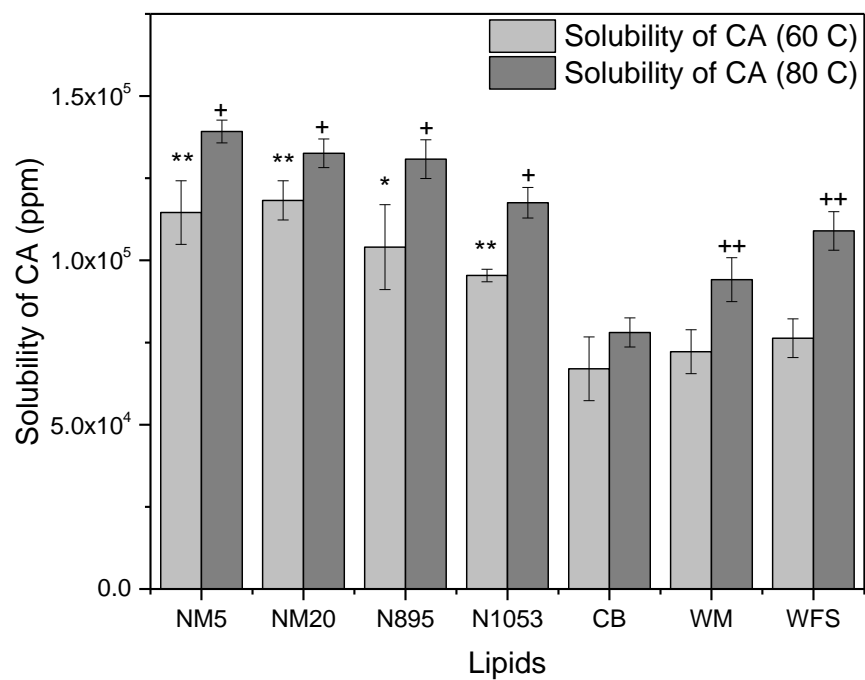


Figure 46 Solubility of carnosic acid (CA) in medium chain triglycerides, Neobee® (NM5, NM20, N895, N1053), cocoa butter (CB) and cocoa butter substitutes, Wecobee® (WM, WFS) at different temperatures (60°C and 80°C). Data shown as n=4, p<0.05

6.3.2 Preparation of Carnosic acid loaded cocoa butter nanoparticles

Different loading of CA in CB nanoparticles were evaluated for stability based on its visual appearance of phase separation and particle size. Different formulations were prepared at 60°C with different amounts of CA shown in Table 16.

High pressure homogenization has proved to be the most effective method to minimize the large particles in the dispersion.⁽¹⁹⁵⁾ To breakdown the emulsion droplets to a nanometric dimension, high energy in form of pressure is required. Smaller the size of the droplet, the higher stability was observed against coalescence.

At pressure 1500 bar and above, the particle size of CA-NP was significantly reduced to 205 ± 13 nm. The number of cycles that allowed the samples were exposed to high pressure had significant effect on the particle size. The hydrodynamic diameter of CA-NP significantly reduced by 50% at 20 cycles compared to that at 10 cycles. Among different pressure and number of cycles conditions for high pressure homogenization, processing at 1500 bar and 20 cycles gave the smallest and stable nanoparticles, as shown as Figure 47 and Figure 48. Different loading % of stable formulations had no effect on the particle size under different processing conditions.

Table 16 Composition and Stability of CA loaded in CB nanodispersions

	CB, g	S60/T60 (9:1), g	CA, g	Water, g	%CA in NP (w/w)	Phase separation of CA from NP
CA-NP-1	10	2	0.1	87.9	0.8	No
CA-NP-2	10	2	0.2	87.8	1.6	No
CA-NP-3	10	2	0.3	87.7	2.4	No
CA-NP-4	10	2	0.4	87.6	3.2	No
CA-NP-5	10	2	0.5	87.5	4.0	No
CA-NP-6	10	2	0.67	87.33	5.3	No
CA-NP-7	10	2	0.8	87.2	6.3	CA crystals observed in emulsion
CA-NP-8	10	2	1	87	7.7	Gelling and CA crystals observed in emulsion

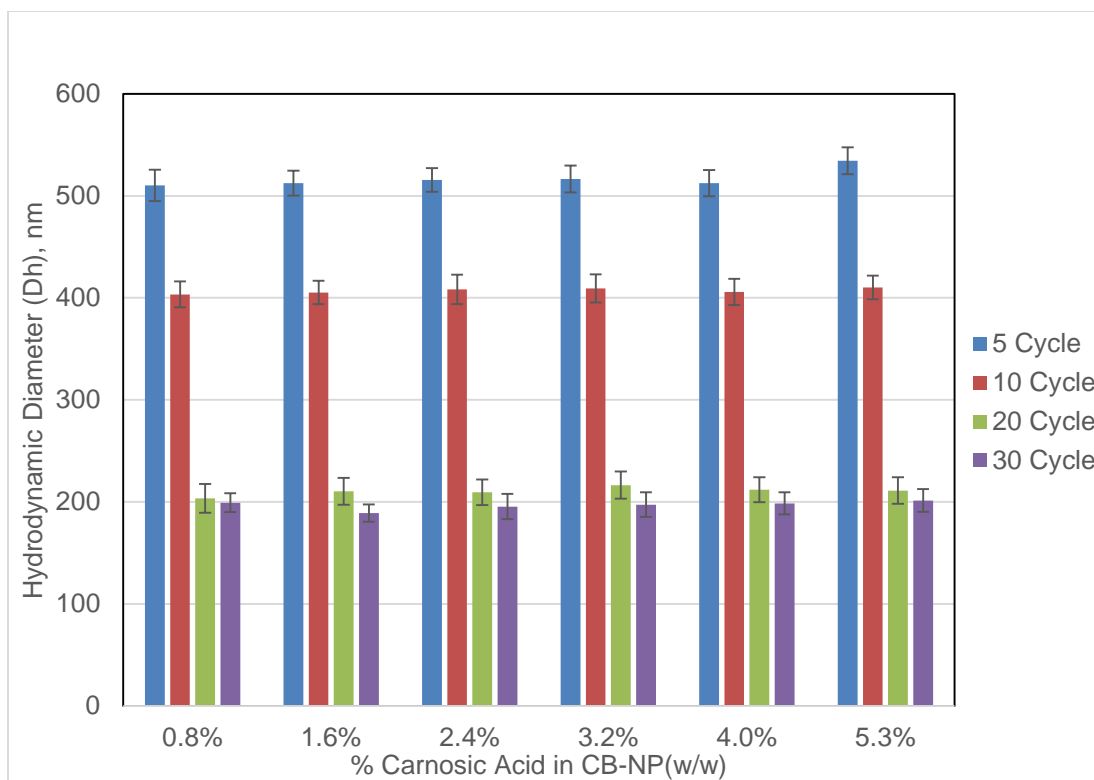


Figure 47 Effect of HPH Cycles on Particle analysis on Stable Formulations (1500 Bar)

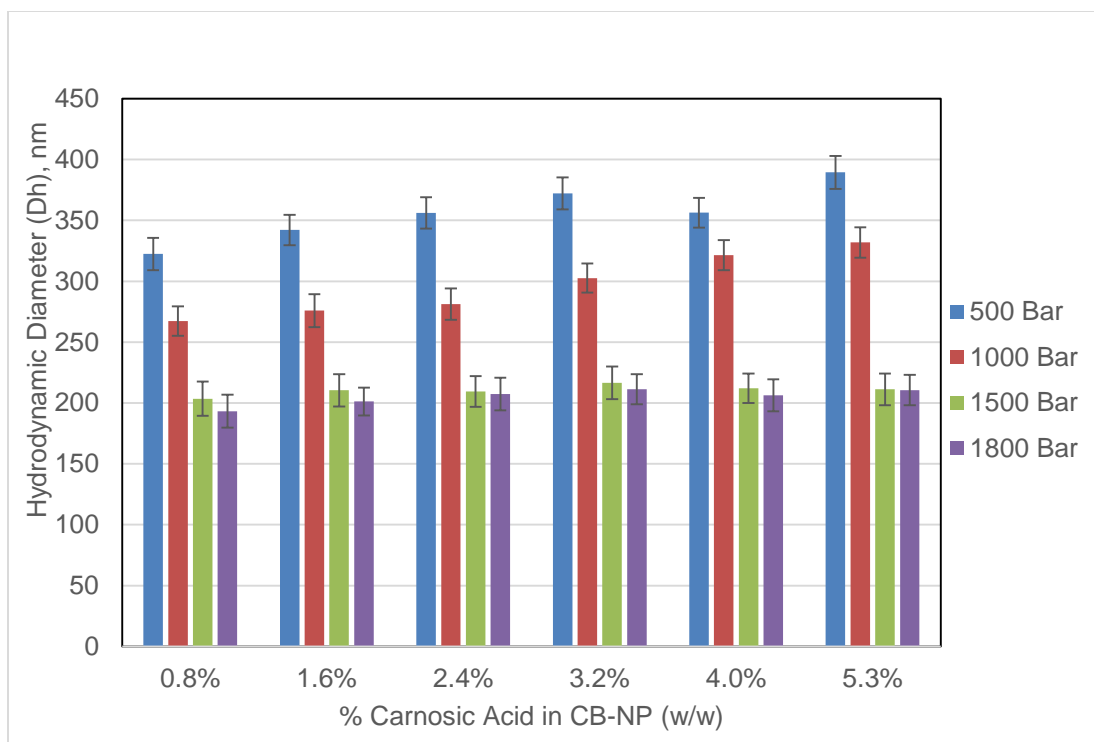


Figure 48 Effect of HPH pressure on Particle analysis on Stable Formulations (20 cycles)

6.3.3 Storage stability of Carnosic acid loaded cocoa butter nanoparticles

The particle size of the stable CA-NP formulations remained consistently same over 1 month of storage at 25°C (Figure 49). During storage, gelation process can occur due to insufficient surfactant mixture, destabilizing composition and recrystallization of the drugs in the lipid matrix. Fluctuating storage temperatures and light exposure are few factors that contribute to any addition of energy into the dispersion system that can destabilize the particles since most of the systems are not at thermodynamic equilibrium.(269, 270) Recrystallization can also lead to phase separation which causes creaming. From Figure 50A-G, all the formulation with CA loading (0.8% - 5.3%) had no destabilizing recrystallization and microphase separation which was seen in formulation with 7.7% CA loading (Figure 50**Error! Reference source not found.** H). The drug payload can significantly affect the crystallization of lipid matrix and can separate into drug crystals when its concentration is higher than the saturation solubility of the formulation. It is observed that formulations that have higher loading than the saturation solubility of CA in bulk CB are highly susceptible for recrystallization and gelling.

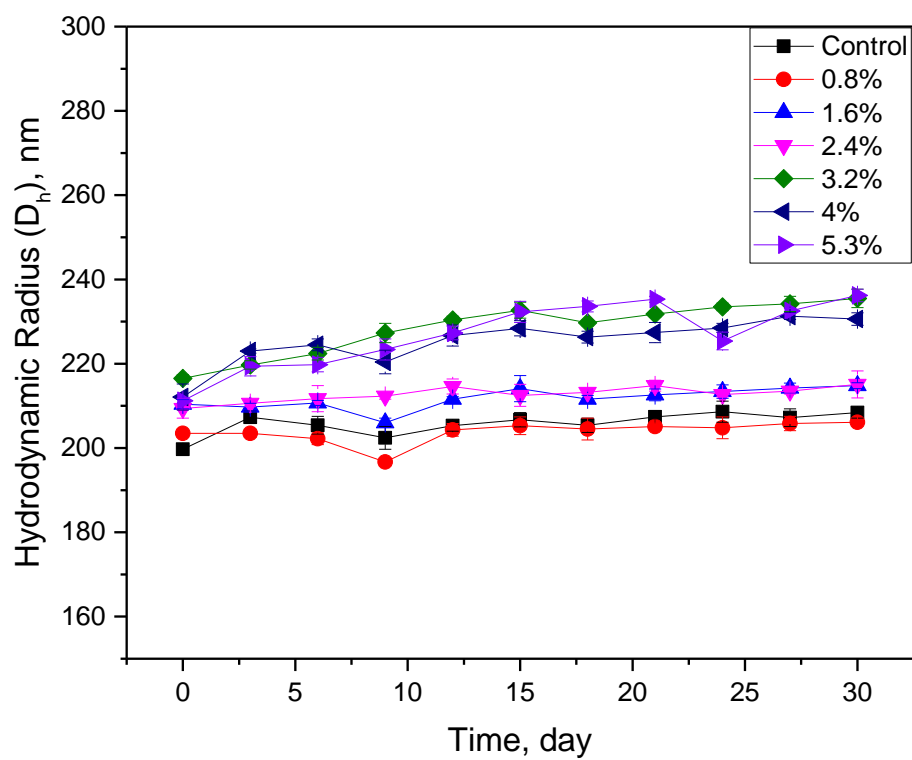


Figure 49 Effective diameter of CA-NP formulation over 4 weeks of storage at 25°C

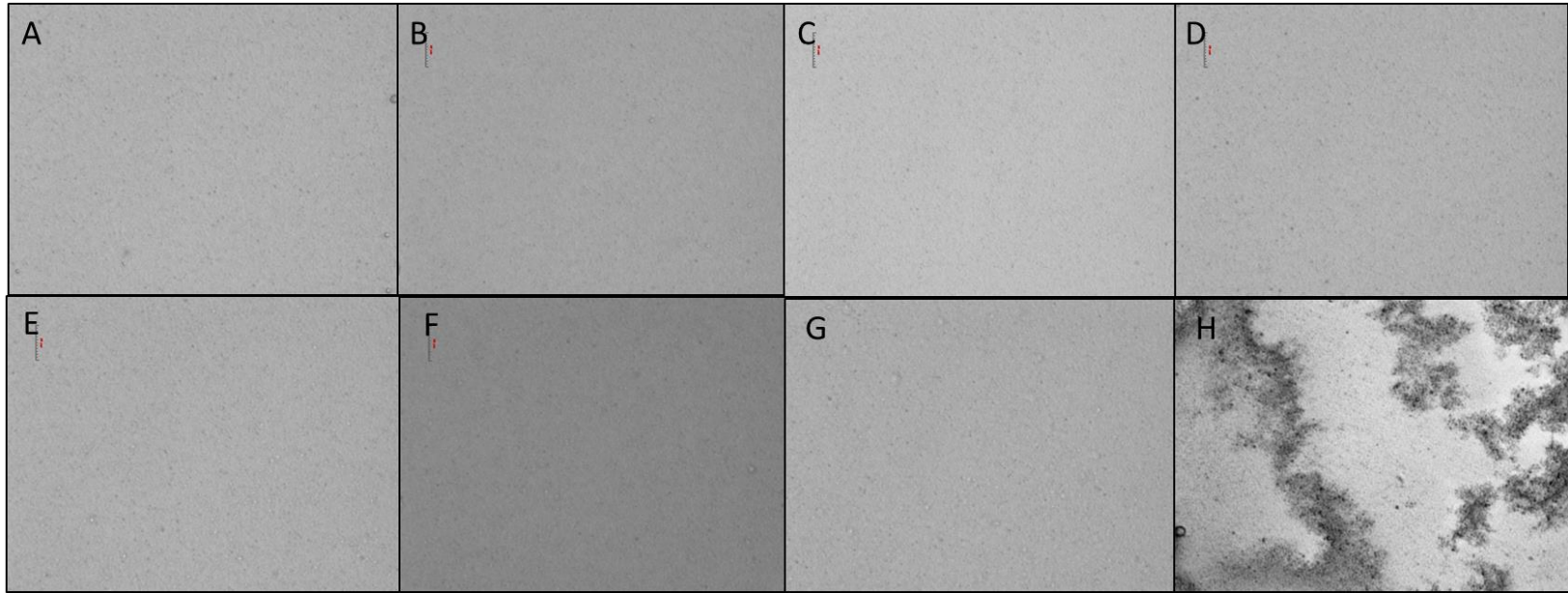


Figure 50 Optical Images of CA-NP formulations after 4 weeks of storage where A = control, B-D = 0.8%, 1.6%, 2.4%, 3.2%, 4%, 5.3% (w/w) of loaded CA in NP and H = 7.7% of loaded CA in NP (400X magnification)

6.3.4 Encapsulation Efficiency of CA loaded CB Nanoparticles

Carnosic acid is effectively encapsulated in cocoa butter nanoparticles with EE% ranging 87-94%. One of the contributing factor to increase encapsulation efficiency is due to polymorphic state of cocoa butter.(239) Since cocoa butter has multiple crystal forms than other hard fats which form ordered crystal structure, (β form)(240). Imperfection in crystals provide space in the lipid matrix for drug molecules to accommodate. This would increase the efficiency of encapsulation.

Encapsulation efficiency of CB NP decreases with increase in CA loading. Due to the crystal order of the lipid matrix, drug payload can be limited. Low loading of CA showed the best EE% because most of CA is entrapped in the lipid core of NP. As concentration of CA increases, the lipid matrix is saturated with CA. Excess CA can remain in the aqueous phase due to emulsification with free surfactants. (Table 17)

Based on these findings, CA-NP-6 formulation with 5.3% (w/w) CA is used as the nano-filler because of its stability and highest amount of encapsulated CA in NP.

Table 17 Encapsulation Efficiency of stable CA-NP formulations

	CA added in bulk CB ($\mu\text{g/g}$)	CA in CB NP form ($\mu\text{g/g}$)	Encapsulation Efficiency, EE%
CA-NP-1	10000	9374.6 ± 32.7	93.7 ± 0.3
CA-NP-2	20000	18128.8 ± 302.1	90.6 ± 1.5
CA-NP-3	30000	26642.0 ± 250.5	88.8 ± 0.8
CA-NP-4	40000	34939.1 ± 335.4	87.4 ± 0.8
CA-NP-5	50000	43088.3 ± 58.5	86.2 ± 0.1
CA-NP-6	67008	58842.6 ± 132.1	87.8 ± 0.2

6.3.5 In-vitro lipolysis studies on CA-CB Nanoparticles

Bioaccessibility of a bioactive released from nanoparticles affect rate of absorption, bioavailability and tissue distribution that determines its nutritive efficiency.(271) Bioavailability of a bioactive is defined by its amount that reaches the systemic circulation after oral administration. The overall bioavailability (F) of poorly soluble actives depends on a number of dependent factors: $F = F_B \times F_A \times F_M$

Here, F_B is the fraction of hydrophobic component released from the delivery system into the lumen of the GIT to become bioaccessible, F_A is the fraction of the released hydrophobic component that is absorbed across the layer of intestinal epithelial cells, and F_M is the fraction of the absorbed hydrophobic component that reaches the systemic circulation without being metabolized.(272)

From studies of in-vitro lipolysis of two forms of delivery strategies: CA+CB mixture and CA encapsulated in CB nanoparticles, extent of lipolysis (release of fatty acids) and bioaccessibility of CA was determined after analyzing CA in aqueous phases by HPLC (Figure 52 and Figure 53). These two type of lipid formulations were evaluated to understand effect of emulsifier and particle size of the formulation on CA release after lipolysis. In fed state buffer, the rate of digestion of CA-NP was significantly higher than CA+CB (

Table 18). For emulsion systems, the rate of FFA (free fatty acids) release is high at the beginning of the lipolysis and gradually decreases until it becomes constant. The rate of FFA release and extent of lipolysis is also significantly dependent on the initial droplet size. The initial droplet size in the digestion buffer is also determined by the physical state of carrier lipid and emulsifier that stabilizes the lipid interface under lipolysis conditions. The extent of digestion of triglycerides in CB is dependent on exposure of digestive enzymes and diffusion of FFA to expose unreacted TAGs in the nanoparticle. Release by action of lipase and diffusion of long-chain fatty acids ($C \geq 16$) is slow compared to that medium chain fatty chains present in liquid oil droplets. Bile salts are crucial in partition of FFA in lipid and aqueous phase and micellar formation. Bioaccessibility of CA was significant in CA-NP than the mixture. Bioaccessibility is dependent on the extent of FFA release and mixed micelles ($\sim 194.47 \pm 4.87$ nm) formed by FFA can solubilize CA in aqueous phase. CA is retained in undigested part of CB, making the mixtures less bioaccessible.

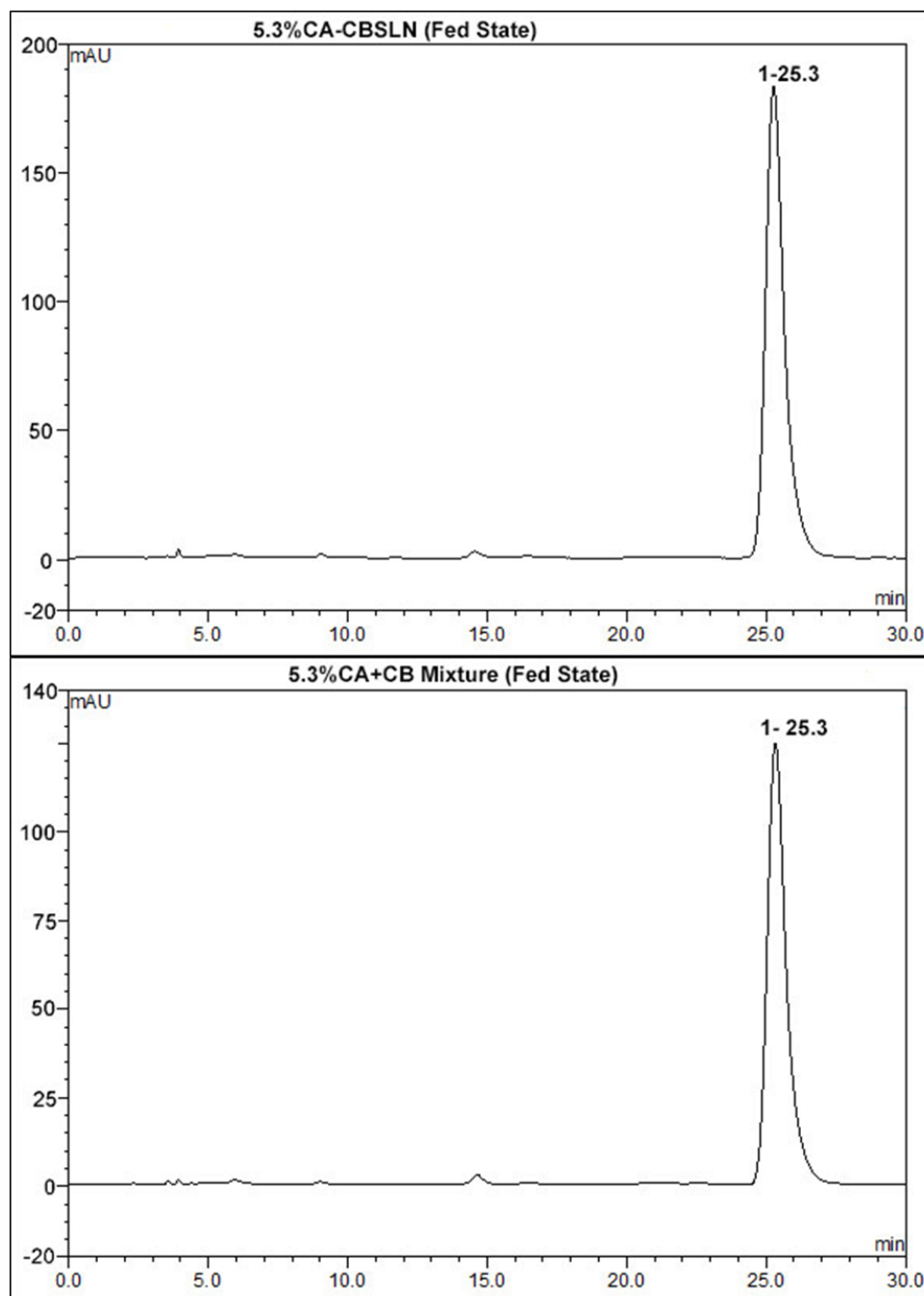


Figure 52 HPLC Spectrogram of aqueous phase of CA & CB Mixture (CA+CB) and CB Nanoparticle with 5.3% CA (CA-NP-6) after in-vitro lipolysis in fed state buffer

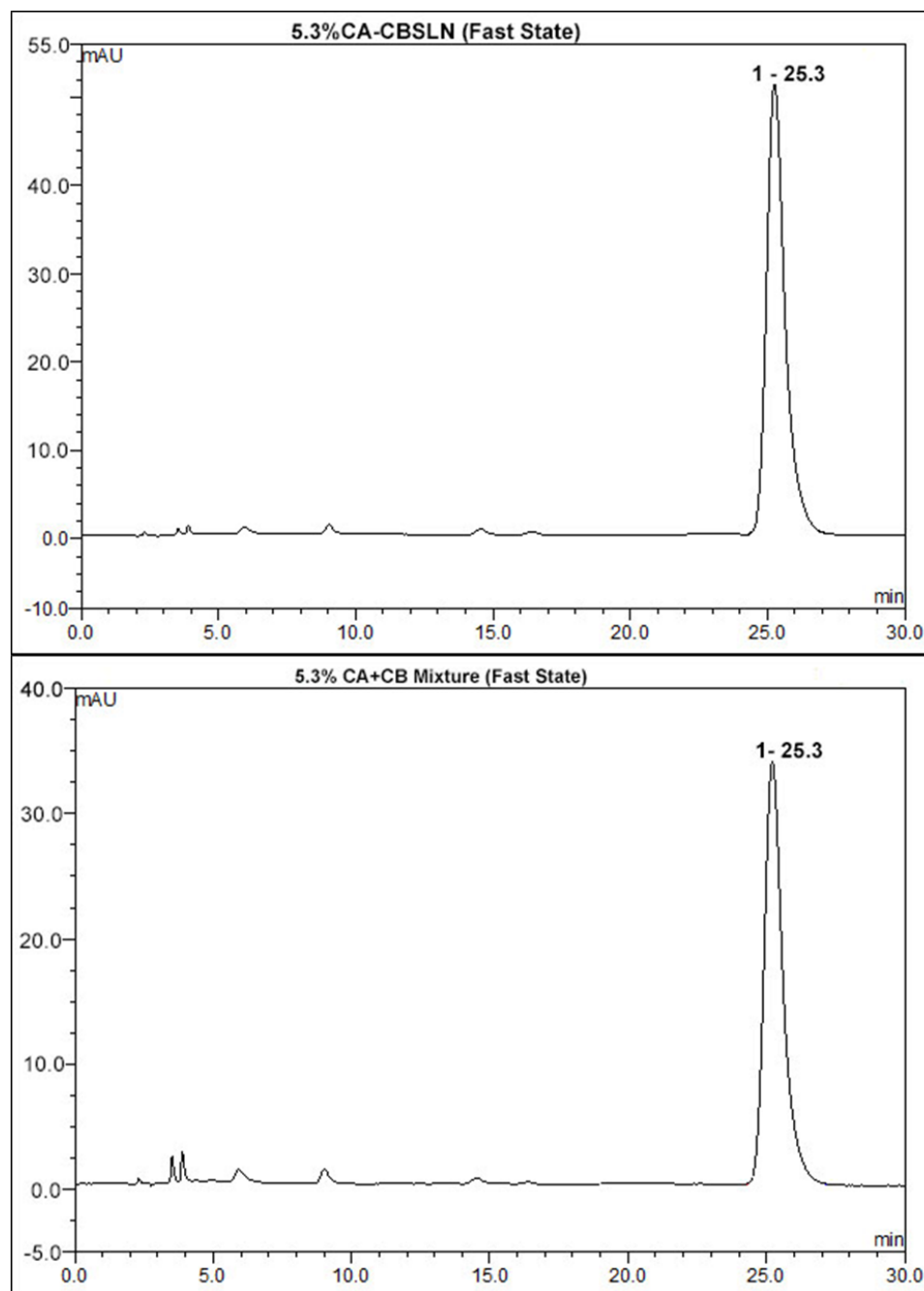


Figure 53 HPLC Spectrogram of aqueous phase of CA & CB Mixture (CA+CB) and CB Nanoparticle with 5.3% CA (CA-NP-6) after in-vitro lipolysis in fast state buffer

Table 18

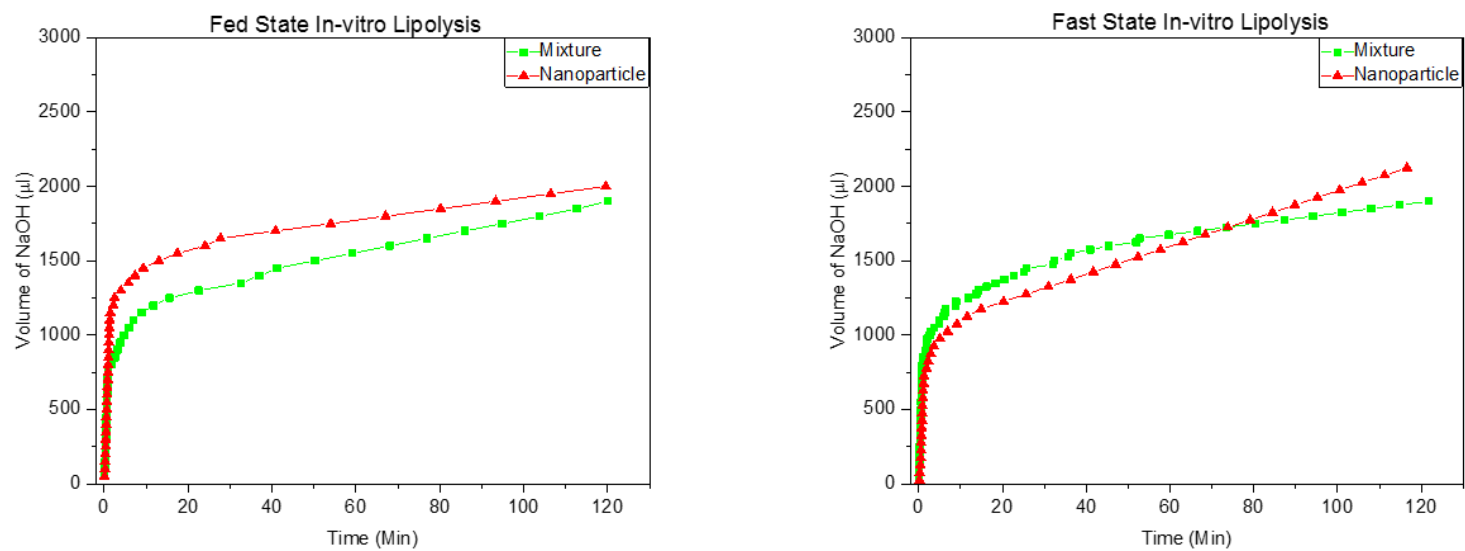


Figure 51 In-vitro Lipolysis of CA+CB mixture (Mixture) and CA-NP -6(Nanoparticle) in fed state and fast state buffers

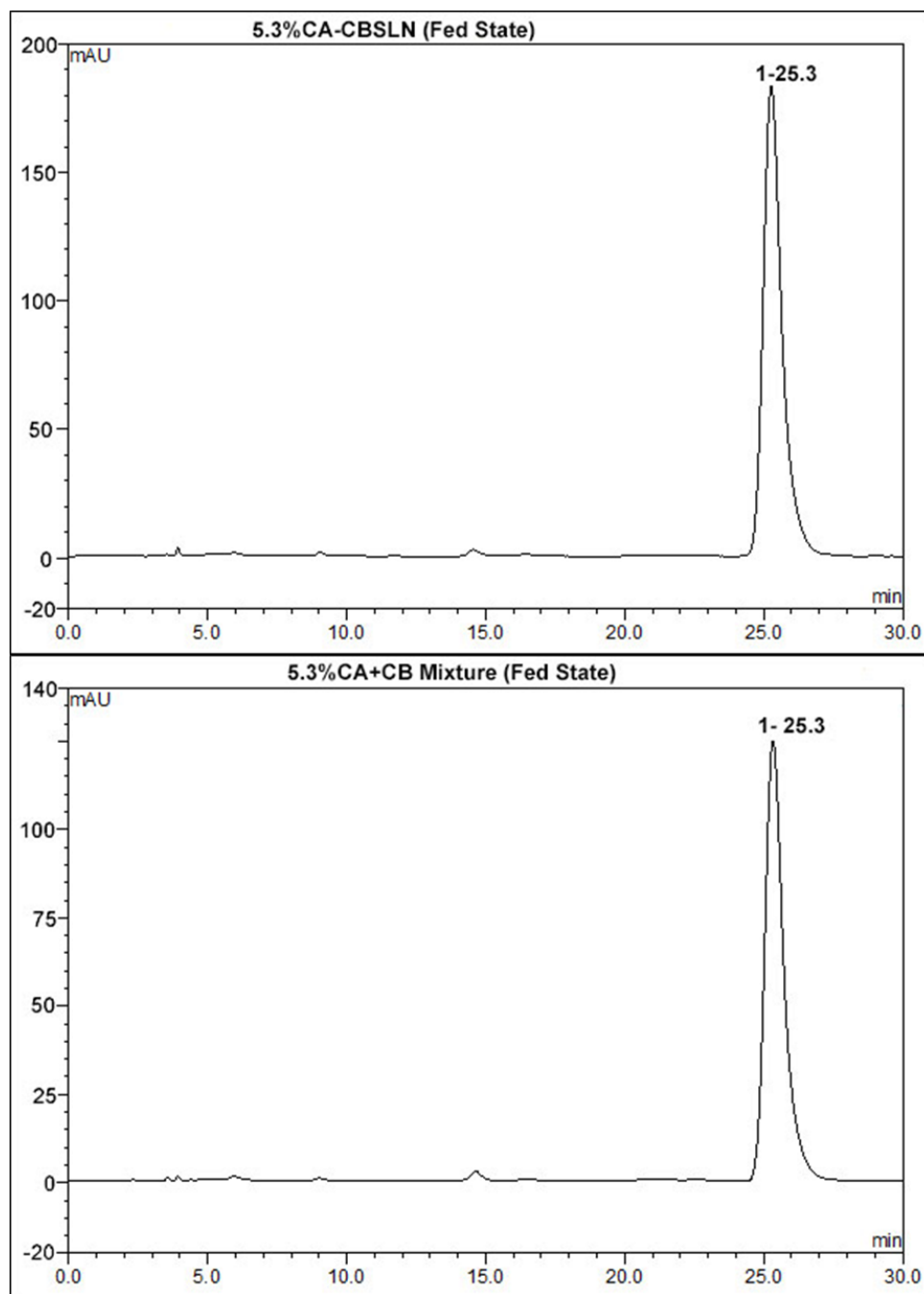


Figure 52 HPLC Spectrogram of aqueous phase of CA & CB Mixture (CA+CB) and CB Nanoparticle with 5.3% CA (CA-NP-6) after in-vitro lipolysis in fed state buffer

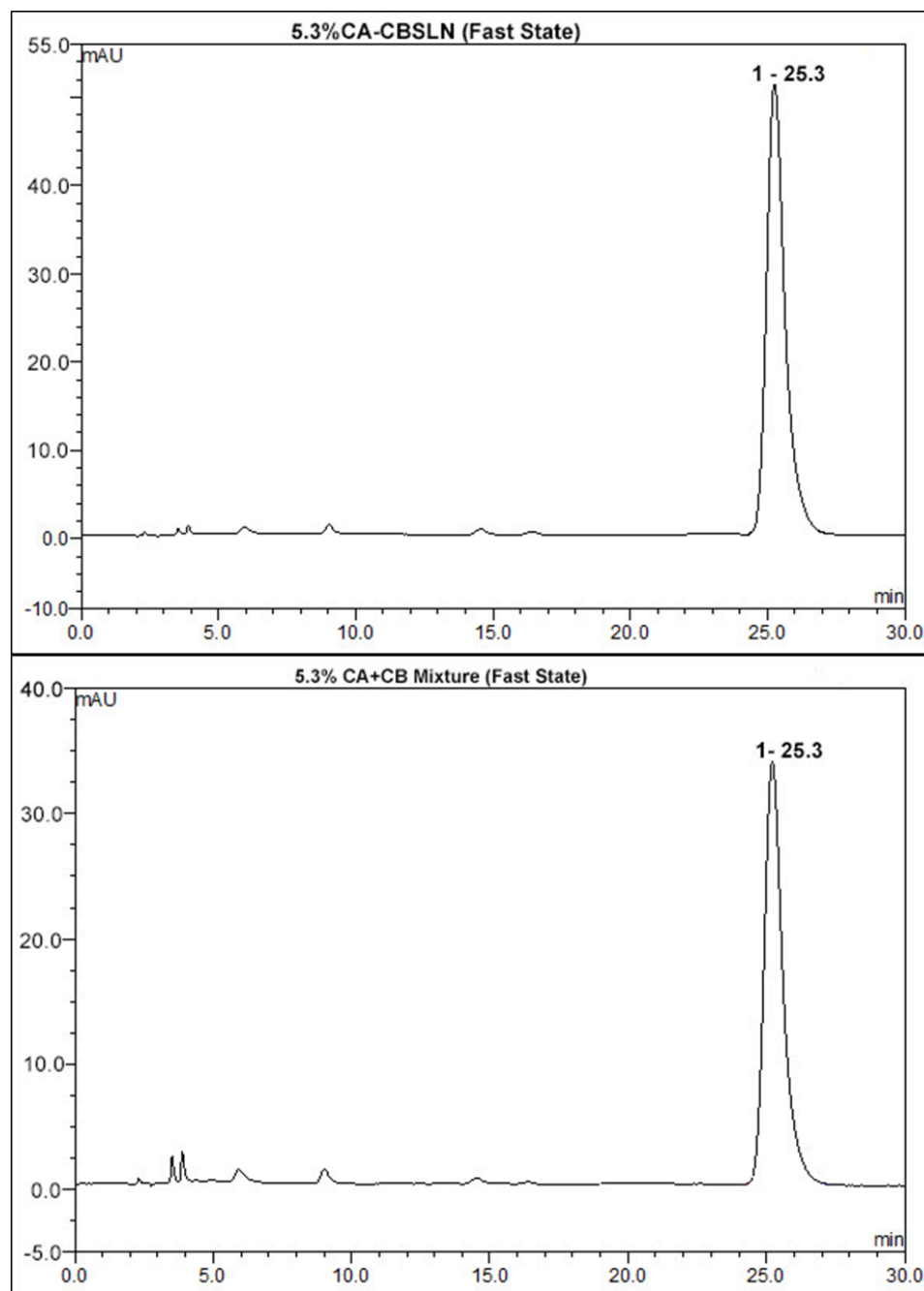


Figure 53 HPLC Spectrogram of aqueous phase of CA & CB Mixture (CA+CB) and CB Nanoparticle with 5.3% CA (CA-NP-6) after in-vitro lipolysis in fast state buffer

Table 18 In-vitro Lipolysis of CA & CB Mixture (CA+CB) and CB Nanoparticle with 5.3% CA (CA-NP-6)

State of Buffer		Extent of Lipolysis (%)	Bioaccessibility (%)
CA+CB	Fed	79.6 ± 4.6	24.7 ± 2.2 ^a
CA-NP-6		80.7 ± 9.3	31.5 ± 0.7 ^b
CA+CB	Fast	82.8 ± 0.1	18.8 ± 0.6 ^c
CA-NP-6		89.9 ± 3.9	23.1 ± 1.4 ^a

6.4 Conclusion

In this study, CB nanoparticle is evaluated as a potential delivery system for carnosic acid. Similar studies that were conducted with CoQ10 as the payload, were performed for carnosic acid so that they can be used to create multifunctional films.

To create a nano-filler for these proposed multifunctional films, stability, encapsulation efficiency and its bioaccessibility of the bioactive need to be studied. Due to high solubility of CA in CB, CA-CBSLN were obtained with very high encapsulation efficiency. The formulation with highest loading of CA was chosen as the nanofiller for the films. Bioaccessibility of CA in CB nanoparticles was assessed in comparison with CB mixture and the results confirm with previous findings that CB in nanoparticle form can improve bioaccessibility effectively than in its mixture for both fed and fast states.

These studies further affirm that C nanoparticles are effective delivery system for different non-polar molecules.

CHAPTER 7. HYDROXYPROPYL STARCH NANOCOMPOSITES WITH CARNOSIC ACID LOADED COCOA BUTTER NANOPARTICLES: PHYSICAL AND ANTIOXIDANT PROPERTIES

7.1 Abstract

Lipid based nanosystems are extensively used in pharmaceutical industry for drug delivery strategies and their potentiality in food applications is the central idea of the current research. The purpose of present project is developing novel multifunctional nanocomposite films using a lipid nanosystems as a filler to extend the shelf life of the food product by improving barrier properties and deliver bioactives on consumption. Hydroxypropylated starch (HPS) is chosen as bulk material of the films due to its excellent film forming properties but hydrophilicity of hydroxylpropyl groups limit its utilization. In this project, nanocomposite of HPS with CA loaded CB NP were prepared. The research objectives focus on characterization of moisture barrier and mechanical properties along with quantification of antioxidative nature of the digested nanocomposite film. The maximum loading capacity of stable CA loaded CB NP was 5.3% dry weight basis with high encapsulation efficiency and improved the bioaccessibility of CA for absorption in in-vitro lipolysis studies. These NP were mixed with solutions of HPS and glycerol as plasticizer to prepare nanocomposite films and their mechanical, moisture barrier and antioxidant properties were studied. Results confirmed that reduced water vapor permeance by 30-40% and stability at a wide range of relative humidity compared to HPS films due to homogenous embedment of NP and low microphase separation. The

mechanical properties of the films did not significantly differ from the control. Antioxidative activity of CA ($IC_{50} 7.44 \pm 2.54$) was observed in the aqueous phase of digested nanocomposite which shows that CA was bioaccessible for absorption. Lipid NP can be utilized to serve both as nano-filler and nutraceutical delivery system in this approach.

7.2 Materials and Methods

7.2.1 Materials

Hydroxypropylated high amylose (80%) corn starch (A1081) with MS (molar substitution) 0.11 was supplied by Penford (Australia). Cocoa butter (manufacturer: Spectrum Chemical Mfg. Corp.) is purchased from vendor, VWR International. Carnosic acid (95%, purity) was purchased Wuling Yangguang Biotechnology Co., Ltd., Hunan province, China. Glycerol and surfactants were acquired from Sigma-Aldrich (St. Louis, MO). Medium chain triglycerides (Neobee®) and cocoa butter substitutes (Wecobee®) are obtained as free samples from Stepan Company (Northfield, Illinois). Other chemicals used for analytical purposes are acquired from Sigma-Aldrich (St. Louis, MO), VWR International (Radnor, PA) and Fischer Chemicals (Hampton, NH).

7.2.2 Preparation of nanocomposite films

8% starch and 4% glycerol were mixed with DI water to prepare solution by heating at 80°C with medium speed stirring using a magnetic stirrer for 30 minutes. Measured amounts of starch solutions and CB nanoparticles with highest loading of CA were mixed to make homogenous film solutions. The 25 ml of film solution were poured in each of clean petri dishes and were air-dried for 2 days.

7.2.3 SEM Imaging

The HPS nanocomposite films were mounted on a flat SEM pin (Tedpella Inc, Redding, CA) for surface images and with aid of 12mm carbon discs (SPI Supplies, West Chester, PA) on to which the sample is adhered. The vacuum dried samples are coated with a 10 nm with gold using in a Polaron (Hatfield, PA) SEM coating system. The specimens were scanned using Field Emission SEM (Zeiss Sigma, Jena, Germany) with Oxford INCA PentaFETx3 EDS system (Model 8100) at an accelerating voltage at 5kV. The images with digitally processed by Smart SEM software (Zeiss Sigma).

7.2.4 Differential Scanning Calorimetry

A differential scanning calorimeter (PerkinElmer DSC Diamond-8000) with a refrigerated cooling system and nitrogen purge gas was used for these experiments. Temperature and heat capacity calibrations were performed using melting point and enthalpies of indium as the baseline. High-pressure stainless steel pans (PE No. B0182901) with gold-plated copper seals (PE No. 042-191758) were used. The DSC samples were heated from 30 °C to 130 °C at a scanning rate of 5 °C/min. Due to the large mass of the steel pans used in the experiment, a slow heating rate was used. The initial and final weights of the pans were registered to assess water loss after scanning. The enthalpy was calculated based on starch films conditioned at 25°C and 50% RH. DSC measurements were performed in triplicates, and the results are presented as the mean.

7.2.5 Mechanical properties

The tensile strength (TS) and elongation at break (EB) of the films (conditioned at 50% RH and 25°C) were measured on Texture Analyzer -Brookfield CT 3 Max Load 2500g (Middleboro, MA) at a speed of 0.1 mm/s. The texture analyzer is equipped with

Texture Pro CT V1.4 Build 17. The appropriate sized films (1.0×10.0 cm) were cut using a razor blade and the gauge length was set at 10.0 mm. For each sample, the measurements were replicated four times. TS was calculated by dividing the maximum load for breaking the film by cross-sectional area, and %E by dividing film elongation at rupture to initial gauge length, and the values were measured both in longitudinal and transverse directions to observe whether any difference in the orientation of polymer chain occurs. Percent elongation is the ratio of extension to the length of the sample. All means were compared with each other, the results of ANOVA indicated significance using Tukey test ($p < 0.05$).

7.2.6 Moisture barrier properties

7.2.6.1 Contact Angle Measurements

The static water contact angle measurements were carried out using a VCA Optima XE Dynamic Contact Angle Analyzer (AST Products Inc., Billerica, MA) at ambient condition. The image was recorded by a CCD camera immediately after the water drop was deposited onto the HGCN film surface. At least six measurements were averaged for each sample.

7.2.6.2 Moisture Sorption Isotherm Measurements

Saturated salt solutions of lithium chloride, magnesium chloride, sodium bromide, sodium chloride, and potassium nitrate were used to obtain different RH combinations having a_w values of 0.11, 0.33, 0.58, 0.75 and 0.94 respectively. These saturated solutions were taken in different desiccators. Prior to keeping the film, specimens were conditioned to 53% RH (desiccator with saturated solution of magnesium nitrate) at 24°C. The initial moisture content of the blend films was measured in duplicate on dry basis (db in %) by

drying in hot air oven at 100 ± 2 °C to constant weight. The sorption experiments were carried out by keeping approximately 1 g of blend films (2 cm x2 cm) in desiccators, removing at frequent intervals and weighing until they reach constant weight (within $\pm 5\%$). All chemicals were of analytical grade from Sigma-Aldrich (St. Louis, MO). The equilibrium moisture content (% db) of the films when the weight of the film reaches a constant value.

$$\text{Equilibrium moisture content (\% db)} = \left(\frac{m_{eq} - m_{dry}}{m_{dry}} \right) \times 100\%$$

Where,

m_{eq} = Weight of the film in equilibrium at a certain relative humidity and temperature 25°C

m_{dry} = Dry weight of a certain relative humidity and temperature 25°C

7.2.6.3 Water absorption Studies

Small pieces of membranes were weighed and immersed in deionized water (30 mL), until equilibrium was reached. The swollen membranes were taken out and extra water was removed by carefully transferring swollen film into a dry dish. The water absorption capacity (WAC) was calculated using the equation:

$$WAC (\%) = \left[\frac{W_s - W_d}{W_d} \right] \times 100$$

Where “ W_d ” is the weight of the dry membrane and “ W_s ” is the weight of swollen membrane at equilibrium.(216) The results were reported as the average of three readings. The swelling response of films was also measured at different pH.

7.2.6.4 Water Vapor Transmission Rate (WVTR) and Water Vapor Permeability (WVP)

The WVTR and WVP of the membranes were analyzed according to the ASTM Method E96/E96 M. Circular test cups were filled with calcium chloride (10.0 ± 0.5 g) as desiccant at 0% relative humidity (RH), and sealed with the test membranes. The membranes were tightly attached and the initial weights of the cups were recorded. The cups were placed in an environmental desiccator set at 25°C and 53% RH. After reaching equilibrium state in the desiccators, cups were weighed daily for 14 days. The WVTR was calculated as the slope of the regression line drawn between elapsed time and the weight change of the test cups. The actual WVTR and WVP of the membranes were calculated using the following equations.

$$WVTR = \frac{G}{A \cdot t}$$

$$WVP = \frac{WVTR}{\Delta P} \cdot x = \frac{WVTR}{S(R_1 - R_2)}$$

Where, G is weight change (g), t is the time (h), A is the test area (m^2), and ΔP is vapor pressure difference (Pa) and S is saturation vapor pressure at test temperature (1.333×10^2 Pa), R_1 = relative humidity at the source expressed as a fraction and R_2 = relative humidity at the vapor sink expressed as a fraction.

7.2.7 Antioxidant activity measurements

Antioxidant activity of aqueous phase of CA-CB mixture, CA-CB nanoparticles and HPS nanocomposites were measured using DPPH radical scavenging assay.

This assay was performed according to the previously reported method.(273) The diluted working solutions of pure CA was prepared in acetonitrile. Aqueous phase of

digested CA-CB mixture, CA-CB nanoparticles and HGCN-2 films were used directly. Digested CA-CB mixture and CA-CB nanoparticle samples are obtained after in-vitro lipolysis method as mentioned. Digested HGCN-2 films were obtained by treating small bits of films with equivalent amount of lipid content to that of CA-CB samples with 2.2 mg of amylase for 30 mins before subjecting them to in-vitro lipolysis. In case of digested films, the aqueous phase was freeze-dried and reconstituted with 2 ml of acetonitrile. Different concentrations of each sample were prepared with acetonitrile in 5 ml test tubes by serial dilution. Each dilution (0.2ml) was added to 3.8ml solution of 0.1 mM DPPH dissolved in methanol. The mixture was shaken vigorously and left in the dark at room temperature for 30 min. The absorbance of the mixture (100 μ l) was recorded at 517 nm using the Synergy HT multimode microplate reader (Bio Tek Instruments Inc., Winooski City, VT, USA). The experiment was repeated three times. The scavenging rate of DPPH free radicals was calculated as:

$$\left[1 - \frac{A_1 - A_2}{A_0} \right] \times 100\%$$

where A_1 was the absorbance of the mixture between sample and DPPH solution, A_2 was the absorbance of the mixture between sample and methanol (control), and A_0 was the absorbance of the mixture between methanol and DPPH solution. The antioxidant activity of the sample was expressed as IC_{50} (μ M), which meant the concentration of the sample while the scavenging rate was 50% and was determined by regression analysis.

Based on calculations of amount of CA present in CB and in CB nanoparticle and film before digestion and including the factor for bioaccessibility, expected antioxidant activity (IC_{50})_{expected} in nanoparticle and from was calculated. Controls for nanoparticles (CB-NP-0) and films (HGCN-0) that didn't have CA were also evaluated for

baseline deduction. $(IC_{50})_{experimental}$ obtained from scavenging rates of DPPH from the digested samples.

Antioxidant Capacity of the samples were calculated as

$$Antioxidant\ Capacity, AOX = \left(\frac{(IC_{50})_{experimental}}{(IC_{50})_{expected}} \right) \times 100 \%$$

7.3 Results and Discussion

7.3.1 Preparation of nanocomposite films

8% (w/v) starch and 4% (w/v) glycerol were mixed with DI water to prepare solution by heating at 80°C with medium speed stirring using a magnetic stirrer for 30 minutes. Measured amounts of starch solutions and CB nanoparticles with highest loading of CA were mixed to make homogenous film solutions as shown in Table 19. The 25 ml of film solution were poured in each of clean petri dishes and were air-dried for 2 days.

Table 19 Composition of the HGCN film solutions

	HPS Starch, g	Glycerol, g	CA-NP, g	Water, g
HGCN-0	8	4	0	88
HGCN-0.5	8	4	0.5	87.5
HGCN-1	8	4	1	87
HGCN-2	8	4	2	86

7.3.2 Microstructure of HGCN films

Study of microstructure of the films gives us information of the arrangement of molecules of different components in the film solution after drying. During drying, the concentration of all the film components which could trigger aggregation or creaming of the lipid nanoparticles leading to phase separation of lipids from polymer matrix. This phenomenon can adversely affect the internal and surface structure of the films and in turn, the physical properties of the films. The microstructure of nanocomposite films, with and without CA loaded CB nanoparticles, was qualitatively studied using Scanning Electron Microscopy (SEM). SEM images in Figure 54 show the surface morphology of the films with increasing amounts of CA-NP-6. The control film HGCN-0 and film with low amount of CA-NP (HGCN-0.5) had smooth surface of a homogenous film matrix. With increase in CA-NP in the film matrix, micro-aggregate sites of lipid appeared increasing. The diameter of the aggregate sites (2-8 μM) increased with the amount of lipid nanoparticles added. The shape of the sites has a distinct shape with a lipid center and ring of surfactant around the aggregates. Coalescence could be a possible mechanism of the phase separation that occurs due to merging of the nanoparticles into a larger droplet.

Figure 55 shows the SEM micrographs of cross-sections of the control and nanocomposite films. From the cross-sectional analysis, the control film has continuous phase of polymer matrix which confirms the homogeneity of the HP starch and glycerol in dry state. Matrices of nanocomposite film are homogenous but appeared very different from that of the control film. No lipid droplets or aggregates were observed inside the matrices which indicates that nanoparticles are well-integrated in the HP starch. No irregular layers of the lipid phase were identified within the matrix which confirms that

there is no phase separation in that region. In HGCN-2 films, there are few irregular regions near the surface of film which could be possibly be lipid aggregates at the surface which complies with its surface morphology in Figure 54.

The microphase separation of the lipids from polymer matrix was evident suggesting that interaction of lipid nanoparticles and the polymers is concentration dependent. The phase separation in films introduces roughness on the surface which could alter its surface properties.

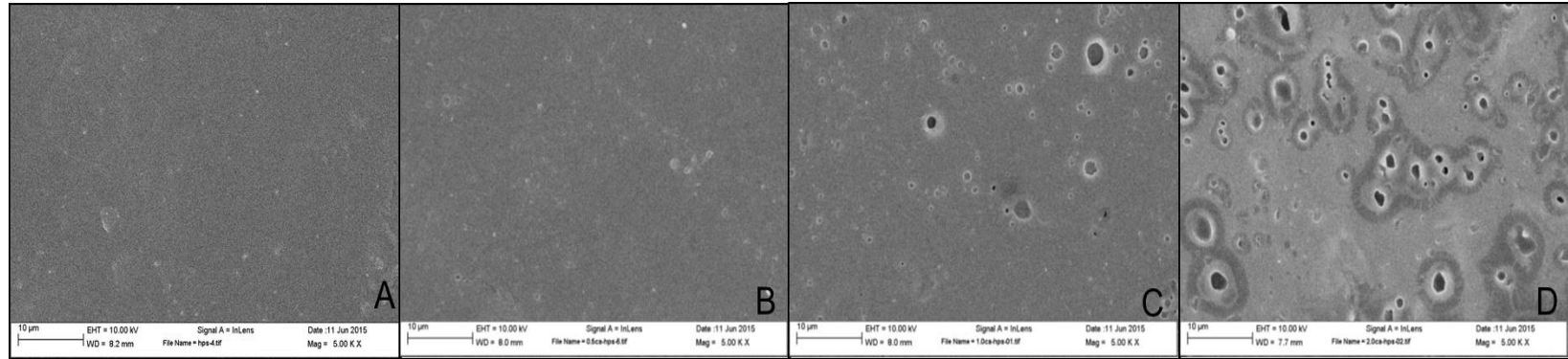


Figure 54 Surface morphology of HP starch (A), nanocomposites HGCN-0.5 (B), HGCN-1 (C) and HGCN-2 (D)

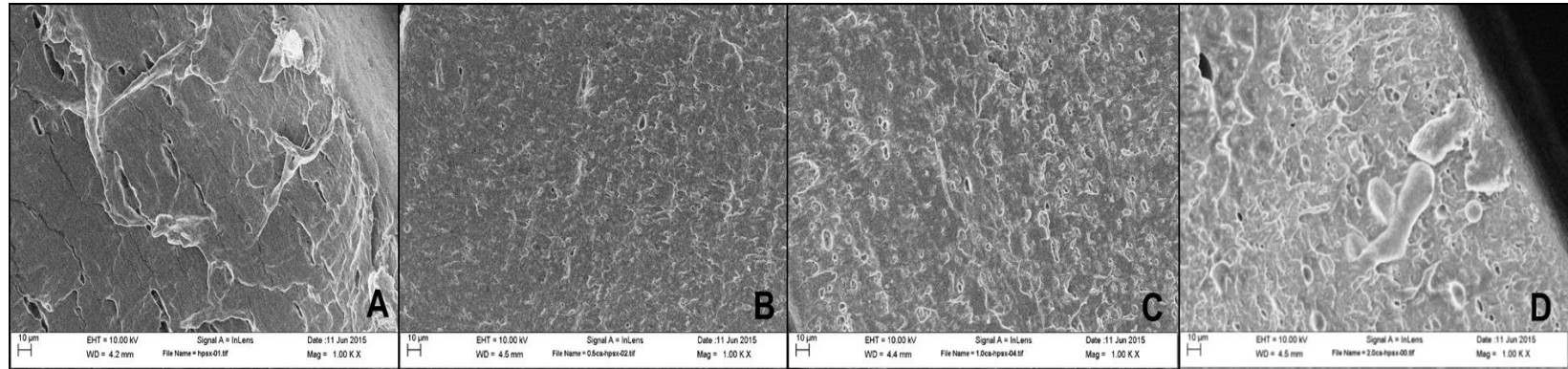


Figure 55 Morphology of the cross-section of films: HP starch (A), HGCN-0.5 (B), HGCN-1 (C) and HGCN-2 (D)

7.3.3 Differential Scanning Calorimetric studies

Multi-phase transitions of the films and lipid nanoparticles during the heating process have been thoroughly investigated by DSC measurements and the results are given in Figure 56 and Table 20. The crystallinity in polymeric materials is generally dependent on the crystallization rate, which follows a bell-shaped curve between the temperatures T_g and T_m . High DSC transition values would correspond mainly to the fusion of the crystals formed from the products of alkaline hydrolysis of starch during storage. Endothermic peak (A) at high temperature in hydropropyl starch film is due to crystallinity. This endothermic peak was not seen in the nanocomposite films. Presence of lipid nanoparticles have a plasticizing effect which increases the mobility of the polysaccharide chains and prevents crystallinity.

DSC thermogram of CA-NP shows 4 melting peaks where P1 and P2 represent different polymorph of CB and P3 and P4 represent Span60 respectively. Peak temperature T_p of P1 is around 20°C corresponds the melting temperature of α -form unstable crystal form of CB whereas P2 corresponds to β -form which is a stable crystal form with a higher melting point. Polymorphism in CB at the lipid core affects the encapsulation efficiency of CA. Presence of α -polymorph which is stabilized by surfactants in a lipid nanoparticle enables higher loading of actives due to its less compact packing between α -crystals compared to those of β -polymorph. This is a desired attribute for this delivery system which is also confirmed by DSC analysis. Endotherm peaks corresponding to CB were observed in the nanocomposite films with shift in T_p to lower melting temperatures. These results further explain the polymorphism of CB in nanoparticles embedded in polysaccharide matrix. The core of lipid nanoparticles is composed of mixed

crystals of different polymorphs of CB which is influenced by its composition and processing parameters. Shift to lower melting points suggest that mixed crystal has higher amounts of α -crystals than the control CA-NP-6.

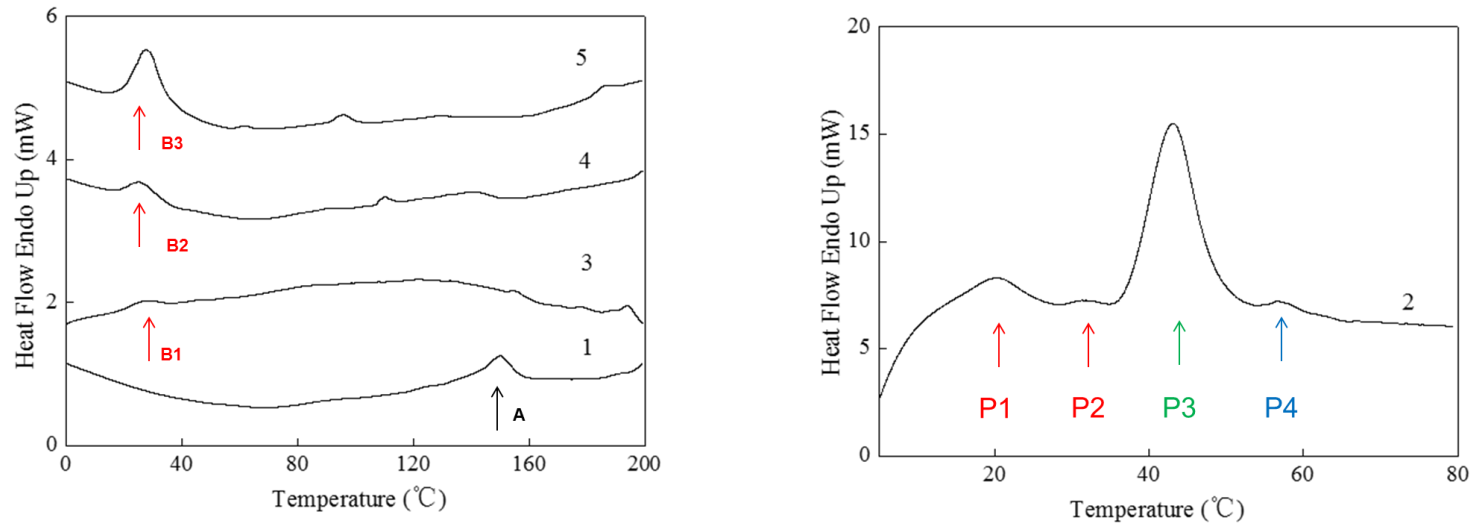


Figure 56 DSC thermograms of HP starch (1), CA-NP (2), nanocomposites HGCN-0.5 (3), HGCN-1 (4) and HGCN-2 (5)

Table 20 Endothermic peaks of HGCN-0 (control), CA loaded nanoparticles and nanocomposites

	Peak	T_o (°C)	T_p (°C)	T_c (°C)	ΔH (J/g)
HGCN-0 (1)	A	138.4	150.2	160.0	2.7
	P1	12.5	20.4	27.6	8.1
CA-NP-6 (2)	P2	28.6	31.3	35.1	0.5
	P3	36.4	43.1	53.1	55.1
	P4	54.1	56.7	60.9	1.0
HGCN-0.5 (3)	B1	16.5	27.2	38.9	0.9
HGCN-1 (4)	B2	15.4	25.7	38.2	2.0
HGCN-2 (5)	B3	17.8	27.8	45.0	7.9

7.3.4 Mechanical Properties of HGCH films

Analysis of mechanical properties of edible films is useful to predict its behavior in its applications in food products. Elasticity modulus , tensile strength and elongation at break are parameters that are studied for describing the mechanical properties of a film, and are closely related with its internal structure.(274)

Typical stress–strain curves of HGCH nanocomposite films obtained at 25 °C and 50% RH are shown in Figure 57. The values of tensile strength (MPa), elongation % and elastic modulus (MPa) are reported in Table 21. Hydroxypropyl starch films (HGCH-0) have higher maximum tensile strength (~ 5MPa) and brittle mechanical behavior as the films broke at slight plastic deformation. Tensile strength in starch films is attributed to the crystallinity in the matrix which occurs due to organized arrangement of polysaccharides chains in the starch. With CA-NP embedded in matrix, films have lower tensile strength compared to the control. Elastic modulus of all films are around 2.65 MPa with their elongation around at 214%. High strain at break property in the films is due to the plasticizing effect of glycerol between polymer chains.

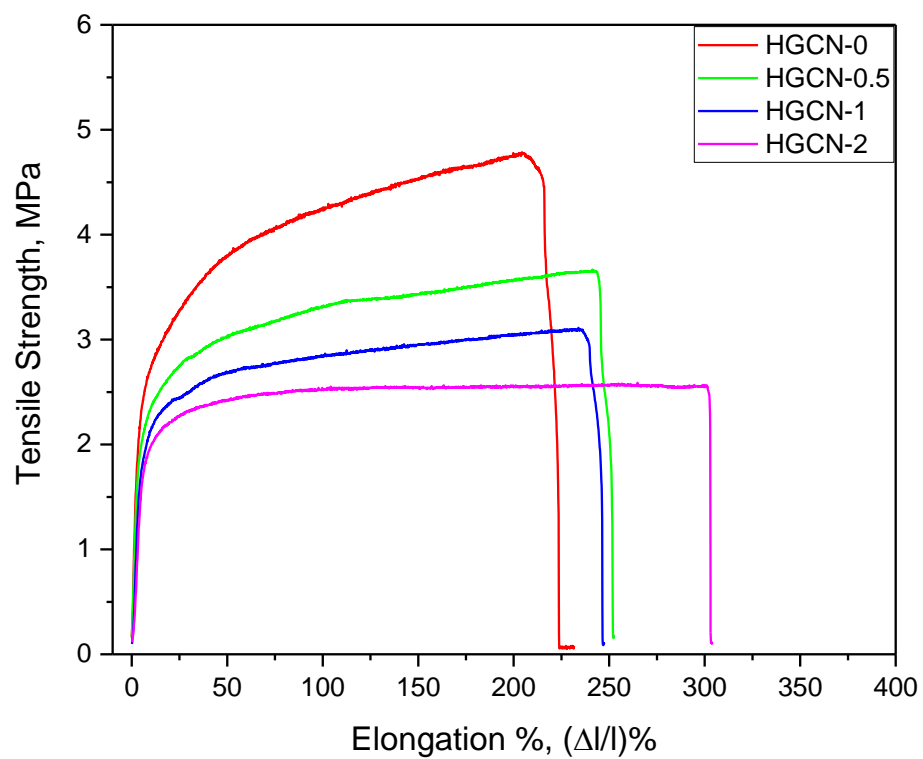


Figure 57 Tensile-strain curves of the films cast at 25 °C and 50% of relative humidity. Water content (17.3% ± 0.3)

Table 21 Mechanical Properties of HGCN films

	Tensile Strength (MPa)	Elongation %	Elastic Modulus (MPa)
HGCN-0	4.7 ± 0.3^a	220.8 ± 26.6^d	3.0 ± 0.2
HGCN-0.5	3.5 ± 0.2^b	234.0 ± 32.8^d	2.2 ± 0.1
HGCN-1	3.9 ± 0.7^{ab}	230.1 ± 101.1^{de}	2.4 ± 0.5
HGCN-2	2.5 ± 0.1^c	140.7 ± 22.8^e	3.0 ± 0.2

7.3.5 Moisture Barrier Properties of HGCN films

7.3.5.1 Contact angle measurements

The hydrophilicity of the films was quantitatively illustrated by measurements of the water droplet absorption kinetics. The kinetics of water absorption is demonstrated by measurements of the initial contact angle of water droplet just after deposition and rate of change of contact angle ($^{\circ}/\text{min}$) which corresponds to the slope of contact angle-time curve (Table 8). There was no significant change in the initial contact angle when low amount of CA-NP was present in the system. In HGCN-1 film, there is a slight increase in hydrophilicity as the initial contact angle was lower than that of the control (HGCN-0). The wetting properties of a film is defined by the molecular interactions of water and molecules that are present at the surface of the film. Roughness or irregularities on the surface can significantly affect the wetting behavior. In figure 15, surface morphology of the films show that the HGCN-0 and HGCN-0.5 have relatively even surfaces than HGCN-1. Due to micro-aggregates of lipids on HGCN-1, the surface roughness greatly increases which explains the decrease in the initial contact angle. Slopes of contact angle-time from absorption didn't significantly change with presence of lipid nanoparticles. Interaction between the water molecules and hydrophilic groups of HP starch influences the absorption kinetics in all the films. No change in slopes of droplet absorption rate further confirms no separation of lipid and polymer phases due to difference in their density and homogeneity of the film matrix.

Table 22 Contact measurements and surface absorption kinetics of HGCN films

	Initial Contact Angle (°)	Change in Contact Angle (°/s)
HGCN-0	67.7 ± 6.0^a	-0.4
HGCN-0.5	61.7 ± 7.1^{ab}	-0.3
HGCN-1	55.2 ± 1.4^b	-0.3

7.3.5.2 Moisture Absorption Isotherms

Temperature and relative humidity effects on water vapor solubility in the polymer can be deduced from water sorption isotherm. In Figure 58 show water vapor absorption kinetics in different films by equilibrating at different relative humidity values. It is observed that at higher humidity ($>75\%$), water absorption rate of control film, HGCN-0 was relatively high due to presence of hydrophilic groups on the polysaccharide chains and presence of glycerol with high water retention capabilities. In case of nanocomposites, water vapor absorption is low over a range of relative humidity values ($< 75\%$) (Figure 59). Possible molecular interactions between the nanoparticles and starch are responsible for low affinity to water vapor. Condensation of water molecules in the film matrix is shifted to higher RH in nanocomposites. In hydrophilic polymers, layers of water are absorbed into the matrix after condensation. Nanocomposites with hydrophobic lipid core and interaction of polymer and lipid or surfactants would hinder the interactions between the water molecules and further prevents condensation. From these observations, the nanocomposite films show poor solubility of water vapor and resilient at higher humidity.

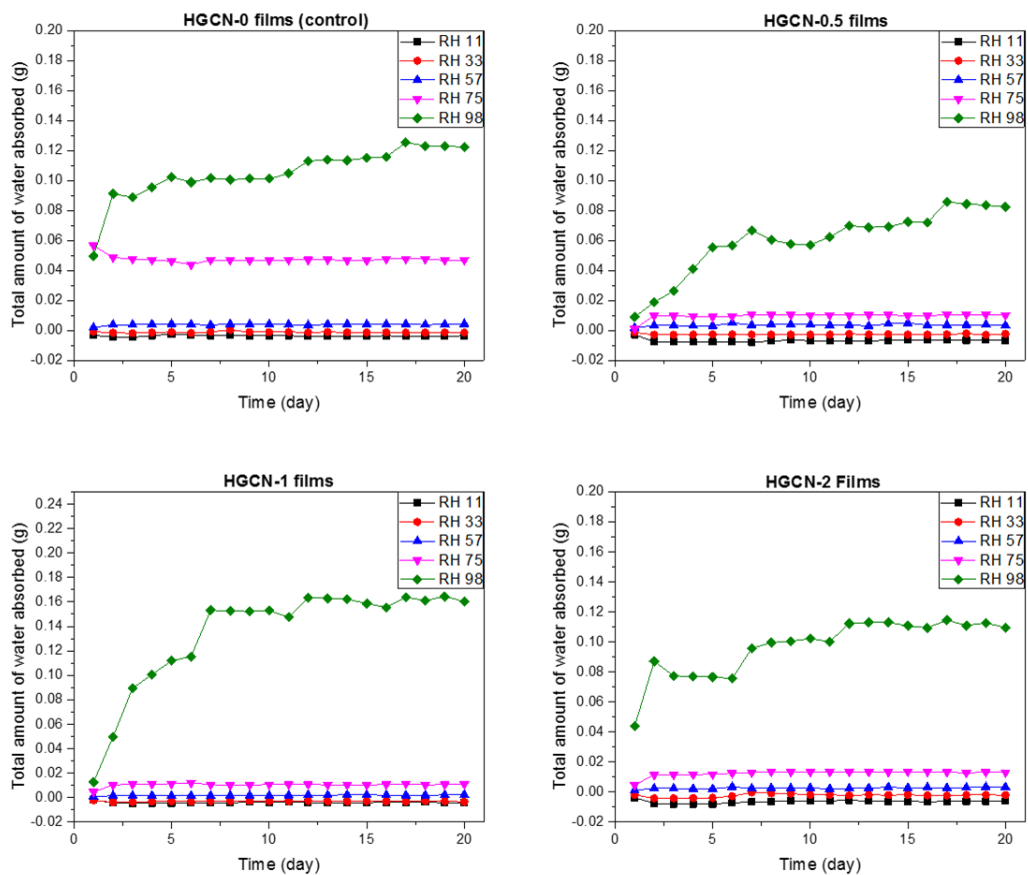


Figure 58 Water sorption isotherm of HP starch and nanocomposite films at different relative humidity at 25°C.

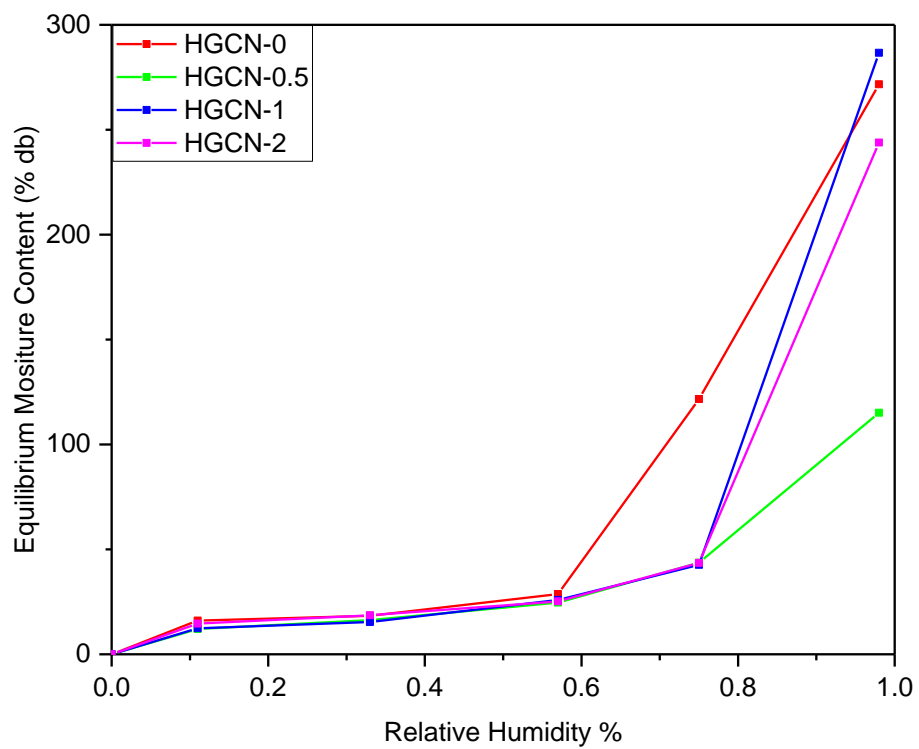


Figure 59 Moisture Isotherms of HP starch (HGCN-0) and nanocomposites (HGCN-0.5, HGCN-1 and HGCN-2) at 25°C

7.3.5.3 Water Uptake studies

Maximum hydration of the films was studied to understand water uptake and swelling behavior. In Figure 60, all the nanocomposites has similar swelling behavior with water uptake around 155% and was 40% lower than the control film (HGNCN-0). Hydration of hydrophilic groups of the polymers and glycerol content % in the starch increases the swelling. By introducing fillers in the film, the nanoparticles occupy the capillary network as the film begins to swell and obstructing the water molecules to interact with starch polymers. Solubility of starch polymers in water is influenced by the strength of interactions between water and intermolecular and intramolecular H bonds between amylose and amylopectin. Substitution of hydroxypropyl groups on starch polymers make it hydrophilic and increases the solubility of HP starch. Glycerol as plasticizer also increases the affinity of water in HP starch film. By introducing fillers in the film, the nanoparticles occupy the capillary network as the film begins to swell and obstructing the water molecules to interact with starch polymers.

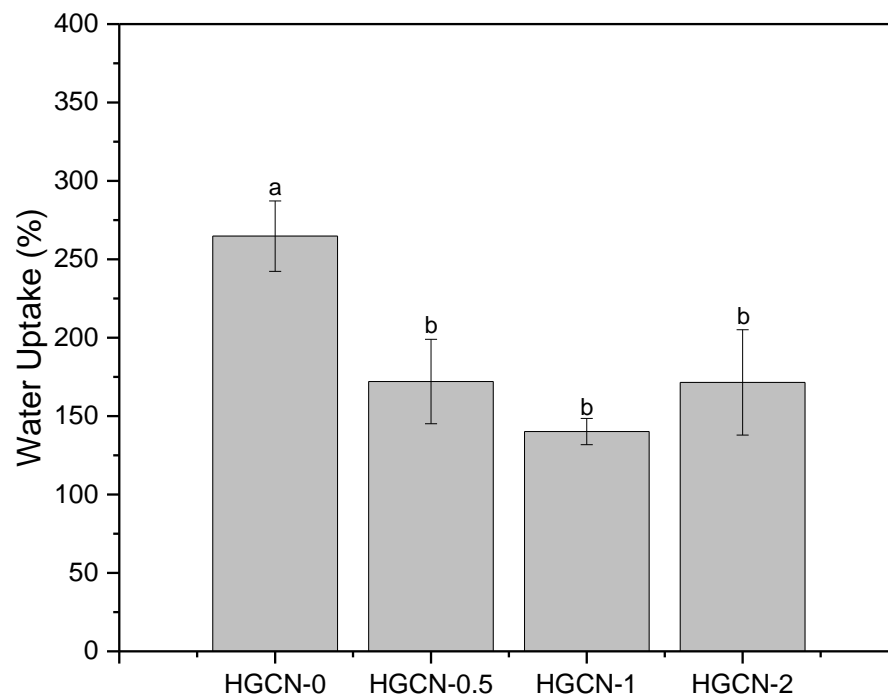


Figure 60 Water uptake % by swelling in HP starch and nanocomposite films

(Mean comparison by Tukey test, $p < 0.05$)

7.3.5.4 Water Vapor Permeability

Mechanisms of water mass transfer and solute-polymers can be studied by water vapor permeability values of edible films. Water vapor permeability results of HGCN films are shown in Figure 23 and all except HGCN-0.5 show no significant difference.

According to the thermodynamics of irreversible process, water chemical potential difference is the driving force of the water transfer through a film. When the process occurs at constant temperature and pressure, the water chemical potential difference results proportional to water vapor concentration difference between the two sides of the films. (275) Permeability can be defined as the product of diffusivity and solubility only when Fick and Henry laws fully apply. For most edible films, the water vapor strongly interacts with polymer structure, which results in diffusion and solubility coefficients dependent on driving force. The physiochemical properties of a films (microstructure, composition and chemical nature of the components) can influence the water transfer from high to low water potential. Plasticizer, glycerol increase chain mobility of the starch by reducing intermolecular forces between the chains and thereby improving the flexibility and extensibility of the films but they also increase diffusion coefficients of gases and water molecules across the films. (276) Effects on addition of lipid nanoparticles as fillers on water vapor transfer is not based on solubility by low affinity of water vapor but it is a complex mechanism that requires better understanding. From the microstructure analysis, HGCN-0.5 had no phase separation and the matrix seemed continuous and homogenous yet difference when comparing with control HGCN-0.

Water interactions in the nanocomposite films is certainly a complex mechanism which could involve interactions between the CB, surfactant, glycerol and starch at

molecular level. Physical behavior of the films can be further investigated by studying and understanding interactions and affinities between triglycerides, amphiphilic surfactants, glycerol, and modified starch by temperature and composition.

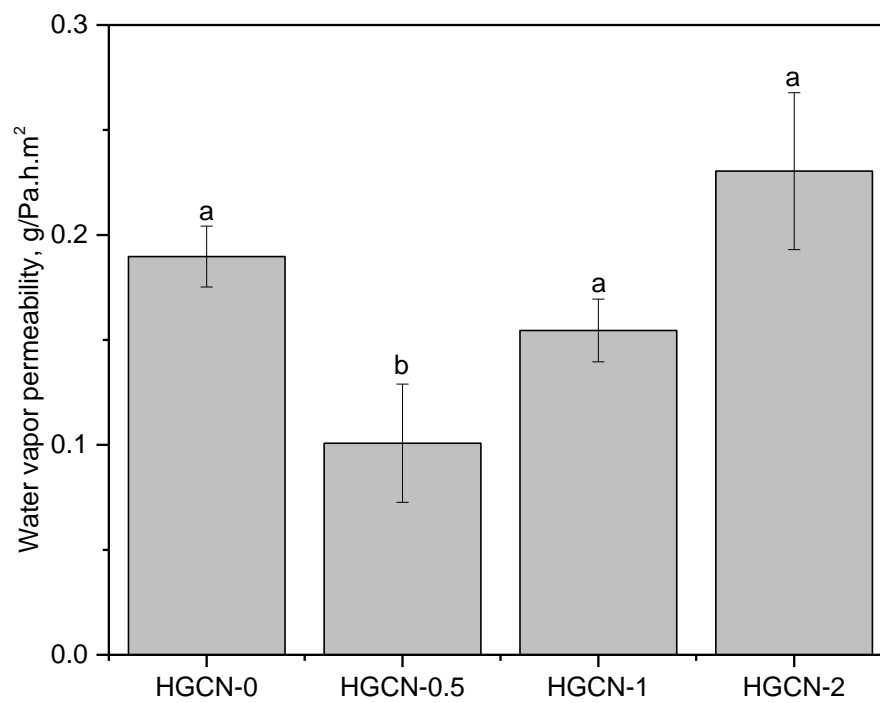


Figure 61 Water vapor permeance of HP starch and nanocomposite films (Mean comparison by Tukey test, $p < 0.05$)

7.3.6 Antioxidant Activity in HGCN films

DPPH radical scavenging assay is one of the standard and easy colorimetric method for assessment of scavenging potential of stable DPPH radicals by an antioxidant compound and thereby, quantify the antioxidant activity of the compound. DPPH[•] radical has a purple color in methanol solution and its absorbance is measured at 517 nm. A change in color is measured by absorbance when DPPH is reduced to DPPH₂ by accepting H atom from antioxidant compound (scavenging molecule) and turning into yellow in solution. In our study, we used fixed time reaction model to calculate the scavenging rate with the assumption that the steady state saturation (maximum decrease in DPPH) is reached within 30 min. IC₅₀ of carnosic acid in acetonitrile is 12.63±1.7 µg/ml. Antioxidant capacity of CA in CB, CB nanoparticle and nanocomposite are listed in Table 23. Antioxidant capacity compares the scavenging rate of DPPH by CA in different delivery system approach. Antioxidant capacity of the CA in CB mixture and CB nanoparticles was 90% and above. Antioxidant capacity is lower than 100% could be possibly be due to conversion of carnosic acid in digestion buffer at pH 7.5 and its instability in solution form.^(50, 266) The phenolic hydroxyl group on CA is easily oxidized and degraded under alkaline conditions. The digested solutions of CA+CB and CA-NP-6 appeared darker due to oxidation. The antioxidant activity didn't significantly change since the degradation products of CA. ⁽²⁷⁷⁾ Digested nanocomposites showed lower antioxidant capacity around 40% and different degradation products were observed in HPLC spectrogram of aqueous phase of the digested nanocomposites (Figure 62). Two possible explanations for this decrease is (i) Incomplete digestion of HP which could have entrapped some of CA-NP during separation of aqueous and insoluble phase of the digested solutions and (ii) possible aggregates due

to interactions of mixed micelles with digested starch polymers. On analyzing solvent extracts of the insoluble phase of digested films, some amount of CA was detected. (Data not shown). Hydroxypropylation of starch influences its digestion by digestive enzymes. With increase in degree of hydroxypropyl group substitution ($<MS$ 0.08) on starch, susceptibility to digestion increased. Bulky substituents on C2 of the glucose unit possibly cause steric hindrance at active-site of α -amylase and obstruct positioning of the substrate which would effectively restrict enzymatic hydrolysis of adjacent glycosidic bonds of unsubstituted glucose units. Starches with MS greater than 0.08 have increased digestibility compared to native starch which is attributed to its swelling behavior.(278) Gelatinization of hydroxypropyl starch has reduced digestibility while ungelatinized starch granules etherified with hydroxypropyl groups allowed better swelling and increased amylolysis.(279) Apparent digestion of raw and HP starch was studied in rats and true digestion in antibiotic treated rats.(280) The extent of digestion and absorption was reduced to a low level, about 50% for hydroxypropylated starch, which was not significantly different from that with the corresponding raw material. Gelatinization of HP starch had no significant effect on digestion. Compared to antibiotic treated rats, metabolism of HP starch by gut microbiota was very limited. Digestion of starch by α -amylase forms maltose and maltotriose as principal chain products by hydrolysis of glycosidic bonds at multiple sites. At the active site of α -amylase, 5 glucose residues of a linear chain get attached. The glycosidic bond between 3 and 4 residues is hydrolyzed in which carboxyl groups of key aspartate and glutamate residues at the active site of the enzyme function as acid-base and nucleophilic catalysts.

Introduction of a hydroxypropyl group on polysaccharide chain would interfere the binding of the residues to the active site. Modification of starch results short starch polymers by enzymatic action of amylase. Digestion products of HP starch can change the specific gravity of the solution and on centrifugation, they formed a layer apart above the insoluble part of the starch. This could form aggregates of CA micelles entrapped in gel-like hydrosylate layer. This could have lowered the concentration of CA in the aqueous phase and making nanocomposites not an effective delivery system for bioactives loaded in CB nanoparticles.

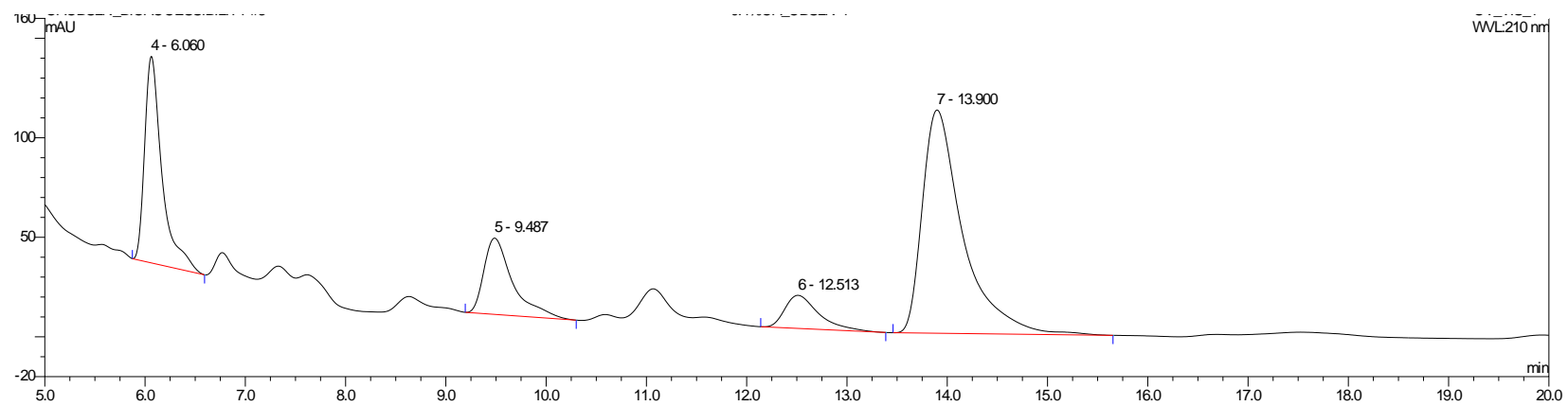


Figure 62 HPLC spectrogram of aqueous phase of digested HGNC-6 nanocomposite film

Table 23 Antioxidant Capacity (%) of CA+CB mixture, nanoparticles and HS nanocomposite film

	Antioxidant Capacity (%)	
	Fed State	Fast State
CA+CB Mixture	93.5 ± 0.5 ^a	88.8 ± 1.3 ^c
CA-NP-6	96.3 ± 2.5 ^b	91.5 ± 1.8 ^{ac}
HGCN-6	43.3 ± 5.6 ^b	37.3 ± 4.7 ^b

7.4 Conclusion

Biopolymer based nanocomposites from edible and renewable resources are suitable alternative to conventional packaging materials which serve similar functions by improving weak mechanical and poor barrier properties. The most common nanocomposite systems are hybrids of organic and inorganic materials like silicates dispersed in polymer matrix on nanoscale and more recently, nanocellulose in composite materials are gaining more attention due to its compatibility with hydrophilic biopolymers. There is a need to explore other alternatives for nanoscale fillers to create novel nanocomposite materials with interesting properties.

The above studies suggest that introduction of solid lipid nanoparticles could serve as filler material in the edible film matrix and deliver hydrophobic bioactives encapsulated in them. Moisture barrier properties are limited to the amount of NP in the matrix as higher amounts of NP (> 4 % dry weight basis) lead to microphase separation between polymer and lipid. The stiffness of the films characterized by tensile strength of the films were significantly reduced by introduction of NP which confirms their plasticizing effect. The release of bioactive in NP from nanocomposite could be dependent on digestibility of biopolymer and solubility of released bioactive in aqueous phase of digested nanocomposite. We conclude that CA loaded CB nanoparticles can be potential nanofillers in creating hydroxypropyl starch nanocomposite edible films with improved moisture barrier properties to overcome hydrophilic nature of the HP starch and can serve as potential drug delivery system.

CHAPTER 8. SUMMARY AND FUTURE WORK

8.1 Summary

From my research, lipid nanoparticles (LN) can perform as nanofiller in biopolymers to improve barrier properties and deliver non-polar bioactives in both beverage and functional edible film applications.

In films, concentration and lipid type chosen can significantly affect its physical properties. Similar to other nanocomposite material literature, low concentration of lipid nanoparticles in biopolymers can improve the barrier properties. Homogeneity of the matrix and type of lipid (based on its chemical structure and crystallinity) can influence the interaction of water with the polymer matrix. To achieve a homogenous composite films, concentration of lipid nanoparticles plays a very important role and is a limiting factor for different properties that were studied. Choice of lipid and characteristics of lipid nanoparticles become crucial factors in developing nanocomposites for specific purposes. For better understanding of potential applications of these lipid based nanocomposites, a scheme of standardized testing need to be performed to quantify its barrier, mechanical and desired properties. A strategic model of different standardized testing can be developed to assess different lipid nanoparticles that can create different nanocomposite films for multiple purposes. In my study, I was able to develop such model to assess performance of 2 different lipid nanoparticles to produce nanocomposite films with improved moisture barrier properties.

8.2 Future Work

8.2.1 Comparative study with other alternative nanocomposite films in real food systems

Future work on lipid NP based nanocomposite films can focus on comparing them with other films that are developed for similar application. For example, there are other lipid based biopolymers films (multilayer films, emulsion type films etc.) reported to have excellent water resistance abilities. Characterization methods described in this research can be extended to other kind of films to understand structure-function relationship to explain the film behavior. This kind of study would put light on relevance and importance of nanotechnology and its approaches in packaging material. Casings and films prepared using these approach can be tested on real food systems (eg. Meats, fresh cut vegeables or capsule material). These studies would highlight practical implications of these novel nanocomposites and can further manipulated to improve the quality and safety of the food.

8.2.2 Response surface methodology for optimization of film composition

Response surface methodology (RSM) is a statistical tool to establish functional relationship between a response of interest, y and a number of associated input variables denoted by x_1, x_2, \dots, x_k which can be approximated by polynomial model of low degree:

$$y = f'(x)\beta + \epsilon$$

where $x = (x_1, x_2, \dots, x_k)$, $f(x)$ is a vector function of p elements that consists of powers and cross- products of powers x_1, x_2, \dots, x_k of up to a certain degree denoted by d (≥ 1), β is a vector of p unknown constant coefficients referred to as parameters, and ϵ is a random experimental error assumed to have a zero mean.(281) Apart from predicting

response values for a given input from the model, one can determine the significance of the factors whose levels are represented by x_1, x_2, \dots, x_k and optimize the input variables to give range of responses of interest.

From this research, we identified the most significant input variables that could influence performance of film in different applications. Type of lipid and amount of lipid nanoparticles in a biopolymer based film are input variables that can affect both moisture barrier and mechanical properties of the film. Central composite design can be adopted for RSM experiments. Fractional factorial design can be used to reduce the number of experiments whereas saturated designs like Plackett–Burman design which is popularly used to develop process conditions to understand the effects of physiochemical, biochemical and sensory variables with least possible number of experiments. Interaction of different factors can be analyzed using full factorial designs.

8.2.3 Lymphatic transport studies for bioactive loaded lipid nanoparticles

Efficacy of a bioactive is dependent on its fate after consumption and delivery system are designed to protect and stabilize to ensure bioactives reach the target tissue without degradation due to physiological processes in the body. Lipid absorption studies have shown that lipid based formulations stimulate production of lipoproteins in enterocytes after their digestion. These lipoproteins along with triglycerides and non-polar bioactives self-assemble to form chylomicrons (80nm – 1mm in diameter) which have low permeability to blood capillary endothelium. This allows chylomicrons to enter the lymphatic route due to its relatively open structure. Since chylomicrons have a lipid based core, the non-polar bioactives with high lipid solubility (> 50 mg/ml) and have higher partition in octanol: water mixture ($\log P > 5$) mostly reside after entering enterocytes as

micelles made of fatty acids, 2-monoglycerides and bile salts. From our studies, it is observed that both Coenzyme Q10 and carnosic acid have high solubility in cocoa butter which confirms that they would preferentially take lymphatic route to reach systematic circulation. Also cocoa butter which is the lipid carrier is composed of long chain fatty acids (greater than C16), lymphatic transport could be a primary mechanism of bioactive transport as increase in fatty acid chain correlates with increase in lymphatic transport.(255)

Simple bioavailability studies give plasma concentration of drugs over time after consumption and doesn't add to the mass balance of drugs due to insufficiency of the approach in these tests. Systemic exposure due to lymphatic transport is needed to understand the absolute bioavailability of the lipophilic drugs. Since traditional pharmacokinetic studies involve lymph intact animals, the data on amount of drug transport in the lymph is ignored which is a crucial factor to be considered. Lymph-cannulated, unrestrained and conscious animal models can be used to evaluate the lymphatic transport of bioactives and proportion of this lymph transported bioactive is absorbed into the blood.

These findings can further our understanding in manipulating these nanoparticles in edible films to create novel functional products. This research was conducted as a proof of concept for usage of lipid nanoparticles as a nanofiller in biopolymer based nanocomposites.

BIBLIOGRAPHY

1. Hauss, D. J., Oral lipid-based formulations. *Advanced Drug Delivery Reviews* **2007**, *59*, 667-676.
2. Fricker, G.; Kromp, T.; Wendel, A.; Blume, A.; Zirkel, J.; Rebmann, H.; Setzer, C.; Quinkert, R.-O.; Martin, F.; Müller-Goymann, C., Phospholipids and Lipid-Based Formulations in Oral Drug Delivery. *Pharm Res* **2010**, *27*, 1469-1486.
3. Mora-Huertas, C. E.; Fessi, H.; Elaissari, A., Polymer-based nanocapsules for drug delivery. *International Journal of Pharmaceutics* **2010**, *385*, 113-142.
4. Torchilin, V. P., Structure and design of polymeric surfactant-based drug delivery systems. *Journal of Controlled Release* **2001**, *73*, 137-172.
5. Weiss, J.; Takhistov, P.; McClements, D. J., Functional Materials in Food Nanotechnology. *Journal of Food Science* **2006**, *71*, R107-R116.
6. McClements, D. J.; Rao, J., Food-Grade Nanoemulsions: Formulation, Fabrication, Properties, Performance, Biological Fate, and Potential Toxicity. *Critical Reviews in Food Science and Nutrition* **2011**, *51*, 285-330.
7. zur Muhlen, A.; Schwarz, C.; Mehnert, W., Solid lipid nanoparticles (SLN) for controlled drug delivery - Drug release and release mechanism. *Eur J Pharm Biopharm* **1998**, *45*, 149-155.
8. H Muller, R.; Shegokar, R.; M Keck, C., 20 Years of Lipid Nanoparticles (SLN NLC): Present State of Development Industrial Applications. *Current drug discovery technologies* **2011**, *8*, 207-227.
9. Jennings, V.; Thunemann, A. F.; Gohla, S. H., Characterisation of a novel solid lipid nanoparticle carrier system based on binary mixtures of liquid and solid lipids. *Int J Pharmaceut* **2000**, *199*, 167-177.
10. Muller, R. H.; Mader, K.; Gohla, S., Solid lipid nanoparticles (SLN) for controlled drug delivery - a review of the state of the art. *Eur J Pharm Biopharm* **2000**, *50*, 161-77.
11. Olbrich, C.; Gessner, A.; Kayser, O.; Müller, R. H., Lipid-drug-conjugate (LDC) nanoparticles as novel carrier system for the hydrophilic antitrypanosomal drug diminazenediacetate. *J Drug Target* **2002**, *10*, 387-396.
12. Pardeike, J.; Hommoss, A.; Müller, R. H., Lipid nanoparticles (SLN, NLC) in cosmetic and pharmaceutical dermal products. *Int J Pharmaceut* **2009**, *366*, 170-184.
13. Siro, I.; Kapolna, E.; Kapolna, B.; Lugasi, A., Functional food. Product development, marketing and consumer acceptance—a review. *Appetite* **2008**, *51*, 456-467.
14. Khan, R. S.; Grigor, J.; Winger, R.; Win, A., Functional food product development – Opportunities and challenges for food manufacturers. *Trends in Food Science & Technology* **2013**, *30*, 27-37.
15. Grunert, K. G., European consumers' acceptance of functional foods. *Annals of the New York Academy of Sciences* **2010**, *1190*, 166-173.
16. Sloan, A. E., The top ten functional food trends. *Food Technology* **2000**, *54*, 33-62.
17. Sloan, A. E., The top 10 functional food trends: the next generation. *Food Technology* **2002**, *56*, 32-57.

18. Sloan, A. E., The top 10 functional food trends 2004. *Food Technology* **2004**, *58*, 28-51.
19. Allen, T. M.; Cullis, P. R., Drug Delivery Systems: Entering the Mainstream. *Science* **2004**, *303*, 1818-1822.
20. Ezhilarasi, P. N.; Karthik, P.; Chhanwal, N.; Anandharamakrishnan, C., Nanoencapsulation Techniques for Food Bioactive Components: A Review. *Food Bioprocess Technol* **2013**, *6*, 628-647.
21. Jennings, V.; Gohla, S. H., Encapsulation of retinoids in solid lipid nanoparticles (SLN (R)). *J Microencapsul* **2001**, *18*, 149-158.
22. Weiss, J.; Decker, E. A.; McClements, D. J.; Kristbergsson, K.; Helgason, T.; Awad, T., Solid lipid nanoparticles as delivery systems for bioactive food components. *Food Biophys* **2008**, *3*, 146-154.
23. Tarr, B. D.; Yalkowsky, S. H., Enhanced intestinal absorption of cyclosporine in rats through the reduction of emulsion droplet size. *Pharmaceutical research* **1989**, *6*, 40-43.
24. Liversidge, G. G.; Cundy, K. C., Particle size reduction for improvement of oral bioavailability of hydrophobic drugs: I. Absolute oral bioavailability of nanocrystalline danazol in beagle dogs. *International Journal of Pharmaceutics* **1995**, *125*, 91-97.
25. Liversidge, G. G.; Conzentino, P., Drug particle size reduction for decreasing gastric irritancy and enhancing absorption of naproxen in rats. *International journal of pharmaceutics* **1995**, *125*, 309-313.
26. Porter, C. J.; Charman, W. N., In vitro assessment of oral lipid based formulations. *Advanced drug delivery reviews* **2001**, *50*, S127-S147.
27. Shackelford, D. M.; Faassen, W. F.; Houwing, N.; Lass, H.; Edwards, G. A.; Porter, C. J.; Charman, W. N., Contribution of lymphatically transported testosterone undecanoate to the systemic exposure of testosterone after oral administration of two andriol formulations in conscious lymph duct-cannulated dogs. *Journal of Pharmacology and Experimental Therapeutics* **2003**, *306*, 925-933.
28. Keck, C.; Fichtinger, A.; Viernstein, H.; Muller, R. In *Oral drug nanocrystals—effect of potential aggregation on bioavailability*, Annual Meeting of Pharmaceutical Scientists (AAPS), Baltimore, MD, 2004; 2004; p 2746.
29. Shellhammer, T. H.; Rumsey, T. R.; Krochta, J. M., Viscoelastic properties of edible lipids. *J Food Eng* **1997**, *33*, 305-320.
30. Toro-Vazquez, J. F.; Morales-Rueda, J. A.; Dibildox-Alvarado, E.; Charo-Alonso, M.; Alonzo-Macias, M.; Gonzalez-Chavez, M. M., Thermal and textural properties of organogels developed by candelilla wax in safflower oil. *J Am Oil Chem Soc* **2007**, *84*, 989-1000.
31. Hagenmaier, R. D.; Baker, R. A., Reduction in gas-exchange of citrus-fruit by wax coatings. *Journal of Agricultural and Food Chemistry* **1993**, *41*, 283-287.
32. Paredes-López, O.; Camargo-Rubio, E.; Gallardo-Navarro, Y., Use of coatings of candelilla wax for the preservation of limes. *Journal of the Science of Food and Agriculture* **1974**, *25*, 1207-1210.
33. Hagenmaier, R. D.; Baker, R. A., Layered coatings to control weight-loss and preserve gloss of citrus-fruit. *Hortscience* **1995**, *30*, 296-298.
34. Donhowe, G.; Fennema, O., Water vapor and oxygen permeability of wax films. *J Am Oil Chem Soc* **1993**, *70*, 867-873.

35. Lipp, M.; Simoneau, C.; Ulberth, F.; Anklam, E.; Crews, C.; Brereton, P.; de Greyt, W.; Schwack, W.; Wiedmaier, C., Composition of Genuine Cocoa Butter and Cocoa Butter Equivalents. *Journal of Food Composition and Analysis* **2001**, *14*, 399-408.
36. Wille, R.; Lutton, E., Polymorphism of cocoa butter. *J Am Oil Chem Soc* **1966**, *43*, 491-496.
37. Loisel, C.; Keller, G.; Lecq, G.; Bourgaux, C.; Ollivon, M., Phase transitions and polymorphism of cocoa butter. *Journal of the American Oil Chemists' Society* **1998**, *75*, 425-439.
38. Crane, F. L., Biochemical functions of coenzyme Q10. *Journal of the American College of Nutrition* **2001**, *20*, 591-598.
39. Ernster, L.; Forsmark-Andree, P., Ubiquinol: an endogenous antioxidant in aerobic organisms. *The clinical investigator* **1993**, *71*, S60-S65.
40. Frei, B.; Kim, M. C.; Ames, B. N., Ubiquinol-10 is an effective lipid-soluble antioxidant at physiological concentrations. *Proceedings of the National Academy of Sciences* **1990**, *87*, 4879-4883.
41. Sarter, B., Coenzyme Q10 and Cardiovascular Disease: A Review. *Journal of Cardiovascular Nursing* **2002**, *16*, 9-20.
42. Mortensen, S. A., Endomyocardial biopsy. Technical aspects and indications. *Dan Med Bull* **1989**, *36*, 507-532.
43. Mizuno, K.; Tanaka, M.; Nozaki, S.; Mizuma, H.; Ataka, S.; Tahara, T.; Sugino, T.; Shirai, T.; Kajimoto, Y.; Kuratsune, H.; Kajimoto, O.; Watanabe, Y., Antifatigue effects of coenzyme Q10 during physical fatigue. *Nutrition* **2008**, *24*, 293-299.
44. Rosenfeldt, F.; Hilton, D.; Pepe, S.; Krum, H., Systematic review of effect of coenzyme Q10 in physical exercise, hypertension and heart failure. *BioFactors* **2003**, *18*, 91-100.
45. Cooke, M.; Iosia, M.; Buford, T.; Shelmadine, B.; Hudson, G.; Kerksick, C.; Rasmussen, C.; Greenwood, M.; Leutholtz, B.; Willoughby, D., Effects of acute and 14-day coenzyme Q10 supplementation on exercise performance in both trained and untrained individuals. *Journal of the International Society of Sports Nutrition* **2008**, *5*, 1-14.
46. Muralikrishnan, D.; Jun, R., The Emerging Role of Coenzyme Q-10 in Aging, Neurodegeneration, Cardiovascular Disease, Cancer and Diabetes Mellitus. *Current Neurovascular Research* **2005**, *2*, 447-459.
47. Roffe, L.; Schmidt, K.; Ernst, E., Efficacy of Coenzyme Q10 for Improved Tolerability of Cancer Treatments: A Systematic Review. *Journal of Clinical Oncology* **2004**, *22*, 4418-4424.
48. Shults, C. W.; Oakes, D.; Kieburtz, K.; Beal, M. F.; Haas, R.; Plumb, S.; Juncos, J. L.; Nutt, J.; Shoulson, I.; Carter, J., Effects of coenzyme Q10 in early Parkinson disease: evidence of slowing of the functional decline. *Archives of Neurology* **2002**, *59*, 1541.
49. Mancuso, M.; Orsucci, D.; Volpi, L.; Calsolaro, V.; Siciliano, G., Coenzyme Q10 in Neuromuscular and Neurodegenerative Disorders. *Current Drug Targets* **2010**, *11*, 111-121.
50. Munné-Bosch, S.; Alegre, L., Subcellular compartmentation of the diterpene carnosic acid and its derivatives in the leaves of rosemary. *Plant physiology* **2001**, *125*, 1094-1102.

51. Masuda, T.; Inaba, Y.; Takeda, Y., Antioxidant Mechanism of Carnosic Acid: Structural Identification of Two Oxidation Products. *Journal of Agricultural and Food Chemistry* **2001**, *49*, 5560-5565.
52. Masuda, T.; Inaba, Y.; Maekawa, T.; Takeda, Y.; Tamura, H.; Yamaguchi, H., Recovery Mechanism of the Antioxidant Activity from Carnosic Acid Quinone, an Oxidized Sage and Rosemary Antioxidant. *Journal of Agricultural and Food Chemistry* **2002**, *50*, 5863-5869.
53. Jimenez, A.; Jose Fabra, M.; Talens, P.; Chiralt, A., Edible and Biodegradable Starch Films: A Review. *Food and Bioprocess Technology* **2012**, *5*, 2058-2076.
54. López, O. V.; Zaritzky, N. E.; García, M. A., Physicochemical characterization of chemically modified corn starches related to rheological behavior, retrogradation and film forming capacity. *Journal of Food Engineering* **2010**, *100*, 160-168.
55. López, O. V.; García, M. A.; Zaritzky, N. E., Film forming capacity of chemically modified corn starches. *Carbohydrate Polymers* **2008**, *73*, 573-581.
56. Park, H.; Weller, C.; Vergano, P.; Testin, R., Permeability and mechanical properties of cellulose-based edible films. *Journal of Food Science* **1993**, *58*, 1361-1364.
57. Imran, M.; El-Fahmy, S.; Revol-Junelles, A. M.; Desobry, S., Cellulose derivative based active coatings: Effects of nisin and plasticizer on physico-chemical and antimicrobial properties of hydroxypropyl methylcellulose films. *Carbohydrate Polymers* **2010**, *81*, 219-225.
58. Osorio, F. A.; Molina, P.; Matiacevich, S.; Enrione, J.; Skurtys, O., Characteristics of hydroxy propyl methyl cellulose (HPMC) based edible film developed for blueberry coatings. *Procedia Food Science* **2011**, *1*, 287-293.
59. Rodionova, G.; Lenes, M.; Eriksen, Ø.; Gregersen, Ø., Surface chemical modification of microfibrillated cellulose: improvement of barrier properties for packaging applications. *Cellulose* **2011**, *18*, 127-134.
60. Kester, J.; Fennema, O., An Edible Film of Lipids and Cellulose Ethers: Performance in a Model Frozen-Food System. *Journal of Food Science* **1989**, *54*, 1390-1392.
61. Rhim, J.-W., Physical and mechanical properties of water resistant sodium alginate films. *LWT - Food Science and Technology* **2004**, *37*, 323-330.
62. Pranoto, Y.; Salokhe, V. M.; Rakshit, S. K., Physical and antibacterial properties of alginate-based edible film incorporated with garlic oil. *Food Research International* **2005**, *38*, 267-272.
63. Olivas, G. I.; Mattinson, D. S.; Barbosa-Cánovas, G. V., Alginate coatings for preservation of minimally processed 'Gala' apples. *Postharvest Biology and Technology* **2007**, *45*, 89-96.
64. Benavides, S.; Villalobos-Carvajal, R.; Reyes, J. E., Physical, mechanical and antibacterial properties of alginate film: Effect of the crosslinking degree and oregano essential oil concentration. *Journal of Food Engineering* **2012**, *110*, 232-239.
65. Eça, K. S.; Machado, M. T. C.; Hubinger, M. D.; Menegalli, F. C., Development of Active Films From Pectin and Fruit Extracts: Light Protection, Antioxidant Capacity, and Compounds Stability. *Journal of Food Science* **2015**, *80*, C2389-C2396.
66. Espitia, P. J. P.; Du, W.-X.; Avena-Bustillos, R. d. J.; Soares, N. d. F. F.; McHugh, T. H., Edible films from pectin: Physical-mechanical and antimicrobial properties - A review. *Food Hydrocolloids* **2014**, *35*, 287-296.

67. Maftoonazad, N.; Ramaswamy, H. S.; Marcotte, M., Moisture Sorption Behavior, and Effect of Moisture Content and Sorbitol on Thermo-Mechanical and Barrier Properties of Pectin Based Edible Films. *International Journal of Food Engineering* **2007**, *3*.
68. Sanchez-Garcia, M. D., *Carrageenan polysaccharides for food packaging*. 2011; p 594-609.
69. Hamzah, H. M.; Osman, A.; Tan, C. P.; Ghazali, F. M., Carrageenan as an alternative coating for papaya (*Carica papaya* L. cv. Eksotika). *Postharvest Biology and Technology* **2013**, *75*, 142-146.
70. Su Cha, D.; Choi, J. H.; Chinnan, M. S.; Park, H. J., Antimicrobial Films Based on Na-alginate and κ -carrageenan. *LWT - Food Science and Technology* **2002**, *35*, 715-719.
71. Alishahi, A.; Aider, M., Applications of Chitosan in the Seafood Industry and Aquaculture: A Review. *Food Bioprocess Technol* **2012**, *5*, 817-830.
72. Elsabee, M. Z.; Abdou, E. S., Chitosan based edible films and coatings: A review. *Materials Science & Engineering C-Materials for Biological Applications* **2013**, *33*, 1819-1841.
73. Leceta, I.; Guerrero, P.; Ibarburu, I.; Duenas, M. T.; de la Caba, K., Characterization and antimicrobial analysis of chitosan-based films. *Journal of Food Engineering* **2013**, *116*, 889-899.
74. Nieto, M., Structure and Function of Polysaccharide Gum-Based Edible Films and Coatings. In *Edible Films and Coatings for Food Applications*, Huber, K. C.; Embuscado, M. E., Eds. Springer New York: 2009; pp 57-112.
75. Mikkonen, K. S.; Rita, H.; Helén, H.; Talja, R. A.; Hyvönen, L.; Tenkanen, M., Effect of Polysaccharide Structure on Mechanical and Thermal Properties of Galactomannan-Based Films. *Biomacromolecules* **2007**, *8*, 3198-3205.
76. Brandenburg, A. H.; Weller, C. L.; Testin, R. F., Edible films and coatings from soy protein. *Journal of Food Science* **1993**, *58*, 1086-1089.
77. Kasongo, K. W.; Shegokar, R.; Muller, R. H.; Walker, R. B., Formulation development and in vitro evaluation of didanosine-loaded nanostructured lipid carriers for the potential treatment of AIDS dementia complex. *Drug Dev Ind Pharm* **2011**, *37*, 396-407.
78. Rhim, J. W.; Gennadios, A.; Handa, A.; Weller, C. L.; Hanna, M. A., Solubility, tensile, and color properties of modified soy protein isolate films. *Journal of Agricultural and Food Chemistry* **2000**, *48*, 4937-4941.
79. Herald, T. J.; Gnanasambandam, R.; McGuire, B. H.; Hachmeister, K. A., Degradable wheat gluten films - preparation, properties and applications. *Journal of Food Science* **1995**, *60*, 1147-&.
80. Tanada-Palmu, P. S.; Grosso, C. R. F., Effect of edible wheat gluten-based films and coatings on refrigerated strawberry (*Fragaria ananassa*) quality. *Postharvest Biology and Technology* **2005**, *36*, 199-208.
81. Mastromatteo, M.; Chillo, S.; Buonocore, G. G.; Massaro, A.; Conte, A.; Del Nobile, M. A., Effects of spelt and wheat bran on the performances of wheat gluten films. *Journal of Food Engineering* **2008**, *88*, 202-212.
82. Marquie, C.; Aymard, C.; Cuq, J. L.; Guilbert, S., Biodegradable packaging made from cottonseed flour - formation and improvement by chemical treatments with

- gossypol, formaldehyde, and glutaraldehyde. *Journal of Agricultural and Food Chemistry* **1995**, *43*, 2762-2767.
83. Marquie, C.; Tessier, A. M.; Aymard, C.; Guilbert, S., HPLC determination of the reactive lysine content of cottonseed protein films to monitor the extent of cross-linking by formaldehyde, glutaraldehyde, and glyoxal. *Journal of Agricultural and Food Chemistry* **1997**, *45*, 922-926.
84. Buffo, R. A.; Weller, C. L.; Gennadios, A., Films from laboratory-extracted sorghum kafirin. *Cereal Chemistry* **1997**, *74*, 473-475.
85. Byaruhanga, Y. B.; Erasmus, C.; Emmambux, M. N.; Taylor, J. R. N., Effect of heating cast kafirin films on their functional properties. *Journal of the Science of Food and Agriculture* **2007**, *87*, 167-175.
86. Buchner, S.; Kinnear, M.; Crouch, I. J.; Taylor, J.; Minnaar, A., Effect of kafirin protein coating on sensory quality and shelf-life of 'Packham's Triumph' pears during ripening. *Journal of the Science of Food and Agriculture* **2011**, *91*, 2814-2820.
87. Adebisi, A. P.; Adebisi, A. O.; Jin, D. H.; Ogawa, T.; Muramoto, K., Rice bran protein-based edible films. *International Journal of Food Science and Technology* **2008**, *43*, 476-483.
88. Shin, Y. J.; Jang, S. A.; Song, K. B., Preparation and mechanical properties of rice bran protein composite films containing gelatin or red algae. *Food Science and Biotechnology* **2011**, *20*, 703-707.
89. Shin, Y. J.; Song, H. Y.; Song, B. K., Effect of a combined treatment of rice bran protein film packaging with aqueous chlorine dioxide washing and ultraviolet-C irradiation on the postharvest quality of 'Goha' strawberries. *Journal of Food Engineering* **2012**, *113*, 374-379.
90. Jangchud, A.; Chinnan, M. S., Properties of peanut protein film: Sorption isotherm and plasticizer effect. *Food Science and Technology-Lebensmittel-Wissenschaft & Technologie* **1999**, *32*, 89-94.
91. Liu, C. C.; Tellez-Garay, A. M.; Castell-Perez, M. E., Physical and mechanical properties of peanut protein films. *Lebensmittel-Wissenschaft Und-Technologie-Food Science and Technology* **2004**, *37*, 731-738.
92. Reddy, N.; Chen, L. H.; Yang, Y. Q., Thermoplastic films from peanut proteins extracted from peanut meal. *Industrial Crops and Products* **2013**, *43*, 159-164.
93. Park, H. J.; Chinnan, M. S.; Shewfelt, R. L., Edible corn-zein film coatings to extend storage life of tomatoes. *Journal of Food Processing and Preservation* **1994**, *18*, 317-331.
94. Yamada, K.; Takahashi, H.; Noguchi, A., Improved water resistance in edible zein films and composites for biodegradable food packaging. *International Journal of Food Science and Technology* **1995**, *30*, 599-608.
95. Rakotonirainy, A. M.; Wang, Q.; Padua, G. W., Evaluation of zein films as modified atmosphere packaging for fresh broccoli. *Journal of Food Science* **2001**, *66*, 1108-1111.
96. Viroben, G.; Barbot, J.; Mouloungui, Z.; Gueguen, J., Preparation and characterization of films from pea protein. *Journal of Agricultural and Food Chemistry* **2000**, *48*, 1064-1069.
97. Choi, W. S.; Han, J. H., Physical and mechanical properties of pea-protein-based edible films. *Journal of Food Science* **2001**, *66*, 319-322.

98. Kowalczyk, D.; Baraniak, B., Effects of plasticizers, pH and heating of film-forming solution on the properties of pea protein isolate films. *Journal of Food Engineering* **2011**, *105*, 295-305.
99. Bisson, A.; Weisenfels, M., Raw sausage production - the use of collagen films with net-wrapped sausage. *Fleischwirtschaft* **1992**, *72*, 1265-1266.
100. Sommer, I.; Kunz, P. M., Improving the water resistance of biodegradable collagen films. *Journal of Applied Polymer Science* **2012**, *125*, E27-E41.
101. Langmaler, F.; Mokrejs, P.; Kolomamik, K.; Mladek, M., Biodegradable packing materials from hydrolysates of collagen waste proteins. *Waste Management* **2008**, *28*, 549-556.
102. Pena, C.; de la Caba, K.; Eceiza, A.; Ruseckaite, R.; Mondragon, I., Enhancing water repellence and mechanical properties of gelatin films by tannin addition. *Bioresource Technology* **2010**, *101*, 6836-6842.
103. Rivero, S.; Garcia, M. A.; Pinotti, A., Correlations between structural, barrier, thermal and mechanical properties of plasticized gelatin films. *Innovative Food Science & Emerging Technologies* **2010**, *11*, 369-375.
104. Gomez-Guillen, M. C.; Perez-Mateos, M.; Gomez-Estaca, J.; Lopez-Caballero, E.; Gimenez, B.; Montero, P., Fish gelatin: a renewable material for developing active biodegradable films. *Trends in Food Science & Technology* **2009**, *20*, 3-16.
105. Cuq, B.; Gontard, N.; Cuq, J. L.; Guilbert, S., Packaging films based on myofibrillar proteins: Fabrication, properties and applications. *Nahrung-Food* **1998**, *42*, 260-263.
106. Shiku, Y.; Hamaguchi, P. Y.; Weng, W. Y.; Tanaka, M., Film-forming mechanism of biodegradable films prepared from fish myofibrillar proteins. *Journal of the Japanese Society for Food Science and Technology-Nippon Shokuhin Kagaku Kogaku Kaishi* **2005**, *52*, 325-329.
107. Cuq, B.; Aymard, C.; Cuq, J. L.; Guilbert, S., Edible packaging films based on fish myofibrillar proteins: Formulation and functional properties. *Journal of Food Science* **1995**, *60*, 1369-1374.
108. Martelli, S. M.; Moore, G.; Paes, S. S.; Gandolfo, C.; Laurindo, J. B., Influence of plasticizers on the water sorption isotherms and water vapor permeability of chicken feather keratin films. *Lwt-Food Science and Technology* **2006**, *39*, 292-301.
109. Ghanbarzadeh, B.; Almasi, H.; Entezami, A. A., Improving the barrier and mechanical properties of corn starch-based edible films: Effect of citric acid and carboxymethyl cellulose. *Industrial Crops and Products* **2011**, *33*, 229-235.
110. Dou, Y.; Huang, X.; Zhang, B.; He, M.; Yin, G.; Cui, Y., Preparation and characterization of a dialdehyde starch crosslinked feather keratin film for food packaging application. *Rsc Advances* **2015**, *5*, 27168-27174.
111. Gennadios, A.; Handa, A.; Froning, G. W.; Weller, C. L.; Hanna, M. A., Physical properties of egg white-dialdehyde starch films. *Journal of Agricultural and Food Chemistry* **1998**, *46*, 1297-1302.
112. Handa, A.; Gennadios, A.; Hanna, M. A.; Weller, C. L.; Kuroda, N., Physical and molecular properties of egg-white lipid films. *Journal of Food Science* **1999**, *64*, 860-864.

113. Hyuga, M.; Omae, K.; Yoshida, H.; Takahashi, R.; Okada, T.; Minoura, N., Physico-Chemical Properties and Lysozyme Activities of Egg White Film. *Kobunshi Ronbunshu* **2012**, *69*, 20-26.
114. Somanathan, N.; Naresh, M.; Arumugam, V.; Ranganathan, T.; Sanjeevi, R., Mechanical properties of alkali treated casein films. *Polym. J* **1992**, *24*, 603.
115. Chick, J.; Ustunol, Z., Mechanical and barrier properties of lactic acid and rennet precipitated casein-based edible films. *Journal of Food Science* **1998**, *63*, 1024-1027.
116. Khwaldia, K.; Perez, C.; Banon, S.; Desobry, S.; Hardy, J., Milk proteins for edible films and coatings. *Critical Reviews in Food Science and Nutrition* **2004**, *44*, 239-251.
117. Shellhammer, T. H.; Krochta, J. M., Whey protein emulsion film performance as affected by lipid type and amount. *Journal of Food Science* **1997**, *62*, 390-394.
118. Fang, Y.; Tung, M. A.; Britt, I. J.; Yada, S.; Dalgleish, D. G., Tensile and barrier properties of edible films made from whey proteins. *Journal of Food Science* **2002**, *67*, 188-193.
119. Zinoviadou, K. G.; Koutsoumanis, K. P.; Biliaderis, C. G., Physico-chemical properties of whey protein isolate films containing oregano oil and their antimicrobial action against spoilage flora of fresh beef. *Meat Science* **2009**, *82*, 338-345.
120. Dutta, P. K.; Tripathi, S.; Mehrotra, G. K.; Dutta, J., Perspectives for chitosan based antimicrobial films in food applications. *Food Chemistry* **2009**, *114*, 1173-1182.
121. Shepherd, R.; Reader, S.; Falshaw, A., Chitosan functional properties. *Glycoconj J* **1997**, *14*, 535-542.
122. Qin, C.; Li, H.; Xiao, Q.; Liu, Y.; Zhu, J.; Du, Y., Water-solubility of chitosan and its antimicrobial activity. *Carbohydrate Polymers* **2006**, *63*, 367-374.
123. Kurita, K.; Sannan, T.; Iwakura, Y., Studies on chitin, 4. Evidence for formation of block and random copolymers of N-acetyl-D-glucosamine and D-glucosamine by hetero- and homogeneous hydrolyses. *Die Makromolekulare Chemie* **1977**, *178*, 3197-3202.
124. Kubota, N.; Tatsumoto, N.; Sano, T.; Toya, K., A simple preparation of half N-acetylated chitosan highly soluble in water and aqueous organic solvents. *Carbohydrate Research* **2000**, *324*, 268-274.
125. Ogawa, K., Effect of Heating an Aqueous Suspension of Chitosan on the Crystallinity and Polymorphs (Analytical Chemistry). *Agricultural and biological chemistry* **1991**, *55*, 2375-2379.
126. Kubota, N.; Eguchi, Y., Facile preparation of water-soluble N-acetylated chitosan and molecular weight dependence of its water-solubility. *Polymer journal* **1997**, *29*, 123-127.
127. Aiba, S.-i., Studies on chitosan: 3. Evidence for the presence of random and block copolymer structures in partially N-acetylated chitosans. *International journal of biological macromolecules* **1991**, *13*, 40-44.
128. Skjak-Braek, G.; Anthonsen, T.; Sandford, P., *Chitin and Chitosan: Sources, Chemistry, Biochemistry, Physical Properties and Applications: Proceedings from the 4th International Conference on Chitin and Chitosan Held in Trondheim, Norway, August 22-24 1988*. Elsevier applied science: 1989.
129. Rinaudo, M.; Pavlov, G.; Desbrières, J., Influence of acetic acid concentration on the solubilization of chitosan. *Polymer* **1999**, *40*, 7029-7032.

130. Rinaudc, M.; Pavlov, G.; Desbrieres, J., Solubilization of chitosan in strong acid medium. *International Journal of Polymer Analysis and Characterization* **1999**, *5*, 267-276.
131. Ravi Kumar, M. N. V., A review of chitin and chitosan applications. *Reactive and Functional Polymers* **2000**, *46*, 1-27.
132. Srinivasa, P. C.; Ramesh, M. N.; Kumar, K. R.; Tharanathan, R. N., Properties of chitosan films prepared under different drying conditions. *Journal of Food Engineering* **2004**, *63*, 79-85.
133. Casariego, A.; Souza, B. W. S.; Cerqueira, M. A.; Teixeira, J. A.; Cruz, L.; Díaz, R.; Vicente, A. A., Chitosan/clay films' properties as affected by biopolymer and clay micro/nanoparticles' concentrations. *Food Hydrocolloids* **2009**, *23*, 1895-1902.
134. Butler, B. L.; Vergano, P. J.; Testin, R. F.; Bunn, J. M.; Wiles, J. L., Mechanical and Barrier Properties of Edible Chitosan Films as affected by Composition and Storage. *Journal of Food Science* **1996**, *61*, 953-956.
135. Srinivasa, P. C.; Ramesh, M. N.; Tharanathan, R. N., Effect of plasticizers and fatty acids on mechanical and permeability characteristics of chitosan films. *Food Hydrocolloids* **2007**, *21*, 1113-1122.
136. Conca, K.; Yang, T., Edible food barrier coatings. *Activities report of the R and D Associates (USA)* **1993**.
137. Nisperos-Carriedo, M. O., Edible coatings and films based on polysaccharides. *Edible coatings and films to improve food quality* **1994**, *1*, 322-323.
138. Despond, S.; Espuche, E.; Domard, A., Water sorption and permeation in chitosan films: Relation between gas permeability and relative humidity. *Journal of Polymer Science Part B: Polymer Physics* **2001**, *39*, 3114-3127.
139. Gallant, D. J.; Bouchet, B.; Baldwin, P. M., Microscopy of starch: evidence of a new level of granule organization. *Carbohydrate Polymers* **1997**, *32*, 177-191.
140. Tester, R. F.; Karkalas, J.; Qi, X., Starch—composition, fine structure and architecture. *Journal of Cereal Science* **2004**, *39*, 151-165.
141. Smits, A.; Kruiskamp, P.; Van Soest, J.; Vliegthart, J., The influence of various small plasticisers and malto-oligosaccharides on the retrogradation of (partly) gelatinised starch. *Carbohydrate polymers* **2003**, *51*, 417-424.
142. Hermansson, A.-M.; Svegmarm, K., Developments in the understanding of starch functionality. *Trends in Food Science & Technology* **1996**, *7*, 345-353.
143. Delville, J.; Joly, C.; Dole, P.; Bliard, C., Influence of photocrosslinking on the retrogradation of wheat starch based films. *Carbohydrate Polymers* **2003**, *53*, 373-381.
144. Tako, M.; Hizukuri, S., Gelatinization mechanism of potato starch. *Carbohydrate Polymers* **2002**, *48*, 397-401.
145. Miles, M. J.; Morris, V. J.; Orford, P. D.; Ring, S. G., The Roles of Amylose and Amylopectin in the Gelation and Retrogradation of Starch. *Carbohydrate Research* **1985**, *135*, 271-281.
146. Eliasson, A., Retrogradation of starch as measured by differential scanning calorimetry. *Progress in biotechnology* **1985**.
147. Eliasson, A.; Gudmundsson, M., Starch: physicochemical and functional aspects. *FOOD SCIENCE AND TECHNOLOGY-NEW YORK-MARCEL DEKKER-* **1996**, 431-504.

148. Eliasson, A. C.; Ljunger, G., Interactions between amylopectin and lipid additives during retrogradation in a model system. *Journal of the Science of Food and Agriculture* **1988**, *44*, 353-361.
149. Kalichevsky, M. T.; Ring, S. G., Incompatibility of amylose and amylopectin in aqueous solution. *Carbohydrate Research* **1987**, *162*, 323-328.
150. Zobel, H. F., Starch Crystal Transformations and Their Industrial Importance. *Starch - Stärke* **1988**, *40*, 1-7.
151. Buléon, A.; Colonna, P.; Planchot, V.; Ball, S., Starch granules: structure and biosynthesis. *International Journal of Biological Macromolecules* **1998**, *23*, 85-112.
152. Buléon, A.; Gérard, C.; Riekkel, C.; Vuong, R.; Chanzy, H., Details of the Crystalline Ultrastructure of C-Starch Granules Revealed by Synchrotron Microfocus Mapping. *Macromolecules* **1998**, *31*, 6605-6610.
153. Tester, R. F.; Morrison, W. R., Swelling and gelatinization of cereal starches. II. Waxy rice starches. *Cereal Chem* **1990**, *67*, 558-563.
154. Fredriksson, H.; Silverio, J.; Andersson, R.; Eliasson, A. C.; Åman, P., The influence of amylose and amylopectin characteristics on gelatinization and retrogradation properties of different starches. *Carbohydrate Polymers* **1998**, *35*, 119-134.
155. Eliasson, A. C., Effect of Water Content on the Gelatinization of Wheat Starch. *Starch - Stärke* **1980**, *32*, 270-272.
156. Garcia, M. A.; Pinotti, A.; Zaritzky, N. E., Physicochemical, Water Vapor Barrier and Mechanical Properties of Corn Starch and Chitosan Composite Films. *Starch - Stärke* **2006**, *58*, 453-463.
157. Mali, S.; Grossmann, M. V. E.; García, M. A.; Martino, M. N.; Zaritzky, N. E., Effects of controlled storage on thermal, mechanical and barrier properties of plasticized films from different starch sources. *Journal of Food Engineering* **2006**, *75*, 453-460.
158. Talja, R. A.; Helén, H.; Roos, Y. H.; Jouppila, K., Effect of type and content of binary polyol mixtures on physical and mechanical properties of starch-based edible films. *Carbohydrate Polymers* **2008**, *71*, 269-276.
159. Arvanitoyannis, I.; Nakayama, A.; Aiba, S.-i., Edible films made from hydroxypropyl starch and gelatin and plasticized by polyols and water. *Carbohydrate Polymers* **1998**, *36*, 105-119.
160. Lourdin, D.; Bizot, H.; Colonna, P., "Antiplasticization" in starch-glycerol films? *Journal of Applied Polymer Science* **1997**, *63*, 1047-1053.
161. Cyras, V. P.; Manfredi, L. B.; Ton-That, M.-T.; Vázquez, A., Physical and mechanical properties of thermoplastic starch/montmorillonite nanocomposite films. *Carbohydrate Polymers* **2008**, *73*, 55-63.
162. Tang, X.; Alavi, S.; Herald, T. J., Barrier and Mechanical Properties of Starch-Clay Nanocomposite Films. *Cereal Chemistry Journal* **2008**, *85*, 433-439.
163. Wilhelm, H. M.; Sierakowski, M. R.; Souza, G. P.; Wypych, F., Starch films reinforced with mineral clay. *Carbohydrate Polymers* **2003**, *52*, 101-110.
164. Avella, M.; De Vlieger, J. J.; Errico, M. E.; Fischer, S.; Vacca, P.; Volpe, M. G., Biodegradable starch/clay nanocomposite films for food packaging applications. *Food Chem* **2005**, *93*, 467-474.
165. Dufresne, A.; Vignon, M. R., Improvement of starch film performances using cellulose microfibrils. *Macromolecules* **1998**, *31*, 2693-2696.

166. Fama, L.; Gerschenson, L.; Goyanes, S., Starch-vegetable fibre composites to protect food products. *Carbohydrate Polymers* **2009**, *75*, 230-235.
167. Angellier, H.; Molina-Boisseau, S.; Dole, P.; Dufresne, A., Thermoplastic Starch–Waxy Maize Starch Nanocrystals Nanocomposites. *Biomacromolecules* **2006**, *7*, 531-539.
168. Rindlav-Westling, A. s.; Stading, M.; Hermansson, A.-M.; Gatenholm, P., Structure, mechanical and barrier properties of amylose and amylopectin films. *Carbohydrate Polymers* **1998**, *36*, 217-224.
169. Wolff, I. A.; Davis, H.; Cluskey, J.; Gundrum, L.; Rist, C. E., Preparation of films from amylose. *Industrial & Engineering Chemistry* **1951**, *43*, 915-919.
170. Myllärinen, P.; Partanen, R.; Seppälä, J.; Forssell, P., Effect of glycerol on behaviour of amylose and amylopectin films. *Carbohydrate Polymers* **2002**, *50*, 355-361.
171. García, M. A.; Martino, M. N.; Zaritzky, N. E., Microstructural Characterization of Plasticized Starch-Based Films. *Starch - Stärke* **2000**, *52*, 118-124.
172. Gaudin, S.; Lourdin, D.; Le Botlan, D.; Ilari, J. L.; Colonna, P., Plasticisation and Mobility in Starch-Sorbitol Films. *Journal of Cereal Science* **1999**, *29*, 273-284.
173. Maran, J. P.; Sivakumar, V.; Thirugnanasambandham, K.; Sridhar, R., Response surface modeling and analysis of barrier and optical properties of maize starch edible films. *International Journal of Biological Macromolecules* **2013**, *60*, 412-421.
174. McHugh, T. H.; Krochta, J. M., Sorbitol- vs Glycerol-Plasticized Whey Protein Edible Films: Integrated Oxygen Permeability and Tensile Property Evaluation. *Journal of Agricultural and Food Chemistry* **1994**, *42*, 841-845.
175. Maran, J. P.; Sivakumar, V.; Sridhar, R.; Thirugnanasambandham, K., Development of model for barrier and optical properties of tapioca starch based edible films. *Carbohydrate Polymers* **2013**, *92*, 1335-1347.
176. Mali, S.; Grossmann, M. V. E.; García, M. A.; Martino, M. N.; Zaritzky, N. E., Barrier, mechanical and optical properties of plasticized yam starch films. *Carbohydrate Polymers* **2004**, *56*, 129-135.
177. Choi, Y. J.; Lim, S.-T.; Iml, S.-S., Preparation of Hydroxypropylated Corn Starch at High Degrees of Substitution in Aqueous Alcohol, and Pasting. **1997**.
178. Vorweg, W.; Dijksterhuis, J.; Borghuis, J.; Radosta, S.; Kröger, A., Film Properties of Hydroxypropyl Starch. *Starch - Stärke* **2004**, *56*, 297-306.
179. Singh, J.; Kaur, L.; McCarthy, O., Factors influencing the physico-chemical, morphological, thermal and rheological properties of some chemically modified starches for food applications—A review. *Food hydrocolloids* **2007**, *21*, 1-22.
180. Tuschhoff, J., Hydroxypropylated starches. *Modified starches: Properties and uses* **1986**, 89-96.
181. Lafargue, D.; Pontoire, B.; Buléon, A.; Doublier, J. L.; Lourdin, D., Structure and Mechanical Properties of Hydroxypropylated Starch Films. *Biomacromolecules* **2007**, *8*, 3950-3958.
182. Wurzburg, O. B., *Modified starches-properties and uses*. CRC Press Inc.: 1986.
183. Rhim, J.-W.; Ng, P. K. W., Natural Biopolymer-Based Nanocomposite Films for Packaging Applications. *Critical Reviews in Food Science and Nutrition* **2007**, *47*, 411-433.
184. Siro, I.; Plackett, D., Microfibrillated cellulose and new nanocomposite materials: a review. *Cellulose* **2010**, *17*, 459-494.

185. de Moura, M. R.; Mattoso, L. H. C.; Zucolotto, V., Development of cellulose-based bactericidal nanocomposites containing silver nanoparticles and their use as active food packaging. *Journal of Food Engineering* **2012**, *109*, 520-524.
186. Asharani, P. V.; Yi Lian, W.; Zhiyuan, G.; Suresh, V., Toxicity of silver nanoparticles in zebrafish models. *Nanotechnology* **2008**, *19*, 255102.
187. Davis, H. T., Factors determining emulsion type: Hydrophile—lipophile balance and beyond. *Colloids and Surfaces A: Physicochemical and Engineering Aspects* **1994**, *91*, 9-24.
188. Becher, P., *Emulsion: Theory and practice*. Reinhold Publishing Group: New York USA, 1957.
189. Stauffer, C. E., *Emulsifiers*. Eagan Press: St. Paul, 1999.
190. Holmberg, K.; Jönsson, B.; Kronberg, B.; Lindman, B., Appendices. In *Surfactants and Polymers in Aqueous Solution*, John Wiley & Sons, Ltd: 2003; pp 519-525.
191. McClements, D. J., *Food emulsions: principles, practice, and techniques*. CRC press: 1998.
192. Yokoyama, N.; Araki, Y. Wax Emulsion. 1984.
193. Kheradmandnia, S.; Vasheghani-Farahani, E.; Nosrati, M.; Atyabi, F., Preparation and characterization of ketoprofen-loaded solid lipid nanoparticles made from beeswax and carnauba wax. *Nanomedicine: Nanotechnology, Biology and Medicine* **2010**, *6*, 753-759.
194. Neslihan Gursoy, R.; Benita, S., Self-emulsifying drug delivery systems (SEDDS) for improved oral delivery of lipophilic drugs. *Biomedicine & Pharmacotherapy* **2004**, *58*, 173-182.
195. Schwarz, C.; Mehnert, W.; Lucks, J. S.; Muller, R. H., Solid Lipid Nanoparticles (SLN) for Controlled Drug-Delivery .1. Production, Characterization and Sterilization. *J Control Release* **1994**, *30*, 83-96.
196. Muller, R. H.; Mehnert, W.; Lucks, J. S.; Schwarz, C.; Zurmuhlen, A.; Weyhers, H.; Freitas, C.; Ruhl, D., Solid Lipid Nanoparticles (SLN) - an Alternative Colloidal Carrier System for Controlled Drug-Delivery. *Eur J Pharm Biopharm* **1995**, *41*, 62-69.
197. Siekmann, B.; Westesen, K., Melt-homogenized solid lipid nanoparticles stabilized by the nonionic surfactant tyloxapol. I. Preparation and particle size determination. *Pharm. Pharmacol. Lett* **1994**, *3*, 194-197.
198. Boode, K.; Walstra, P., Partial coalescence in oil-in-water emulsions 1. Nature of the aggregation. *Colloids and Surfaces A: Physicochemical and Engineering Aspects* **1993**, *81*, 121-137.
199. Helgason, T.; Awad, T. S.; Kristbergsson, K.; McClements, D. J.; Weiss, J., Effect of surfactant surface coverage on formation of solid lipid nanoparticles (SLN). *J Colloid Interf Sci* **2009**, *334*, 75-81.
200. Hunter, R., *Foundations of Colloid Science*. Oxford University Press: Oxford, UK, 1986; Vol. 1, p 31.
201. zurMuhlen, Z.; zurMuhlen, E.; Niehus, H.; Mehnert, W., Atomic force microscopy studies of solid lipid nanoparticles. *Pharm Res* **1996**, *13*, 1411-1416.
202. Li, J.; Huang, Q., Rheological properties of chitosan–tripolyphosphate complexes: From suspensions to microgels. *Carbohydrate Polymers* **2012**, *87*, 1670-1677.

203. Shahgaldian, P.; Da Silva, E.; Coleman, A. W.; Rather, B.; Zaworotko, M. J., Para-acyl-calix-arene based solid lipid nanoparticles (SLNs): a detailed study of preparation and stability parameters. *International Journal of Pharmaceutics* **2003**, *253*, 23-38.
204. Bunjes, H., Structural properties of solid lipid based colloidal drug delivery systems. *Curr Opin Colloid In* **2011**, *16*, 405-411.
205. Rosenblatt, K. M.; Bunjes, H., Poly(vinyl alcohol) as Emulsifier Stabilizes Solid Triglyceride Drug Carrier Nanoparticles in the α -Modification. *Mol Pharmaceut* **2008**, *6*, 105-120.
206. Bunjes, H.; Koch, M. H. J.; Westesen, K., Effect of Particle Size on Colloidal Solid Triglycerides. *Langmuir* **2000**, *16*, 5234-5241.
207. Westesen, K.; Siekmann, B., Investigation of the gel formation of phospholipid-stabilized solid lipid nanoparticles. *International Journal of Pharmaceutics* **1997**, *151*, 35-45.
208. Unruh, T.; Bunjes, H.; Westesen, K.; Koch, M. H. J., Observation of Size-Dependent Melting in Lipid Nanoparticles. *The Journal of Physical Chemistry B* **1999**, *103*, 10373-10377.
209. Illing, A.; Unruh, T.; Koch, M. J., Investigation on Particle Self-Assembly in Solid Lipid-Based Colloidal Drug Carrier Systems. *Pharm Res* **2004**, *21*, 592-597.
210. Unruh, T.; Westesen, K.; Bösecke, P.; Lindner, P.; Koch, M. H. J., Self-Assembly of Triglyceride Nanocrystals in Suspension. *Langmuir* **2002**, *18*, 1796-1800.
211. Jores, K.; Mehnert, W.; Drechsler, M.; Bunjes, H.; Johann, C.; Mader, K., Investigations on the structure of solid lipid nanoparticles (SLN) and oil-loaded solid lipid nanoparticles by photon correlation spectroscopy, field-flow fractionation and transmission electron microscopy. *J Control Release* **2004**, *95*, 217-227.
212. Schubert, M. A.; Harms, M.; Müller-Goymann, C. C., Structural investigations on lipid nanoparticles containing high amounts of lecithin. *Eur J Pharm Sci* **2006**, *27*, 226-236.
213. Schubert, M. A.; Muller-Goymann, C. C., Characterisation of surface-modified solid lipid nanoparticles (SLN): Influence of lecithin and nonionic emulsifier. *Eur J Pharm Biopharm* **2005**, *61*, 77-86.
214. Esposito, E.; Fantin, M.; Marti, M.; Drechsler, M.; Paccamiccio, L.; Mariani, P.; Sivieri, E.; Lain, F.; Menegatti, E.; Morari, M.; Cortesi, R., Solid lipid nanoparticles as delivery systems for bromocriptine. *Pharm Res* **2008**, *25*, 1521-1530.
215. Morales-Rueda, J. A.; Dibildox-Alvarado, E.; Charo-Alonso, M. A.; Weiss, R. G.; Toro-Vazquez, J. F., Thermo-mechanical properties of candelilla wax and dotriacontane organogels in safflower oil. *Eur J Lipid Sci Tech* **2009**, *111*, 207-215.
216. Kim, S. J.; Park, S. J.; Kim, S. I., Swelling behavior of interpenetrating polymer network hydrogels composed of poly(vinyl alcohol) and chitosan. *Reactive and Functional Polymers* **2003**, *55*, 53-59.
217. Zhai, M.; Zhao, L.; Yoshii, F.; Kume, T., Study on antibacterial starch/chitosan blend film formed under the action of irradiation. *Carbohydrate Polymers* **2004**, *57*, 83-88.
218. Goldstein, J.; Newbury, D. E.; Joy, D.; Lyman, C., Scanning electron microscopy and x-ray microanalysis. In Kluwer Academic/Plenum Publishers: New York, USA, 2003.

219. Garbassi, F.; Morra, M.; Occhiello, E., *Polymer surfaces : from physics to technology*. Wiley: Chichester, UK, 1994.
220. Suyatma, N. E.; Tighzert, L.; Copinet, A.; Coma, V., Effects of Hydrophilic Plasticizers on Mechanical, Thermal, and Surface Properties of Chitosan Films. *Journal of Agricultural and Food Chemistry* **2005**, *53*, 3950-3957.
221. Adam, N., The Adsorption of Gases and Vapours. *Nature* **1945**, *155*, 154-155.
222. Srinivasa, P.; Ramesh, M.; Kumar, K.; Tharanathan, R., Properties and sorption studies of chitosan–polyvinyl alcohol blend films. *Carbohydrate Polymers* **2003**, *53*, 431-438.
223. Bano, I.; Ghauri, M. A.; Yasin, T.; Huang, Q.; Palaparthi, A. D. S., Characterization and potential applications of gamma irradiated chitosan and its blends with poly(vinyl alcohol). *International Journal of Biological Macromolecules* **2014**, *65*, 81-88.
224. Nunthanid, J.; Puttipipatkachorn, S.; Yamamoto, K.; Peck, G. E., Physical properties and molecular behavior of chitosan films. *Drug development and industrial pharmacy* **2001**, *27*, 143-157.
225. Zheng, H.; Du, Y.; Yu, J.; Huang, R.; Zhang, L., Preparation and characterization of chitosan/poly(vinyl alcohol) blend fibers. *Journal of Applied Polymer Science* **2001**, *80*, 2558-2565.
226. Chen, C. H.; Wang, F. Y.; Mao, C. F.; Yang, C. H., Studies of chitosan. I. Preparation and characterization of chitosan/poly (vinyl alcohol) blend films. *Journal of applied polymer science* **2007**, *105*, 1086-1092.
227. Costa-Júnior, E. S.; Barbosa-Stancioli, E. F.; Mansur, A. A. P.; Vasconcelos, W. L.; Mansur, H. S., Preparation and characterization of chitosan/poly(vinyl alcohol) chemically crosslinked blends for biomedical applications. *Carbohydrate Polymers* **2009**, *76*, 472-481.
228. El-Hefian, E. A.; Nasef, M. M.; Yahaya, A. H., The Preparation and Characterization of Chitosan / Poly (Vinyl Alcohol) Blended Films. *E-Journal of Chemistry* **2010**, *7*, 1212-1219.
229. Ochoa, E.; Saucedo-Pompa, S.; Rojas-Molina, R.; de la Garza, H.; Charles-Rodriguez, A. V.; Aguilar, C. N., Evaluation of a candelilla wax-based edible coating to prolong the shelf-life quality and safety of apples. *American Journal of Agricultural and Biological Sciences* **2011**, *6*, 92.
230. Chen, X. G.; Xing, K.; Park, H. J., Antimicrobial properties of chitosan and mode of action: A state of the art review. *International Journal of Food Microbiology* **2010**, *144*, 51-63.
231. Wang, X.; Jiang, Y.; Wang, Y.-W.; Huang, M.-T.; Ho, C.-T.; Huang, Q., Enhancing anti-inflammation activity of curcumin through O/W nanoemulsions. *Food Chemistry* **2008**, *108*, 419-424.
232. Thanatuksorn, P.; Kawai, K.; Hayakawa, M.; Hayashi, M.; Kajiwara, K., Improvement of the oral bioavailability of coenzyme Q10 by emulsification with fats and emulsifiers used in the food industry. *LWT - Food Science and Technology* **2009**, *42*, 385-390.
233. Kommuru, T. R.; Gurley, B.; Khan, M. A.; Reddy, I. K., Self-emulsifying drug delivery systems (SEDDS) of coenzyme Q10: formulation development and bioavailability assessment. *International Journal of Pharmaceutics* **2001**, *212*, 233-246.

234. Rabinow, B. E., Nanosuspensions in drug delivery. *Nat Rev Drug Discov* **2004**, *3*, 785-796.
235. Porter, C. J. H.; Pouton, C. W.; Cuine, J. F.; Charman, W. N., Enhancing intestinal drug solubilisation using lipid-based delivery systems. *Advanced Drug Delivery Reviews* **2008**, *60*, 673-691.
236. Suresh, G.; Manjunath, K.; Venkateswarlu, V.; Satyanarayana, V., Preparation, characterization, and in vitro and in vivo evaluation of lovastatin solid lipid nanoparticles. *AAPS PharmSciTech* **2007**, *8*, E162-E170.
237. Garti, N.; Sato, K., Crystallization and polymorphism of fats and fatty acids. *Surfactant science series (USA)* **1988**.
238. Cavalli, R.; Caputo, O.; Carlotti, M. E.; Trotta, M.; Scarnecchia, C.; Gasco, M. R., Sterilization and freeze-drying of drug-free and drug-loaded solid lipid nanoparticles. *Int J Pharmaceut* **1997**, *148*, 47-54.
239. Lutton, R. L. W. a. E. S., Polymorphism of cocoa butter. **1966**.
240. Toro-Vazquez, J. F.; Perez-Martinez, D.; Dibildox-Alvarado, E.; Charo-Alonso, M.; Reyes-Hernandez, J., Rheometry and polymorphism of cocoa butter during crystallization under static and stirring conditions. *J Am Oil Chem Soc* **2004**, *81*, 195-202.
241. Teeranachaidekul, V.; Souto, E. B.; Junyaprasert, V. B.; Müller, R. H., Cetyl palmitate-based NLC for topical delivery of Coenzyme Q10 – Development, physicochemical characterization and in vitro release studies. *Eur J Pharm Biopharm* **2007**, *67*, 141-148.
242. Westesen, K., Novel lipid-based colloidal dispersions as potential drug administration systems – expectations and reality. *Colloid Polym Sci* **2000**, *278*, 608-618.
243. Hsu, C. H.; Cui, Z.; Mumper, R. J.; Jay, M., Preparation and characterization of novel coenzyme Q10 nanoparticles engineered from microemulsion precursors. *AAPS PharmSciTech [electronic resource]* **2003**, *4*.
244. Rossell, J., Phase diagrams of triglyceride systems. *Adv. Lipid Res* **1967**, *5*, 353-408.
245. Sek, L.; Porter, C. J. H.; Charman, W. N., Characterisation and quantification of medium chain and long chain triglycerides and their in vitro digestion products, by HPTLC coupled with in situ densitometric analysis. *Journal of Pharmaceutical and Biomedical Analysis* **2001**, *25*, 651-661.
246. Yu, H.; Shi, K.; Liu, D.; Huang, Q., Development of a food-grade organogel with high bioaccessibility and loading of curcuminoids. *Food Chemistry* **2012**, *131*, 48-54.
247. Ting, Y.; Li, C. C.; Pan, M.-H.; Ho, C.-T.; Huang, Q., Effect of a Labile Methyl Donor on the Transformation of 5-Demethyltangeretin and the Related Implication on Bioactivity. *Journal of Agricultural and Food Chemistry* **2013**, *61*, 8090-8097.
248. Cohen, M.; Morgan, R. G. H.; Hofmann, A. F., Lipolytic Activity of Human Gastric and Duodenal Juice Against Medium and Long Chain Triglycerides. *Gastroenterology* **1971**, *60*, 1-15.
249. Armand, M.; Borel, P.; Ythier, P.; Dutot, G.; Melin, C.; Senft, M.; Lafont, H.; Lairon, D., Effects of droplet size, triacylglycerol composition, and calcium on the hydrolysis of complex emulsions by pancreatic lipase: an in vitro study. *The Journal of Nutritional Biochemistry* **1992**, *3*, 333-341.
250. Armand, M.; Pasquier, B.; André, M.; Borel, P.; Senft, M.; Peyrot, J.; Salducci, J.; Portugal, H.; Jaussan, V.; Lairon, D., Digestion and absorption of 2 fat emulsions with

different droplet sizes in the human digestive tract. *The American Journal of Clinical Nutrition* **1999**, *70*, 1096-1106.

251. Sek, L.; Porter, C. J. H.; Kaukonen, A. M.; Charman, W. N., Evaluation of the in-vitro digestion profiles of long and medium chain glycerides and the phase behaviour of their lipolytic products. *Journal of Pharmacy and Pharmacology* **2002**, *54*, 29-41.

252. Tomono, Y.; Hasegawa, J.; Seki, T.; Motegi, K.; Morishita, N., Pharmacokinetic study of deuterium-labelled coenzyme Q10 in man. *International journal of clinical pharmacology, therapy, and toxicology* **1986**, *24*, 536-541.

253. Kalenikova, E. I.; Gorodetskaya, E. A.; Medvedev, O. S., Pharmacokinetics of Coenzyme Q(10). *Bulletin of Experimental Biology and Medicine* **2008**, *146*, 313-316.

254. Åberg, F.; Appelkvist, E.-L.; Dallner, G.; Ernster, L., Distribution and redox state of ubiquinones in rat and human tissues. *Archives of Biochemistry and Biophysics* **1992**, *295*, 230-234.

255. Caliph, S. M.; Charman, W. N.; Porter, C. J. H., Effect of short-, medium-, and long-chain fatty acid-based vehicles on the absolute oral bioavailability and intestinal lymphatic transport of halofantrine and assessment of mass balance in lymph-cannulated and non-cannulated rats. *J Pharm Sci-US* **2000**, *89*, 1073-1084.

256. Gershkovich, P.; Hoffman, A., Uptake of lipophilic drugs by plasma derived isolated chylomicrons: Linear correlation with intestinal lymphatic bioavailability. *Eur J Pharm Sci* **2005**, *26*, 394-404.

257. Charman, W. N. A.; Stella, V. J., Estimating the maximal potential for intestinal lymphatic transport of lipophilic drug molecules. *International Journal of Pharmaceutics* **1986**, *34*, 175-178.

258. Katayama, K.; Fujita, T., Studies on lymphatic absorption of 1',2'-(3 H)-coenzyme Q 10 in rats. *Chemical & pharmaceutical bulletin* **1972**, *20*, 2585-92.

259. Holm, R.; Porter, C. J. H.; Edwards, G. A.; Müllertz, A.; Kristensen, H. G.; Charman, W. N., Examination of oral absorption and lymphatic transport of halofantrine in a triple-cannulated canine model after administration in self-microemulsifying drug delivery systems (SMEDDS) containing structured triglycerides. *Eur J Pharm Sci* **2003**, *20*, 91-97.

260. Zhang, Y.; Åberg, F.; Appelkvist, E.-L.; Dallner, G.; Ernster, L., Uptake of Dietary Coenzyme Q Supplement is Limited in Rats. *The Journal of Nutrition* **1995**, *125*, 446-453.

261. Reahal, S.; Wrigglesworth, J., Tissue concentrations of coenzyme Q10 in the rat following its oral and intraperitoneal administration. *Drug Metabolism and Disposition* **1992**, *20*, 423-427.

262. Ernster, L.; Dallner, G., Mitochondrial diseases Biochemical, physiological and medical aspects of ubiquinone function. *Biochimica et Biophysica Acta (BBA) - Molecular Basis of Disease* **1995**, *1271*, 195-204.

263. Scalori, V.; Alessandri, M. G.; Mian, M.; Giovannini, L.; Bertelli, A. A., Plasma and tissue concentrations of coenzyme Q10 in the rat after its oral administration. *International journal of tissue reactions* **1988**, *10*, 95-7.

264. Scalori, V.; Alessandri, M. G.; Giovannini, L.; Bertelli, A., Plasma and tissue concentrations of coenzyme Q10 in the rat after intravenous, oral and topical administrations. *International journal of tissue reactions* **1990**, *12*, 149-54.

265. Miles, M. V., The uptake and distribution of coenzyme Q(10). *Mitochondrion* **2007**, *7*, Supplement, S72-S77.
266. Richheimer, S. L.; Bernart, M. W.; King, G. A.; Kent, M. C.; Beiley, D. T., Antioxidant activity of lipid-soluble phenolic diterpenes from rosemary. *J Am Oil Chem Soc* **1996**, *73*, 507-514.
267. **!!! INVALID CITATION !!!**
268. Landfeld, A.; Novotna, P.; Strohal, J.; Houska, M.; Kyhos, K., Viscosity of cocoa butter. *International Journal of Food Properties* **2000**, *3*, 165-169.
269. Freitas, C.; Muller, R. H., Correlation between long-term stability of solid lipid nanoparticles (SLN (TM)) and crystallinity of the lipid phase. *Eur J Pharm Biopharm* **1999**, *47*, 125-132.
270. Freitas, C.; Müller, R. H., Effect of light and temperature on zeta potential and physical stability in solid lipid nanoparticle (SLNTM) dispersions. *Int J Pharmaceut* **1998**, *168*, 221-229.
271. Fernández-García, E.; Carvajal-Lérida, I.; Pérez-Gálvez, A., In vitro bioaccessibility assessment as a prediction tool of nutritional efficiency. *Nutrition Research* **2009**, *29*, 751-760.
272. McClements, D. J., Edible lipid nanoparticles: Digestion, absorption, and potential toxicity. *Progress in Lipid Research* **2013**, *52*, 409-423.
273. Chen, Y.; Wang, J.; Ou, Y.; Chen, H.; Xiao, S.; Liu, G.; Cao, Y.; Huang, Q., Cellular antioxidant activities of polyphenols isolated from Eucalyptus leaves (Eucalyptus grandis× Eucalyptus urophylla GL9). *Journal of Functional Foods* **2014**, *7*, 737-745.
274. Peressini, D.; Bravin, B.; Sensidoni, A., Tensile properties, water vapour permeabilities and solubilities of starch-methylcellulose-based edible films. *Italian Journal of Food Science* **2004**, *16*, 5-16.
275. Bertuzzi, M. A.; Castro Vidaurre, E. F.; Armada, M.; Gottifredi, J. C., Water vapor permeability of edible starch based films. *Journal of Food Engineering* **2007**, *80*, 972-978.
276. Guilbert, S., Technology and application of edible protective films. In " Food Packaging and Preservation. Teory and Practice", ed. M. Mathlouthi. *Elsevier Applied Science Publishing Co., London, England* **1986**, *9*, 37.
277. Frankel, E. N.; Huang, S.-W.; Aeschbach, R.; Prior, E., Antioxidant Activity of a Rosemary Extract and Its Constituents, Carnosic Acid, Carnosol, and Rosmarinic Acid, in Bulk Oil and Oil-in-Water Emulsion. *Journal of Agricultural and Food Chemistry* **1996**, *44*, 131-135.
278. Hoover, R.; Hannouz, D.; Sosulski, F., Effects of Hydroxypropylation on Thermal Properties, Starch Digestibility and Freeze-Thaw Stability of Field Pea (Pisum sativum cv Trapper) Starch. *Starch-Stärke* **1988**, *40*, 383-387.
279. Östergård, K.; Björck, I.; Gunnarsson, A., A study of native and chemically modified potato starch. Part I: Analysis and enzymic availability in vitro. *Starch-Stärke* **1988**, *40*, 58-66.
280. Björck, I.; Gunnarsson, A.; Østergård, K., A study of native and chemically modified potato starch. Part II: Digestibility in the rat intestinal tract. *Starch-Stärke* **1989**, *41*, 128-134.

281. Khuri, A. I.; Mukhopadhyay, S., Response surface methodology. *Wiley Interdisciplinary Reviews: Computational Statistics* **2010**, 2, 128-149.